Dielectric Elastomer Tape Actuators

by

Tizoc Cruz-Gonzalez

A dissertation submitted in partial fulfillment
of the requirements for the degree of
Doctor of Philosophy
(Mechanical Engineering)
in the University of Michigan
2024

Doctoral Committee:

Professor Diann Erbschole Brei, Co-Chair
Associate Research Scientist Jonathan E. Luntz, Co-Chair
Professor Daniel J. Inman
Professor Kon-Well Wang

Tizoc Cruz-Gonzalez

tizoc@umich.edu

ORCID iD: 0000-0002-2782-7783

Dedication

To my family and to those who never, ever give up. I never have and I never will.

Acknowledgment

I want to thank my family, partner, friends, co-workers, advisors, therapists, and those who have helped on this journey. I also want to thank General Motors for sponsoring my research.

Table of Contents

List of Tables

List of Figures

Abstract

Actuators enable movement across the expanse of human invention; their role in technological advancement cannot be overstated. Revolutionary technological developments have accelerated the need for new actuators for aerospace, automotive, consumer, and medical applications: actuators that perform fast, large-strain actuation in a compact, conformable package while doing external work. Despite tremendous advances in materials, architecture, fabrication, characterization, and modeling of dielectric elastomer (DE) actuators, challenges remain: no architecture possesses all the desired actuation properties, and design process methodological issues persist. Because material and actuator properties vary with strain state and exhibit hysteric and viscoelastic behaviors, only complex viscoelastic analytical models have effectively predicted performance over a wide range of operating conditions, limiting actuator design to researchers with specialized expertise. This dissertation addresses technological and methodological issues in DE actuators. The primary technical contribution is a new DE tape actuator architecture that utilizes a novel flexible release frame, silicone elastomer, single-wall carbon nanotube (SWNT) electrodes, and innovative multifunctional tape connectors. The architecture performs fast, lightweight, conformable, large-strain actuation while doing external work; it is compact and modular to facilitate scaling; over time, it is repeatable and robust; and it supports a simplified design process, enabling predictable and controllable design with variable performance. The research established a new categorization rubric for frame configurations, created a new flexible release frame, and developed pioneering multifunctional tape connectors. The dissertation delineates a design approach – characterization, modeling, and system design – based on the actuator's application context, encompassing the application situation, actuation requirements, and actuator architecture. Given the material and actuation property complexities, hysteric behavior, and viscoelasticity associated with DE actuators, application context dictates characterization requirements and provides a simple process for full actuator characterization. Viscoelastic performance can be simplified into the quasi-static force-deflection realm without losing critical information, while data simplification facilitates analytical modeling of actuators'

viscoelastic behavior without requiring complex time-dependent models. The resulting model enables a simple quasi-static design process that accurately predicts the performance of the actuator/device. This dissertation establishes a process for characterizing cyclical steady-state actuation – defined as the repeated actuation performance level reached after some number of cycles when the long-term transient viscoelastic properties, Mullins effect, or actuator shakedown, have settled out – that captures key mechanical and electrical actuation properties which drive performance. The dissertation also presents a new variable shear Gent strain energy model for terminated primary creep steady-state cycling actuation, created from first principles. The elegance of this model is that the new variable shear term is only dependent on the driving voltage, yet it effectively encompasses all the relevant viscoelastic effects over the whole actuation range for steady-state cyclical actuation. The model calibration requires data from only two actuation performance curves operating at different voltages yet provides virtually the same accuracy as if the model was calibrated at each desired operating voltage level. The new model enables simple quasi-static model-based design for DE actuators while promoting an intuitive understanding of how the parameters impact the performance of the actuation system. Three case studies are used to validate the technological and methodological advances. The outcomes of this research – a new DE actuator architecture, characterization paradigm, predictive design model, and design methodology – provide a foundation for future progress to enable wider adoption and advancement of DE actuators.

Chapter 1 Introduction

Actuators enable movement across the expanse of human invention. The crucial role of actuators traversing all areas of technological advancement cannot be overstated. With revolutionary changes in the size and capabilities of electronics over the past several decades, frontiers for actuation are expanding and evolving at an exceptional pace. In particular, rapid developments in medicine and medical devices, transportation technologies, and consumer products have exposed gaps in existing actuation technology and crystallized the demand for actuators with expanded capabilities. Actuators displaying the following characteristics will be required. First, actuators must be lightweight and accommodate fast, large-strain actuation while performing external work. They need to be conformal, compact, and modular to enable scaling. Their behavior must be robust and repeatable. For the purposes of this dissertation, robust refers to being insensitive to environmental conditions, resistant to material impurities, and having a low failure rate, pushing the performance close to the material limits. Finally, they should support a simplified design process that allows for predictable and controllable design with variable performance. This research aims to create a new dielectric elastomer (DE) actuator architecture and develop a foundation for the systematic, model-based design of DE actuators for industrial applications.

This chapter identifies evolving actuation needs in light of current and promising technological advancements. Dielectric elastomer actuators, their potential to meet the developing need for fast, large-strain, conformable, compact, modular, robust, and repeatable actuation, and current factors inhibiting the adoption of DE actuators are reviewed. From these challenges, the research issues and approach for this dissertation are identified to lay the groundwork for future advances in the field of dielectric elastomer actuation.

1.1. Ever-Growing Need for Actuation

Technological innovation over the past half-century has increased exponentially. These advancements have been driven by the decreasing size and increasing electronics capability. The

miniaturization of electronics coincides with a surge in their capabilities. The same is true of batteries and power electronics. These developments have made it possible to incorporate actuation into devices and technology in previously inconceivable ways [1–9].

Conventional actuators have been improving for more than a century. Tremendous advancements in efficiency, power, and size have enabled them to be used in more and more places, from consumer applications. In addition to advances in conventional actuators, there have been improvements in smart material actuators to address situations where conventional actuators are not reasonably capable. These showcase the greatest near-term potential for dielectric elastomer actuators. Advancing and growing application fields are typically where these gaps or mismatches of technology can be found.

Lead adopters of new actuation technology include medicine and medical technology; transportation technology, particularly the aerospace and automotive industries; and consumer products. Applications in these cutting-edge fields require lightweight, energy-efficient, large-strain actuation and compact actuators all at a low cost [10–13]. Specifically regarding medical advances, a lightweight, fast, large-strain actuator capable of doing external work in a conformable and compact package with robust and repeatably action would assist in designing prosthetics and artificial organs. In prosthetics, there is a need for lightweight large-strain actuators that can act in the 0.1 – 1.5 Hz frequency range [14]. Biomedical research into muscles, lungs, and cardiac and gastrointestinal tissues is challenging because it is difficult to mimic the mechanical-biological forces applied to these tissues in vivo [15]. Self -inflating hydrogel tissue expanders offer a significant advance in the reconstructive techniques available for the surgical restoration of a wide variety of soft tissue defects [16]. While traditional saline expanders enable soft tissue expansion, they result in high infection rates. Conformable actuators are those that can modulate their shape to match irregular surfaces [10,17–23], or as noted by Gua [24], “conform to the uneven surface of an object, allowing efficient yet delicate grasping of multiple items with unknown geometry, moduli, and weights.” Conformability is particularly critical in applications such as soft tissue and automotive applications like door seals, where exactly conforming to an irregular surface is critical. The shift towards lightweight materials and electric vehicles in the automotive industry is prompting the review and replacement of mechanical actuators, including replacing cooling hoses, which currently require pumps, with active hoses where pumping is achieved through nonmechanical actuation within the hose material itself. Drones and micro air

vehicles (MAV) seek actuators to control surfaces and pumps and drive flapping. Morphing control surfaces and aero profiles will enable aircraft to be more efficient and operate under a wider range of varying flight conditions [25]. New morphing aircraft require large-strain actuation (greater than 100%) [13]. These applications require lightweight, fast, large-strain actuation with conformal and compact packaging. In the expansive field of consumer products, the need for lightweight, conformable, compact, and repeatable actuation ranges from goods relying on haptics, such as mobile devices and game controllers, to noise-canceling headphones to peristaltic pumps used for mobile medication dosing. Soft robotics seeks to mimic advantages of living systems, including improved flexibility, adaptability, and reconfigurability [10,26–28].

Each of these domains has seen the implementation of new actuation technologies enabled by advancements in electronics, batteries, and power electronics. Actuation improvements consist primarily of improved performance while reducing weight and size. However, there are numerous applications in these fields where actuation technology lags behind other technological advancements. There is an ongoing need for actuation technology to accommodate, enhance, and enable other technological advances, for example, in applications where modern actuation technologies are incapable of being integrated or where the integration challenges lead to infeasible devices as the negative trade-offs required for integration negate any benefits from new actuation. A new actuation technology with different performance capabilities could eliminate the trade-off necessary to integrate existing actuator technologies. The critical properties required of new technologies include being lightweight, capable of fast, large-strain actuation while performing external work in a conformable and compact package with the ability to scale modularly, exhibiting robust and repeatable action, and offering a predictable and controllable method to achieve variable performance.

1.2. Actuation Current State of the Art to Meet New Needs

Advances in actuation drive and empower technological progress. While there have been significant advances in actuator technology in recent years, science has not yet identified or developed an actuation system that simultaneously accommodates fast, large-strain actuation while having conformable properties and is in a compact package [29–31]. Conventional actuators are characterized by using electric, electromagnetic, hydraulic, and pneumatic sources to produce and control movement. These are well suited for traditional applications where large,

one-directional movement is required and a larger actuation mechanism can be accommodated. However, they are ill-suited for newer applications requiring lightweight, conformable, compact actuators. Actuator technology has advanced significantly over the past 40 years with the proliferation of smart materials, that is, materials responsive to alterations in their external environment, such as temperature, moisture, magnetic fields, etc. With significantly higher energy densities than conventional actuators, smart material actuators hold great potential for providing compact and lightweight actuation to meet evolving needs. Ceramic piezoelectric actuators convert electrical energy into linear motion. Piezo actuators are well suited for applications requiring strict accuracy and precision, including miniature medical devices and smartphone technology. However, they are constrained to very low-strain applications that require linear movement or a complex system that turns a high force at very high frequency with low-strain actuation into large-strain actuation with lower force. This transformation requires additional mass and space while being very rigid. Shape memory polymers (SMPs) and shape memory alloys (SMAs) soften and deform in response to heat, light, electricity, or magnetism and then revert to their original shape when the external stimulus is removed. SMPs are very slow actuators, which severely limits their application spaces. SMAs are very fast for transforming their crystalline structure one way but act at slow speeds when used in cyclical actuation and are typically limited to strains less than 10% [32]. SMAs can achieve much larger strains using more complex architectures or packaging, but there is a trade-off of higher complexity, and they cycle at low actuation frequencies. SMAs are typically used in binary actuation applications since they are also difficult to control. Pneumatic artificial muscles (PAMs), also known as soft pneumatic actuators, are designed to mimic biological muscles. Inflatables are actuators that expand to create movement. PAMs and inflatables require pumps, limiting their suitability for compact and lightweight applications. As their name suggests, electroactive polymers (EAPs) change in size or shape when exposed to an electric field. While there are numerous types of EAPs, they are generally considered slow acting and may require the use of liquids, except dielectric elastomers, a particular type of EAP.

1.2.1. History of Dielectric Elastomers

A dielectric elastomer is a specific type of EAP that is lightweight and highly stretchable. The use of DEs for actuation was introduced in the early 1990s when a group at SRI

International recognized the potential application of DEs to actuation [33–36]. While focusing on the performance and characteristics of DEs, the group determined that applying an electrostatic charge to particular elastomer films could produce large-strain actuation. From its initial publication in the 1990s until the early 2000s, only a few research groups closely tied to SRI were investigating DEs. They mainly focused on exploring new materials and discovering new methods to improve actuation performance [37–39]. They also worked on creating devices that would exhibit the best properties of DE actuators of large-strain actuation [21,40–42].

During the early to mid-2000s, there was some small growth in research groups using dielectric elastomers. These groups continued to explore and discover new materials for DEs, but they also started to build the fundamental knowledge to understand how DEs function. This knowledge included comparing materials, actuator modeling, control methods, and failure modes.

From the mid-2000s to 2010, there was a significant growth in research groups that were still creating or discovering new and better materials while finding more applications for dielectric elastomers. During this time, the fundamental knowledge of fabrication [43,44], experimental characterization [45–51], failure modes [52–55], and higher fidelity modeling [56–76] of DEs continued to mature. Researchers added knowledge and maturity enabled these groups to develop even more impressive gizmos (i.e., one-off devices constructed by researchers to demonstrate specific actuator properties) [77–88] for a range of applications, including haptics and robotics, as well as to utilize DEs as energy harvesters. The application of actuators as gizmos or energy harvesters was primarily focused on demonstrating the unique capabilities of DE actuators. While this "gizmo phase" focused mainly on establishing the usefulness and potential of DE actuation technology, it did not significantly progress DE technology to industrial applications.

Since 2010, there has been a mix of widgets and material research in general; however, there has been a significant increase in exploring the adoption of DE actuation in various fields. In many application spaces, including haptics [89–98], prosthetics [14], and soft robotics [10,26–28], researchers have found that DE actuators still need significant technological development before they can be employed [29,99,100]. However, one application space where DE actuation has been adopted is in cellular research in which bioreactors are used for in-situ cellular research [101–107]. In this instance, DE actuators are used to discover the impacts of mechano-

transduction and other standard cellular investigatory practices. In considering other industrial applications, many of the advances required for DE actuator technology adoption relate to non-experts in DE technology attempting to use DE actuators for specific tasks in their fields [31,108–112]. Because material and actuator properties vary with strain state and exhibit hysteric and viscoelastic behaviors, only complex viscoelastic analytical models have effectively predicted performance over a wide range of operating conditions, limiting actuator design to researchers with specialized expertise.

1.3. Dielectric Elastomer Actuator Potential

Dielectric elastomer actuators hold great promise for meeting evolving actuation needs. With DE actuators, large fast strain actuation is a key capability that separates them from other smart material actuators [113]. Dielectric elastomer actuators consist of a thin elastomer covered by a conductive electrode on both surfaces. When a differential voltage is applied to the two conductive surfaces, a Maxwell stress on the surfaces, created by the voltage differential, causes the elastomer to become thinner and grow in area. The total volume of the elastomer remains constant before and after actuation. Elastomers are made from a large conglomeration of polymer chains with relatively weak molecular bonds. They are capable of large deformations due to a combination of elastic and viscous properties caused by their atomic structure, and their chemical structure causes them to be lightweight and conformable. The elastic and viscous material properties facilitate a fast, large, distributed strain response to external forces. The principal benefits of DE actuators derive from their unique properties of being lightweight, accommodating large, fast actuation strain; and being composed of inexpensive materials [113,114]. Gu et al. identified characteristics of DEs, including distributed actuation, high energy, and ease of control [29], that make them a superior choice for applications requiring those properties.

1.3.1. Architecture

A dielectric elastomer actuator is a composite structure with a thin elastomer film and compliant conductive electrodes on the top and bottom of the film, as shown in Figure 1. The intrinsic force-displacement properties of a DE actuator are based on the mechanical properties of the elastomer's and the electrodes' combined structure and an applied voltage difference across

the DE material and the bottom surfaces. This force causes the incompressible elastomer to expand in plane, also shown in Figure 1. This Maxwell stress is a function of the applied voltage difference as well as of the dielectric properties of the elastomer.

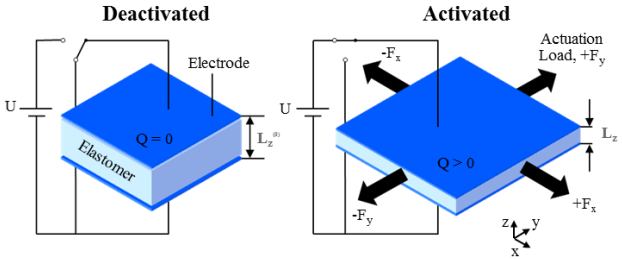

Figure 1. Basic Dielectric Elastomer Actuator

Composition of a dielectric elastomer actuator and the basic principle of actuation.

A DE actuator is often integrated into a frame that provides a pre-stretch to the elastomer film to modify the actuator's initial strain state, as shown in Figure 2. A DE actuator's external force and work depend significantly on the external force it is working against, as well as on the properties of the elastomer, the electrodes, the initial pre-stretch of the actuator, and the driving voltage.

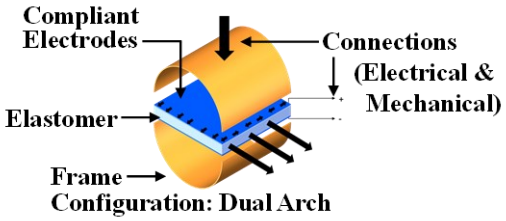

Figure 2. Dual-Arch Frame Configuration Dielectric Elastomer Actuator.

Dielectric elastomer actuator with a dual-arch frame configuration. The individual components of a typical dielectric elastomer are identified: elastomer film, compliant electrodes, electrical and mechanical connections, and the configuration frame.

The base performance characteristics of DE actuation are defined by the elastomer's stress-stretch curve, also known as a hyperelastic curve. A hyperelastic curve is the characteristic shape of any stress-stretch of an elastomer and is inherently a dynamic property. Since all elastomers have some viscoelastic properties, the standard stress-stretch curve is measured under a constant strain rate. Elastomer properties are often tested using a very slow strain rate, which measures quasi-static performance.

Elastomers experience creep whenever a constant load or stress is applied. Creep in hyperelastic elastomers involves primary, secondary, and tertiary. The primary creep, also known as transient creep, starts when a force is applied and concludes when the creep rate stabilizes, indicating the beginning of secondary creep. Secondary creep proceeds at a slow, consistent strain rate and ends when the elastomer hits its elastic limit. Tertiary creep refers to plastic deformation due to the slippage of polymer chains, which is linked with necking and void formation [115–120]. Secondary and tertiary creep may not significantly impact dielectric elastomer actuation. However, they could influence long-term actuator life. [19,121]

For Elastomer, stretch is defined as the current length, l, over the reference length, l_0. A typical elastomer's hyperelastic curve, shown in Figure 3, has three regions: an initial relatively stiff region (Region I) at small stretches, a middle compliant region (Region II) over a wide range of stretches, and a final stiffening region (Region III) at large stretches where the material approaches an asymptotic stretch limit. The figure shows a dot where a dielectric elastomer actuator is under no external forces, so the equilibrium point is zero on the stress-stretch curve. When Maxwell stress is applied on the surfaces, the planar tension stress on the elastomer increases, and the elastomer stretches to a new equilibrium point. The change in stress results from the applied Maxwell stress and the change in stretch can be considered the operating stroke from the applied Maxwell field. The DE actuator in the figure is also shown with an initial pre-stretch applied to the actuator. This pre-stretch moves the initial point up the stress-stretch curve into the middle compliant plateau portion of the curve, or Region II, of the stress-stretch curve. When the same Maxwell stress is applied to the actuator at the second equilibrium point, the planar tension stress in the film decreases by the same amount. The total energy in the system remains the same because of the applied strain energy from the Maxwell stress. In the second case, the biased operating stroke is significantly longer because the stress-stretch curve has a much lower stiffness in this region, and the applied Maxwell stress lowers the elastomer strain energy. This simple example demonstrates the significant variability in actuation performance when one actuator parameter changes. The pre-tension in the film supplied by an external force enables the Maxwell stress to relieve the stress in the system rather than add to the stress. As a result, vastly enhanced performance can be achieved.

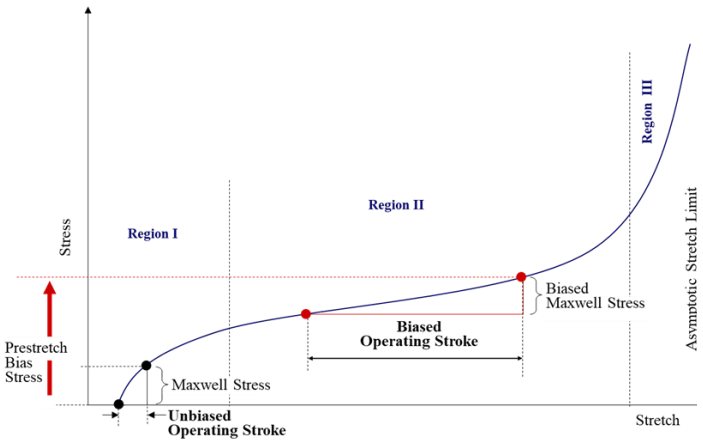

Figure 3. Dielectric Elastomer Stress-Stretch Curve.

Dielectric elastomer stress-stretch curve and actuator performance.

A second approach to the DE actuator operation is to consider it a quasi-static actuator switching between two states. The actuator has two force-displacement curves, a LOW-voltage curve, and a HIGH-voltage curve, causing a voltage difference across the elastomer. As shown in the previous figure, this extra stress acts as an additional in-plane bias and extends the material length, effectively shifting the material's force-displacement curve downward, as shown in Figure 4. If the voltage differential is zero, then the LOW curve is equivalent to the quasi-static force-displacement curve shown by the blue line. The HIGH curve is the force-displacement curve with the Maxwell stress applied to the actuator shown by the blue line. With an external load applied and the Maxwell stress off, the DE actuator will stretch until it achieves an equilibrium position, shown by the blue dot (Voltage Off Equilibrium). If the applied load remains constant and the Maxwell stress is applied, the actuator will reach a new equilibrium position, shown by the red dot (Voltage On Equilibrium). The change in the displacement between these two points is defined as the stroke of the actuator. Thus, a DE actuator stroke is a function of the externally applied force and the applied voltage differential. This approach is useful because the two curves depict the dynamic system behavior, making it easier to understand.

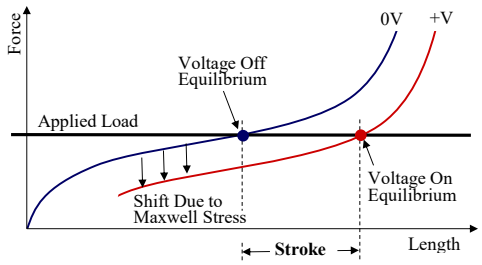

Figure 4. Force Length Performance Curves.

Dielectric elastomer actuator performance curves with voltage OFF and ON force-length curves.

1.3.2. Operation

A dielectric elastomer's mechanism to convert the Maxwell stress into an actuation force depends on the actuator design, including its fundamental frame configuration and initial conditions. Recall that a typical hyperelastic curve has three sections: an initially stiff region, a strain-softening region, and a stiffening region as the material reaches its hyperelastic limit. In the previous section, it has been shown how the same Maxwell stress results in significantly different actuation strokes depending on the pre-stretch in the elastomer. Changing the initial conditions of the actuator by applying a pre-stretch to the elastomer film enables the actuator to actuate in the strain-softening plateau region, where the best actuation performance can be achieved. The pre-stretch also causes secondary impacts, such as enhancing the dielectric properties of the elastomer. The in-plane strain caused by the Maxwell stress is an isotropic phenomenon. When the pre-stretch in the elastomer material is biaxial, it matches the reaction of the isotropic Maxwell stress and enables the best actuation stroke performance. However, applying different pre-stretches in different directions to a DE actuator is possible, making it appear to have anisotropic actuation properties. A DE actuator integrated into a system can be designed to achieve the maximum operating stroke performance using an external force to provide the initial biasing force.

It has already been shown that the same applied Maxwell stress changes the operating stroke depending on the initial pre-stretch in a dielectric elastomer actuator. This phenomenon can also be seen in the force-length and force-stroke graphs in Figure 5. As shown on the left graph, The previous pre-stretch applied to the actuator becomes an applied force in the force-length domain. If the external constant force varies across the actuator's complete force domain, the ON and

OFF voltage equilibrium point difference is the actuation stroke, as shown on the right graph. This stroke curve is valid for all externally applied forces if the ON voltage level remains constant.

In the previous example of the different operating strokes from an applied pre-stretch, a large change in pre-stretch is shown to result in a large change in operating stroke. However, this is not always valid and depends on the shape of the performance curves. An example of the typical ON and OFF performance curves is shown in Figure 5.

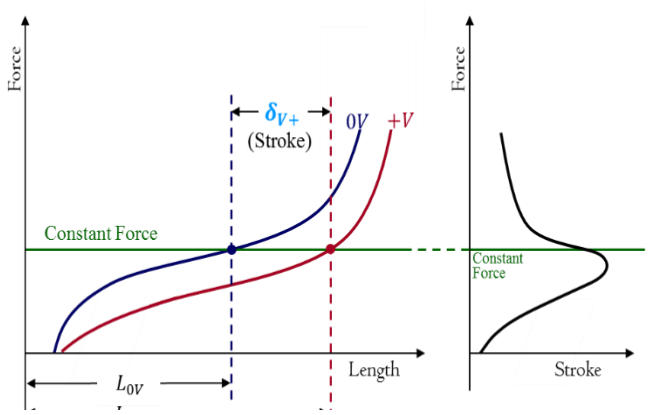

Figure 5. ON and OFF Voltage Performance Curves and Actuator Stroke.

The plot on the left shows the ON and OFF voltage performance curves in the force-length space for a dielectric elastomer actuator as well as the equilibrium points when a constant force is applied to the actuator. The plot on the right shows the actuation stroke for the same actuator when the external constant force is varied across the entire actuator's range.

Although there is a distinct maximum stroke location, the regions around the peak have very similar strokes. There are two regions where the stroke is relatively stable: near the peak and at high loads. These locations have low design sensitivity, meaning that if the applied external load is adjusted in small amounts, the stroke performance does not change. If the actuation stroke has a large slope, the location is said to have high design sensitivity. The source of the sensitivity is that small adjustments to the applied load will substantially impact the actuation stroke. If the stroke curve has a positive slope and the externally applied force is less than the desired level, the stroke will be less than desired. On the other hand, if a slightly larger external force is used, the actuator will move farther than desired. Higher loads produce lower strokes for the negative slope regions, and lower extremity forces result in higher actuation strokes.

This section has focused only on what happens when the externally applied force is varied. It is assumed that the ON voltage level is constant. However, with modern electronics, controlling the applied voltage level is easy. Any increase in the applied ON voltage level will increase the actuation stroke. The voltage level can be increased until an electrical or mechanical limit is reached. In the actuation stroke regions with low sensitivity, varying the applied voltage can achieve the desired stroke for a given externally applied load. The result is an actuation system in which the dielectric elastomer is completely controllable and can achieve any intermediate position.

1.3.3. Application Spaces

While there are myriad potential application spaces for DE actuators, three notable fields where advancements have exposed gaps or mismatches of actuator technology that DE actuators can address include medical, transportation, and consumer products. Applications in these fields require large-motion actuation in a conformal and compact package. Dielectric elastomer actuators hold great promise in addressing this need. Explosive growth in medicine and medical technology provides tremendous opportunities for the application of DE actuators. Replicating human tissue, including the in-vivo environment of cells and human muscle for organ transplantation, requires cyclical actuation [122], complex 3D deformations [15], and environmental insensitivity [30]. Likewise, next-generation prosthetics must be lightweight, reliable at high-performance levels, and attain large strain with low power. Research has shown that pneumatic cyclical compression of the calf can prevent deep-vein thrombosis [123]. These pneumatic devices require pumps that can be bulky and uncomfortable. One possible improvement would be to replace the whole compression scenario with a distributed actuator that can provide cyclic compression with the moderate force required to decrease the chances of deep-vein thrombosis complications. In aerospace, there has been a growth of unmanned aerial vehicles (UAVs) and micro-UAVs, which have much tighter packages for actuators [25]. Bats and small birds inspire many micro-UAVs to achieve better mobility [124–126]. While nature achieves this through morphing, current technology struggles to mimic this behavior. Attempting to match animal performance leads to a need for either a morphing skin that can achieve large, distributed shape changes or a new compact distributed actuator that can be used to create variable control surfaces at an intermediate frequency required for control. In the automotive

industry, there has been substantial growth in the number of actuators in vehicles [127], with many operations becoming powered to enhance the customer experience. One area of frequent customer complaint relates to weather-stripping or door seals [128–132]. Currently, these are constructed of passive rubber, which requires a design trade-off between door-closing properties and good sealing. A conformal and compact actuator could eliminate this trade-off to achieve large-strain, distributed actuation along the seal.

Conventional actuators have been improving for more than a century. Tremendous advancements in efficiency, power, and size have enabled them to be used in more and more places, from consumer products to industrial applications. In addition to advances in conventional actuators, there have been advances in smart material actuators to address situations where conventional actuators are not reasonably capable and to showcase the greatest near-term potential for dielectric elastomer actuators. These new actuation requirements of fast, large-strain motion, conformal and compact packaging, and cyclical actuation for the aerospace, automotive, and medical fields are difficult to accomplish with traditional actuators. Identifying potentially useful fields of application is important; however, that is only part of the story when investigating the possible uses for DE actuators. This technology is based on compliant elastomers with complex behavior because their properties are based on the interaction of long polymer chains. When elastomers are repeatedly stretched or cyclically strained, their behavior is known to settle into a predictable pattern. By narrowing the application space to areas that require cyclical actuation, it is further possible to narrow the performance requirements for the actuation technology. The application fields previously identified can also use cyclical actuation [15,122,133,134] to accomplish walking [29,135–143], flapping [42,142,144–147], and pumping [63,85,96,148–165]. These actions can be performed at constant frequencies varying from fast to slow, where all transient creep behavior has ended during each half period. In the case of DE actuators, actuation with transient creep ended is defined as a period when all the viscoelastic properties of the actuator have settled enough so that there are no significant changes in properties during the desired time frame. There are, in fact, many applications that can use a type of cycling actuator and for which the inherent advantages of DE actuators would be well suited.

1.4. Advantages of Dielectric Elastomer Actuators

The inherent advantageous characteristics of DE actuator technology are derived from their unique material properties. These actuators are based on thin, compliant elastomers. Therefore, these actuators will be characteristically flat, conformable, and compact. The Maxwell stress for actuation is inherently distributed, enabling a large actuation strain when the initial strain energy is manipulated to be favorable. These characteristics exemplify why this actuation technology has the potential to fulfill the actuation gaps identified previously. However, the value of DE actuators extends beyond the actuators' material properties to include the actuation's nature and their utility in the design process. Therefore, the advantages of DE actuators can be broadly categorized as properties of DE actuators, the characteristics of DE actuation, and features related to designing for DE actuation. This dissertation will refer to the following summary of these key properties.

Properties of Dielectric Elastomer Actuators: Dielectric elastomer actuators are distinguished by their lightweight and compact qualities. Their lightweight characteristics enhance their suitability for prosthetics, electric vehicles, and aerospace technology use. Similarly, the compact nature of DEs makes them well -suited for use in mobile devices and consumer electronics. Compactness is particularly applicable in medicine: the compact form of DE actuators enables them to be used directly in cell research under microscopes [166]. Dielectric elastomer actuators hold great promise as modular actuators due to their compact actuation shape and the simple ability to activate more than one actuator at a time. A modular DE actuator can potentially use multiple modules in a larger architecture to compensate for inherent limitations like low force [167–170]. Two types of scaling are possible with DE actuators: scaling based on the size of the elastomer film and modular scaling based on the number of DE actuator modules combined to make a single actuator. Elastomers are inherently scalable because their size is variable. Therefore, the scale of a DE actuator’s performance can be changed simply by increasing or decreasing the size of the elastomer film. At the lower end, miniature scalability in the range of millimeters and smaller has been demonstrated for MEMS applications [171–178] and microfluidics [112,179–188]. At the other end of the spectrum, DE actuation has been used in aerospace applications, such as for a five-meter blimp [83,88], where the scale ranges to multiple square meters [189–191]. However, modular scaling is also available with DE actuators. DE actuators can be scaled by combining layers of elastomer film and attaching a larger frame to

the new structure. Compared to a DE actuator footprint consisting of actuator length and width, the total thickness of the DE actuator is insignificant. When scaled using multilayer actuators, the footprint does not change, and the thickness remains insignificant.

Actuation Characteristics: Dielectric elastomer actuation is inherently fast, large-strain, conformable, and distributed. As noted by Madsen et al. in 2016, the ability to accommodate large-strain actuation is the principal advantage of DE actuators over other transducers [113]. Dielectric elastomers can expand well over 100%; in 2013, the Su research group from Harvard created DEs using a VHB film and carbon grease that expanded over 1692% [192]. More importantly, DE actuators perform external work while achieving large-strain actuation. As noted, large-strain actuation is critical for medical and transportation technology applications. Actuation speed is a remarkable quality of DE actuators. From the outset of research into DEs, it has been known that fast response times on the order of one millisecond were possible for DE actuators constructed with low-viscoelasticity elastomers [193]. This ability to achieve fast actuation in combination with large-strain actuation is particularly notable. In 2018, the Shea research group from EPFL demonstrated large, fast, uniaxial actuation strain for cell culture substate: -12% to 38% strain with sub- millisecond response time [194]. Dielectric elastomer actuators are energy efficient and possess high energy [34]. They are fundamentally energy storage devices, as they are compliant capacitors. For actuation, an external electrical source is used to apply a voltage potential across a DE material. The DE actuator stores the applied electrical energy as elastomer strain energy. Later, the elastomer strain energy can be converted back into electrical energy when the actuator is deactivated. Storing the energy as a capacitor is beneficial because no additional power is required to hold the actuator in place for continuous operation. As a result, DE actuators demonstrate efficiencies as high as 80 % to 90 % [193,195,196]. In addition, DEs have specific elastic energy densities up to 0.15 J/kg [23,193,195], comparable to the energy density of human muscle and pneumatics [197]. The particular material used can also contribute to the energy efficiency of DE actuators: silicone DE actuators have been shown to have low viscoelastic and electrical losses [23,193,195]. The dual characteristics of being distributed and controllable greatly enhance the functionality of DE actuators. The ability to distribute movement across the surface of the elastomer is a distinguishing characteristic of DE actuators, setting them apart from actuators that operate at a single point or edge. This distributed actuation, coupled with the ability to control the movement

across the elastomer's surface, transforms the actuator's capabilities. This movement, the "programmable shape change" [198] of DE actuators, is enabled by the simple physics of the applied electric field to control the actuation while remaining compliant. Note: because the ability to distribute movement across the elastomer is inherent to dielectric elastomers, this characteristic is implicitly included in the traits featured in a DE actuator architecture and is therefore not included in the list of factors to be addressed in a new architecture.

In addition to single-use performance characteristics, DE actuation can be characterized as robust and repeatable over extended use. For this dissertation, robust is defined as having three distinguishing qualities: first, insensitivity to environmental factors such as heat and humidity, light abrasion, and the impacts of handling and traveling; second, resistance to minor material flaws or imperfections, generally due to the ability to self-heal; third, a low failure rate, such that the performance is pushed close to the material limits. With these lifetime properties being robust and repeatable, DE actuators maintain a low failure rate, and the actuation performance remains consistent over the life of the device. Minor flaws or imperfections can be overcome using self-healing properties, pushing the performance close to the material limits ensuring long life.

Design Properties: An additional benefit of using DE actuators arises from their simple actuation physics which can enable predictable and controllable with variable performance. The resulting actuation can be predicted and controlled based on selected inputs.

While each attribute is noteworthy, they set DE actuators apart as a superior actuation solution in combination. Actuators capable of fast, large-strain actuation while performing external work in a conformable and compact package with the ability to scale modularly, exhibiting robust and repeatable actions, and offering predictable and controllable variable performance over time hold great promise for satisfying current unmet needs, as well as for future applications that have yet identified. However, although these attributes have been demonstrated individually in DE actuation and DE actuators, a DE actuator architecture showing these attributes in combination had not been established before this dissertation. Creating an architecture that can present these properties in combination will be a principal focus of this research.

1.5. Dielectric Elastomer Actuator Technology and Research Issues

The first decade of significant research into the field of DE actuators saw strong development of fundamental actuator materials – the base elastomer and the compliant electrodes – as well as many configurations to imbue actuators with a significant pre-stretch. However, to further advance DE actuator technology, the research focus must shift to accentuate the technology's fundamental advantages and identify methodological approaches that will facilitate the adoption of DE technology. Addressing both categories of adoption issues – technological and methodological – is necessary to achieve progress in adopting DE actuator technology. Technological improvements to DE actuators, the initial area of focus for this dissertation, include creating an architecture that possesses the following qualities in combination: able to achieve fast, large-strain actuation while performing external work; conformable, that is, able to provide distributed actuation over the desired surface area; compact package even when scaled modularly; robust, such that the actuation performance extends to the limits of the materials because minor flaws and impurities can be self-healed while maintaining repeatable and predictable actuation over the life of the device.

The second area of focus addresses methodological challenges in DE technology that limit the wider adoption of these actuators. Dielectric elastomer actuators may fill the growing need where conventional actuator technology is extremely limited or virtually impossible without significant compromises, but issues with characterization, modeling, and the design process present obstacles to their implementation. The complexities presented by dielectric elastomers and DE actuators require a new, cohesive approach to the design process. Actuation performance characterization must address actuator stroke as a function of forces and voltages, limitations like the maximum dielectric breakdown strength, and losses such as current leakage. Likewise, DE actuator modeling needs to account for simple viscoelastic behavior; Characterization methods that mimic and represent the limited type of actuation required by these applications allow for targeted characterization, which in turn allows for simpler and more accurate characterization. Limiting the desired application spaces also enables the development of a targeted analytical model that can be simple and accurate. To further ease the adoption of DE actuator technology, design challenges encountered by novice users need to be considered and addressed. In addition, design processes and methods that allow novice designers to bridge the existing and emerging actuation gaps successfully must be developed.

1.5.1. Actuator Architecture Issues

While there exist many fantastic and ingenious examples of DE actuators that demonstrate novel forms of actuation or are integrated into a previously challenging application and environment, identifying a combination of individual actuator sub-components to form an actuator architecture that can be applied more universally to complex technologies continues to elude researchers.

Four main components of any DE actuator architecture will be analyzed: the frame configuration, the elastomer film, the compliant electrode, and the mechanical and electrical connections. The frame configuration is defined as the structure that comprises both the external connection and the structure that provides the initial pre-stretch to the elastomer film. The elastomer film and the compliant electrodes are self-explanatory. Finally, the practical implementation of the external mechanical and electrical connections must be considered.

1.5.1.1. Frame Configuration

One of the early advances of DE actuator technology was the discovery that adding pre-stretch to the actuator before actuation dramatically increased the actuation strain potential for DE actuators [46,199–201]. This pre-stretching is a form of shifting the performance curve up the hyperelastic curve. Using nonuniform pre-stretches also introduces advantages. It enhances the work mechanically and electrically. The mechanical advantage of a nonuniform pre-stretch is that the pressure from the surface actuation can be directed by controlling the initial strain state of the elastomer material.

Typically, the pre-stretch in the elastomer is achieved by bending a flexible frame configuration or using rigid components to maintain the pre-stretch. Using the flexible frame to store strain energy and provide the pre-stretch significantly reduces the amount of external work the actuator can perform. Using a rigid or stiff frame configuration reduces or eliminates the conformal properties of the actuator. Likewise, a hard, thick frame limits the ability to use multiple actuators because of the increased bulk resulting from multiple frames. It is critical to identify a frame configuration that will maintain the initial pre-stretch, which allows the actuator to have a large actuation stroke while keeping the DE actuator's conformal properties. Dielectric elastomer actuators are typically categorized using two methods: application or shape/properties

of the frame configuration (roll, strip, spot, membrane, diaphragm). However, this classification provides limited insight into DE actuators' full potential capabilities and uses.

1.5.1.2. Elastomer Film

Dielectric elastomer actuators have unique requirements for the base elastomer. The coupling of the electrical and mechanical film properties determines actuation performance. Material selection is, therefore critically important to achieve the desired properties [202,203]. A good elastomer film for a large-stroke DE actuator will have a small slope force-length profile, low viscoelasticity, high dielectric permittivity, and high dielectric breakdown strength. For a robust actuator, the elastomer material should also be environmentally insensitive. The film will have a consistent thickness and limited defects/inclusions. A film fabricated with these properties will have uniform stress, allowing it to achieve maximum material properties. Foreign inclusions/defects in the elastomer film will lower the dielectric breakdown strength, lowering the maximum actuation strain of a DE actuator.

Focusing on only the basic electrical and mechanical properties contributing to actuation stroke neglects other attributes important for adopting dielectric elastomers outside of research. For example, the speed of actuation under cyclical loading [29,133] must be considered. Consistent performance over long cycling periods is imperative for many applications [134,204]. Selecting a relatively insensitive material to environmental conditions leads to more consistent actuation performance with less variability [205]. For example, acrylic elastomers are particularly susceptible to temperature fluctuations; silicones are more impervious to temperature changes as their elasticity remains constant [206]. Another consideration is the viscoelastic properties of the elastomer. Viscoelastic properties can be broken into two categories: short-term and long-term effects. Short-term effects mainly pertain to the actuation; while these can limit the applications, they can be incorporated into the design of an application. The long-term viscoelastic properties can have more detrimental effects on the use of DE actuators. Large-strain DE actuators require a large pre-stretch. Long viscoelastic creep can cause the elastomer to relax, which can change the actuator's performance over time. This creep can eventually lead to actuator failure, which introduces a shelf life to the actuator that will detract from its ability to be used in an application [207]. While silicone elastomers display the advantages of producing

repeatable and reproducible actuation over time, currently, their availability is limited to off-the - shelf materials rather than those developed for this specific use in DE actuators [113].

1.5.1.3. Compliant Electrodes

Compliant electrodes are critical in enabling DE actuators to achieve their large strains. The primary purpose of compliant electrodes is to distribute the electrical charge across the entire surface of the elastomer. The distributed electrical charge produces an electric field that generates the Maxwell stress, which drives the actuator.

Maintaining conductivity over a wide stretch range without increasing stiffness poses a significant challenge for most materials [191]. The only materials that can easily overcome this obstacle are viscous. Viscous materials can flow, allowing them to move along with elastomer stretching without adding stiffness. However, viscous materials are impractical for industrial applications because they are not robust: the electrodes can be removed with abrasion and dry out over time, and it is challenging to pattern the electrodes [206]. Therefore, since this research aims to advance the technology toward industrial application, another solution must be found.

Conduction is defined as the ability of a material to transfer electrons. All materials have a percolation limit, the minimum density limit at which the material can no longer transfer electrons to adjacent elements. This limit is defined according to the density of the material where it no longer transfers charge. Dielectric elastomer actuators are capable of very large stretches; therefore, it is very important that the electrode material not reach its percolation limit during the expansion, which would cause the electrode to be the limiting factor for actuation stroke [208]. The simple solution to achieving the full actuation strain is to increase the starting density of the electrode material so that the electrode density is well above the percolation limit at maximum stroke. Then, the percolation limit of the compliant electrodes is not the actuator's limiting factor. However, as the density and thickness of the material are increased, there will typically be a corresponding increase in the stiffness of the elastomer material, which will diminish the actuation stroke. Another consideration is to ensure that the time required to distribute the electric charge across the compliant electrode is orders of magnitude less than the desired actuation. This time for electric charge distribution is typically calculated from the RC time constant. Too high electronic resistance in the electrode can affect the rate at which the "capacitor" can charge. The concern for high resistance in the electrode and slow charging is

typically unimportant because very high voltages, several kilovolts, are typically used to drive DE actuators. Therefore, the time required to fill the capacitor will typically be orders of magnitude lower than the strain rate of the material, which is dependent on the elastomer's viscous properties. However, depending on the application requirements and the materials selected, the compliant electrode density and resistance issue must be accounted for in any analysis.

One common failure point of DE actuators is a dielectric breakdown in the elastomer film, which causes an electrical short. This failure typically occurs where there is a defect or inclusion in the elastomer film. This type of fault can be avoided in three ways: the defect in the elastomer can be minimized or eliminated in the film fabrication process, the electric field applied for actuation can be limited to a level significantly below the elastomer film dielectric breakdown strength, or the short can be self-healed where the electric charge is not conveyed to the location of the short. No film fabrication process is perfect, so there will always be defects. Minimizing film defects requires higher and tighter requirements for the elastomer film, resulting in higher, even prohibitive, fabrication costs. The applied electric field drives the actuation, and the higher the applied field, the greater the stroke performance. A large stroke is one of the principal advantages of a DE actuator and is required to fulfill many evolving applications. While the electrode material will dictate the electromechanical performance of a DE actuator, the electrode material's performance is contingent on the electric field [206]. Therefore, it is imperative to have an applied electric field that is as close as possible to the elastomer film dielectric breakdown strength. An actuator with a high-quality film with minimal defects and a limited applied electric field can still encounter an electrical short. If the compliant electrode continues to convey an electric charge to the location of the dielectric breakdown in the film, the actuator will remain broken. However, if the conductivity in the compliant electrode around the short can be eliminated, the actuator can regain function. Self-healing electrodes accomplish this isolation task using a current spike that burns away the conductive material around the electrical short. Thus, the self-healing of the electrode causes the percolation limit to be reached locally around the short. Although there will still be a short in the elastomer film, the compliant electrode will not transfer a charge to the location of the short. Thus, the actuator can be said to be robust to defects in the fabrication process and can use an electric field close to the breakdown strength of the film. The electrode’s ability allows DEs to tolerate flaws and is a striking advantage of this

electrode approach [206]. The additional robustness of self-healing electrodes is a potentially important quality to consider when selecting a compliant electrode. Being robust to errors increases the total robustness of the actuator.

One final issue that also falls under robustness or manufacturability is the electrode's ability of the elastomer. The applied pattern must remain where it is placed. If electrodes migrate, there is the possibility of introducing stress concentration from the Maxwell stress, which can cause overall failure of the actuator. This robustness can be addressed using a passive sealing layer; however, this reintroduces the problem of increased stiffness. As O'Halloran et al. noted [206], "Continued research into the development of more sophisticated compliant electrodes is essential in the further development of dielectric elastomer actuator technology as a whole." The proper selection of material and fabrication technique can enable a compliant actuator to have all the properties required for a particular application. Specifically, new applications will require compliant electrodes that can be firmly attached to the DE and exhibit high elasticity, conductivity, and a low shear modulus [206].

1.5.1.4. Electrical and Mechanical Connections

The selection of frame configuration, elastomer material, and compliant electrode material dictate the requirements for the electrical and mechanical connections. Dielectric elastomer actuators with external frame configurations have internal and external electrical and mechanical connections. The internal connections link the active portion of the actuator, where there is conductive material on both sides of the elastomer material, to the frame configuration. The external connections link the frame configuration electrically and mechanically to the external world. For the electrical connection, an additional mid-electrical connection can link the internal and external electrical connections. The ease of integrating a DE actuator into an application is dependent on the electrical and mechanical connections.

The internal mechanical connection has two components: the link from the active region of the actuator to the frame configuration and the method of joining the internal side of the frame configuration to the elastomer. While the internal material linking the active region to the frame configuration is usually the same base elastomer, it does not have to be. The physical connection between the elastomer film and the internal side of the frame configuration can be made through adhesion, friction, clamping, co-bonding, or any other physical phenomena that can link two

materials. Ideally, the internal mechanical connection should have a higher strength than the ultimate strength of the elastomer. The transition between the frame configuration and the elastomer should avoid stress peaks or discontinuities. Also, structurally compliant elastomer film should not be allowed to slip relative to the internal frame configuration.

The external mechanical connection is the method by which the frame configuration is attached to the actuated item. This connection must have a higher ultimate strength than the elastomer film. The more simple the method of external attachment, the easier it will be to integrate the actuator into many different systems. Ideally, the mechanical connection between the frame configuration and the external system will not add significant stiffness.

The internal electrical connection attaches the actuator's active electrode region to the actuator's inactive part, often integrated into or attached to the frame configuration. This link is typically made of the same material as the compliant electrode. Thus, the internal mechanical electrical connections should be fabricated at the same time as the active region of the actuator. One consideration related to the electrical and mechanical connections is that the active region should be separated or contain a transition zone to the frame configuration. Otherwise, if the active area is directly connected to the frame configuration, the active region will attempt to pull away when the actuator is energized. This interface often results in premature failure of the actuator. The resistance of the internal electrical lead must be low enough not detrimentally to affect the RC charging speed of the actuator.

The external electrical connection links the voltage supply to the actuator. This external connection must be securely attached to the elastomer film and compliant electrode; conversely, it must be solidly connected to the external electrical source. Depending on the material selected for the actuator and the type of external electrical connection, these two connections may have different requirements. In the case of competing requirements, it is helpful to use an additional intermediate electrode material that satisfies the internal and external electrical connection requirements. Actuation requires only one external electrical connection to each side of the film and corresponding compliant electrodes. One of the connections will be for the low-voltage side and one for the high-voltage side of the power supply. To facilitate more utility, secondary connections to both the low- and high-voltage plane electrodes somewhere else on the frame configuration are advisable. The secondary connection adds flexibility for connections.

The goal of advancing DE actuators for industrial applications makes the mechanical and electrical connections significantly more important because they must be robust and useful in many different situations and configurations. Absent a configuration with wide utility and modularity, each application of the actuator would require a redesign of the mechanical and electrical connections, which increases the complexity of the design process and ultimately decreases the functionality of the design.

1.5.2. Fabrication Issues

Industrial applications require that actuators be relatively insensitive to changes in environmental conditions and maintain consistent performance over the short and long term because they will not be confined to locations with stable environmental conditions. Variable environmental conditions lead to the selection focus on silicone materials, which are relatively insensitive to environmental conditions and can be designed to have the electrical and mechanical properties required for large-stroke DE actuators. At the onset of this research in 2010, purchasing commercial thin, soft films with superior electrical and mechanical properties for DE actuators in industrial applications was impossible because there was no previous need for thin elastomers with countervailing mechanical and electrical properties. In recent years, there has been some commercial progress in creating new robust elastomers for DE actuators. However, even now, these commercial elastomers have a somewhat high stiffness, making them easier to manufacture with very low viscosity, which is mostly useful for small-stroke actuators operating at higher frequencies. This type of actuation is useful; however, closing the more significant gap in current technology requires a large-stroke actuator.

When the research for this dissertation began, handmade custom thin silicone film was used for the dielectric elastomer and custom electrodes. The result was substantial variability in actuator performance. The primary goal at that time – finding materials with great potential for improved actuator performance – required only a limited experimental demonstration of the performance and allowed for a focus on best-performance data for each material. This focus on max achievable performance is precisely the correct thing to do when exploring new materials; however, industrial uses require robust and repeatable performance. Achieving reliable and repeatable performance necessitates consistently fabricating high-quality materials instead of individually constructing numerous materials and simply reporting on the actuators with the

greatest performance. Even today, most DE actuators are fabricated by hand. A significant barrier to the large-scale adoption of DE elastomer actuators is that hand fabrication continues to be an issue with DE actuator technology [29,111].

Elastomer film for a large-stroke DE actuator requires a low-compliance material, but low compliance is typically linked to high viscosity, which significantly limits the utility of the material. The dielectric permittivity of the elastomer, as well as the dielectric strength, are often thought of as constants, but they can change significantly with the strain energy in the elastomer film. Thus, the elastomer compliance, viscosity, dielectric permittivity, and dielectric strength will depend on the fabrication process as well as on the strain energy of the actuator configuration.

Dielectric elastomer actuators are highly dependent on the properties of the thin elastomer. However, the fabrication and integration of the compliant electrode's electrical and mechanical connections and the frame configuration all play significant roles in the performance and robustness of the actuator. As noted by Chen et al. in 2017 [202], "Careful selection of materials based on design requirements is paramount for the fabrication of successful DE actuators." These components can be combined to enhance certain properties and reduce other limitations.

1.5.3. Characterization Issues

Difficulty characterizing dielectric elastomer actuation performance arises from the complexities of dielectric elastomer materials, their behavior, and the connections between the elastomer and the external world. Current characterization methods focus on these elements separately rather than as a system, limiting the accuracy of the characterization. Methodological issues about actuation performance characterization need to address actuator stroke as a function of forces and voltages, limitations such as the maximum dielectric breakdown strength, and losses from current leakage.

For the initial decade of DE actuator research, the characterization of elastomers for DE actuators focused on using simple basic electrical and mechanical characterization tests. The primary method for evaluating the practicality of the material for DE actuators was to use test materials in a membrane/spot actuator. These membrane/spot actuators stretch an elastomer equally and biaxially inside a stiff frame and create a conductive spot at the center of the membrane. The spot is far enough away from the perimeter that the strain field is uniform in the

center. When a voltage differential is applied, the spot will grow in diameter. This architecture performs well at isolating the strain actuation properties and allows comparisons between materials [200,209–215]. Characterizing spot actuators to evaluate materials properties has limited utility for determining the fully configured DE actuator performance in an application [29,109,198,216]. The conditions of a DE actuator can be substantially different. A primary driver of this difference is that the strain state of the elastomer during actuation and the initial strain state may differ significantly from the material property characterization tests. Many standard elastomer property tests use controlled displacement to characterize properties, but authority is closely linked to force and displacement in actuation control. Elastomers are extremely complex because macro properties result from statistical interactions of many polymer chains [217]. Viscosity is related to the settling of interactions of different polymer chains at a low-energy state. The lowest energy state for elastomers will depend on the strain-state frequency of actuation, number of cycles, and relaxation time [218].

It is extremely challenging to characterize actuator performance when many actuator properties are characterized in standalone, isolated experiences that simplify the characterization of the material parameters. These applications do not account for the interaction of the parameters when they are being used in the full actuator context. To produce the best material characterization results for an actuator's performance, selecting a methodology that is characteristic of the desired application and reflects how the actuator will function is advisable.

1.5.4. Modeling Issues

Similar to the issues with characterization, challenges in modeling dielectric elastomer actuation arise from the complexities inherent in the dielectric elastomer materials and the connections between the elastomer and the external world. Methodological issues related to DE actuator modeling include accounting for or representing simple viscoelastic behavior, using calibration data to identify model parameters, and minimizing the required calibration data.

Elastomers are constructed from a very large quantity of interacting long polymer chains. The individual chains have extremely complex behavior and can significantly change depending on how they are manipulated. However, at a macro scale, the complexity of the entire elastomer material can be simplified considerably. The macro statistical interaction of the polymer chains gives elastomers their very large hyperelastic stretch range. Simple elastomer models predict the

quasi-static, or fully elastic, stress-strain performance curve. More advanced elastomer models incorporate viscoelastic properties by adding viscous terms to the elastic stress-strain curve.

A plethora of analytical models have been developed to predict the elastic performance of polymers. The most basic is a simple spring model with a force spring constant. Beyond the basic spring model, other elastic models have additional terms and can better represent the complex hyperelastic shape. At the extreme, models with unlimited terms can very closely predict the elastic performance. However, as the number of model parameters increases, the characterization becomes more complex, and more expertise is required to understand and use these unlimited-term models.

Since large-strain actuation is a primary advantage of DE actuators, models considering large strains are necessary to describe this behavior [113]. Likewise, models must account for the nonlinear, viscoelastic properties inherent in elastomers, which fundamentally impact DE actuation [29,133]. While Pelrine's initial tactic in modeling was useful for assessing the electromechanical response of DE actuation [34,37], it fails to accommodate DE actuators' nonlinear elasticity and large deformed nonlinearity [9].

Dielectric elastomer actuator models use the Maxwell stress caused by the voltage differential on the film's surface simply as a boundary condition. For example, the Gent model uses two parameters to model a hyperelastic curve, which can then be relied upon to forecast the behaviors of DE actuators [59,178,219–225]. Any additional mechanical connections to the elastomer film represent other boundary conditions needed to analyze an actuator's performance. O'Halloran et al. [206] noted, "Much work is required to accurately model the behavior of electric elastomers by coupling both electrical and mechanical behavior to accelerate the development of new improved actuators."

Many analytical models either capture the simplest performance approximation or accurately capture the full complexity of the performance. However, the simple models do not capture enough of the complexity to be used for more than the most basic gizmo design, while the complex models require significant expertise to use. Attention to the application space and type of actuation needed allows for a focus on the requirements for the analytical model. The goal is a simple model that is easily understood while capturing the important viscoelastic effects without adding a significant number of terms. For non-experts to predict the performance of DE actuators, models need to be more accurate with improved ease of use [29,31].

1.5.5. Design Issues

Dielectric elastomers are still new materials, and very few people know of their capabilities, challenges, and methods to make the greatest use of their abilities. Dielectric elastomer actuators do not function like most traditional actuators: in some ways, they can be described as reverse actuators because, when activated, they produce less force. Furthermore, because they are under tension, which is required for large-strain actuation, electrical activation results in the stroke of the actuator. The materials are complex, and determining the optimal initial strain energy to achieve the desired actuation is difficult. These actuators are based on soft elastomers and have relatively low force authority. There are ways to use leverage and other mechanisms to modify the force profiles to match the material's performance. There needs to be a simple, approachable design process. There is also a need for design models and processes that can lower the expertise required to design DE actuators.

Specific issues that need to be addressed in a design methodology include the ability to easily increase both the actuation force and stroke to meet the requirements of an application. The design of DE actuators must provide for accurate prediction of the actuation strain for repeated actuation at a range of driving voltages [219]. Utilizing a modular design may be one way to tackle the issues related to incremental changes in force and stroke.

1.6. Research Goals and Objectives

This research aims to create a new dielectric elastomer (DE) actuator architecture and develop a foundation for the systematic, model-based design of DE actuators for industrial applications. Meeting five research objectives is necessary to achieve this goal.

1. **Architecture for Enhancing Actuator Properties:** Identify a DE actuator frame configuration, elastomer and compliant electrode materials, and electrical and mechanical connections that enable a fast, large-strain actuator that performs external work in a conformable and compact package that can scale modularly and meet requirements for industrial applications. Those requirements include exhibiting robust and repeatable action over the life of the device while offering the design qualities of having predictable and controllable variable performance.

2. **Characterization Process:** Develop an approach for characterizing dielectric elastomer actuators for applications that use DE's inherent advantages, support actuator modeling, and a simple design.
3. **Analytical Modeling for Design:** Develop an analytical model that predicts a DE actuator's performance, which is useful for designing actuation systems. The model should utilize a minimum number of parameters to predict performance, require a minimum number of calibration data points, and finally, aid in the intuitive understanding of how modification of parameters and variables impact the performance of a dielectric elastomer actuator.
4. **Design Methodology:** Create a framework for understanding and designing dielectric elastomer actuators in device and actuation systems. Identify the limitations of a dielectric elastomer actuator's performance and methods to minimize or compensate for the disadvantages; finally, identify common or useful actuator systems for the DE actuators and methods or processes that can be utilized to generate the best performance from a dielectric elastomer actuator.
5. **Case Studies:** Use case studies are needed to validate the potential of dielectric elastomer actuators for industrial applications and to validate new characterization processes, models, and design approaches.

1.7. Research Approach

This research approach is three-pronged: the initial area of focus aims to establish a new actuator architecture to exploit the advantages of dielectric elastomers; the second area of focus seeks to establish a system-based methodology to facilitate the characterization, modeling, and design of DE actuators; the third and final area of focus involves the validation of the new architecture and system-based methodology. Five tasks aim to accomplish these three focuses, address the identified research problems, and establish the research fundamentals to advance DE actuator technology. The first task involves identifying an actuator configuration, materials, and design that meet specified performance and integration requirements driven by targeted application uses. Tasks two through four encompass identifying cohesive methodologies integral to the design process. The second task focuses on creating and validating experimental characterization techniques that accurately capture the actuation form's actuator performance and

material properties. This actuator characterization is necessary as material properties are known to change under large and complex strain states. The third task aims to develop a simple analytical model encompassing all the essential information to design actuation systems. The fourth task seeks to exemplify the critical design knowledge required to create actuation systems using a dielectric elastomer actuator. The fifth and final task involves demonstrating and validating all the dielectric elastomer actuator science fundamentals, using the developed information in case studies.

Identifying and selecting an application context for this dissertation is a fundamental and overarching element of the research approach as it ties together and is integral to each of the five tasks. Dielectric elastomer actuators are well suited to a wide range of applications, from aerospace and automotive to consumer products and medical applications and beyond. With this extensive variety of application spaces comes a commensurate range of performance requirements. For example, the performance requirements of camera focus adjustment require fast, extremely stable, and accurate displacement characteristics, whereas an active automotive seal requires conformal distributed actuation in a compact package that needs long life and durability under harsh environmental conditions. Therefore, the application context, i.e., the performance requirements specific to a particular industrial application or category of applications, is foundational to determining the characteristics and design parameters required for an actuator. In other words, actuator performance requirements depend and vary based on how the actuator is used. Consequently, material selection, characterization, modeling, and design derive from the specific application context. This context can vary from the needs of the actuation type (one movement, several movements, one frequency cycling, multiple frequency cycling, etc.) to performance requirements to the environmental conditions. Temperature conditions can range from conditions that are lab controlled (25 °C) for medical experiments to automotive applications that have a wide range (-30 °C to 120 °C), to consumer products with a smaller critical range similar to personal electronics (0 °C to 50 °C) or minimal for toys which may not have any temperature requirements. Actuation context consists of three components to account for these variations: actuator situation, actuation requirements and the specific dielectric elastomer actuator. Steady -state cyclic actuation is a simple, useful, and important application context because it captures uses in medical research from mimicking in-situ mechanical stress on cells to pumping for microfluidic or transportation of fluids to displacement control in small

packages. Steady-state cyclic actuation is defined as repeated actuation at a constant period where the outputs measured are constant for the same inputs. This dissertation utilizes the steady-state cyclic application context to demonstrate characterization, modeling, and design methodologies. Note that there are other useful contexts, such as impulse actuation and constant varying frequency actuation, that can be developed in the future using this framework, but the scope of this dissertation is limited to this particular context.

1.7.1. Actuator Configuration, Materials, and Integration

The research approach for identifying a frame configuration and materials suitable for industrial applications began with a survey of the current state of the art. Before this research, dielectric elastomer actuators were categorized based on three primary components: frame configuration, elastomer material, and compliant electrode material. This research identified a fourth important category: external electrical and mechanical connections. These connections significantly impact actuation performance. Although research papers occasionally mention external electrical and mechanical links briefly, their importance warrants including them as a separate category for actuator classification.

This research established a categorization paradigm that identifies four existing frame configuration types: frameless, full flexible frame, full rigid frame, and rigid released frame. All four of these frame configurations use advantageous components of dielectric elastomers; however, each has deficiencies that do not allow them to attain the full potential capabilities of a dielectric elastomer actuator. These findings were used to develop a fourth DE actuator frame configuration: a flexible released frame capable of achieving the pre-stretch required for large-strain actuation while maintaining the conformal advantage inherent in dielectric elastomer actuators.

Elastomer material was the second component of the DE actuator to be evaluated. While many hyperelastic materials are compatible with dielectric elastomer actuators, the three primary types used for dielectric elastomer actuators are acrylic, silicone, and polyurethanes. This research selected silicone as the most viable elastomer material for industrial applications due to its ability to achieve large actuation strains with minimal viscoelastic properties and consistent performance over time.

A plethora of materials can be used as compliant electrodes for dielectric elastomers. The most common and useful materials for compliant electrodes utilize carbon- or metal-based conductors. Other novel compliant electrodes typically have fabrication or longevity challenges, which have limited their adoption. The carbon-based conductors come in three forms: powder, grease, and chains. The metal-based electrodes typically use a thin, patterned material; however, their actuation strain range is limited due to the low elastic limits of metals. All three carbon-based electrode forms have advantages and disadvantages that must be matched to the desired industrial application.

The next step was to identify new or different electrical and mechanical connectors that do not take away from the advantages of dielectric elastomer actuators and potentially allow for addressing inherent deficiencies of dielectric elastomer actuators like low force. This consisted of pinpointing the weaknesses of current electrical and mechanical connections in dielectric elastomer actuators and determining how to lessen these liabilities. Failure points often occur at intersections in joints, so special attention was paid to the electrical and mechanical connections to minimize premature electrical breakdown [216]. Since current literature contains limited information on the subject, it is an area where improved performance is required. Using multiple actuators together in larger architectures is a technique used with other smart materials to address actuators' inherent limitations. Utilizing larger architectures is simplified when an actuator is designed as a module and contains the mechanical and electrical connection points to connect to another module. Due to the broad width of achievable performance characteristics from dielectric elastomer actuators, it was necessary to determine which properties to prioritize for industrial applications to make proper choices on configurations and materials. The identified desirable properties for industrial applications include low cost and robust and repeatable performance, ease of manufacturing, and tailorable performance.

A new DE actuator architecture was established using these elements: the DE tape actuator. The new architecture exploits the advantages of using dielectric elastomers for actuation by enabling fast, large-strain actuation while performing external work in a conformable and compact package with the ability to scale modularly, exhibiting robust and repeatable actions and offering predictable and controllable variable performance.

1.7.2. Experimental Actuator Characterization and Validation

The new DE tape actuator architecture created the need to identify a characterization methodology for steady-state cyclical actuation to characterize a DE actuator accurately. In 2015, a significant portion of the dielectric elastomer community combined to create a paper that identified the best methods for calculating or characterizing the components of dielectric elastomer actuators and sensors [216]. These standards are important because they allow the systematic comparison of different materials concerning performance. Standard material characterization tests are typically designed to characterize a few properties while holding the other material properties fixed. The paper also clearly states that there are multiple limitations to these standardized characterization techniques and that new methodologies may be required.

Developing the characterization methodology and conducting validation tests were predicated on specifying the application context as steady-state cyclic actuation since the application context established the performance requirements for the actuator. Developing a characterization methodology followed five general steps: identify the application context; use current state-of-the-art characterization techniques to identify any physics or performance factors not captured with these techniques; develop an initial experimental characterization methodology; validate and refine design and fabrication parameters; and establish the final characterization methodology. The first step, determining how the actuator needs to perform and identifying specific actuation properties, flows from the selected application context of steady-state cyclic actuation. Based on its ability to accommodate large actuation, Silpuran was identified as the desired elastomer material for this DE tape actuator. The second step involves using first engineering principals and current state-of-the-art characterization techniques to evaluate actuation performance and identify any physics and component interactions that are not being fully characterized. The third comprises exploring the characterization performance in the specific application context to identify a characterization methodology that can mimic the behavior of the actuator for the given application context. This process consists of experimentally exploring the performance properties when used in the application context and then developing a theory of characterization methodology that will provide consistent results when used in the specific application context. The fourth step involves validating the fabrication methods and refining the initial characterization and performance parameters. The final step of this process is to establish a characterization methodology for the architecture and test its

performance. Transient creep-terminated steady-state cyclic actuation is the resulting characterization for the DE tape actuator in this dissertation.

A significant issue in characterizing dielectric elastomers is their base of hyperelastic materials, which are in themselves complex. Simple material tests have been developed to identify properties related to a fixed or known strain energy state. However, many of the material properties of hyperelastic materials change with stretch, and since DE actuators utilize a large pre-stretch of the elastomer to achieve large actuation strains, these material tests do not fully characterize the material properties of the actuators used. The complex properties of hyperelastic materials are not fully understood and are still being researched. One such phenomenon not fully defined is how hyperelastic materials respond from repeated stretching and how the response changes over repeated cycles. The material response is categorized under the Mullins effect and viscoelastic properties. These combine to make it difficult to characterize dielectric elastomer properties. Therefore, the best method to overcome these issues is to characterize the material properties in the states under which they will be used in a dielectric elastomer actuator. The viscoelastic characterization effects can be accurately accounted for if there is an understanding of the performance requirements of the particular application. In this case, we are focusing on steady-state cyclic actuation; therefore, the initial hysteric effects, known as the Mullins effect, are known to shake out after a certain number of cycles. When the actuation frequency is low, and the secondary creep phase is reached during every state change or half cycle, we can overlook the initial transient creep and shakedown effects. This is permissible as long as the long-term repetitive performance is captured during the characterization. This situation can also be described as primary creep-terminated steady-state cyclical actuation. Given that we know the form factor of the DE actuator and the type of actuation approximately, we can develop techniques that accurately and consistently provide the necessary material and performance properties for practical application and design.

1.7.3. Analytical Modeling towards Device Design

The approach to creating an analytical model is to survey the current state of the art for modeling DE actuators. Early on, modelers used the hyperelastic material model with correct boundary conditions. Hyperelastic material modeling is an extensive field, so that many models can be used in DE modeling. Simple elastomer models approximate the hyperelastic material

performance as an elastic spring with complex spring stiffness. Advanced elastomer models add a viscous component to the elastic spring representation. While no model perfectly represents these complexities, the goal is to find a simple analytical model capable of predicting the performance of a DE tape actuator within the range of the actuator's performance. The characteristics of a silicone elastomer and the desire for steady-state cyclical actuation present an opportunity to simplify the required analytical models to predict the displacement while still capturing important viscous effects. The ultimate goal is to predict the actuation stroke from the system inputs; therefore, the model evaluation will focus on actuator length and stroke. After a model is identified or developed, it must be validated, the accuracy range specified, and its limitations found. The potential industrial application again allows for simplifying this process because a particular set of requirements is needed for steady-state cyclic actuation in industrial applications. There needs to be repeatable and consistent actuation performance over many repeated cycles, which means it is possible to eliminate transient effects that do not impact the long-term cyclical performance.

1.7.4. Designing Dielectric Elastomer Actuators for Performance

An existing graphical design process methodology was chosen because it enables the effective design of quasi-static systems using other smart material actuators. Using DE actuator performance curves, developed experimentally or analytically, the graphical design process will allow a designer to qualitatively predict the performance impact of changing device/system parameters or architectures. The shape of a DE actuator’s quasi-static performance curve can be related to the basic material properties or design parameters. Assuming a known configuration and material properties for an actuator, it is possible to qualitatively predict the impacts of changes on a device or system level. However, there are limits to how much the system performance can be modified by changing properties or parameters. Performance can be further modified using larger architectural structures to minimize or ameliorate the limits and disadvantages but at the cost of increased complexity. To enhance the understanding of the advantages and disadvantages of larger architectures on device/system performance when using DE actuators, a set of six devices/actuation systems are identified and evaluated. These devices/systems occur in common actuation circumstances and demonstrate how DE actuators

can be used to achieve their greatest performance. These example devices/systems will be evaluated for their performance capabilities and limitations.

1.7.5. Case Study Validation

Case studies were conducted to demonstrate and validate the dissertation's theoretical findings. The first case study used an active seal for a vehicle to illustrate the conformal properties and compact packaging of the DE tape actuator. It also demonstrates the modular properties of the DE tape actuator, using multilayer actuators to enhance the force-displacement performance of the actuation system.

In the second case study, a gravity-driven reverse bias panel was employed to demonstrate DE tape actuators' very large strain actuation potential. This example relied heavily on accurate characterization and modeling to achieve the large-strain reverse bias leverage performance.

The third case study exemplified and validated many of this dissertation's findings through an antagonistic reverse bias acoustic panel. The performance of the DE tape actuators revealed their great promise for future industrial applications. Specifically, the operation of the flexible released frame configuration and the modular properties enabled by the multifunctional tape connector demonstrated the conformal and compact package characteristics of the new architecture. This case study exemplified a use-case where the steady-state cyclical actuation is germane, making the steady-state cyclical actuation characterization methodology critical for characterizing performance. Furthermore, the new variable shear Gent strain energy model accurately reflected the actuation performance, and the quasi-static design process was applied to achieve the desired actuation performance. In short, the final case study confirmed the significance of the findings and contributions resulting from this research.

1.8. Outcomes and Contributions

This research resulted in several notable outcomes that show immense promise for future DE actuator research and application. These contributions can be broadly categorized as technological and methodological, where the technological contributions pertain to the creation of the new DE tape actuator architecture, and the methodological contributions relate to the development of a system-based process for characterization, modeling, and design. The quest to develop a DE actuator that would exemplify the advantages of elastomers successfully created

the innovative DE tape actuator. In that effort, additional notable outcomes included categorizing actuator frames and designing and applying the multifunctional tape connectors. This new actuator uses a frame configuration that enhances the performance (force, stroke, and work), uses the fundamental characteristics (conformal, compliant, and low mass) of dielectric elastomers, and enables scaling to mitigate the local force authority limitations. The DE tape actuator is designed to meet a critical gap in current actuation technologies, namely, an actuator that achieves a fast, large-strain actuation while doing external work in a conformable and compact packaging with the ability to scale modularly and maintains repeatable and robust functionality throughout the life of the device. Finally, the technology enables a simple actuator design that offers predictable and controllable variable performance.

The application context paradigm was conceived to enable this new technology to serve more applications. While a single application will require specific packaging needs and a specific type of actuation, an application context is not confined to a particular application. Rather, an application context encompasses a family of applications defined by performance requirements. Using the application context paradigm enables researchers and designers to identify the desired performance parameters for the desired type of actuation and establish the characterization, modeling, and design methodologies that best fit those parameters. For this dissertation, steady-state cyclical actuation best reflects the kind of actuation in potential application areas. Given this application context, this new characterization methodology was developed to simplify the design and allow for the parameters required to develop an analytical model. Therefore, the characterization methodology addresses the actuator's final application and configuration.

The significant development of the variable shear Gent model and the corresponding design methodology established through this dissertation will facilitate future research and expedite industrial applications of DE tape actuators. The design model was developed to capture important performance values while minimizing complexity. Dielectric elastomers should be understood as part of a complete system because their performance significantly changes under different implementations. This research applies a simplified yet powerful graphical force-displacement design technique to the DE actuator for quasi-static applications. The research also demonstrates how to manipulate DE tape actuator performance to match different systems' unique requirements.

The products of this research – the new DE tape actuator architecture, the paradigm for steady-state cyclical actuation characterization, the variable shear Gent predictive design model, the design methodology, and the supporting case studies – lay the groundwork for future advances in DE tape actuators and their application in various industrial spaces.

Chapter 2 Dielectric Elastomer Tape Actuator Architecture

Dielectric elastomer (DE) tape actuators are promising for providing fast, large-strain actuation while performing external work in a conformable and compact package that can scale modularly. They offer a significant advantage of enabling scaling by stacking or laying out in series. The process of creating a new DE tape actuator architecture requires close examination and categorization of the current state of the art of the four components of a DE actuator, frame configuration, elastomer material, compliant electrode material, and electrical and mechanical connections, that will allow for the fabrication of an actuator with the desired properties and performance capabilities that can eventually meet the requirements for industrial applications. Separately, each element is critical, but the elegance of this new architecture becomes apparent when the pieces are combined to create a new fast, large-stroke, and controllable actuator that has the potential to meet current and evolving needs in medical and transportation technology as well as in consumer products.

2.1. Review of Dielectric Elastomer Actuators

The basic components of a DE actuator include its configuration, external electrical and mechanical connections, elastomer film, and electrodes. There has been extensive research into many actuator configurations, film materials, and electrode materials; however, there has been less research into the external electrical and mechanical connections that play a crucial role in the robustness of an actuator and that do not compromise a DE's inherent advantages, such as conformability and compactness.

2.1.1. Frame Configurations

The configuration represents the external structure to which the elastomer film and electrode materials are attached. The configuration of a DE is important because it controls the general magnitude of the actuation strain range. A DE configuration without a frame (frameless) is capable of actuation strain performance in the range of 1–10% strain, while a configuration that uses a frame to provide a pre-stretch to the elastomer can achieve actuation strains of more than

100% strain [226]. To better understand the capabilities of DE actuators, a new categorization system that groups actuators by their forms and functions was created during this research. The current configurations of DEs can be organized into four categories: frameless, rigid frame, flexible frame, and rigid release frame. The frameless actuators take advantage of the compliant and conformal properties of DEs. The rigid frame actuators achieve extremely large actuation strains. The flexible framed actuators achieve large actuation and maintain the conformal compliant properties of DEs. The rigid release frame actuators achieve large actuation and can easily do useful external work. All these configurations take advantage of some of the inherent benefits of DEs; however, they are unable to take advantage of all the good DE properties while at the same time mitigating the challenging aspects of working with DEs.

2.1.1.1. Frameless

A frameless configuration is an actuator that does not have an external frame. This type of actuator consists of a free-standing thin film with compliant electrodes on the top and bottom surfaces. The outline of the actuator can be any shape, with a square or circle being the most common, as seen in Figure 6. The electrodes typically cover the entire surface except for a small region around the perimeter, which is left blank to avoid arcing between the two electrodes. When a voltage is applied, the electrodes come together, and the structure's thickness decreases by 10–20% [227,228]. This change in thickness is the dominant form of actuation for a frameless actuator. Frameless actuators are typically used as multilayer actuators to achieve larger useful strokes.

Figure 6. Dielectric Elastomer Actuators with Frameless Configurations.

Dielectric elastomer actuators with frameless configurations in multilayer stacks ; circle and square shapes for contractile actuation [345–347].

The frameless configuration has many inherent advantages. These include being a distributed surface actuation, having a relatively large force because of the uniform direct

actuation, and being compliant and compact since there is no other bulky or hard external support material. One main disadvantage of a frameless configuration is the limited actuation strain. Therefore, many layers of a frameless configuration are required to achieve a useful stroke. A second limitation with a large stack of frameless configuration actuators is that the resultant stack actuator becomes very similar in packaging to a conventional actuator that may have better actuation performance in a comparable package. It is also challenging to connect a frameless configuration to an external connection since the surface tries to actuate [229–237]. One potential application for this type of actuation is in haptic feedback systems with compact packaging [238].

2.1.1.2. Rigid Frames

A second type of DE configuration is a rigid frame actuator, which uses a rigid frame completely attached to the perimeter of the film. The main purpose of the rigid frame is to support a pre-stretch in the elastomer material that enhances the actuation strain potential for the dielectric elastomer to more than 100% strain [226].

The advantages of the rigid frame configuration include large motion, large relative force, and external load -enhanced actuation. The rigid frame enables large actuation strains by supporting a large pre-stretch in the elastomer, which puts externally stored energy into the system [239]. Using the elastomer film in the plane with a high pre-stretch enables a large relative force. These actuators can have multiple degrees of freedom of motion by using patterns of electrodes to actuate selective regions of the actuator, as shown in Figure 7. The rigid frame also makes attaching the actuator to external structures and electrical and mechanical connectors easier. However, including a large, stiff mating structure eliminates the conformal properties of the actuators. The larger rigid frames also increase the package size of the actuators, which further reduces the advantages of a DE actuator. Many of these rigid frame actuators have complex actuation strains [240,241]. The complex state of strain means that some of the actuation authority is lost as it is not being used to the limit of the material. The rigid frame also poses challenges for extracting external work from an actuator. An abrupt transition from the soft, active material to the rigid frame can cause electrical and mechanical problems.

Figure 7. Dielectric Elastomer Actuators with Rigid Frame Configuration.

Examples of rigid frame configuration dielectric elastomer actuators [193,348,349].

2.1.1.3. Flexible Frames

The flexible frame configuration uses a flexible material around the perimeter of the active material, which is used to maintain a pre-stretch in the elastomer film. The pre-stretched elastomer bends the flexible frame and deforms until the bending stress in the frame matches the stress in the film. The frames typically bend in or out of the plane, as shown in Figure 8.

Figure 8. Dielectric Elastomer Actuators with Flexible Frame Configuration.

Examples of a flexible frame configuration of dielectric elastomer actuators showing in-plane and out-of-plane flexibility [242,274,350].

A flexible frame configuration has the advantages of large actuation strain, conformal properties, complex shapes, and distributed actuation. The large actuation strain is achieved because the flexible frame maintains the pre-stretch in the film. The bending of the flexible frame can be used to magnify the stroke of an actuator [242]. The bending can also conform to complex shapes while providing distributed actuation [243]. However, the downside of the flexible frame configuration is that it typically uses much of its actuation authority to bend and flex the frame [244]. Therefore, it typically has moderate to low external force capability. This lower actuation force range further limits the possible application space. Another challenge with a flexible frame configuration is integration into a system when everything is compliant. There has been an exploration of using flexible configuration actuators for conformable grippers, hopping robots, and haptic feedback [245–247].

2.1.1.4. Rigid Released Frames

The fourth category of configuration for DE actuators is the rigid released frame, which consists of a rigid external frame attached to two ends of a dielectric elastomer, while the other edges are allowed to be free, as shown in Figure 9. The rigid edges enable the configuration to maintain a unidirectional pre-stretch parallel to the edge support, while the free edges enable the pre-stretch in the active region to change as a function of an applied external force.

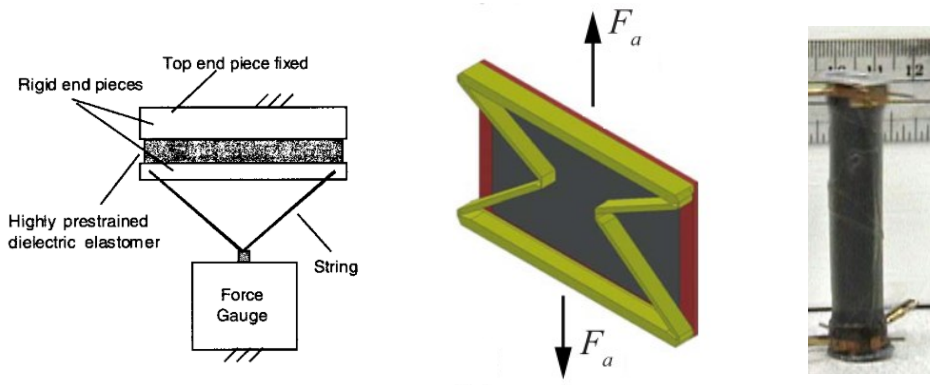

Figure 9. Dielectric Elastomer Actuators with Rigid Release Frame Configuration.

The advantage of this type of configuration is that it can provide the large pre-stretch needed to enhance actuation, which results in actuators that can achieve extremely large actuation [248]. The freedom to move allows the system to do external work easily. These configurations often require preloading from an external system to achieve optimal performance. The advantage of using the external force to provide some of the desirable pre-stretching is that the actuation is directly working against the external source in an unleveraged fashion, which increases the force-displacement actuation capabilities [249]. These actuators perform a distributed actuation across the whole edge surface, which is a strong advantage that DEs have over most other actuation technologies. These actuators are also easy to integrate because the mechanical and electrical external connections can be incorporated into the two rigid frames [250]. One issue with using a rigid frame is that one of the main conformal advantages of DE actuators is lost. Also, while rigid frames permit modular scaling, their bulk greatly increases the packaging size of the actuator.

2.1.1.5. Configuration Summary

Four categories of configurations for DEs have been introduced: frameless, fixed frame, flexible frame, and rigid released frame. Each configuration has advantages and disadvantages that could be suited to niche applications. However, because as an actuator technology, DEs are competing for use in applications against conventional and other smart material actuators, DE actuator configurations should focus on the main advantages of DE technology (fast, large-strain, distributed, conformable, and in a compact package), while minimizing the main disadvantage of DEs (low force actuation). Although frameless configuration actuators are excellent at distributed conformal actuation, they are low-strain actuators. Fixed frame actuators are large-strain actuators with high relative force potential, but the stiff frame removes the conformal advantage of DEs and significantly adds to the packaging size of the actuators while making it challenging to do external work. The flexible frame actuators have high actuation strain while performing external work in conformable and compact packaging; however, they are very low force, limiting their applications. The rigid release frames are high force and strain and easy to integrate into external work applications, but the rigid frame limits the conformability and increases the packaging size. There is currently no single configuration that enhances the fundamental advantages of DE actuators while, at the same time, mitigating all the main disadvantages.

2.1.2. External Electrical and Mechanical Connections

One aspect of DE actuators critical to robust performance and longevity is the external mechanical and electrical connections [189,251,252]. Both the electrical and mechanical connections are challenging because, in general, they are transitioning from a very low stiffness (DE actuator) to a much higher stiffness (electrical supply and mechanical support). A gradual transition would be more robust, while an abrupt transition would be more prone to failures due to a stiffness mismatch. The most basic technique connects a flexible wire to the conductive electrode [252]. The electrical connection may also be made with carbon grease, even when the compliant electrode is made from another material [253]. One technique used with rigid frame configurations is to embed a conductive region in the rigid structure that matches the compliant electrodes, which can be produced with a printed circuit board (PCB) [254]. Using a PCB provides an easy method for patterning the electrical leads but still relies on an abrupt stiffness transition. The mechanical connection must link the soft DE actuator to a more rigid external

world. The mechanical connection for configurations with a pre-stretched elastomer must also support or transfer the stress from the pre-stretch of the film. The film can be connected to the external support through a chemical bond or mechanical friction [255]. When the DE actuator is composed of a tape, such as 3M™ VHB™ (Very High Bonding), the mechanical connection can be easily completed by attaching the tape to any appropriate substrate [256]. An external glue or mechanical friction joint must be used if the film has no inherent tackiness. The advantage of a chemical/glue bond is that it can be very thin. With the correct selection of materials, the bond can be very strong. The disadvantage of glue bonds is that they are susceptible to peeling forces, and the glue will need to be bonded to another surface to provide mechanical support. When a DE is actuated, the glue layer can have substantial shear and move if it is too thick, reducing the actuation performance. Mechanical compression/friction joints require two stiff supports to sandwich the elastomer and support a distributed pressure. A challenge for compression/friction joints is determining the correct compression because the elastomer is compliant and will compress when pressure is applied. Too large a pressure may damage the elastomer, while too little pressure will allow the elastomer to break free. Both the external electrical and mechanical connections are critical to creating a robust DE actuator and must overcome the challenge of mating two materials with dissimilar degrees of stiffness.

2.1.3. Elastomer Films

DE actuators have unique requirements for good actuation performance of the base elastomer material. The elastomer film determines the actuation performance because it transforms an applied electric field into mechanical work, and this transformation is dependent on the film's properties. The key properties of the film are the force-displacement profile, viscoelasticity, dielectric permittivity, and dielectric breakdown strength. A low force-displacement profile enables a large stroke; low viscoelasticity enables fast actuation; large dielectric permittivity enables large actuation from a low electric field; and high dielectric breakdown strength allows a large electric field to be applied. Regarding benefits for actuation strain, these elastomer properties are inversely related, where the improvement of one property will detrimentally affect the other properties [257]. Therefore, a trade-off between material properties must be made when selecting an elastomer. There has been a wide exploration of materials, but the types of elastomers that have shown the best promise for general DE actuators

are acrylics and silicones [258]. Other elastomers have shown promise for niche applications, such as polyurethanes for high-force and low-strain applications [259]. The material type will control the material properties' general magnitude [193,260,261], directly correlating to the achievable performance. The specific material properties also vary with the state of strain and the environmental conditions [262,263]. Some general goals drive the selection of the elastomer, such as large actuation strain, low viscoelastic properties, and temperature insensitivity, but the actual choice of the best material depends on many factors, including the application requirements and interaction between DE actuator subcomponents. The application requirements can include strain, force, work, and operating environment.

One of the earliest materials, and still the most common material for film in DEs, is an acrylic foam, 3M™ VHB™ 4910 [262,264]. VHB-based DE actuators can produce extremely large actuation strokes because of a combination of the dielectric permittivity, the dielectric breakdown strength, and the low stiffness of the material [265]. In addition to enabling the large actuation performance, the fact that the material is a double-sided tape enables a simple external mechanical connection. VHB is used in many research gizmos for its great strain performance; however, its use for other applications is limited because of its high viscoelasticity and temperature sensitivity [54].

There has been a wide exploration of commercially available silicone elastomers; however, even today, many more possibilities have not been explored [258]. Silicone elastomers have many commercially available properties, including low force-displacement profiles, high dielectric constants, and high dielectric breakdown strength. The challenge is to find a silicone material with a good trade-off between the conflicting material properties for DE actuation. Silicones are also, in general, relatively insensitive to environmental conditions and much less viscoelastic compared to VHB. Some silicone elastomers that have shown potential for DE actuators are Elastosil, Silpuran, and RTV410 [51,249,266]. At the same time, there has been a wide exploration of creating custom silicones by doping base silicone materials with other materials to enhance their properties or change cross-link densities [51,257,267–270]. Silicone has properties that limit the ability of many materials to adhere to it, which poses challenges when fabricating a compliant electrode on the film's surface for a DE actuator [189]. However, the low viscosity, environmental insensitivity, and high actuation strain performance make silicone a promising material for DE actuators.

Polyurethane is an elastomer material explored in DEs, specifically for high-force applications that do not require large strains [258,259]. The high stiffness of polyurethane provides a high actuation force with the trade-off of a low actuation strain. The material properties are also generally insensitive to environmental conditions.

2.1.4. Compliant Electrodes

DEs can achieve large-strain actuation performance; one key component that enables this is their compliant electrodes. The conductive electrode must increase in area and maintain conductivity as a dielectric elastomer actuator strain, and the film surface area becomes larger. The primary electrode properties that affect the actuation strain are the conductivity of the electrodes as a function of strain and the stiffness and robustness of the electrodes. The Robustness of an electrode is defined in terms of the electrode's adherence to the elastomer and its functionality over repeated use. For conductive materials, a trade-off exists between electrode compliance and conductivity as a function of stretch so that as one improves, the other will be negatively affected. The compliant electrode material primarily controls these properties. However, the fabrication process can also influence the final properties when the electrode material is integrated into a dielectric elastomer actuator.

Compliant electrodes can be most readily grouped into three general categories: carbon-based, metallic, and other novel electrodes [189]. The carbon-based electrodes can be sorted into four subcategories: powders, viscous fluids or liquids, polymers, and other structures (single or multiwall carbon nanotubes). Metallic electrodes are typically very thin films or patterned in flexible shapes.

Carbon powders are mainly composed of carbon black or graphite and are deposited on the film surface to form a conductive electrode. The advantage of carbon powder electrodes is that they do not significantly increase the actuator's stiffness when used as a compliant electrode. There are two main challenges when using powder as a compliant electrode for DE actuators: maintaining conductivity under actuation and the robustness of the electrode. As a DE actuator expands, the distance between particles will increase and eventually lose conductivity by falling below their percolation limit, where particles lose conductivity to adjacent particles, limiting further strain of the actuator. The electrode's robustness depends on the carbon particles' ability to remain attached to the film's surface [195,271]. If the elastomer has no sticky surface, the

carbon particles will sit on the surface and depend on Van der Wall forces to keep the particles attached. Since particles have a low surface area, they have low attractive forces to keep them attached to the elastomer.

Conductive liquid or conductive viscous fluid electrodes consist of conductive carbon particles suspended in a viscous fluid. Fluid electrodes can maintain conductivity over a very large stretch range because of their ability to flow. Fluid electrodes typically have a negligible impact on the stiffness of the electrode, but this depends on selecting an appropriate viscosity for the fluid medium [272]. The most common form of fluid electrode for DEs is carbon grease. Moreover, the largest actuation with DEs, over 1000% strain, has been achieved using carbon grease [273]. Viscous fluids are a challenge to pattern because liquid flows, but it depends on the viscosity of the fluid medium [274]. The liquid can also evaporate or dry over time, affecting the conductive properties. Fluid electrodes are not robust because they can flow when not in use or be rubbed off with contact from another surface, which can cause failure of the actuator.

Conductive polymer electrodes consist of conductive carbon particles suspended in a polymer matrix. The conductivity of the electrodes depends on the ratio of the conductive material to the polymer matrix and the surface area of the carbon black. The percolation limit for the conductive particles has been shown to vary from 1% to 24% [275]. The stiffness of the polymer electrodes depends on both the thickness of the polymer and the polymer matrix properties. The advantage of conductive polymer electrodes is that they are robust and can be patterned accurately [276]. By trapping the conductive particles in a polymer matrix, the electrodes become resistant to abrasion and electrode drift. The disadvantage of polymer electrodes is that they increase the stiffness of a DE actuator and are a challenge to attach to the dielectric film. The increased stiffness depends heavily on the type and thickness of the polymer [252]. The additional work required to stretch the electrodes detracts from the total possible work the actuator can perform.

The carbon nanotube electrodes form a highly stretchable electrode because of their large aspect ratio of length to diameter. When deposited on a surface, the long tubes form a crisscrossing pattern that allows the tubes to pivot over each other when stretched and maintain conductivity. The electrode mat can have a low stiffness, but the stiffness of the electrode depends on its thickness and fabrication methods. The advantage of carbon nanotube electrodes is that they can maintain conductivity over a very large stretch range, greater than 700% while

having minimal impact on a DE actuator's stiffness [277]. Another advantage of using carbon nanotubes as electrodes is that they can self-heal, enhancing the robustness of a DE actuator [278]. Self-healing occurs when an electrical breakdown in the elastomer causes a current to transfer through the film. The flowing current burns off the electrode around the electrical short's location, eliminating the conductive path through the dielectric film. A challenge of carbon nanotube electrodes is that they depend on surface attraction to maintain contact with the elastomer, similar to loose carbon particles, but because of their large surface area, they have better adhesion properties [251].

Two main types of metal electrodes are used in dielectric elastomer actuators: thin films and patterned films. The thin metallic electrode films can have a maximum elastic strain in the range of 2% – 3%, after which they will crack and cease to function as an electrode [252]. This electrode type provides great conductivity and can be useful for very high speeds where the actuation strain is very low (for dielectric elastomers). Metal electrodes can be made to have much larger stretch ranges when they are patterned. There are two categories of patterns: ones that rely on an in-plane pattern to allow stretch and maintain conductivity and ones that use a 3-D or out-of-plane patterning to allow conductivity over a large range [279,280]. Both pattern types typically consist of shapes that enable thin metal strips to bend and result in large stretch ranges without stretching or exceeding the elastic stretch limits of the metal. The advantage of metal electrodes is detailed patterning and adhering well to the film's surface, using fabrication techniques already developed for micro-electromechanical systems (MEMS) applications and other uses [189]. The electrode can also provide good conductivity and stretch ranges greater than 100%, but, again, the metal electrodes significantly limit maximum potential actuation strain since elastomers can produce much larger strains [281]. Another advantage is that if the electrodes are made small enough and thin enough, metal electrodes exhibit self-healing behavior [282,283]. The disadvantages of patterned metal electrodes are that they significantly increase the actuator's stiffness and limit the full range of a dielectric elastomer.

2.1.5. Summary

In the field of dielectric elastomers, there has been tremendous progress in advancing the underlying technologies that support DE architectures. These include innovative configurations, custom elastomers with modified chemical compositions for improved properties, and an

assortment of compliant electrodes that can be selected depending on the application requirements. Many of the advances have focused on individual aspects of the architecture; however, there are now opportunities to combine multiple advances into a new DE actuator architecture that can enhance DE's fundamental advantages while mitigating the disadvantages.

2.2. Tape Actuator Architecture

The principal inherent advantage of dielectric elastomer actuators is that they consist of large-strain actuation performing distributed external work in a conformal and compact package. One of the main challenges of a DE actuator is its low-force capabilities. One way that the low-force attribute can be minimized is to use a larger architecture that uses multiple actuators acting in parallel to scale up the force, but the fundamental architecture must accommodate this aspect and enable it. Each type of current configuration enhances some of the essential advantages of DEs, but none fully uses all their potential benefits. There is a need for a DE actuator that uses moderate force levels while also being able to be used in a large architecture for enhanced force capabilities. This new actuator technology also needs to maintain the advantages of DE actuators, including being conformal and having distributed actuation.

The rigid released frame actuator is The configuration closest to providing all these advantages. However, rigid release frame configuration actuators have rigid components that prevent them from taking advantage of the DE being soft and conformal, one of its most unique and important aspects. Also, modular scaling using rigid -release frame configurations rapidly increases total packaging size because the ridged frames typically have substantially more thickness than the film and electrode. This dissertation establishes a new architecture. I have designed a DE tape actuator architecture that uses a new flexible release frame configuration and a new multifunctional tape connector (MTC). The flexible release frame configuration combines the advantages of the flexible full frame and rigid release frame configurations by replacing the stiff support in the rigid release frame with a thin, extensible support material. The new MTC is a composite structure that uses embedded conductive regions and tape to create a thin, inextensible, conformable connector that handles the DE tape architecture's external electrical and mechanical connectors.

2.2.1. Flexible Release Frame Configuration

The flexible release frame configuration has many advantages that enhance the fundamental benefits of DE technology: it enables large-strain actuation, producing moderate distributed force while doing external work in a conformal and compact package. The flexible release frame configuration uses two thin, inextensible, and flexible frames to connect to two separate edges of a rectangular, active DE region while the other two remain free. The flexible release frame configuration can achieve large actuation strains by supporting a large film pre-stretching in the lateral direction (parallel to the support frames), while the externally applied load provides pre-stretching in the axial direction (actuation direction). Thus, by delivering pre-stretch in both directions independently, achieving an effective pre-strain that enables large unidirectional motion is possible. The strain field and thickness of the entire film are relatively uniform, which allows the actuator to push the full mechanical or electrical performance limits. Using the external load to provide the pre-stretch in the axial direction allows for the direct actuation of the external load, which enables a maximum amount of the actuation authority to be used for external work. The DE tape actuator maintains the lateral pre-strain without rigid frames by using a thin, flexible, inextensible frame material bonded to two of the edges of the actuator. Although the frame material is inextensible, it is very thin, which allows the support material to be flexible out of the plane. The two independent edges can be easily attached to the external structure and provide external work capabilities. Both frames can also make external electrical connections, enabling scaling. One challenge of the flexible release frame configuration is that the free, unsupported edges of the actuator have nonuniform stress fields. To reduce the impact of these nonuniform stress fields on actuation and to minimize their size, the actuators must have a large aspect ratio for their lateral width to axial length. There is also the challenge of attaching the electrical connection to the flexible release frame configuration without any hard point that would reduce the conformal properties and introduce failure points.

2.2.2. Flexible Release Frame Configuration

Critical components that enable a DE's capabilities are the mechanical and electrical connections that link the actuator's active area to the external world. These connections are combined into a multifunctional tape connector (MTC) for a DE tape actuator. In addition to incorporating the mechanical and electrical connections, the MTC also supports the film's lateral

pre-stretch and enables larger architectures with multiple actuators while still allowing the conformability of the tape actuator. The MTC achieves its functionality by using thin, compliant, conductive materials for the electrical leads to maintain the conformability of the actuator while not significantly increasing the size of the actuator; employing an inextensible material with adhesive on both sides to provide the structural support and external mechanical connections, and providing a layout of the electrical leads that allows series and parallel electrical connections.

The DE tape actuator requires different properties for the electrical connection on the film side from the external side. On the film side, the connection must be flexible and adhere well to the film while making a strong electrical connection to the compliant electrode. The MTC uses two conductive materials to form an electric path that joins the soft, compliant electrode on the surface to a stiffer external electrical connection. The internal conductive material is chosen to make a solid electrical connection to the compliant electrode and the base elastomer. The connector will be robust By mating well to the film and the complaint electrode while maintaining conformal properties. This first connector removes the electrical connection from the active material and transitions to the external conductive material, which is stiffer but still flexible because it is very thin. The external material has a very light conductive glue on the surface, which makes it capable of being used as a reusable external electrical connection. This connection must have conductivity on both the top and bottom surfaces to make an electrical connection from either direction.

Robust internal and external mechanical connections are created using a thin, inextensible material with adhesive applied to both sides is used as the base support. The adhesive is matched in thickness and type to adhere well to the base elastomer and the external attachment. To minimize the peel forces, the MTC uses two support pieces that are individually attached to the top and bottom edges of the active DE region. The strength of the adhesive bond must exceed only the strength of the elastomer. The thickness of the supports is on the same scale as the elastomer, which maintains the actuator’s conformal properties and allows for minimizing the packaging size increase due to the supports. Access holes are cut into the supports above the locations of both the positive and negative external electrical connections on both the top and bottom support surfaces. This conductive path provides electrical access to the external electrical connection regardless of the orientation of the actuator.

The layout of the electrical leads on the MTC, the adhesive of both the support and the external electrical connections, and the inclusion of MTC on both edges of the release frame configuration enable the creation of a modular actuator that can be easily assembled into a larger architecture. The location of the electrical leads is aligned on the actuator such that the negative and positive electric leads on both ends of the release frame are aligned axially. This axial alignment allows modular actuators to be connected in series or stacked on each other. The fact that both the electrical and mechanical connections are made of tape and that it is flat and conformal means it becomes very easy to integrate the dielectric elastomer actuator into an existing application without substantial modification.

2.2.3. Architecture Advantages of Dielectric Elastomer Tape Actuators

One of the advantages that a DE tape actuator has over other actuators is that it is a distributed actuator. Conventional actuators typically achieve distributed actuation by using a support structure with a high bending stiffness to distribute a point of actuation across an edge. The total force required to actuate an entire edge of a surface with a single-point actuator may be large, but the local distributed force and stress will be substantially smaller. A DE tape actuator can be used in a distributed format where multiple actuators are distributed across an edge, and each one actuates a region. All the actuators act in parallel, increasing the total force. The distinct advantage of this format is that a stiff support structure is no longer needed to distribute the force across the entire edge of the moving material. This distributed actuation across multiple actuators also increases the fault tolerance, as the other actuators can still function if a single actuator fails.

A DE tape actuator is a modular actuator designed to be used individually or in a larger architecture in parallel or series with other modules. A multi-module DE tape actuator architecture enables a larger application space by expanding the force and stroke performance while not substantially increasing the packaging size. Multi-module architecture improves the performance range and provides possible redundancy with the trade-off of increased complexity. If well-designed, it is possible to create a system with enough performance space to account for the failure of individual components. One challenge with using multiple actuators in a larger architecture is the need for assembly, which will have manufacturing tolerances. The manufacturing tolerance for DEs can be larger and more forgiving than traditional actuators because of the flexible nature of the DE actuators. Geometric misalignments can be overcome

with additional pre-stretch or reduced pre-stretch, depending on the fabrication error, without seriously affecting the actuation performance of the whole system.

The advantages of the dielectric elastomer tape actuator architecture are conferred by the selection of elastomer and compliant electrode materials, a flexible release frame configuration, and multifunctional tape connectors. Each aspect of the architecture contributes to overall benefits, but these are typically closely related to or limited by one or more subcomponents. Due to its viscoelastic properties, the elastomer material limits the actuator's maximum speed. The frame configuration enables large-strain actuation while performing external work. The frame configuration and multifunctional tape connectors control the conformable properties and overall package compactness while enabling modularity. The elastomer and compliant electrodes significantly impact robust and repeatable actions over the actuator's lifespan. Predictable and controllable variable performance depends on the complete architecture, the characterization process, ease of modeling, and a model-based design process.

In Chapter 3, experimental characterization tests demonstrate the performance advantages of fast, large-strain actuation and robust and repeatable action over the actuator's lifecycle. These benefits are attributed to the chosen silicone elastomer material and the pre-extended single-wall carbon nanotube compliant electrodes. Fast actuation is highlighted in Sections 3.3 and 3.6. Section 3.5.3.1 illustrates the robust and repeatable action through dielectric breakdown strength characterization and a full actuator characterization in Section 3.6. While no specific actuator lifetime characterization tests were conducted, the experimental characterization process ensured that many individual actuators were handled consistently and underwent more than 10,000 actuation cycles.

The flexible release frame configuration and multifunctional tape connector confer the actuation advantages of large-strain actuation while performing distributed external work in a conformable and compact package and with the potential to scale modularly. Each of these advantages is proven in the subsequent chapters. The properties of large-strain actuation producing moderate distributed force while doing external work are shown in an experimental study in Section 3.6 and proven in three validation case studies in Sections 6.1, 6.2, and 6.3. The frame configuration's conformal properties are visually demonstrated in Section 2.4 and validated in the active seal case study, Section 6.1. A brief experimental exploration of the impact on actuation performance indicated that higher curvatures produced smaller actuation strokes

when conformal properties were required. The compact package is visually shown in Section 2.4, and the active seal case study is in Section 6.1. Compactness and modularity are proven in Section 3.7, where a stack actuator is assembled using seven tape actuator modules, and the actuation force scales while the actuator footprint remains the same. The full stack also occupies virtually the same packaging space.

2.3. Tape Actuator Prototype Fabrication

For a DE tape actuator to maintain many inherent advantages of dielectric elastomer technology, such as distributed conformal actuation in a tight package, the material choices and fabrication techniques used to create it are critical. For this research, a DE tape actuator prototype was fabricated using a flexible release frame configuration with a silicone elastomer, single-wall carbon nanotube compliant electrodes, and a multifunctional tape connector. The fabrication process of a dielectric elastomer tape actuator can be broken down into its constituent parts: *film*, *electrodes*, and *MTC*.

2.3.1. Film Fabrication

Dielectric elastomer actuators can fast large-strain actuation in a comformable and compact package. The elastomer film determines the actuation performance by transforming an applied electric field into mechanical work. This transformation depends on the film's properties, with the key properties being the force-displacement profile, viscoelasticity, dielectric permittivity, and dielectric breakdown strength. A low force-displacement profile enables a large stroke, low viscoelasticity enables fast actuation, large dielectric permittivity enables large actuation from a low electric field, and high dielectric breakdown strength allows a large electric field to be applied. These elastomer properties are inversely related to benefits for actuation stroke; improving one property will detrimentally impact the others [203,284–287]. Therefore, a design trade-off must be made when selecting the ideal properties. The elastomer properties are influenced by many factors, including the type of elastomer, the film's fabrication process, the state of strain, and the environmental conditions. The kind of elastomer, acrylic, polyurethane, or silicone, will control the general magnitude of the material properties. The fabrication process influences the material properties, including the liquid polymer preparation, the method used to create the thin film, and the film curing process. Finally, the material properties can vary with the

state of strain and the environmental conditions. Therefore, the desired actuation properties, strain, force, or work and the operating environment will determine the desired elastomer material, fabrication process, and strain state.

A good elastomer film for a large-stroke dielectric elastomer actuator will have a low-slope force-displacement profile, low viscoelasticity, high relative dielectric permittivity, and high dielectric breakdown strength. The elastomer material should also be environmentally insensitive to make a robust actuator. The film should have limited defects/inclusions and a consistent thickness so that the actuator will have uniform stress and achieve maximum material properties. Although acrylic elastomers, typically 3M VHB, have been shown to have the largest actuation strain range, their performance is sensitive to environmental conditions and highly viscoelastic. While polyurethanes have shown good temperature insensitivity and low viscosity, they have low actuation strain. On the other hand, silicone-based elastomers have large, consistent actuation strains across a wide temperature range and low viscoelastic properties, making them a good choice for applications outside of a lab where conditions are not controlled [113].

To demonstrate the influence of the fabrication process on the elastomer film, a silicone film, Wacker Silpuran 6000/10, was chosen as the typical base elastomer material. Silpuran was selected as a base for the dielectric elastomer actuator because it has been shown to have a large actuation strain and low viscoelasticity, and it is relatively environmentally insensitive [288]. Silpuran is manufactured as a two-part silicone, Part A and Part B. Part A contains the high-temperature activated cross-link. Both silicone components are combined with a solvent to create a low-viscosity liquid polymer mixture. The viscosity of the liquid polymer mixture affects the thickness and quality of the film and can be controlled by varying the proportion of the solvent to the silicone. Isopar G is an effective solvent for Silpuran [288,289]. One advantage of a custom-made two-part silicone is that the proportion of cross-linking sites can be controlled by varying the amount of cross-linker in the liquid polymer mixture by Lowering the elastomer's cross-link density, resulting in a film with a softer force-displacement profile. Cross-linking sites must be distributed equally through the liquid polymer for consistent properties. The liquid polymer preparation should minimize foreign inclusion, including air bubbles or particulates that would lower the dielectric breakdown strength [215]. Drop-casting is an effective technique for creating soft, thin films for dielectric elastomer actuators. The solvent evaporation and film curing can influence the material properties [190]. In the following sections, the specific fabrication steps

for creating a thin Silpuran film will be reviewed; however, the techniques for determining fabrication impacts, general trends on the film properties, and dielectric elastomer actuation performance can be applied to the general fabrication of thin films for use in dielectric elastomer actuators.

2.3.1.1. Liquid Silicone

Fabrication of a thin elastomer film requires a low-viscosity liquid polymer solution. The liquid polymer solution combines the raw silicone with a solvent, mixes the resultant solution, and finally out-gasses the solution, as shown in Figure 10. Each of these fabrication steps influences the final film material properties.

The viscosity of the liquid polymer is a key driver of the film thickness and thickness uniformity. A low-viscosity liquid polymer is needed to combine the two silicone components accurately and to enable drop-casting. The low-viscosity liquid silicone polymer solution is created by combining the raw silicone, which is highly viscous, with a low-viscosity solvent. Too low or too high a viscosity will harm final film properties. A high -viscosity mixture is incompatible with drop-casting because the liquid polymer will not distribute evenly over a deposition surface, thus creating a nonuniform thickness film. Too low a viscosity mixture creates very thin films, where defects can impact properties more. Very thin films also result in lower yield from the complete DE fabrication process because of the difficulty of working with very thin films. The thickness of the final film impacts the final film's electrical properties. Nonuniform films affect dielectric elastomer actuation performance because the actuation limits are related to the minimum film thickness. Isopar G is a good solvent for Silpuran. A liquid polymer solution with an effective viscosity can be created with a density of 20% Silpuran and 80% Isopar G by weight [55,179,269,270,286,290]. Weighing the components is an effective method for accurately combining the silicone components and the solvent.

Figure 10. Film Preparation.

Silpuran components are combined with a solvent to create a low viscosity fluid usable for drop-casting. A paint shaker, Blair Tornado II, is used to fully mix the final solution.

Effective mixing of the two liquid silicone components evenly distributes the cross-link sites through the mixture and results in consistent properties. The final film properties, both mechanical and electrical, are influenced by the number of cross-link sites in the final mix, which is controlled by the ratio of Silpuran Part B to Part A, which contains the chemical cross-linker. The coupling of the electrical and mechanical properties determines actuation performance. Sensitivity experiments in the following chapter, Section 3.5.2.2, show that a lower cross-link density results in a lower-stiffness elastomer, which improves the actuation strain even though the dielectric permittivity is also decreased. A final ratio of 10% Part A to 90% Part B silicone was shown to have the largest actuation strain, which was determined from the sensitivity study in Section 3.5.2. The diluted liquid polymer components Part A and Part B, 20% silicone and 80% Isopar G by weight, can be accurately combined using a volume measurement with a pipet since the combined liquid has a low viscosity. A paint shaker, Blair Tornado II, was used for 30 minutes to mix the solvent and the raw silicone. The shaker was used a second time for 15 minutes to combine the liquid polymers Parts A and B.

Inclusions in the liquid polymer, including foreign particles from contamination or air bubbles from mixing, when trapped in the final film, act as defects and lower the film's dielectric strength [190]. A clean working environment can minimize foreign particle contamination. The liquid polymer is held in a vacuum chamber, Yamato® Scientific Model DP-43, at a low pressure of 0.1 kPa for a minimum of 1 hour to eliminate trapped air bubbles. The liquid polymer will appear to boil for approximately 15 minutes as the air bubbles escape the liquid polymer.

2.3.1.2. Drop-Casting

Drop-casting creates a thin film by depositing a low-viscosity liquid polymer mixture on a flat substrate. The mixture contains a solvent that evaporates, leaving a uniform polymer layer distributed across the substrate. Drop-casting relies on the volume of liquid deposited, liquid viscosity, liquid surface tension, and gravity to create a uniform -thickness film. Gravity causes the liquid to distribute over the surface of the substrate because the low-viscosity liquid cannot support shear forces. However, the liquid surface tension can limit the spread of the liquid. The surface tension increases when the fluid reaches the perimeter and prevents the liquid from flowing over the edges of the substrate. The surface of the liquid will curve down and attach itself to the perimeter of the substrate, which results in a different thickness on the perimeter. Due to this variation in thickness, the edge region should not be used in the final dielectric elastomer actuator. As discussed earlier in the liquid silicone section, a specific range of viscosities results in a uniform film. The final thickness of the film after the solvent evaporates depends on the volume of the liquid mixture deposited and the percentage of silicone in the liquid polymer. Too small a volume of deposited liquid allows the surface tension to limit the liquid's flow. If too large a volume of liquid polymer is used, the liquid can overcome the edge surface tension and cause the liquid to overflow the boundary of the substrate. Overflowing the boundary leaves an indeterminate amount of liquid on the surface, which causes a batch of films to have significant thickness variations. Inconsistent thickness reduces electrical breakdown strength and nonuniform stress in the film, which would lower the limits of a DE actuator.

For a mixture of liquid polymer of 20% Silpuran and 80% Isopar G by weight, a volume of 2.5 ml deposited on a 2" by 2" glass slide will result in a uniformly thin film of approximately 130 μm. A mechanical pipette, Fisherbrand Finnpipette II, can be used to accurately control the volume of the liquid polymer deposited, as shown in Figure 11.

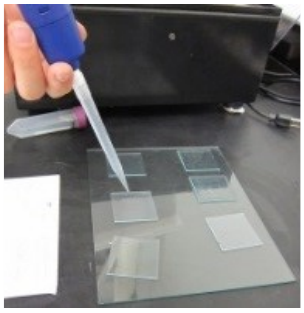

Figure 11. Drop-Casting Films.

Dielectric elastomer film fabrication using drop-casting. An automatic pipettor is used to cast an equal volume for each film sample.

2.3.1.3. Curing

The curing process includes the evaporation of the solvent and the use of thermal energy to activate the cross-linking sites. Creating the cross-links transforms the liquid polymer into an elastomer. The evaporation process, curing temperature, and time at temperature can all affect the elastomer properties. The evaporation process uses a laminar flow hood to create a clean environment, which minimizes foreign inclusions while the solvent evaporates. The uncured film with the evaporated solvent is placed in a preheated oven to activate the cross-linking sites. The oven temperature and the duration at temperature affect the number of cross-links formed. The number of cross-links and any defects from inclusions affect both the mechanical and electrical properties, which control the actuation properties, as shown in Figure 12.

An Iso 5 (Class 100) laminar flow hood, AirClean Systems model H-6595-2, was used to store the cast films for at least 48 hours to allow the solvent to evaporate. The films are then cured for 2 hours at 175°F. An experimental sensitivity study was conducted to determine the range of temperatures that can cure a Silpuran film and the impacts on actuation from changing the curing temperature, while the 2 hours is the manufacturer's recommended cure time. (See Section 3.5.2.) The experiments were inconclusive in determining an optimal temperature because the electrical and mechanical properties were affected. However, a range of temperatures, 170–200°F, was identified to enable good actuator strain results.

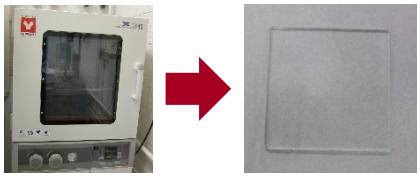

Figure 12. Film Curing with A Vacuum Oven.

Dielectric elastomer film is cured using a vacuum oven.

2.3.2. Pre-Extended Compliant Electrodes

Dielectric elastomers have demonstrated large-strain actuation performance, and one key component that enables this large actuation strain is their compliant electrodes. The conductive electrode must increase in area and maintain conductivity as a dielectric elastomer actuator strains, and the film surface area becomes larger. The primary electrode properties that affect the actuation strain are the conductivity of the electrodes as a function of strain, the electrodes' stiffness, and the electrodes' robustness. The robustness of an electrode can be defined in terms of the electrode's adherence to the elastomer and its functionality over repeated use. For conductive materials, a trade-off exists between electrode compliance and conductivity as a function of stretch so that as one improves, the other will be negatively impacted. The compliant electrode material primarily controls these properties. However, the fabrication process can also heavily influence the final properties when the electrode material is integrated into a dielectric elastomer actuator. The most common electrode materials are carbon -based, including carbon grease, carbon powder, conductive polymers with carbon particles, and carbon nanotubes. Carbon grease has the lowest trade-off between conductivity and stiffness because it is a viscous fluid and can maintain conductivity over a very large stretch range while having negligible stiffness. The electrode can flow, but the viscous medium can cause lowered robustness by flowing to undesired areas, drying out, or being removed by contact or abrasion. Carbon particles also have negligible stiffness; however, they will reach their percolation limit and lose conductivity. Conductive polymers can have great robustness and maintain conductivity over a large stretch range but can add significant stiffness. Carbon nanotubes have good robustness and a large conductivity range, but they have a range of stiffnesses that depend heavily on

fabrication. Each type of elastomer requires its fabrication process; however, the general requirements for all electrodes include preparation of the film, creation of a pattern mask to isolate the conductive region, preparation of the electrode material, and deposition of the electrode. Depending on the type of conductive material, the electrode fabrication process can substantially impact the trade-off between conductivity as a function of stretch and stiffness [54,55,189,202,269,291–294].

The fabrication process for creating a SWNT-compliant electrode is used to demonstrate the impacts of the compliant electrode on the performance of a dielectric elastomer actuator. The carbon nanotube electrodes were selected as the base material because they enable high actuation strain performance and they are self-healinghealing, providing a robustness advantage. The fabrication process for carbon nanotube compliant electrodes heavily influences the trade-off between conductivity as a function of stretch and stiffness. Each step in the fabrication process, film *pre-stretch*, *pattern mask*, electrode *mixture*, and electrode *deposition*, plays a role in determining the completed actuator's compliant electrode properties and robustness. The film preparation allows for the pre-stretching of the film to create a pre-extended electrode that provides an enhanced conductivity stretch range. The pattern mask is key to isolating the conductive region to prevent shorts, but it also enables conductive leads that be removed from the active area, further improving robustness. The electrode mixture, in combination with the deposition technique, controls the quality and thickness of the final electrode. The following section will describe the fabrication techniques for using SWNT electrodes as compliant electrodes; however, the impacts of the fabrication process can be translated to other materials for dielectric elastomers.

2.3.2.1. Pre-Stretch

The *film pre-stretching* is a key step in the fabrication process because it shifts the operating point of the dielectric elastomer on the force-displacement curve and enables the creation of pre-extended electrodes. The film will be stretched biaxially, as shown in Figure 13, with a different stretch ratio for the axial stretch, the direction of motion of the actuator, and the lateral stretch, which is the stretch ratio that the multifunctional connectors will fix. The lateral stretch substantially impacts the strain actuation performance of the dielectric elastomer. A low lateral pre-stretch will result in high film thickness, which requires a higher voltage to operate. Part of

the Maxwell pressure will be needed to push the film laterally, decreasing the axial actuation, and the film will be susceptible to pull-in instability when actuated, which lowers the actuation strain range [46,295,296]. A large lateral pre-stretch causes the elastomer to be near the maximum stretch limit, impeding the actuator from achieving a large actuation strain because the elastomer will quickly approach the asymptotic stretch limit. An axial pre-stretch of the film before the creation of the electrode enables the fabrication of a pre-extended electrode, which improves the trade-off between electrode conductivity as a function of strain and stiffness. Pre-extended electrodes are fabricated in an extended state. Therefore, when the electrodes are later stretched during actuation, they will experience a lower strain because they were initially fabricated at a larger strain state.

The lateral pre-stretch strain, 150% strain, is chosen to provide good strain performance of the actuator over a broad range of axial loads when the actuator is released, as shown in Figure 13. Comparing the strain actuation performance between 100%, 150%, and 200% lateral pre-stretch showed that 150% showed good performance while being easy to manufacture. The axial pre-stain, 100% strain, is chosen to ensure that the electrodes are conductive throughout the entire actuation range without significantly increasing the overall stiffness. A paper scale is used to make a 1.5” x 1” box on the film that is then stretched to 3” x 2.5” onto an acrylic frame that has a 2” x 2” box cut out of the interior. The interior region eventually becomes the base of the actuator. Only the interior region of a film is used in the actuator to avoid any edge thickness variations.

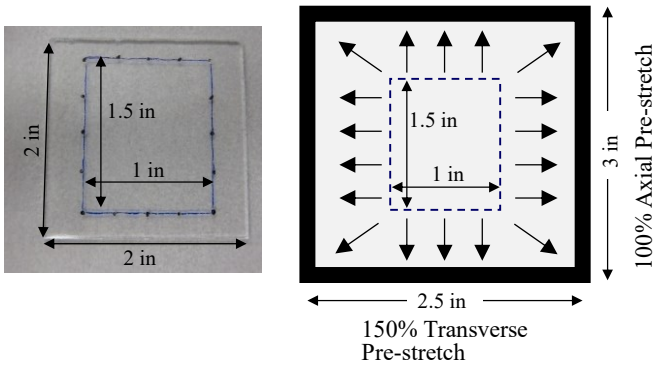

Figure 13. Film Markings for Fabrication for Pre-Stretching.

Axial and transverse pre-stretch of the elastomer film.

2.3.2.2. Pattern Mask

The pattern mask isolates the actuation regions, separates the external electrical connection from the active region, and enables electrical connections to adjacent actuators. The actuation region is isolated to the areas with an electrode on both the top and bottom surfaces, as shown in Figure 14. Controlling the active region minimizes the area prone to electrical failures and limits the required conductive material. The mask blocks the film edges from being conductive, which prevents electrical shorts across the free-side edges. The electrical tabs are the conductive regions that extend from the active region, move the external electrical connection away from the active area, and exist in both frame components. The electrical tabs minimize electrical failures in the lead and allow a transition to the stiffer external electrical connections away from the active area. Minimizing the use of additional conductive materials enhances the conformal properties of the final actuator. All the electrical tabs are also accessible from both the upper and lower face of the frames, enabling the tape actuator to be easily connected in series and parallel, enhancing the force and stroke with a larger architecture.

The masks are cut from a 0.03" polyethylene terephthalate (PET) sheet using a CO_2 laser cutter. The masks are placed on the upper and lower surfaces of the thin film, with the electrical leads on opposite sides, left and right of the top and bottom surfaces. A clean surface of PET adheres well to the stretched film and keeps the mask fixed on the film.

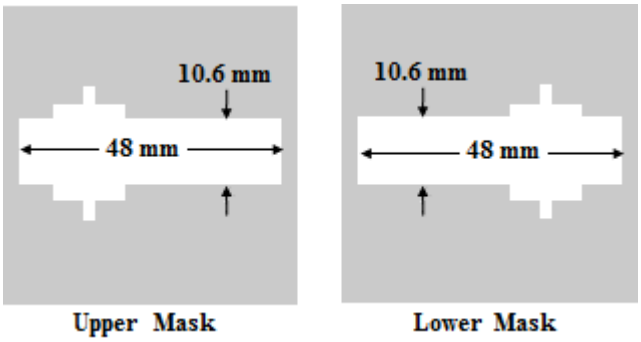

Figure 14. Electrode Spray Masks.
Upper and lower PET spray masks with electrical leads.

2.3.2.3. Mixture

A mixture of SWNT in a solvent affects the properties of the compliant electrodes, which plays an important role in the actuation capabilities of a dielectric elastomer. The important

properties are the conductivity as a function of stretch and the stiffness of the compliant electrode, which are both affected by the density and quality of the mixture. The density of the mix is defined as the SWNT mass per solvent volume. The density, along with the volume of the mixture deposited on the compliant electrode, controls the thickness of the electrode. Although the same mass of conductive material deposited can be attained with any specific combination of the ratio between density and volume, the quality of the compliant electrode will decrease if the density is too high because it is difficult to evenly distribute the conductive material on the surface of the elastomer. A low-density mixture will require a greater mixture volume to be deposited, increasing the fabrication time. A high-quality mixture, or evenly distributed SWNT in the solvent, results in an evenly distributed mat of conductive material when deposited on the surface of the elastomer. A high-quality mixture is achieved by drying out any moisture from the electrode material before it is combined with the solvent and by vigorously shaking the mixture to distribute the conductive material in the solvent fully. An evenly distributed mat will have the best conductivity as a function of stretch and the lowest stiffness, which enables the best dielectric elastomer actuation performance.

The SWNTs, Carbon Solutions P3-SWNT, are effective conductive materials and can be used with a solvent of isopropanol [54,55,269,293,294]. An effective mixture density of 1 mg/20 mL was determined from an experimental sensitivity study of the effects of electrode density on a DE actuator's performance. (See Section 3.5.2.7.) The mass of SWNT is measured by placing the vial on a scale and then measuring the mass of SWNT added to the vial. After adding the desired amount of SWNT, the vial is placed in a 50°C oven for 24 hours. After drying, the solvent is added to the vial. The mixture is placed in an ultrasonic mixer, Fisher® Scientific; 13 qt. (12.3 L) Capacity: 120 V 50/60 Hz, 4 A, 510 W, for a minimum of 8 hours to ensure good dispersion of the SWNT. After mixing, the solution looks black and has no large visible clumps.

2.3.2.4. Depositions

The deposition process, which consists of airbrushing a fixed volume of mixture onto the film's surface, affects the critical electrode material property, i.e., conductivity as a function of stretch and stiffness. The quality and thickness of the electrode are the two factors of the deposition process that affect the key compliant electrode properties. The quality of the electrode is mainly a function of the deposition process. A good process results in an even distribution of

conductive material on the film's surface, resulting in consistent conductive properties. The pressure of the airbrush, the nozzle diameter, and the spraying technique all together influence the deposition quality. These three factors need to be chosen such that the solvent evaporates quickly and does not pool on the film's surface, which would cause the SWNT to clump and not form a uniformly distributed electrode. A nonuniformly distributed electrode will negatively affect the conductivity as a function of the stretch and stiffness of the electrode. The volume of the conductive mixture deposited controls The thickness of the electrode. Too thin an electrode will have low stiffness but lose conductivity when stretched. Too thick an electrode, and the stiffness of the electrode will increase enough to limit the stretch range thereby limiting the conductivity as a function of stretch. There is an intermediate range that provides sufficient conductivity for the desired stretch range with a minimum stiffness.

The deposition of the SWNT is performed with an airbrush, Iwata Eclipse HP-CS, with a 0.35" nozzle and a supply pressure of 18 psi, which is a technique adopted from the literature [54,55,269,293,294]. A volume of 2 mL of the SWNT and solvent mixture at a density of 0.05 mg/mL is used to create a single compliant electrode as determined experimentally, as discussed in Section 3.5.2.7. the airbrush nozzle is approximately 4 cm from the film's surface for deposition. The nozzle is moved in a slow circular pattern that traces the edge of the mask. A small circle is visible when the liquid mixture hits the surface but quickly evaporates. The circle's edge should remain inside the cutout region of the mask so that most of the SWNT will land on the film surface. The spray pattern masks are removed from the film after forming the compliant electrodes for the top and bottom surfaces. A composite structure remains with two compliant electrodes on the exterior surface and the dielectric film between them.

2.3.3. Multifunctional Tape Connector Fabrication

Dielectric elastomer actuators have unique properties because they are based on elastomers that make them conformable while capable of extremely large distributed actuation strains. The mechanical and electrical connections that link the actuator's active area to the external world are critical components that enable these capabilities. These connections are combined into a multifunctional tape connector (MTC) for a dielectric elastomer tape actuator. In addition to the mechanical and electrical connections, the MTC also supports the film lateral pre-stretch and enables larger architectures with multiple actuators while still allowing the conformability of the

tape actuator. The MTC needs to be more robust than the film, maintain functionality while matching the conformability of the film, and be thin to minimize the increase in the packaging size. There is a trade-off between the conformability of the multifunctional connector and the strength and robustness of the electrical and mechanical connection, which is required to support the lateral pre-stretch. However, the materials and fabrication process of the MTC can minimize the necessary trade-off between the strong robustness functions and the level of conformability of the tape actuator. The mechanical connection can be made with either a clamping force or a chemical bond. A clamping force requires a distributed force on the surface, which requires a stiff support material to distribute the clamping pressure. This stiff support material would eliminate the conformal advantages of the actuator. A chemical bond connection is stronger than the base elastomer and can be made to match the conformal properties of the elastomer. The type of elastomer film will dictate the material selection for the electrical and mechanical connectors since they must bond with the film. The electrical connection requires different properties on the film and external sides. On the film side, the connection must be flexible and adhere well to the film while making a strong electrical connection to the compliant electrode. On the external side, the connection must make strong reusable connections while being a good conductor. These two conductive property requirements can be fulfilled by using multiple materials. The lateral pre-stretch can be supported with either a stiff support structure or an inextensible support. A stiff support structure would decrease the conformability of the actuator. A thin, inextensible material can maintain the lateral pre-stretch and, at the same time, enable conformal properties by having minimal out-of-plane stiffness. The modular properties of the actuator are supported by having electrical connections on each end of the actuator that are accessible on both the upper and lower surfaces. Multiple electrical connections enable the structure of the multifunctional tape connector to connect numerous actuators in parallel or series. The fabrication of the MTC can be separated into the subcomponents of the electrical connection, mechanical connection, and release of the actuator from the fabrication frame. Each of these components influences the final properties of the MTC.

2.3.3.1. Electrical Connections

The electrical connection makes a conductive path from the external electrical leads to the compliant electrode while having minimal impact on the conformal properties. The electrical

connection has different requirements on the film and external sides. The film side requires a permanent connection, while the external side requires a robust, reusable connection that is conductively accessible from both the top and bottom surfaces. These two roles are fulfilled by using two different materials: an electrically conductive silicone adhesive tape (3M™ XYZ-Axis Electrically Conductive Adhesive Transfer Tape 9719) and a conductive fabric tape (3M™ Fabric Tape CN-4490). The advantage of using a dual-material external electrical connection is that it creates a very strong and flexible connection at the joint with the SWNT and then gives a reusable electrical connection at the external connection site. The layout of the electrical and mechanical components that make up the MTC is shown in Figure 15. The silicone adhesive tape is placed on the electrically conductive tabs such that the edge of the tape is several millimeters (a minimum of 2 mm) from the active region and up to the edge of the windows in the flexible external support. The conductive fabric is then connected to the conductive silicone tape and the area beneath the windows in a flexible structural support. The fabric tape is conductive only on one surface, so it is folded over itself with the conductive material facing outward before placement. This folding allows a conductive path to both the upper and lower surfaces. Using two materials for the electrical connection allows selecting material properties to match the desired properties.

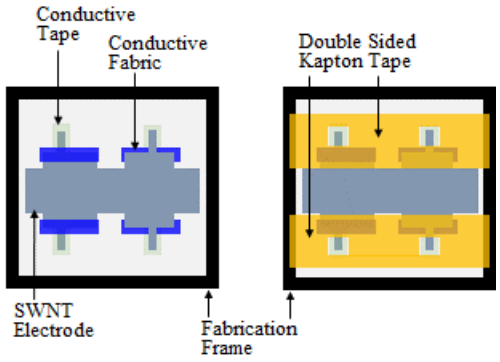

Figure 15. Fabrication of External Electrical and Mechanical Connections.

Fabrication steps of the external electrical and mechanical connections.

2.3.3.2. Mechanical Connections

The flexible external support is applied After the external electrical connections are made. The mechanical connection material needs to support the lateral pre-stretch, adhere well to the

silicone film, be flexible to maintain the conformal properties of a dielectric elastomer, adhere to external structures, and have conductive regions so that the external electrical connections can be made. The mechanical connections are made with double-sided polyimide tape, PPTDE-3, silicone adhesive, and windows cut out for the external electrical connection. The mechanical connector is created by laser cutting it from a large sheet. Four external support pieces are needed for a single tape actuator. Two connectors are sandwiched on each side of the tape actuator. They are all placed such that there is a 1-mm clearance between the edge of the connector and the compliant electrode. The electrical leads are then placed underneath the support material with the external electrical connection framed by the windows in the support material. The actuator now has two MTCs that provide external mechanical and electrical connections without sacrificing the conformal properties.

2.3.4. Actuator Release from Fabrication Frame

The final step in the manufacturing process is to release the actuator from the rigid frame. This process must be completed without damaging the edges because edge defects can propagate and cause the film to fail catastrophically. A fabric roll cutter cuts the edge in one smooth, fast motion, resulting in a clean and uniform cut. The film must also be cut out from the conductive windows to have a conductive path from the upper to the lower surface. The completed tape actuator has a typical thickness of 250 µm, as shown in Figure 16.

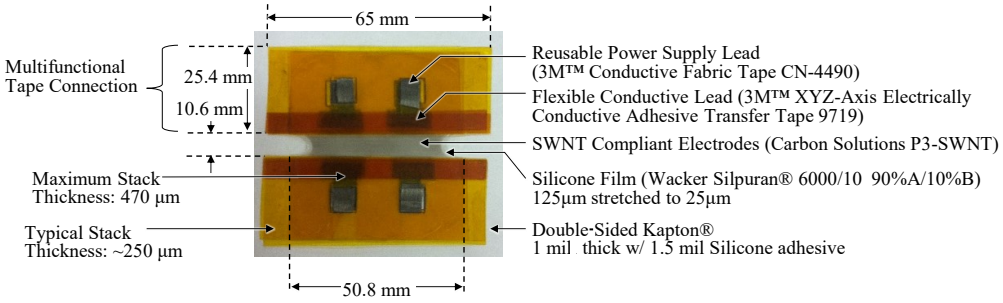

Figure 16. Completed Tape Actuator.

Tape actuator example with components and dimensions labeled.

2.4. Dielectric Elastomer Tape Actuator Conceptual Demonstration

With the new DE tape actuator architecture conceived and assembled, a helpful next step is to confirm that it exhibits the desired material and actuation properties. The DE tape actuator

should be validated in a way that highlights the critical design features that enable it to fulfill needs not currently met by other DE actuators. The advantages of the DE tape actuator architecture derive from the flexible release frame configuration and multifunctional tape connectors (MTCs). This section provides a conceptual demonstration of the new DE tape actuator architecture's properties and functionality. Key elements to be validated include the flexible release frame, which enables the actuator to conform to complex shapes, and the MTCs, which allow for compact packaging and modular scaling. While the following discussion of the various elements of the DE tape architecture is intended to confirm the material and actuation properties of the new architecture, they are strictly conceptual: this section is not intended to validate the research findings experimentally or numerically, rather it is meant to display the advantageous properties of the new architecture physically.

The DE tape actuator is a large-strain, conformal, and compact actuator. The frame configuration and the MTCs enable these capabilities. The primary benefits of the flexible release frame in combination with the dielectric elastomer film are two-fold: effective and efficient use of external force and the ability to conform to complex shapes. The flexible release frame lets the actuator directly use external force to stretch the elastomer. Using the external force as part of the elastomer pre-stretch results in an extremely effective and efficient use of external force and maximizes the work potential. Likewise, the ability to conform to complex shapes directly results from using elastomer film in conjunction with the flexible release frame. While the flexible release frame is attached to the DE at either end, along the free edges, the elastomer matches whichever shape is presented.

The multifunctional tape connectors also contribute to the conformable properties of the DE tape actuator while enabling the actuators to be compact and modularly scalable. The electrical and mechanical connections within the MFT are inherently flat since they are based on thin tape. Consequently, they enhance rather than prevent or interfere with the elastomer's conformability. Additionally, the mechanical connections adhere to complex shapes and support forces greater than the maximum strength of the elastomer film. The electrical connections easily adhere to external electrical connections and provide a transition from the film's stiffness to that of the external world. The tape supports easy electrical and mechanical connections to the external world from both sides of the actuator.

Both the active material and the frame configuration are compact, such that the length and width of the actuator are at least 50 times greater than its thickness. Therefore, stacking the actuators will have insignificant impacts on the overall actuator thickness. Similarly, the DE tape actuator's frame configuration, MTCs, and material properties allow it to be combined in series and parallel. The significant consequence of the DE tape actuator architecture's compact and modular properties is its scalability in series, parallel, and stacking.

The configuration performance can be validated with the actuation force, displacement, and work, while the MTC can be validated in a basic manner by showing that it successfully fulfills the requirements for the electrical and mechanical connections in a conformal and compact package.

The conformal and compact package properties are inherent properties of the tape actuator and are demonstrated through the repeated performance of many actuators tested over many cycles. The MTC is validated in the proof of its conformal properties and its thinness. After making over 90 actuators and testing them for tens of thousands of cycles, the MTC was robust and capable of performing without failures. Both the electrical and mechanical connections were consistent and robust. The conformal properties of the actuator are seen in Figure 17, where DE tape actuators are attached to an apple and a banana.

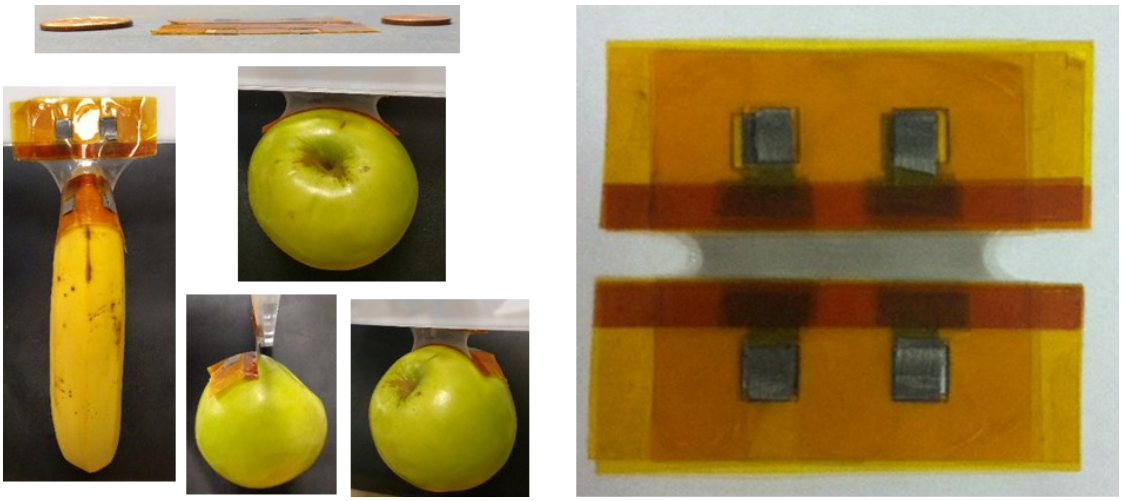

Figure 17. Demonstration of Tape Actuator Packaging Properties.

Tape actuator demonstrating conformality, compactness, and distributed properties. Thickness compared to a penny and quarter. Conformal properties demonstrated bridging flat and curved surfaces. Distributed actuation across whole surface.

The MTC is a key component of a DE tape actuator. It serves two important functions: it is responsible for electrical and mechanical connections and supports the elastomer pre-stretch. The

electrical connections for DEs are challenging because they must bridge the soft, compliant nature of the DE and the harder, stiffer external world. The electrical connection must provide an electrical connectivity to the external power supply or the electrical connections to the adjacent actuators. The quality of the mechanical connection is measured by how well the MTC can attach to the thin, highly pre-stretched elastomer film and by how well it maintains the lateral pre-stretch. The strength of the external and internal connections should be greater than the strength of the elastomer so that the actuators are not limited to anything lower than their material strengths. The properties of the MTC were experimentally demonstrated in the external work performance of a DE tape actuator. The electrical and mechanical connections were validated implicitly by serving their purposes for electrical and mechanical connections in a compact package and not failing mechanically or electrically. The mechanical connection maintained the lateral pre-stretch, did not cause rips or tears in the elastomer, supported the external loads transferred through the actuator without failure, and allowed conformality of the actuator. The electrical connections maintained conduction between the external connector and the active DE material. They did not experience any typical issues with electrical connections, including localized shorts where the electrical connection connects to the active material or loss of connectivity over time as a function of time or as the actuator is bent.

2.5. Dielectric Elastomer Tape Actuator Architecture Conclusion

Dielectric elastomers are a new smart material actuator with great potential. As the technology progresses, they will eventually be able to compete with and surpass conventional actuator technology in certain applications. Soon, however, dielectric elastomer tape actuators will find industrial adoptions in applications that require lightweight, fast, large-strain actuators that perform external work in a conformable and compact package with the ability to scale modularly, exhibit robust and repeatable action over their lifetime and offer the design quality of having predictable and controllable performance that can be easily varied to accommodate changing application needs.

Conventional actuator technology currently outperforms DE tape actuators in many existing generic applications. Dielectric elastomer tape actuators can be adopted Where conventional actuators are infeasible or extremely difficult to match due to size, packaging, or type of actuation. The near-term advantage of DE actuators is that they can perform types of actuation

that are virtually impossible for conventional technology. Tape actuators also have a flat form factor that allows them to be placed in locations not possible by other actuator technologies. The other main advantage of DEs is that they are flexible and can be used as conformal actuators. A DE tape actuator maintains the inherent benefits of elastomers while enabling easy integration as an actuator into devices. The distributed nature allows the use of the actuator for flexible actuation, where it is desirable to have no hard components. The distributed nature can also enable the removal of the support material required to distribute point actuators.

Dielectric elastomer tape actuators have shown great promise because they enable large-strain actuation. However, they have not achieved their full potential as large-strain actuators with conformal and distributed properties because the typical architectures required to achieve a large stroke use stiff frames. A DE actuator with a stiff supporting frame loses the conformability properties inherent in DEs and their thinness and compact packaging advantages. A DE tape actuator uses a released frame architecture with a silicone film, single-wall carbon nanotubes in pre-extended configuration for compliant electrodes, and a multifunctional tape connector for pre-stretch support and external electrical and mechanical connections. The multifunctional tape actuators enable the inherent conformal properties and allow large actuation stroke performance. Including the electrical connection within the MTC makes the whole actuator thin and enables performance scaling through multilayer actuators. Finally, their dimensions are inherent in the compactness, thinness, embedded electrodes, and the architecture of the multifunction tape actuator's electrical connection. These properties may also be validated if used in a multilayer tape actuator.

Chapter 3 Application Context Approach to Dielectric Elastomer Actuator Characterization

Reliable methods for characterizing actuators are crucial in developing new actuator technologies. Due to the complexity of their material and actuation properties, standard characterization procedures for smart materials often do not exist. Dielectric elastomer's research history is younger than many other smart materials, so, unsurprisingly, there is no systematic or standard experimentally characterized actuation performance.

Establishing standard characterization processes is not just important, it is crucial and necessary for comparing actuator performance across different architectures and materials. In 2015, dielectric elastomer researchers created a characterization standards guide. While it provided processes to measure and test material and electrical parameters, many of these are similar to material science tests where as many parameters as possible are fixed. These tests can result in a highly accurate measurement given all the testing conditions, but a single test point cannot accurately encapsulate the viscoelastic behavior when the parameters are known to change with the strain state. The standards guide explicitly highlights that electrical material parameters are known to change significantly. Therefore, typical material science characterization techniques cannot effectively capture all the viscoelastic actuation behavior of a dielectric elastomer actuator.

Given the absence of standards for characterizing dielectric elastomer actuators, it may be necessary to resort to a characterization process from literature, an adaptation to an existing methodology, or an entirely new characterization process to gather all relevant performance data for a targeted application. However, a more efficient approach that avoids requiring a new characterization process for every application is to identify categories of actuators in applications that demand similar actuation performance. This categorization can be achieved by grouping actuators based on their intended applications and the performance metrics they must meet.

This chapter introduces a practical and innovative system to characterize actuation performance, model it analytically, and design a process that uses similar information. The characterization of dielectric elastomer actuators can be made more straightforward by adopting

a new methodological approach: the application context. This approach includes required actuation performance metrics, the actuator's architecture, and the actuator situation, encompassing all other relevant information. This approach is not just a theoretical concept but a practical tool that can be readily applied.

A literature search into dielectric elastomer actuator characterization processes revealed a common type of cyclical actuation in many applications and research papers. Focusing on cyclical actuation can reduce the information needed to capture the actuation performance fully. Further investigation revealed a consistent and repeatable subset of steady-state cyclical actuation. The application context characterization approach is demonstrated by applying it to dielectric elastomer cyclical actuation, which is discussed in detail throughout the rest of this chapter.

This chapter's work encompasses the characterization methodology development and experimental demonstration for steady-state cyclical actuation. The fundamental behavior and characteristics of DE actuators undergoing cyclical actuation are explained, and an experimental methodology is developed to characterize the steady-state cyclical performance that captures the essential behavior. The resulting characterization methodology focuses on a DE actuator's capabilities and potentailly accelerates their adoption as potential solutions in evolving technologies.

3.1. Application Context Approach to Steady-State Cyclical Actuation Characterization

Dielectric elastomer actuators can be used in myriad applications, ranging from active weather stripping for automotive, aerospace, and buildings to prosthetics to medical research applications. Each use brings different actuation requirements, necessitating different materials and material properties to achieve the desired performance. Identifying the specific application context dictates the entire actuator design process, from material selection to characterization and validation throughout the development and design. Application context consists of three components: actuation situation, actuation requirements, and the specific dielectric elastomer actuator. Actuation situation refers to conditions that may affect actuator performance, such as environmental conditions during fabrication or actuation, factors associated with integrating the actuator into a system, frequency of actuation events (constant, continuously variable, etc.), and actuation type (one-time, rapid on-off, continual responding and varying to an external source,

etc.). Actuation requirements relate to standard basic numerical metrics for actuation, such as force, stroke, work speed, etc. Identifying the application context was the precursor to the design process activities associated with this dissertation. While the specific application context will dictate the actuator's performance requirements and, therefore, the characterization, the following characterization process can be used regardless of the application context. The process established and used here has five required components plus an optional step at the end:

1. Identify a specific application context that considers various factors ranging from the actuator materials, to actuation requirements to environmental conditions.
2. Use current state -of -the -art characterization techniques to identify any physics or performance metrics not fully captured by these techniques.
3. Develop a characterization process that captures the essential actuation data. Identify an appropriate simplification method to condense the myriad variables into one or two effective material parameters that reflect the actuation performance. A binary actuation paradigm is one possible solution to simplifying the results data.
4. Evaluate the actuator’s performance, limitations, and losses. Based on these findings, modify the actuator to improve performance and account for the losses and limitations.
5. Fully characterize the actuator's performance.

Bonus Step: Identify similar application contexts that can use the same characterization process.

These steps are briefly described below, and the remainder of this chapter provides a detailed walkthrough of the characterization and validation process used in this research. Identifying the application context is the first step in this process. As noted above, the application context encompasses the actuator situation, actuation requirements, and the specific dielectric elastomer actuator. Steady -state cyclical actuation was selected as the application context for this research because it exemplifies the type of actuation found in many industrial applications. It can be used in applications such as a pumping or flapping motion, walking, or repeated for many cycles. Expanding the application space for dielectric elastomer tape actuators requires that their performance be characterized to predict these types of motion. Repeated actuation at a steady-state simplifies the inherent complexity of the elastomer's material properties because transient viscoelastic effects will settle. Steady -state cycling is defined as maintaining the same cycle at a single frequency. Steady -state cycling is generally achieved after an initial period when cycle

variation gives way to the same cycle. The cycling for these actuation requirements can work at various frequencies, ranging from 10s Hz to slow transient creep-terminated frequencies. During steady-state cyclical actuation, the actuator switches repeatedly between two binary states where the actuator is either fully contracted or fully extended. With the proper characterization methodology, a dielectric elastomer's performance can be distilled to the minimum information needed to predict the performance for cyclical actuation, which is the identification of the fully contracted and fully extended lengths as a function of load and voltage. The advantage of distilling the characterizing method for a specific type of actuation is that one can effectively predict the actuator's performance for the kind of actuation desired while minimizing testing. Establishing that the application context is steady-state cyclic actuation leads to determining how the actuator will need to perform for this application context and to identify specific actuation properties. A thorough review of existing literature will help identify materials that will best meet actuation requirements for a particular application. For this dissertation, Silpuran was identified as a silicone elastomer material useful for large actuation strokes. This dissertation will be characterizing the DE tape architecture developed in Chapter 2.

Once the application context is defined and the actuator architecture is selected, the second step involves using first principles and current state -of -the -art characterization techniques to evaluate actuation performance and identify any physics and component interactions that are not fully characterized.

The third step consists of exploring the characterization performance in the specific application context to identify a simple characterization methodology that can mimic the behavior of the actuator for the given application context. This process consists of experimentally exploring the actuator's performance properties when used in the application context and then developing a theory on characterization methodology that will provide consistent results when used in the specific application context. For this research, experimental exploration included looking at single stretching, cyclical stretching to a fixed length, and repeated stretching to new greater lengths each time and smaller total lengths each time.

The fourth step involves validating and refining the initial methodology identified in the exploratory phase. In particular, the fabrication methods require validation, and additional testing will refine the characterization and performance parameters. This research concludes that repeated cycling causes the performance of the DE tape actuator to become consistent and

repeatable after several initial cycles. The characterization methodology used many cycles to account for initial shakedown cycles and achieve consistent and predictable performance. When the actuator is stretched to its maximum potential length and cycled a certain number of times initially, this shakedown process will minimize the impact of the Mullins effect on performance for all smaller actuator lengths, or at least make the Mullins effects insignificant on the actuator's performance.

Based on the findings of this testing, refinement, and validation, the fifth step uses the new characterization process to characterize the actuator performance for the application context. This involves changing the control variables and actuator parameters to measure the performance for the entire desired range of actuation and evaluating the limits and losses of larger architectures that use multiple modules. For this dissertation, steady-state cyclic actuation is the resulting characterization of the DE tape actuator.

An optional final step in the process is to use similarities and categorization to identify any larger family or category of actuation that encompasses the application context. If one is found, the newly developed characterization process may be used for broader applications with similar actuator requirements.

This chapter will expand on the characterization process and detail the development of the characterization methodology for the DE tape actuator architecture for the application context of steady-state cyclical actuation.

3.2. Experimental Characterization Test Setups

A significant amount of testing was performed throughout the development and validation of the characterization methodology. The various test setups are detailed below and are referred to throughout this chapter.

3.2.1. Dynamic Mechanical Analyzer Experimental Test Setup

The function of the test setup is to enforce the displacement on the DE tape actuator at a fixed rate and to control an applied voltage to the actuator while also measuring the force as a function of the inputs. The force-displacement controlled portion of the experiment is done with a dynamic mechanical machine, TA Instruments RSA3 Dynamic Mechanical Analyzer (DMA). The machine is typically designed for material testing. Custom chunks are created to place a

released frame actuator into the system. The custom chunks consist of a stiff acrylic T-shaped frame. The horizontal or top part of the T is used to hold the lateral pre-stretch of the actuator and the vertical leg of the T is used to mount the support to the DMA machine. The acrylic frame also electrically isolates the actuator from the DMA machine. (See Figure 18.)

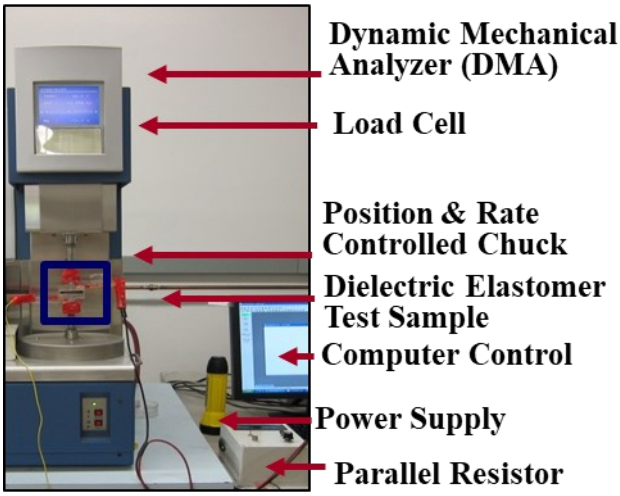

Figure 18. Actuator Characterization with DMA Machine.

Dynamic mechanical analyzer experimental test setup with a released frame actuator.

The high-voltage power supply is a custom power supply that can output a voltage of up to 5000 V. The power circuit includes a 40.1 MOhm resistor in series on the negative side of the circuit to limit the current draw in case of an electrical short in the actuator. The power supply provides a constant voltage differential to the actuator. (See test setup in Figure 19.)

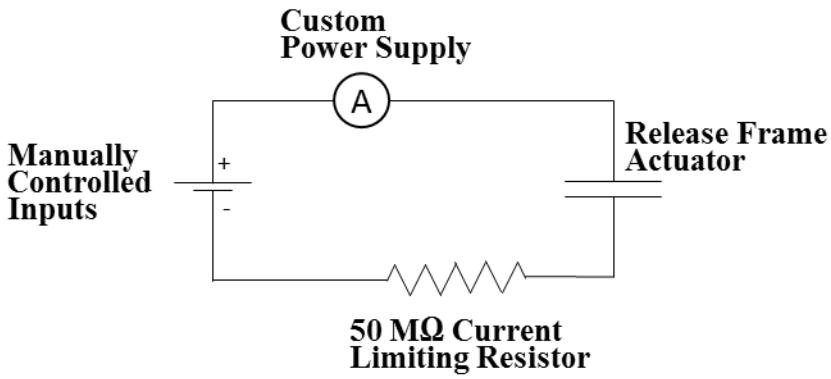

Figure 19. Electrical Schematic of Test Setup.

The voltage level is manually controlled, and on the negative terminal, there is a 50 Mega ohm resistor in series to limit current in case of an electrical short.

3.2.2. Custom Constant Force Experimental Test Setup

A custom experimental setup was created to characterize the steady-state cyclical actuation of a dielectric elastomer tape actuator. The setup was used to apply a constant force and an applied voltage while measuring the displacement of the actuator and the supplied voltage and current. The setup is shown in Figure 20. The actuator was mounted so that the lateral direction would be parallel to the mount, normal to the direction of gravity, and centered on the first pulley. The multifunctional tape connectors were aligned to make electrical contact with the electrical leads embedded in the support structure. Both electrical and mechanical connections were made by simply attaching the actuator to the support frame with finger pressure since the electrical connections were reusable tape. A calibrated mass and gravity were used to create a constant external force. A Kevlar string is routed through two low-friction pulleys attached to the external load of the actuator. The lower pulley ensured the external load was pulled directly in line with the actuator and minimized swaying. A high-voltage power source, Trek High Voltage Amplifier model 10/10B HS, applied the voltage differential to activate the tape actuator. A 30-Mohm resistor was put in series between the actuator and the electrical ground. The resister limited the current from the power supply when there was a short in the actuator, enabling the actuator to self-heal without causing severe damage. The actuator displacement was recorded with an optical encoder, US Digital B00-1000-9000 Rev B, attached to the lower pulley, which was transformed into an analog voltage with a US Digital Encoder Digital-to-Analog Converter (EDAC2). Although the encoder was capable of measuring relative displacement, it was not

capable of measuring the initial length of the actuator. Therefore, the initial length was measured optically before each experiment with a Cannon S90 camera by referencing a fixed dimension in the photo. The encoder and the high-voltage power supply were computer -controlled through a DAQ, NI USB-6341.

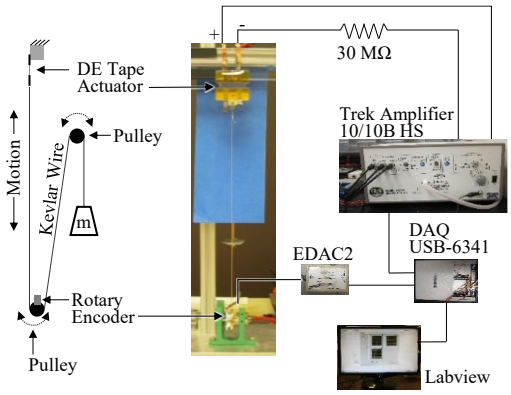

Figure 20. Experimental Setup.

Constant force force-displacement experiment setup.

3.2.3. Custom Displacement Controlled Experimental Setup

A custom force-displacement setup was created to perform a blocking force test on the dielectric elastomer tape actuators, as shown in Figure 21. The function of the setup is to enforce displacement and measure the force response while a supply voltage is applied to the actuator installed in the test fixture. The displacement of the actuator is controlled with a stepper motor, Hayden 43L4Y-2.33-015ENG, with a chopper drive, Hayden micro stepper driver DCM8055/8028, which is used to drive a low-friction slide, LPSK-100A. The motor is driven with a computer-controlled drive amplifier. The grounded side of the actuator is attached to a Honeywell load cell, AL311AP,1M,2U,4A,6E,15C; the slide, the stepper motor, and the load cell are affixed to a machined metal plate to ensure alignment of the components.

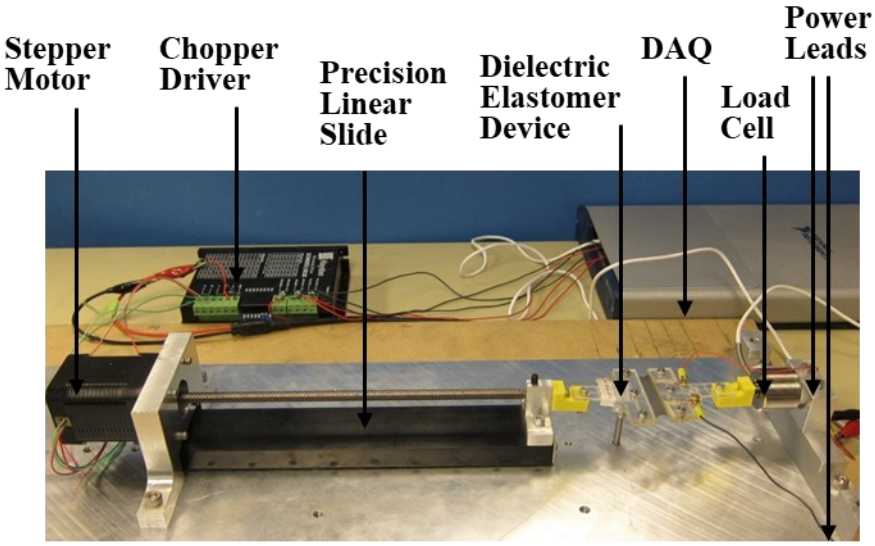

Figure 21. Automated Film Characterization Experimental Setup.

Custom test setup which using a stepper motor to contorl displacement and a load cell to meaure force controlled by a custom LabVIEW program.

A diagram of the electrical setup is shown in Figure 22. The setup uses a LabView program to control and record the experimental results. The power is supplied to the actuator by sending an electrical signal to a high-voltage Trek Amplifier 10/10B-HS. The amplifier can source and sink current, enforcing the actuator's high- and low-voltage potential. A voltage limiting resistor, 40.1 MΩ, is also in series with the actuator. This large resistance limits the current draw from the amplifier when there is an electrical short. Limiting the current allows for self-healing of the electrode around the short by burning away the electrodes locally. The limited current enables the burnoff of the electrode without enough current to heat the film and cause significant or permanent damage to it.

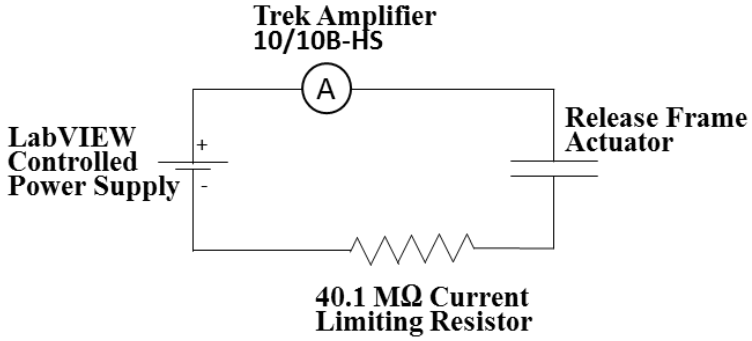

Figure 22. Circuit Diagram with Current Limiting Resistor.

Electric circuit schematic.

3.3. Experimental Exploration of Steady-State Cyclical Actuation Performance

Steady -state cyclical actuation is an important type of actuation that has many uses. It can be used in applications such as a pumping or flapping motion, walking, or repeated for many cycles. Expanding the application space for dielectric elastomers requires that their performance be characterized to predict these types of motion. Repeated actuation at a steady-state simplifies the inherent complexity of elastomers' material properties because transient viscoelastic effects will settle. During steady-state cyclical actuation, the actuator switches repeatedly between two binary states where the actuator is either fully contracted or fully extended. With the proper characterization methodology, a dielectric elastomer's performance can be distilled to the minimum information needed to predict the performance for cyclical actuation, which is the identification of the fully contracted and fully extended lengths as a function of load and voltage. The advantage of distilling the characterizing method for a specific type of actuation is that one can effectively predict the actuator's performance for the kind of actuation desired while minimizing testing.

Elastomers are challenging materials to characterize experimentally because of their large stretch, viscoelastic behavior, and complex material response in general [297]. There is an American Society for Testing and Materials (ASTM) industry standard for experimentally characterizing elastomer materials, ASTM D 1388-96. However, these methodologies are limited in capturing the important characteristics for use in DEs [298]. Many of the issues are caused by the materials moving with complex internal stresses rather than passively deforming. In 2016, the dielectric elastomer research community proposed guidelines for the characterization of generic dielectric elastomers, and the proposed standard methods work well to characterize elastomers for simple dielectric elastomer actuators and simple situations. However, they have limitations when characterizing a more complex actuation, such as steady-state cyclical actuation [297,299]. Therefore, there is a need for an experimental actuator characterization that is relevant to how a dielectric elastomer functions in cyclical operation.

The following sections will review the standard material characterization techniques and the experimental modification needed to capture the steady-state cyclical actuation. A new methodology for characterizing the steady-state cycling behavior of dielectric elastomers will be explained. The performance characteristics of dielectric elastomers undergoing cyclical actuation will be theoretically explained along with the behavior of key metrics. A methodology is

proposed to summarize the complex steady-state cycling behavior into binary actuation and present the data in the force-displacement space. Creating a new DE actuator is to enable use in industrial applications. Requirements for industrial applications include stability over a wide range of environmental conditions, including temperature, humidity, and aging. Another industry consideration is which material makes the best actuator, and that will depend strongly on the application. Industrial application of dielectric elastomers currently occurs in places where the fundamental abilities of a DE provide functionality that is very difficult or impossible for current technology. The best application takes advantage of DE actuators' inherent properties, including their large distributed actuation. There is always a trade-off between speed, force, and stroke when dealing with actuators. DE actuators always struggle with force because they are based on polymers. Their advantage lies in their ability to create fast, large-strain actuators. Therefore, the two properties that should be maximized with elastomer material are large-strain actuation and speed of actuation.

Although 3M^{TM} VHB^{TM} tapes 4905 and 4910 have been used as elastomer films that can achieve large performance, their high viscosity and large property changes with temperature make them less than ideal for industrial applications [133,300]. Searching for a material with relatively independent properties to temperature and low viscosity leads to the selection of silicone as a good candidate for the elastomer. There is active research into developing enhanced silicone materials for dielectric elastomers[113,301–306], but a commercially available elastomer material that has shown promise for DE actuators is Wacker Chemicals Silpuran 6000\10 silicone. Silpuran is a polydimethylsiloxane (PDMS) in which methyl groups are used. It is the most common type of silicone elastomer. The material combines a two-part mixture, Part A and Part B, cross-linked with high-temperature vulcanization. This study aims to evaluate the force-displacement profile of a tape actuator when it is pulled to a certain stretch length for the first time compared to when it has been cycled multiple times at the same stretch length. Elastomers have one-time viscoelastic effects known as Mullins effects. The maximum stretch is the maximum length the actuator has been extended. When a polymer is stretched, it causes the polymer chains that make up the elastomer to unwind and interact, enabling the large stretch. As the elastomers return to the unstretched state, they will again interact. As the elastomers are subsequently stretched to the same length, the polymer chains will stretch out again; however, they do not move in the same manner as the first time, which results in a stress-softened material.

The stress-softening is when the elastomer has a lower force for the same displacement than the previous time it was stretched out. The stress-softening will continue to occur over several cycles but will eventually settle into a steady-state force-displacement profile after a certain number of cycles. The number of cycles will depend on the elastomer material. Although more stress-softening may occur, it is likely small and insignificant. When an elastomer is stretched to a length greater than it has previously been stretched, the force in the new region of stretch will stiffen significantly and will match the previous first stretch to the last maximum length. If the elastomer is cycled to this new maximum length, the material will stress-soften again and settle into a steady-state force-displacement profile. This behavior is critical in evaluating dielectric elastomers because the first actuation will have a different performance level than the subsequent actuation. Most of the previous analysis with elastomers has been done with dog bone tensile specimens, so the effects of having a highly laterally pre-stretched elastomer from repeated cycling need to be understood. The hypothesis is that the highly stretched elastomer will experience the same shakedown behavior. The test is designed to help determine the number of cycles needed to achieve a repeated performance level.

The test setup uses a dynamic mechanical analysis machine to experimentally determine the force-displacement profile of a dielectric elastomer tape actuator. The DMA machine enforces a displacement and measures the force response. The machine is computer -controlled, and the displacement rate can be controlled. The stretch length and the number of cycles can also be pre-programmed into the machine to test various conditions. More details of the setup can be found in Section 3.2.1.

The test setup uses a DE tape actuator to assess the impact of the first stretch cycle compared to multiple stretch cycles at the same maximum stretch ratio. Using a tape actuator ensures that the results include the effects of compliant electrodes. The details of the fabrication process can be found in Section 2.3. The elastomer material is Silpuran 6000/10 with 50% Part A and 50 % Part B. The film is made by drop-casting 2.0 ml of a solution made of 20% by weight silicone material and 80% by weight Isopar G. After waiting for 48 hours for the Isopar G to evaporate, the films are cured at 180° on a hotplate for 2 hours. The films are then pre-stretched onto a frame with 100%transverse pre-stretch and 50%axial pre-stretch. The compliant electrodes are each made with an 8 mL solution with a density of 0.4 mg/mL of SWNT in isopropanol. The test aims to determine the force-displacement profile for the first-time stretch to

a certain maximum length and compare it to the force-displacement profile of stretching to the next maximum length on the subsequent cycle. The actuator is first stretched to 12 mm, 17 mm, 19 mm, 21 mm, 23 mm, 25 mm, 27 mm, and 29 mm.

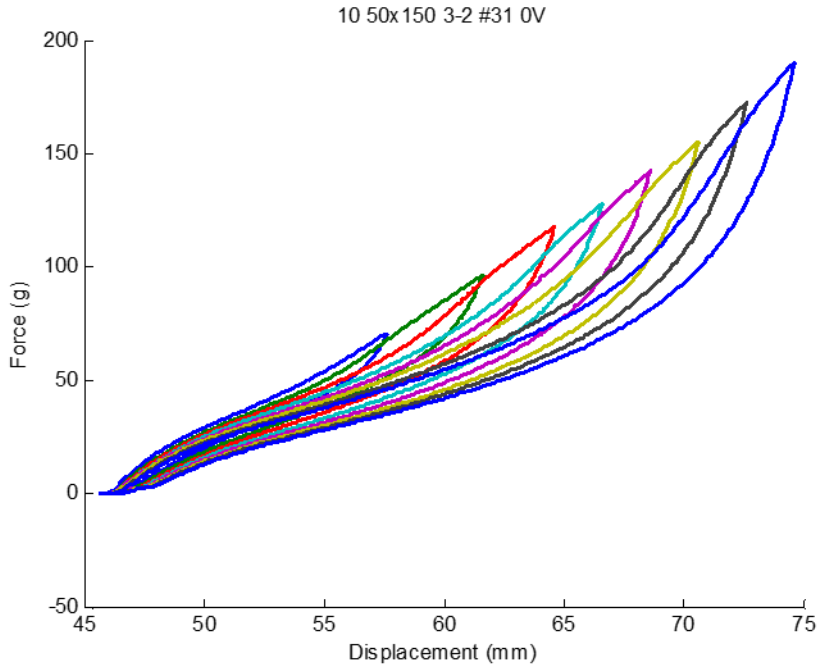

Figure 23. Repeated Pullout Characterization with Greater Displacement.
Characterized using DMA test setup.

The results from the repeated pullout tests, with each test pulled to a greater maximum distance (as shown in Figure 23), show that stress-softening occurs when an actuator is repeatedly cycled. The force for a given distance is less than or equal to the performance from the previous cycles. Once the length of the actuator passes the previous maximum length, it returns to an approximate representation of the path of a single pullout test. Linking all the highest force regions from each cycle would produce a curve approximately equal to what would exist for a single pullout test at an equivalent rate of 1 mm/s. In the lower lengths of the actuator, the pullout curves converge in their force-displacement profiles. This path convergence is because the actuator has been repeatedly cycled to these lengths, so complete stress-softening has occurred, and the actuator has come to a consistent viscoelastic response to the pullout test. It is necessary to cycle the actuator to achieve repeatable performance; otherwise, a temporary viscoelastic effect will be captured.

Inherent material properties cannot be changed with the manufacturing process; therefore, when selecting a material for the conductive electrode, the first step is to evaluate the inherent characteristics to see whether they match the final desired properties. Since the goal for a dielectric elastomer is to have a large, repeatable actuation strain, the use of carbon particles can be eliminated because they have a hard conductivity limit, and the use of carbon grease can be eliminated because, by its ability to flow, it is inherently a nonrobust material[190,220,307].

3.3.1. Determining Shakedown Cycles to Steady-State Cyclic Performance

The Mullins effect characterization consists of stretching a test sample repeatedly, after which the number of cycles to steady-state performance can be determined. The test sample is placed into the DMA and cycled five times from a fully relaxed gap length of 2 mm to 7 mm. The test is performed at a displacement rate of 0.1 mm/s, a quasi-static rate that will be validated later. The results of the experiment can be seen in Figure 24.

The testing sample is made using the fabrication process detailed in Section 2.3. The parameters used for fabricating the film are the following: The elastomer material is Silpuran 6000/10 with 50% Part A and 50% Part B. The film is made by drop-casting 2.0 ml of a solution made of 20% silicone material and 80% by weight Isopar G. The films are drop-cast with a total liquid volume of 2 ml, which results in a characteristic film thickness of approximately 100 μm. After 48 hours for the Isopar G to evaporate, the films are cured at 180° on a hotplate for 2 hours. The films are then pre-stretched onto a frame with 100%transverse pre-stretch and 50% axial pre-stretch. A sonically mixed 8-mL solution of SWNT in isopropanol, with a density of 0.4 mg/mL, is then airbrushed onto each side of the film to form the compliant electrodes. A rigid acrylic support frame is added to enable easy installation into a DMA machine.

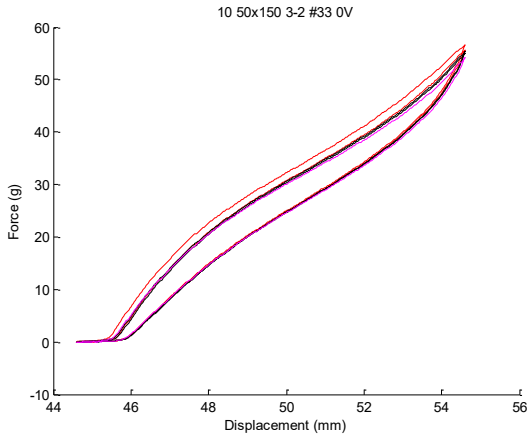

Figure 24. Typical DMA Results.

Typical force-length data from a dynamic mechanical analysis stretching the actuator for many cycles.

The characteristic data for each test consists of a loop, as seen in Figure 24. The length of the actuator at the zero force represents the stress-free state in the axial direction of the actuator. Because of the Poisson effect, the lateral pre-stretch of the elastomer causes the actuator to have an initial length smaller than the analytical zero axial stress state. During a pullout test, the loop's top half represents the elastomers' stretching, and the bottom half represents the relaxation of the actuator. The difference in the stretching and relaxing curves is due to viscoelastic effects. An initial stiff region represents the initial untangling of the elastomer's polymer chains. After approximately 1 mm of travel, the actuator starts to strain- soften, and the slope of the elastomer decreases. The decreased slope represents the middle stretch of the elastomer range. At the end of the stretch range, the elastomer starts to stiffen, which is caused by the elastomer entering the final region, where it reaches its hyperelastic limit.

The first stretch cycle is stiffer than the subsequent cycles, which are all approximately the same within 5%. Pre-stretch cycling of the elastomer two times, a shakedown, to the maximum limit of testing should be performed to eliminate one-time effects like the Mullins effects.

The second step is to start the relaxation experiment, which allows the actuator and the elastomer to come to a relaxed equilibrium before the start of the blocking force experiment. All the blocking force experiments are done at a length of an axial stretch ratio of lambda, a stretch ratio of current length over an initial length of 3, which is a 200%axial strain. Since the actuator is fabricated with an initial upstretched length of 4 mm, it is stretched to 12 mm. The actuator is moved at a rate of 10 mm/s to apply the force as quickly as possible. The actuator is then just

held at that length for 100 s to allow the relaxation of the viscoelastic forces in the elastomer. There are many different time constants in the viscoelastic forces of the Silpuran material. Several tests were executed to over 5,000 s to access the required time to come to a transient creep-terminated equilibrium, and it has been determined that at 100 seconds, the actuator has achieved 96%of the 5,000 s equilibrium position. The characteristic results for the strain relaxation test can be seen in Figure 25.

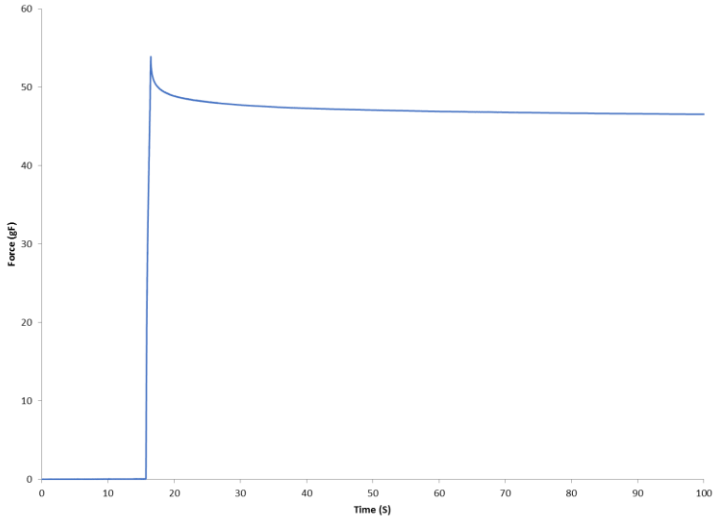

Figure 25. Relaxation Test Before Blocking Force Test.
Viscoelastice relaxation from DMA characterization setup.

3.3.2. Characterizing Viscoelastic Performance Data

Comparing viscoelastic elastomer material stiffness properties is simplified when the testing for material stiffness is done quasi-statically. A quasi-static displacement rate will have to be determined experimentally for the test sample with a DE tape actuator and has been shaken down for Mullin's effects. An added complexity to tape actuators is that they sometimes contain an active electric field. The impact of an applied electric field and Maxwell stress on the transient creep-terminated displacement rate will also be investigated.

The testing sample is made using the fabrication process detailed in Section 2.3. The parameters used for fabricating the film are the following: The elastomer material is Silpuran 6000/10, with 50% Part A and 50% Part B. The film is made by drop-casting 2.0 ml of a solution made of 20% weight silicone material and 80% by weight Isopar G. The films are drop-cast with a total liquid volume of 2 ml, which results in a characteristic film thickness of approximately

100 µm. The films are cured for 2 hours at 180° on a hotplate after 48 hours to allow the isopar G to evaporate. The films are then pre-stretched onto a frame with 100% transverse pre-stretch and 50% axial pre-stretch. A sonically mixed 8-mL solution of SWNT in isopropanol, with a density of 0.4 mg/mL, is then airbrushed onto each side of the film to form the compliant electrodes. A rigid acrylic support frame is added to enable easy installation into a DMA machine.

The experimental displacement rate study consists of cycling the test sample at two rates with no voltage applied, followed by repeated cycling at the same rates but with a voltage applied. The test sample is placed into the DMA machine and shaken down by cycling the sample two times from 2mm to 7mm. The sample is then cycled from 2 mm to 7 mm at two rates, 0.1 mm/s, and 0.01 mm/s, with no voltage applied to the actuator. The same sample is then cycled again at the same two rates but with an applied voltage of 1600 V., Both sets of the results are plotted in Figure 26.

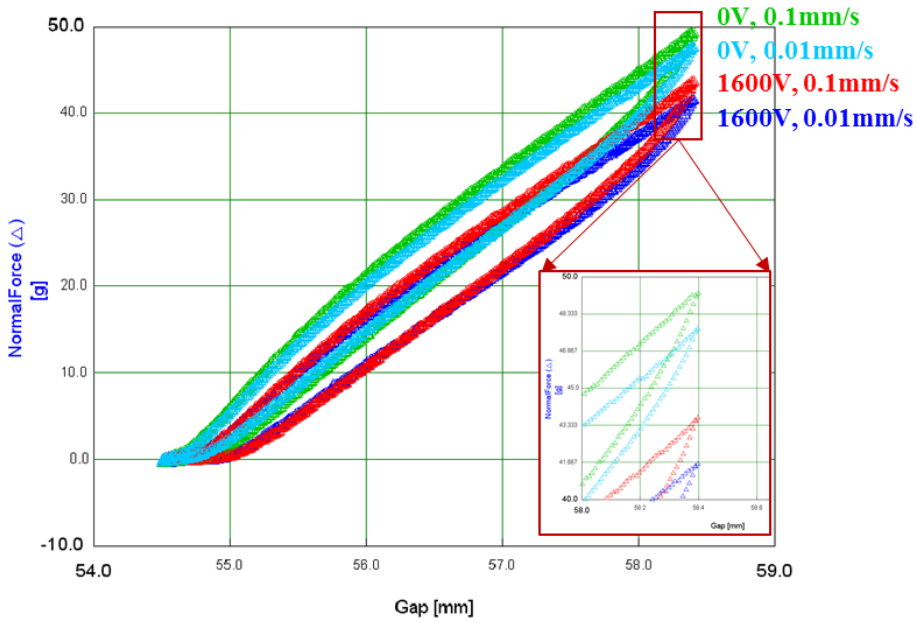

Figure 26. Pull-Out Characterization at Multiple Rates.

Pull-out testing results at 0 V and 1600 V at 0.1 mm/s and 0.01 mm/s.

The result of the pullout test is a loop with the material being stiffer on the pullout and softer on the relaxation of the sample. For a given displacement, the corresponding force level is higher for the pullout stroke than for the force level of the relaxation stroke. Comparing the force levels for the different displacement rates allows for determining the impact of the changing rate. The

slower displacement has a lower corresponding force at the maximum displacement for the two OFF voltage curves at 0.1 mm/s and 0.01 mm/s, and The higher rate displacement, 0.1 mm/s, compared to the slower displacement rate, 0.01 mm/s, results in a force that is at a maximum 3%higher. The performance difference between the two curves is very similar for the two ON voltage curves, with an ON voltage of 1600 V. For the ON voltage pulled at a rate of 0.1 mm/s, the force level at the maximum displacement is 5% greater than the ON voltage curve with a displacement of 0.01 mm/s. With an experimental result within 5%, with an order of magnitude change in displacement rate from 0.01 mm/s to 0.1 mm/s, it is then possible to use a displacement rate of 0.1 mm/s.

3.4. Develop Characterization Process and Simplify Complex Viscoelastic Performance

The typical way to characterize elastomers is to stretch them constantly and measure the stress response. The constant stretch rate is often quasi-static but can be at any relevant strain rate for elastomer characterization [308]. Material tension tests are typically done to failure, but this is unnecessary in the context of dielectric elastomer because the material becomes very stiff near the breaking point and loses the capacity to stretch farther under action. Therefore, testing must only be performed when the elastomer becomes asymptotically stiffer. The typical specimen is a thin film with a large height-to-width aspect ratio, which gives a uniaxial tension test. However, a uniaxial tension test has limited value for DE actuators because they have complex internal stress states [297,299]. The complex internal stress is caused by the need for the material to be highly pre-stretched to achieve large actuation. Another issue with stretching the elastomers a single time to get the stress-stretch behavior is that elastomers experience strain-softening when they are repeatedly stretched to the same length [309]. The strain-softening and, therefore, the stress-stretch performance curve of the elastomer is a function of how far the elastomer has been stretched and how many times the elastomer has been stretched to that distance [309]. If the elastomer is repeatedly stretched to the same length, the stretch stress curve will eventually settle and behave the same way each time [309]. If the elastomer has reached steady-state stress-stretch curves for a length equal to or greater than the current stretch length, then the elastomer will have a steady-state repeatable performance.

DE actuator performance is typically characterized by displacement or force control [298]. The current common method uses a displacement control test to determine the cyclical actuation

performance [248,250] experimentally. This method does not fully capture the transient viscoelastic behaviors when the actuator is force-controlled in applications. Missing the transient viscoelastic effects may significantly impact predicting an actuator's performance [270,310]. Although steady-state performance can be achieved with either technique, the actuator's viscoelastic complexities will be better captured with the force control method.

Dielectric elastomers are complex materials, and their large stretch and use of surface Maxwell stress for actuation make the definitions of their dimensions important. The "length" of a dielectric elastomer tape actuator is the distance between the two multifunctional tape connectors. The terminology "length" is typically used for the initial characterizing of the actuators because experiments usually measure the actuator length versus time and voltage versus time. Actuators are typically defined in terms of force versus displacement. Therefore, when the tape actuator performance is discussed, the length will be described as the displacement. “length” and “displacement” are synonymous with dielectric elastomers. The term “displacement” for dielectric elastomers includes initial unstretched length so that the displacement is nonzero at zero applied force on a force-versus-deflection graph. Another important term to define is the "stroke" of the DE tape actuator. The "stroke" is the change in displacement due to the change in applied voltage.

3.4.1. Characterizing Steady-State Cyclical Actuation

Steady-state cyclical actuation for a Dielectric Elastomer (DE) actuator is defined as consistent actuation at a constant frequency long enough to conclude transient macro viscoelastic effects. This means each cycle has the same as the previous and following ones. The steady-state condition indicates that the measured performance from cyclical actuation will remain constant for a given set of inputs. Initially, when dielectric elastomers undergo cyclical actuation, their performance varies due to the material transitioning from a non-actuating to an actuating state—This performance shift results from the viscoelastic properties of the elastomer.

3.4.1.1. Characterization Process for Steady-State Cyclical Actuation

In the literature on dielectric elastomer actuators, the author could not identify a generally applicable characterization process for the steady-state cyclical actuation for pure shear or strip frame configuration actuators. The following experimental investigations led to the developing

of a new general characterization process for shear actuators that effectively captures the critical behaviors during steady-state cycling. The definition of steady-state cycling from the previous section requires that the characterization process specify the following inputs: external load, desired LOW and HIGH voltage differentials, cycling frequency, duty cycle, and the rates for energizing and de-energizing the actuator.

After cycling begins with constant input variables and parameters, the actuator will eventually achieve a steady-state where all cycles are identical. The onset of steady-state cyclical actuation can be identified either by the elapsed time from the start of the test or by the number of cycles needed to reach a steady-state condition after the start. Either measure can be used because their relationship remains constant due to the constant frequency. This dissertation will use the number of cycles for comparison purposes, as this non-dimensional measure simplifies comparisons across different frequencies.

A diagram of characteristic inputs and outputs of a dielectric elastomer undergoing cyclical actuation under a constant external force is shown in Figure 27. The figure shows the system's electrical inputs on the top and the measured mechanical outputs on the bottom as a function of time. At time zero, the electrical input starts at an applied voltage in a LOW state, while the mechanical output begins at an initial length, L_o, from a constant external force and the LOW voltage differential. The input voltage difference across the dielectric elastomer film then alternates between the LOW, V^L, and HIGH, V^H, states as a function of time. This voltage differential between the LOW and HIGH states, ΔV, creates an electric field that increases the stress on the elastomer, the maxwell stress. The increased stress causes the elastomer to lengthen, as shown in the bottom half of the figure.

In this example, the voltage switches at a fixed frequency with a square wave and a 50%duty cycle. In the actuator displacement chart, the end of each half-cycle input at LOW and HIGH voltages are marked with a circle and a triangle, respectively. As the actuator is initially cycled, the length of the actuator at the end of each half-cycle is longer than the previous cycle. The length of the actuator at the end of each HIGH voltage input, triangles, increases on each cycle until the third cycle, where its length is repeated on the next cycle. The actuator length of the LOW voltage input also increases until the third cycle. The actuator has reached steady-state cyclical actuation in the third cycle since every subsequent cycle has the same displacement at the end of each LOW, circle, and HIGH triangle voltage input.

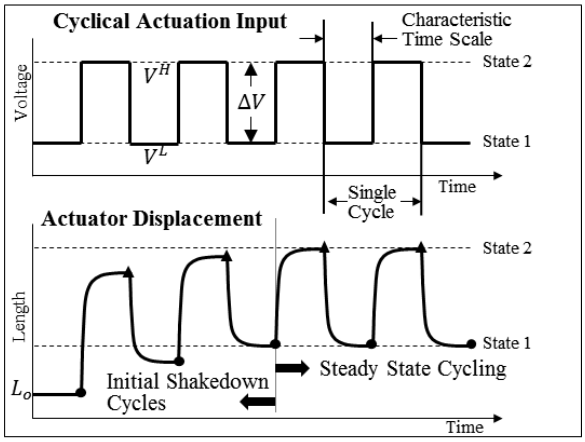

Figure 27. Typical Plots of Voltage and Length Versus Time.

Typical electrical inputs into a dielectric elastomer for steady-state cyclical actuation and the corresponding mechanical outputs for the dielectric actuation.

The number of cycles needed to reach steady-state cyclical actuation depends on the materials, initial conditions, and inputs. The steady-state length at the end of each LOW and HIGH voltage input also depends on the inputs. The example shown in Figure 27 has a frequency such that each switch in voltage allows the length to reach a maximum since the transient creep has ended. A higher frequency would result in lower actuator displacement lengths, while a lower frequency would yield the same nominal performance. The transient creep-terminated displacement is an important metric because it is the longest actuator length achievable, resulting in the largest actuation stroke.

This steady-state cyclical test can be repeated with the same LOW voltage, V_o^L, and a different HIGH voltage level, V_2^H, resulting in similar behavior, as shown in Figure 28. The actuator increases in length over the first few cycles and eventually reaches steady-state behavior. The same characteristic time-length curve results in the transient creep behavior ending in each cycle even though the actuator is increasing in length. With the HIGH state, V_2^H, now larger than the original HIGH state, V_1^H, the actuator increases in length for the HIGH state, as expected. Even though the actuator sees the same LOW voltage state during both tests, the actuator with the higher voltage state has a longer length for the LOW voltage state. Again, the changes in performance levels are caused by viscoelasticity in the elastomer.

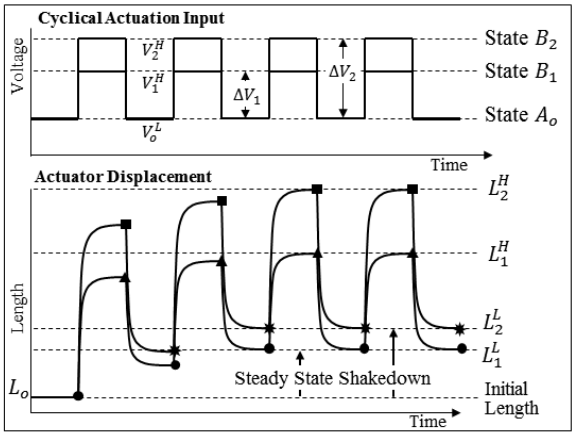

Figure 28. Time Plots Showing the Input Voltages and Actuator Lengths.

Cyclical performance for multiple voltage levels.

3.4.1.2. Using a Binary Actuator Paradigm to Simplify Viscoelastic Actuation Performance

There are many ways to analyze the performance of a dielectric elastomer, but the best method will depend on the application and how the information will be used. The DE tape actuators are intended for doing external work for an application that requires an actuator. Work is a function of the force and the displacement. Therefore, the best way to present the data would be in the force-displacement space. The cyclical length data in Figure 28 can be simplified by representing only the steady-state LOW and HIGH states for a given voltage. These two states can be graphed in a force-displacement space, as shown in Figure 29. The force is constant, as shown, while the length of the two states, LOW, L_1^L, and HIGH, L_1^H, are plotted. When the steady-state cyclical test is repeated at different force levels with the same LOW and HIGH voltage levels, the HIGH and LOW lengths will create a continuous curve. These LOW and HIGH states are represented by blue and red curves, respectively. The LOW voltage curve (in blue) resembles a typical hyperelastic material curve. It has an initially stiff region, after which its strain-softens and the actuator's stiffness decreases. As the actuator is farther stretched, the elastomer approaches its hyperelastic limit and stiffens. The HIGH voltage curve (in red) has the same appearance; however, the curve is shifted to the right, representing the additional displacement caused by the higher voltage.

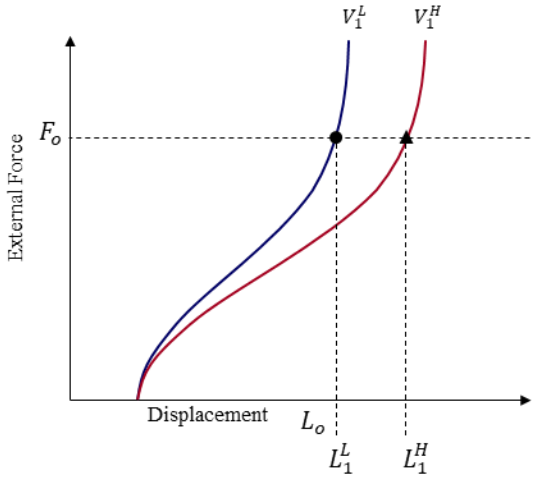

Figure 29. Tape Actuator Plot in Force – Displacement Space.

Plot summarized steady-state cyclical performance as binary LOW and HIGH lengths in a force-displacement graph for a given voltage.

This same force-displacement graph can also represent the data at multiple voltages. The result is a family of curves representing the steady-state cyclical behavior in a single graph, as shown in Figure 30 below.

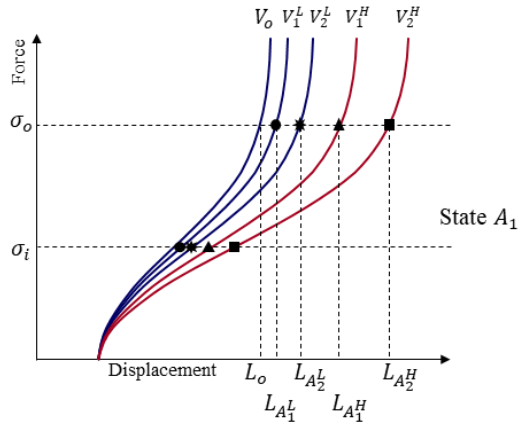

Figure 30. Tape Actuator Performance Plot at Multiple Voltage Levels.

Summarized steady-state cyclical performance as binary LOW and HIGH lengths in a force-displacement graph at multiple voltages.

The summarized data in the force-displacement curves make it easy to predict the actuator's performance for a given force and voltage.

3.4.2. Quasi-Static Actuator Performance Representing Steady-State Cyclical Actuation

A simple way to summarize the actuation performance of a DE tape actuator undergoing steady-state cyclical actuation is to present it visually as a force-displacement graph, per the methodology described in Section 3.4.1.1. The steady-state cyclical experimental characterization procedure of Section 3.4.1.2 is used to produce the characterization data needed to summarize the actuation performance for a fixed voltage.

The summarized characterization data are shown in Figure 31. The graph shows the performance data for forces from 10 gf to 50 gf at LOW (voltage OFF) and HIGH (voltage ON) voltage levels of 0 V and 2300 V, respectively. The experimental data are displayed as pink circles with a best-fit cubic spline fitted to the data. Both the OFF and ON performance curves display the typical hyperelastic material characteristics with an initial stiff region, followed by a strain-softened plateau, and finally stiffening when approaching the hyperelastic limit. The OFF and ON voltage curves are generally similar, except that the ON curve is shifted to the right. At low loads, the ON voltage curve has shifted less from the OFF curve than in the middle region. This larger shift is caused by having a fixed voltage, which results in a higher electric field in the middle region. The higher electric field is due to a thinner film caused by the higher stretch resulting from the high external force. At larger displacements, after the middle region, the ON voltage curve increases stiffness faster than the OFF voltage curve, causing the ON voltage curve to shift less to the right at higher loads. Although the electric field is higher at larger loads, the elastomer stiffening counteracts the additional Maxwell stress. Therefore, even with a larger electric field, the actuator cannot stretch as far as when the elastomer is in the middle region where the slope of the curves is relatively constant.

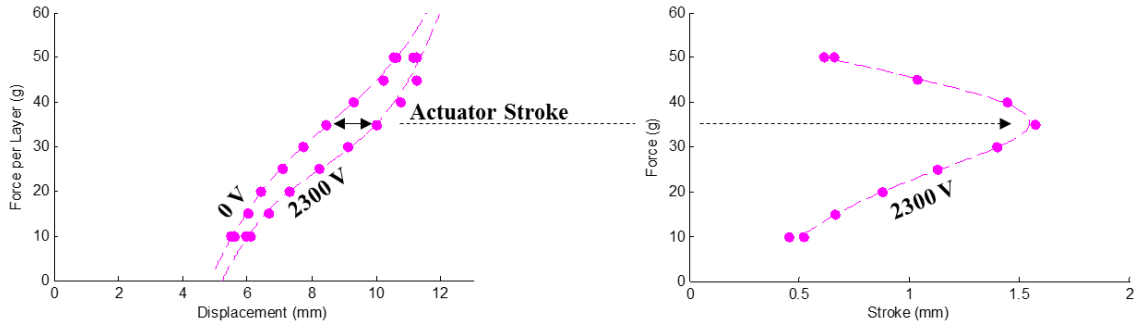

Figure 31. Force-Displacement and Force-Stroke Plots.

Summarized steady-state cyclical performance in force-displacement and force-stroke of actuator space at 2300 V.

The data can be replotted as the force-stroke to simplify the results further, as shown in Figure 31. The stroke is the relative displacement between the OFF and ON curves. The force-stroke data look approximately like a parabola rotated 90° counterclockwise. The stroke starts low at small loads and increases approximately linearly until it reaches a maximum value and then decreases until the maximum load is reached. With a peak stroke location, there is now an optimal location for the design and use of the actuator when a large stroke is required. Because a larger stroke is a key component of the successful application of a dielectric elastomer, the peak of the curve indicates the optimal load that should be used in its design.

Another way that the data can be analyzed is to present it in the force-work space, as shown in Figure 32. The work is the force times the stroke and represents the amount of external work the actuator can perform. The curve is very similar to the force-stroke curve, where the work starts small at low loads and then increases to a peak, after which the work decreases. One significant difference is that the peak work location occurs at a higher external force than the peak stroke, 35 gf versus 40 gf. Therefore, a trade-off exists between a larger stroke and performing more external work.

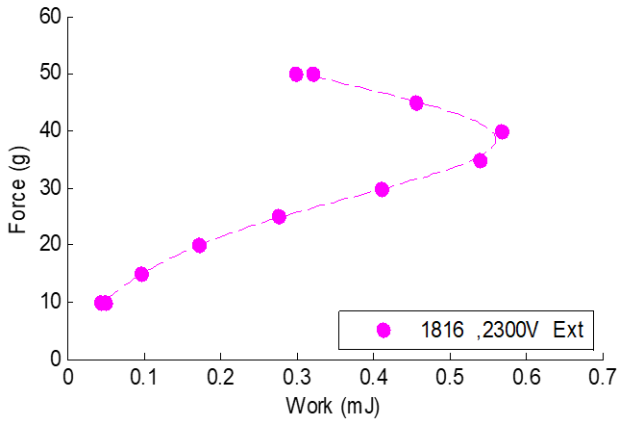

Figure 32. Force-Work Performance Plot.

Steady-state cyclical tape actuator binary performance in the force-work space.

These performance results demonstrate the ability of DE tape actuators to do external work, and they show the large actuation stroke that can be achieved. Although a single DE tape actuator can perform a large stroke, it is limited by how much work it can perform because DE actuators' actuation is inherently based on a compliant elastomer.

3.5. Steady-State Cyclical Actuator Characterization, Validation, and Actuation Performance

When developing new technology that requires material and actuator component fabrication, basic validation tests are needed to ensure that the resulting product meets expectations and that the fabrication process yields consistent results. Although previous studies using spot actuators have shown the usefulness of Silpuran as a possible elastomer with the potential for dielectric elastomers, there is still a need to analyze the material in a released frame architecture further because the complex strain state can impact the performance [133,216,311]. It is necessary to examine the drop-casting process to evaluate the ability to fabricate consistently thin films to ensure repeatability and accuracy. The drop-casting process is an integral component of creating custom thin, soft films; therefore, an experiment is needed to analyze the thickness consistency of a single film and the consistency of film thicknesses across a batch of individual films. The compliant electrode fabrication process is another critical step that must be evaluated to ensure consistency and performance. After evaluating the film thickness and compliant electrodes, the performance variability of the entire actuator is measured when the cross-link density in the elastomer changes when characterized in a rigid released frame configuration. This study

analyzes the macro influences of the cross-linking density on the actuator's mechanical and electrical properties and actuation performance. Creating an effective and reliable DE tape actuator involves many fabrication parameters for the film and electrodes. Understanding these parameters and their relative impact on the function of the actuator will assist in determining how to maximize actuator performance. The sensitivity of the following parameters will be evaluated. Parameters impacting elastomer cross-linking density include static and dynamic mechanical material properties and dielectric permittivity. Also assessed will be the sensitivity of the DE tape actuator performance to the following parameters: elastomer cross-linking density, film curing temperature, and electrode density. Finally, the DE tape actuator performance properties in steady-state cyclic actuation will be characterized to facilitate maximum performance. The following DE tape actuator performance properties will be characterized: electric field breakdown strength, current leakage, actuator performance with SWNT self-healing electrodes, and the performance from pre-extended electrodes. These validation tests are detailed below, and a summary of the results is included at the end of this section.

3.5.1. Fabrication Processes Validation

When investigating technology that requires new or unvalidated fabrication techniques, it is critical to ascertain the reliability of the fabrication processes and ensure that the fabricated prototype has very similar properties. In future experimental studies, it will be known that any change in performance is caused by a purposeful shift in a variable or parameter and not the variability of the fabrication process. For DE actuators the two key components that control a DE actuator's performance are the elastomer film and the compliant electrode. Therefore, the repeatability and accuracy of the fabrication of these two components must be evaluated.

3.5.1.1. Uniformity of Elastomer Film Thickness

Film thickness is important because dielectric elastomers function as capacitors with a charge separated by the film to create an electric field. The region of the film with the lowest thickness will have the highest electric field. The area with the highest electric field will likely be the first to fail and represents total failure. The DE tape actuator fabrication process uses drop-casting to create the thin custom film. It is, therefore, necessary to measure the film thickness and validate that the drop-cast films have a consistent thickness. For the elastomer film, thickness consistency is defined in two manners. One definition is the consistency of thickness in the film thickness uniformity across a single film. A second definition is the repeatability of the fabrication process to create consistent thickness films across a batch of films. The thickness uniformity is experimentally validated by measuring an array of points across a single film and comparing the thickness measurements. After validation of the thickness uniformity, the batch thickness consistency is experimentally studied by measuring the thickness of a set of samples. The thin films'' thickness and consistency are vital to DE tape actuators' performance.

Table 1. Film Fabrication Parameters for Film Uniformity Study.

The following parameters were used to create all the samples for the film uniformity studies.

Film Parameters	**Solvent Mixture**					
	Material Preparation			**Drop Cast**		
Silpuran ID	**% Silicone in Isopar G**	**Part A (%)**	**Part B (%)**	**Area (in^2)**	**Volume (ml)**	**Evaporation (Hr)**
6000/10	80	10	90	4	2	48

Film Preparation				**Each Electrode**	
Curing		**Film Pre-Stretch**		**SWNT & Isopropanol**	
Temp (°)	**Time (Hr)**	**Axial (%)**	**Transverse (%)**	**Volume (mL)**	**Density (mg/mL)**
180	2	50	100	NA	NA

Measuring the film's thickness after being removed from the glass fabrication substrate is difficult because the film is easily stretched and hard to handle. Therefore, the film is measured indirectly in two steps. The first measurement measures a stack's glass substrate, film, and mask. After removing the film from the glass substrate, a second measurement is taken at the same location with only the glass substrate and the mask. The film thickness is then the difference between these two measurements. A Mitutoyo 293-349 micrometer is used for the thickness measurements.

Measuring a thin and soft film is challenging; special care is needed when measuring through contact. The thickness measurement is taken by placing the film and substrate vertically and tightening the micrometers until they barely touch the surface; the micrometers are then used to lift the stack of components. If there is insufficient pressure, the stack of components will not move. With the lightest pressure, the stacked components rotate around the micrometers. If the pressure is too great, the sample is lifted without rotation. This technique enables the measurement of the thickness of the stack without compressing the soft, thin film.

A study of the thickness uniformity of the drop-cast films is performed to verify that high-quality uniform-thickness films are being created. Table 1 contains the elastomer film fabrication parameters. The surface of the 2" by 2" glass slides and the film is divided into a grid pattern of five across and five down, which results in 25 possible measurement locations. The perimeter thickness measurements are ignored due to edge variations caused by the drop-casting process. The edges are not included in the final DE actuator. The 13 measurement locations are highlighted in pink in Figure 33 and labeled 3, 7, 8, 9, 11, 12, 13, 14, 15, 17, 18, 19, and 23.

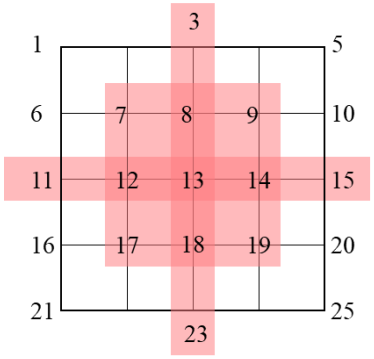

Figure 33. Film Thickness Measurement Locations.

Location for measurements on films while on glass fabrication substrate.

The experimental process consists of five rounds of measurement of the thickness of the film. Each location is measured once in a single pass with the thickness recorded. After all measurements are taken in a single round, the process is repeated four times for five independent measurements at each location. Between each measurement round, the micrometer's zero gap length is verified to correspond to zero. The film is removed from the glass substrate after the five rounds of thickness measurement. The removed film can then be used to fabricate a dielectric elastomer actuator. After removing the slide, the thicknesses are measured. The mask

and the glass substrate are easy to measure accurately because they are relatively incompressible. The full results of these measurements can be seen in Figure 34.

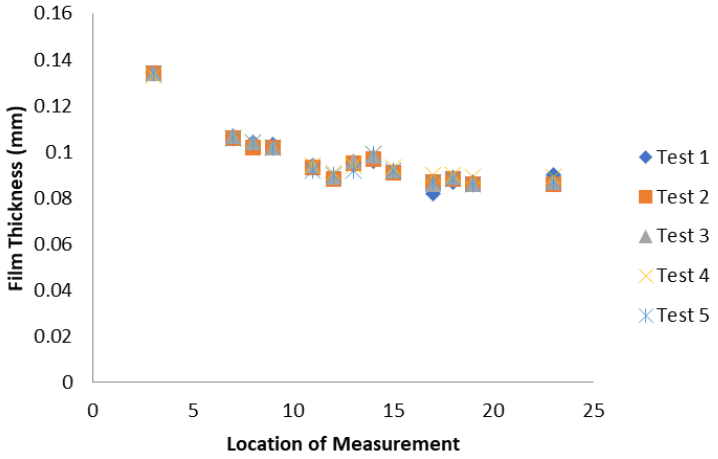

Figure 34. Film Thickness Consistency Comparison.
Consistency of film thickness across samples.

The total stack thickness measurements by location vary from 0.134 mm to 0.087 mm. The spread in the measurements is much larger than in the individual repeated measurements at each location, as shown in Figure 34. The maximum spread in the individual measurement is 4 µm. The average standard deviation at each measurement location is 1 µm. There is a strong trend of the thickness decreasing as a function of the distance from the top; this change in thickness results from the surface used in the evaporation stage not being level. There is no apparent unevenness in the horizontal direction. Replotting the thickness data for the middle nine points as a function of the distance from the top shows the variation in the thickness from not being perfectly level. (See Figure 35.)

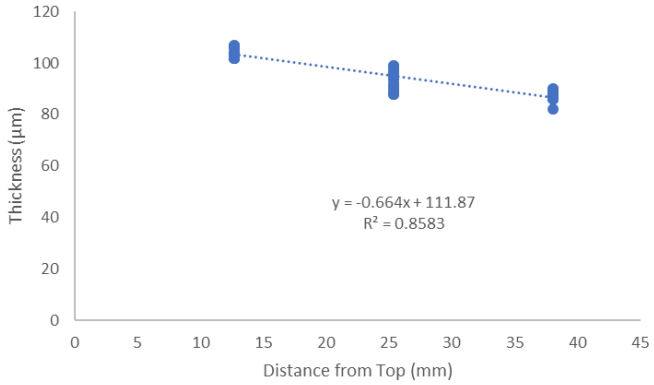

Figure 35. Film Thickness as a Function of Thickness.

Film Thickness as a function of the distance from the top of the sample.

The average thickness and the standard deviation as a function of the distance from the top are 104 μm and 2 μm, 94 μm and 3 μm, and 87 μm and 2 μm. The change in thickness as a function of location is greater than the standard deviation of the measurements at a single distance. A linear regression of the data provides a slope of change in the thickness of $-0.664\ \mu m/mm$. Using this slope and the height of a DE tape actuator, it is possible to determine the maximum variation caused by the uneven surface. The height, 5.3333 mm, times the slope is 3.8 μm. The impact of this thickness variation is that the electric field will vary. One way to analyze the importance of this variation in the thickness is to evaluate the effect on the actuator's actuation authority caused by the electric field's Maxwell pressure. The change in thickness from the center will then be half the thickness change due to unevenness, which is 1.9 μm. The 1.9 μm is equal to a 45 V difference if a 2300 V is applied to actuate a DE actuator. Because the force of actuation is related to the voltage squared, this results in a maximum of 4%change in the actuation authority. In summary, the drop-casting technique can produce a high-quality film with relatively uniform thickness.

3.5.1.2. Batch Consistency of Elastomer Film Thickness

The batch film thickness consistency was studied by measuring the thickness of a batch of nine films cast simultaneously; see Table 1 for actuator fabrication parameters. Each film's thickness was measured at nine locations to validate the thickness uniformity fully. In F, the locations are labeled as 7, 8, 9, 12, 13, 14, 17, 18, and 19. The measurement technique used for

the thickness is the contact measurement process described in Section 3.1.1. The results of the measurement are shown in Figure 36.

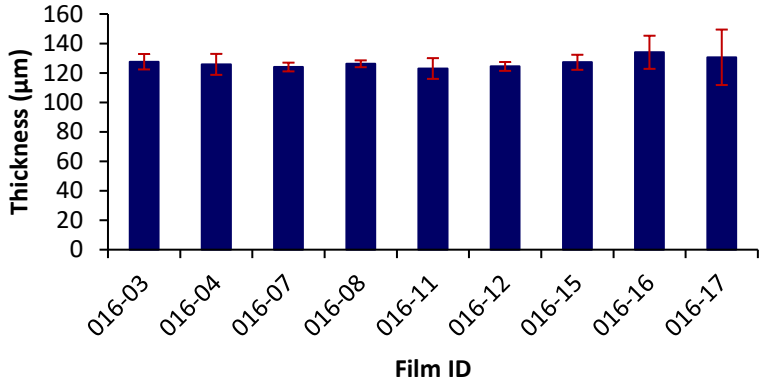

Figure 36. Film Thickness with Standard Deviation.

Average thickness of all measurement points and standard deviation for nine film samples from one batch.

From the volume control drop-cast process, the standard deviation in the thickness was calculated to be less than 4% of the average film thickness to assess the uniformity of the elastomer film thickness. The standard deviation of the thickness across the batch of nine films is calculated to be 1.1% of the mean film thickness. The result is a high-quality film that can create a reliable actuator with a potentially long life. Creating films with equal thickness is key to having the performance scale as they are used in larger architectures.

3.5.1.3. Repeatability of Compliant Electrode Fabrication

Repeatable and reliable performance is a requirement for any technology to advance. The main purpose of the compliant electrode is to conduct the differential voltage charge across the whole surface of the DE tape actuator without adding stiffness to the actuator. SWNT mats have been shown to have the necessary properties to be good compliant electrodes; however, there is currently no standard procedure for creating high-quality compliant electrodes. The density of the compliant electrode is controlled by the volume of the SWNT solution sprayed on the surface of the masked film, the pressure of the airbrush spray, and the spraying technique. Measuring the conductivity of the fabricated electrodes is one method to validate the fabrication process. See Table 2 for actuator fabrication parameters. These measurements enable the evaluation of the repeatability of the electrode fabrication process.

Table 2. Film Fabrication Parameters for Electrode Repeatability Study.

The following parameters were used to create all the samples for the electrode repeatability study.

Actuator Parameters	Solvent Mixture					
	Material Preparation			Drop-Cast		
Silpuran ID	% Silicone in Isopar G	Part A (%)	Part B (%)	Area (in^2)	Volume (ml)	Evaporation (Hr)
6000/10	80	10	90	4	2	48

Film Preparation				Each Electrode	
Curing		Film Pre-Stretch		SWNT and Isopropanol	
Temp (°)	Time (Hr)	Axial (%)	Transverse (%)	Volume (mL)	Density (mg/mL)
180	2	50	100	4.0	0.4

The conductivity of both compliant electrodes and the capacitance of the actuator is measured during the fabrication process. The resistance measurement is taken after the multifunctional tape connectors are assembled on the actuators and before the actuator is released from the frame. A DE tape actuator has two electrical leads embedded in the multifunctional tape connectors for each compliant electrode. These electrodes provide a simple and repeatable location to measure the resistance and capacitance across the actuator. A FLUKE 287 multimeter is used to measure the resistance of the compliant electrode on both film surfaces. The capacitance of the actuators is measured using an AMPROBE LCR55A. The results of characterizing the electrode are shown in Table 3.

Table 3. Capacitance and Electrode Resistance Characterization Results.

A series of 18 films were fabricated and characterized for their capacitance and electrode resistance.

	Mean	σ	σ/Mean × 100
Capacitance (pF)	524	15	2.8 %
Upper Electrode Resistance (KΩ)	2.85	1.04	36.4 %
Upper Electrode Resistance (KΩ)	7.11	3.05	42.9 %

The measurement of the capacitance of the actuator indicates that the electrode is forming an acceptable conductive mat. The low variation in the standard deviation, 2.8%indicates the consistency of the thickness of the film. The mean electrode resistance measurements for the two sides vary by 150% from 2.85 kΩ for the upper electrode to 7.11 kΩ for the lower electrode. The

percent error of the standard deviation to the mean for the upper and lower surfaces is within 7 percent from 36%to 43%In the broader context of compliant electrodes for a dielectric elastomer, the consistency of the electrodes ensures conductivity with low enough impedance that the resistance does not slow down the actuation. The RC time constant for the capacitor is 4 microseconds. The short-time constant means that the variation in conductivity will not detrimentally slow the speed of the actuation.

3.5.2. Performance Sensitivity to Architecture Parameters During Steady-State Cyclical Actuation

Creating a DE actuator requires many fabrication parameters for the film and electrodes. Understanding a DE actuator's performance sensitivity to key fabrication parameters is important for reliable performance. The key elastomer fabrication parameters are the cross-linking density and the curing temperature. Walker Chemical specifies certain material properties when the silicone parts are combined equally, and a film is cured within a specified temperature range. The actuation performance and performance sensitivity to variations in these fabrication parameters must be characterized to ensure that the best DE actuator performance is achieved for the desired actuator context. The density of the electrode material in isopropanol solution and the volume of the mixture used for each electrode control the electrode's properties and characteristics. Characterizing the sensitivity of a DE actuator's performance relative to the compliant electrode fabrication parameters must be understood to create the best compliant electrode.

3.5.2.1. Static Mechanical Properties Sensitivity to Elastomer Cross-Link Density

The actuation performance of a dielectric elastomer tape actuator is highly dependent on the thin elastomer film's material properties. The film's material properties depend on the type of polymer material, the fabrication process, and the strain state. The greatest effects on the properties come from the kind of polymer and the cross-link density. Cross-links are the chemical links that connect two adjacent polymer chains. The cross-link density controls the interaction of the long polymer chains and gives an elastomer film its fundamental mechanical properties. The chemical cross-links are formed in the film fabrication process and can be controlled by varying the number of chemical cross-linkers within one of the chemical parts of the raw silicone.

The following three studies experimentally characterize the sensitivity of material properties concerning the density of cross-links and evaluate the impacts on DE actuation performance.

The material properties are the mechanical static and dynamic properties and the electrical material properties. For each study, three cross-linked densities are explored: 50% Part A and 50% Part B, 30% Part A and 70% Part B, and 10% Part A and 90% Part B. See Table 4 for the actuator fabrication parameters. The results of these studies identify the tailorable and adjustable material properties range of a tape actuator made with Silpuran 6000/10 A/B.

The appropriate material and actuator properties are determined by directly testing DE actuators. The experimental characterization procedure for determining the mechanical material properties is a multistep process that includes an initial shakedown, a mechanical characterization, and a combined electrical and mechanical characterization. The initial shakedown eliminates one-time effects, such as the Mullins effects. The actuators are characterized in both the OFF and ON voltage states to capture passive material properties compared to the ON voltage properties.

Table 4. Film Fabrication Parameters for The Cross-Link Density Film Studies.

The same fabrication parameters were used to create all the samples for the study except for changing the density of the cross-linking in the films by varying the proportion of Silpuran Parts A and B.

Actuator Parameters	**Solvent Mixture**					
	Material Preparation			**Drop-Cast**		
Silpuran ID	**% Silicone in Isopar G**	**Part A (%)**	**Part B (%)**	**Area (in^2)**	**Volume (ml)**	**Evaporation (Hr)**
6000/10	80	50, 30, 10	50, 70, 90	4	2	48

Film Preparation				**Each Electrode**	
Curing		**Film Pre-Stretch**		**SWNT & Isopropanol**	
Temp (°)	**Time (Hr)**	**Axial (%)**	**Transverse (%)**	**Volume (mL)**	**Density (mg/mL)**
175	2	50	100	4.0	0.4

The mechanical property characterization experiments consist of cycling the actuator test sample at a fixed rate with no voltage applied and subsequently with an array of voltages. A rigid acrylic support frame enables the easy installation of a DE actuator into the Dynamic Mechanical Analysis (DMA) machine. See Section 3.2.1 for details of the experimental test setup. A test sample is placed into the DMA machine and shaken down by cycling the sample two times from 2mm to 7mm. The sample is then cycled from 2 mm to 7 mm at two rates, 0.1 mm/s, with no voltage applied to the actuator. The sample is subsequently tested with an array of applied

voltages starting at 200 V and increasing to 1400 V in 200-V increments. Characteristic data for the pullout stretching data from the experiments are plotted in Figure 37.

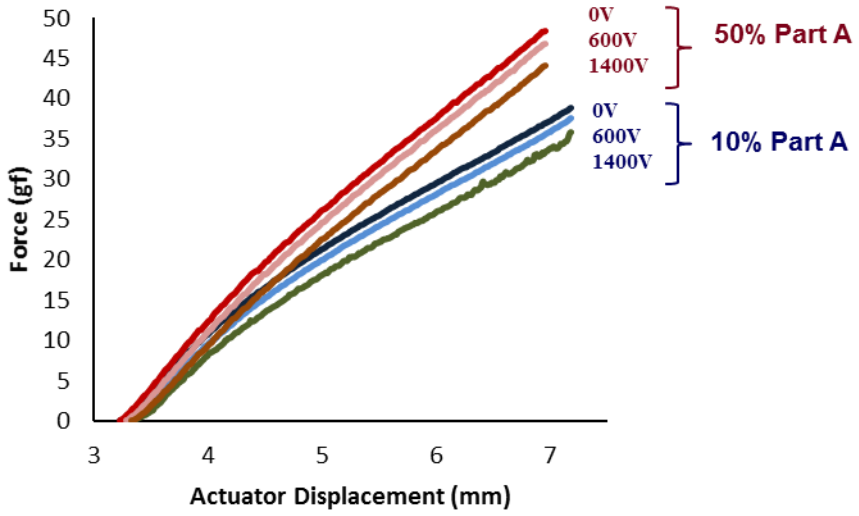

Figure 37. Extension Data from Actuator Pullout Characterization.
Pullout force displacement for 50% Part A and 10% Part A.

The mechanical and the active electrical data are plotted in Figure 13 for 0 V, 600 V, and 1400 V for actuators with a 50% by weight Part A and 10% by weight of silicone. The mechanical change and impacts of cross-linker density can be derived from comparing the two OFF voltage curves. The two curves, dark red and dark blue, have fundamentally similar profiles: they both have an initial stiff region, after which they stress-0soften and have a lower stiffness. Initially, both materials have similar stiffness. This initial stiffness is driven by the uncoiling of the long polymer chains and is primarily dependent on the length of the chains. Because both films are based on the same components, they have the same size polymer chains and are expected to have the same initial stiffness. The stress-softening occurs because the polymer chains have uncoiled and are starting to be stretched out. The stiffness in this middle region is driven by the interaction of the adjacent polymer chains, which in turn is driven by the number of cross-links. The 50% Part A Silpuran has more cross-links than the 10% Part A. As expected, the 50% Part A stiffness is greater than the 10% Part A. There is an approximate 40% reduction in the stiffness of the elastomer with the change from 50% Part A to 10% Part A.

The active force-displacement profile of a dielectric elastomer is a function of the applied voltage differential. The Maxwell stress supplied by the electric field reduces the stiffness or shifting of the OFF force-displacement curve down. The Maxwell stress goes with the square of

the electric field. Since the voltage is being held constant for each pullout test, the field will change as a function of the stretch. Elastomers can be assumed to be incompressible, and since the width is considered fixed for a released frame architecture, the increase in length corresponds to a decrease in the thickness. The differences in the performance curves for both cross-link densities have similar behavior. There is a shift down for the ON voltage curves. In the initial region, there is little separation between the ON and OFF voltage curves. The electric field goes with the square of the thickness. The material is relatively thick in the initial area, with a low electric field, which results in minimal differences between the ON and OFF voltage curves. After the stress-softening occurs and the elastomer is in the second middle region, there is a more significant difference between the ON and OFF voltage curves. Generally, the ON and OFF voltage curves are parallel but shifted down.

One way to compare the static mechanical properties of the materials is to compare the local stiffness in the two approximately constant regions: the initial stiffness region and the stress-softened region. The initial stiffness region is insensitive to the cross-link density; however, the stress-softened region substantially differs in stiffness. The stiffness for the stress-softened region, between 5 mm and 7 mm, is plotted below each voltage in Figure 38.

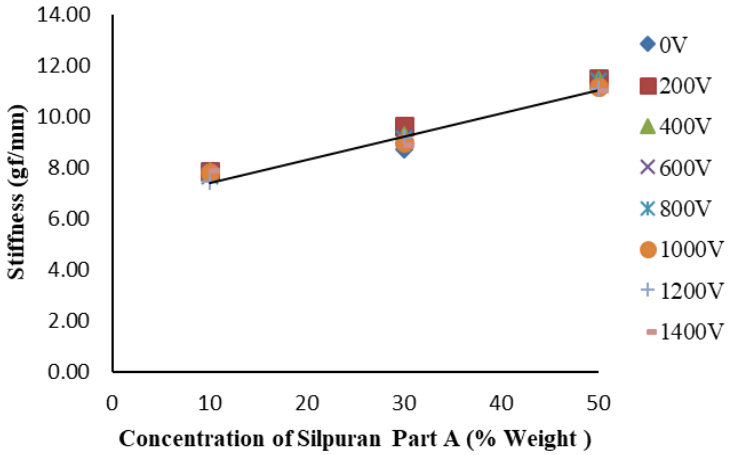

Figure 38. Custom Film Stiffness Comparison.

Three custom films made with varying percentages of Silpuran Part A into the composition. The stiffness as measured in a DMA pullout test is compared at a range of voltages.

The stiffness is independent of the applied voltage and is strongly dependent on the cross-link density. There is a 33% stiffness reduction from 50% to 10% Part A cross-link density

concentration. This reduced stiffness equates to a larger stroke for the actuator if the viscoelastic and electrical properties remain relatively constant.

3.5.2.2. Derived Actuation Stroke Sensitivity to Elastomer Cross-Link Density and Voltage

Another way to analyze the results from the previous study is to determine the sensitivity of the actuation stroke as a function of force from variable cross-link density. A constant force external system is chosen to evaluate the performance of a DE actuator. Using a constant force as the metric to judge performance will drive the preferential performance to an elastomer if everything else is constant due to the geometric relationship between the slope of the actuator and external system curves. Although there is an inherent bias to the choice of a constant force system, the preference for a softer material reinforces the primary advantages of a dielectric elastomer: large stroke and soft conformal properties.

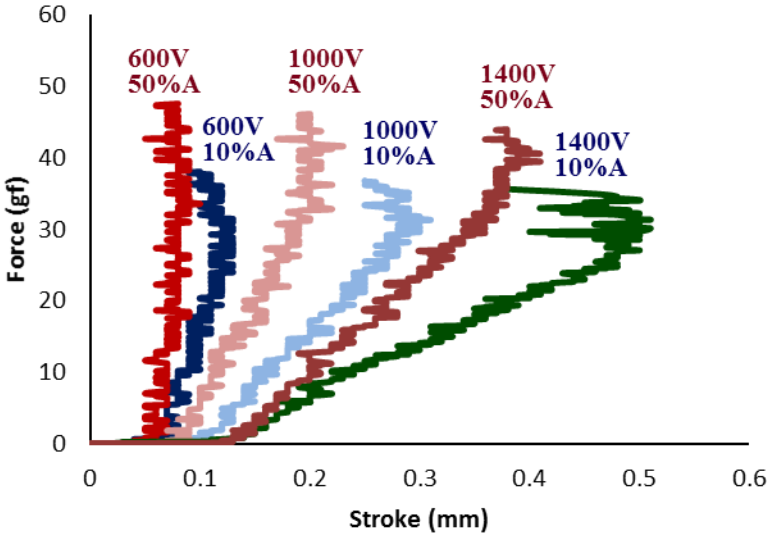

Figure 39. Custom Film Force-Stroke Comparison.

Pullout force stroke graph for 50% Part A and 10% Part A at 600 V, 1000 V, and 1400 V.

The force-stroke curves for a constant external force from the data plotted in Figure 38 are shown in Figure 39. Three voltage levels, 600 V, 1000 V, and 1400 V, are plotted for 50% Part A and 10% Part A. These curves are derived by finding the difference in length of the actuator's curves in the force-displacement space between the OFF and ON voltage curves. Therefore, there is a stroke for each ON and OFF voltage curve, but, by definition, the OFF voltage stroke will be zero. The actuator's stroke for both Part A concentrations increases as a function of voltage. For

a given force level and voltage level, the stroke is greater for the softer elastomer. For the range of performance, a peak stroke is identifiable for the 10% Part A actuator and the 50% Part A actuator. The peak stroke for the 10% Part A is 0.5 mm, while the peak stroke for the 50% Part A is 0.4 mm. The 10% Part A elastomer has a 0.1 mm or 25% greater stroke than the stiffer material. The trade-off for the larger stroke is that the peak stroke for the 10% Part A occurs at a force level of 30 gf compared to 40 gf for the 50% Part A. Depending on the stroke and force requirements, it is possible to tailor elastomer properties to match the desired actuator performance.

3.5.2.3. Viscoelastic Properties Sensitivity to Elastomer Cross-Link Density and Voltage

The viscoelastic properties of an elastomer can substantially affect the performance of tape actuators because they change the force-displacement profile while also affecting the speed of actuation and the creep of the actuator when holding position. Silpuran, in the formulation with 50 percent Part A, has low viscoelastic properties, making it useful for dielectric elastomer tape actuators. Decreasing the cross-link density has the positive actuation effect of lowering the stiffness. However, the effects on viscoelasticity are unknown. This study will experimentally characterize the force-displacement profile of a 10% Part A elastomer at different displacement rates. The results will be compared to the 50% Part A data, and the viscoelastic properties will be compared. The results of these experiments will allow the selection of the material properties as a function of cross-link density. See Table 4 for actuator fabrication parameters.

The experimental displacement rate study involves cycling the test sample at three rates with no voltage applied using the test setup described in Section 3.2.1. The test sample is placed into the DMA machine and shaken down by cycling the sample two times from 2mm to 7mm. The sample is then cycled from 2 mm to 7 mm at three rates, 1.0 mm/s, 0.1 mm/s, and 0.01 mm/s, with no voltage applied to the actuator. The results are plotted in Figure 40.

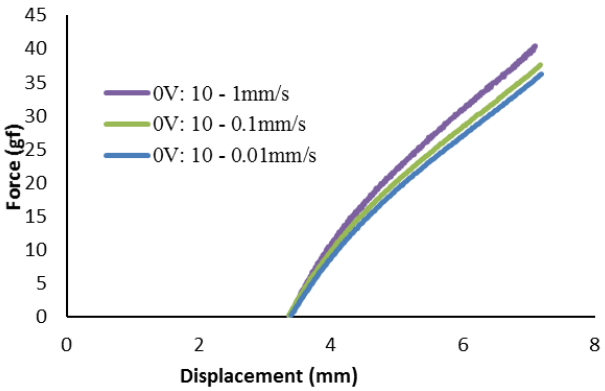

Figure 40. Film Characterization at Multiple Displacement Rates.

Pullout force displacement at rates 1mm/s, 0.1mm/s, and 0.01mm/s.

The results of the pullout tests at the three rates of 1.0 mm/s (purple curve), 0.1 mm/s (green curve), and 0.01 mm/s (blue curve) for a Silpuran film with 10% Part A and 90% Part B are plotted in Figure 40. Each curve has the same basic shape. All the curves have an initial stiff region at the beginning of the pullout, and then they stress-soften and reach a second stiffness level that is less than the original stiff region. There is a 100-fold difference in the rates from 0.01 mm/s to 1.00 mm/s, and the difference in the force response at 7 mm is approximately 5 gf, which, at a force level of 35.4 gf, equates to an increase of 14.2%of force caused by the increased strain rate. The 0.10 mm/s and the 0.01 mm/s rates for the Silpuran films with 10% Part A have a very similar performance with a difference of under 5%, with the increase over the 35.4 gf being 1.6 gf. Both have an identical initial stiffness and stiffen in the second region after the stress-softening.

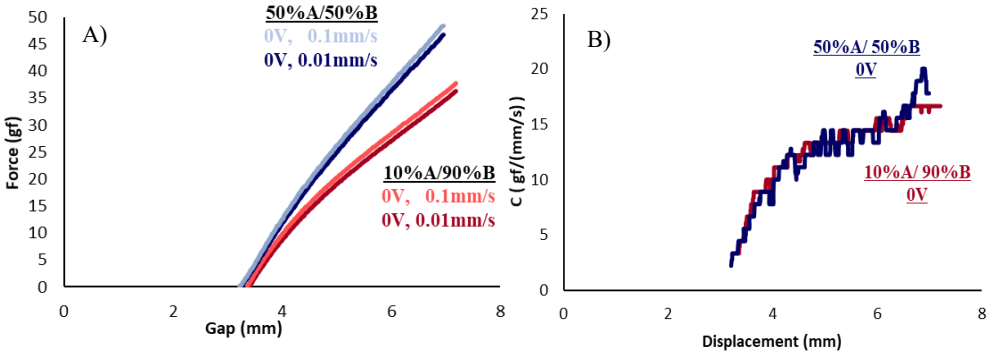

Figure 41. Force-Displacement Profiles (a) and Local Damping Coefficients (b).

A comparison of the force displacement profiles and local damping of custom silicone films characterized at displacement rates of 0.1 mm/s and 0.01 mm/s. The term “Gap” is an alternate name for displacement.

The Silpuran films made with 10% Part A have a difference in the viscoelastic effects, but they are very similar to the impact of the 50% Part A from the results shown in Figure 41. The two different stiffness regions introduce the possibility of using the elastomer in the various strain ranges to give different damping effects. It is possible to tailor the rigidity of the whole structure by controlling the pre-stretch applied to the actuator. The local damping coefficient properties can be determined for each cross-link density for the 0.1mm/s pull rate, shown in Figure 41. The rates are virtually identical except at the maximum displacement. Varying the cross-link density from 50 percent Part A to 10% Part A does not detrimentally change the viscoelastic effects of the material. The elastomer's stiffness can be changed by varying the cross-link density without causing detrimental effects.

3.5.2.4. Dielectric Permittivity Sensitivity to Elastomer Cross-Link Density

The stiffness and the dielectric permittivity mainly control the transient creep-terminated actuation stroke performance of a dielectric elastomer actuator. The elastomer stiffness has already been determined to decrease with lower cross-link density. The dielectric permittivity or dielectric constant is critical because it determines the Maxwell pressure from the applied voltage. In the previous section, the total actuator displacement increased with a decreased cross-link density; however, separating the effects of change in stiffness and dielectric permittivity is challenging. Therefore, it is desirable to determine the impact of cross-link density on the dielectric permittivity. Although dielectric permittivity is often considered a constant, it has been shown to change with stretch, although the change is not typically large. The high pre-stretch of a dielectric elastomer tape actuator and using an electric field to stretch the elastomer further require a custom process to determine the dielectric permittivity while under a high pre-stretch and an applied electric field. This study will evaluate the dielectric permittivity sensitivity to cross-link density by measuring the force change in a DE tape actuator when a voltage is applied during a blocking force test. See Table 4 for actuator fabrication parameters. One advantage of testing the dielectric permittivity in the actuator configuration is that all components will be the same as when the actuator is in use.

The function of the test setup is to enforce displacement and measure the force as a voltage is applied to the actuator. This test uses the same DMA setup detailed in Section 3.2.1; however, the experimental procedure differs. The test procedure for the blocking force consists of cycling

the actuator from 2 mm to 15 mm two times and then moving the actuator to 15 mm in length. The actuator then relaxes for 10 minutes before initiating the blocking force test. The test consists of cycling the voltage ON and OFF at 1/20 Hz, with a duty cycle of 50%. At each cycle, the voltage is increased by 100 V until failure is reached. For all portions of the cycle where the voltage is OFF, the voltage level is set to 0 V. The typical test results for the blocking test are shown in Figure 42.

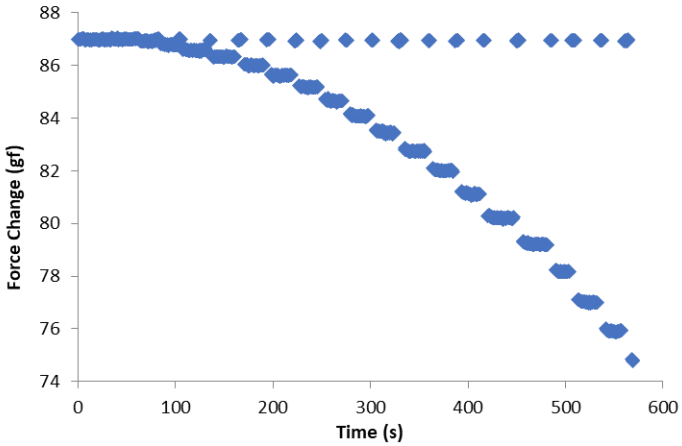

Figure 42. Active Blocking Force Characterization.

Active cyclical blocking force characterization: the applied voltage is cycled at a frequency of 1/20 Hz, with a duty cycle of 50%. At each cycle, the voltage is increased by 100 V until failure.

Each ON voltage step shows the force decreasing in a quadratic shape, which is expected because of the increasing electric field because the force is proportional to the voltage squared. During the blocking force test, the elastomer's geometric dimensions are fixed, which means the change in the electric field is directly coupled to the change in force. Each ON voltage of the actuation experiences a small amount of creep. For each test, the data are summarized by taking the force at the end of the cycle. The dielectric permittivity is the constant that can be derived for each ON and OFF voltage step. The summary of the dielectric permittivity as a function of voltage and cross-link density is plotted below in Figure 43.

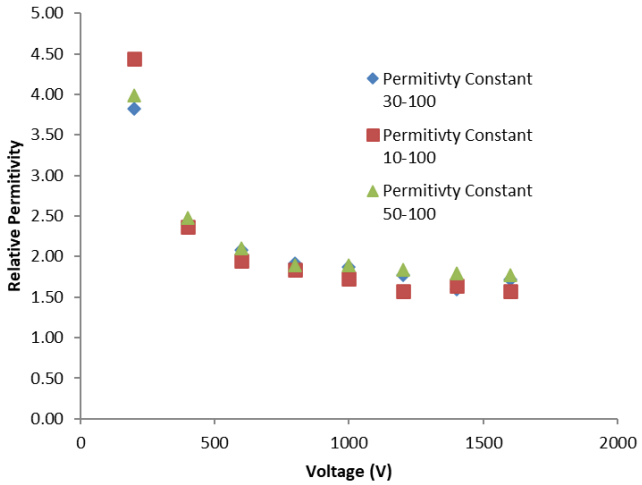

Figure 43. Custom Silicone Relative Dielectric Permittivity Constant Plotted.

Results of deriving the elastomer relative dielectric permittivity constant from blocking force experiments at three densities of elastomer cross-links.

The plot shows the dielectric permittivity as a function of the applied voltage for three cross-linking densities: 50% Part A in grey triangles, 30% Part A in blue diamonds, and 10% Part A in orange squares. There is a trend of the dielectric constant decreasing as the voltage level is increased.

The dielectric permittivity for the 10% Part A does appear to be less than for the 50 % Part A. The 30% Part A has a dielectric constant between the 10% and 50% Part A. If the values are averaged over the whole data set, then the dielectric permittivity for 10% Part A is 9.0% less than 50% Part A, and 30% Part A is 3.8%less than 50% Part A. One source of error in the measurements is the small change in force at small voltage differences. As the voltage increases, a larger force differential lowers the error in the dielectric permittivity measurement. Although there is a small loss in the dielectric permittivity, it is not large enough to offset the advantages of decreasing the material's stiffness. The actuation of a dielectric elastomer is a trade-off between the dielectric permittivity and the material's stiffness. In the case of Silpuran, the decrease in stiffness is more important and advantageous to offset the small reduction in the dielectric permittivity.

3.5.2.5. Performance Sensitivity to Elastomer Film Curing Temperature

This study examines the effect of changing the curing temperature on the material properties of a Silpuran 6000/10 film. The Silpuran 600/10 manufacturer, Wacker Chemicals, recommends

curing at a range of temperatures from 165°C to 200°C and from 5 minutes to 6 hours for both curing and post-curing. The curing temperature is the temperature at which the cross-links are formed, and the elastomer transforms from a polymer gel into an elastomer. The temperature and the time for curing can affect the material properties of the film because they affect the number of cross-links made and how they are made. Therefore, the curing temperature and time are important variables in fabricating a high-quality film for dielectric elastomers. Twenty-five films were fabricated at five different temperatures, 100°C, 140°C, 160°C, 170°C, 200°C, and 215°C, for the film curing temperature study. See Table 5 for the actuator fabrication parameters.

Table 5. Film Fabrication Parameters for Film Curing Temperature Study.

The same fabrication parameters were used to create all the samples for the study except for changing the curing temperature.

Actuator Parameters	**Solvent Mixture**					
	Material Preparation			**Drop Cast**		
Silpuran ID	**% Silicone in Isopar G**	**Part A (%)**	**Part B (%)**	**Area (in^2)**	**Volume (ml)**	**Evaporation (Hr)**
6000/10	80	10	90	4	2	48

Film Preparation				**Each Electrode**	
Curing		**Film Pre-Stretch**		**SWNT & Isopropanol**	
Temp (°)	**Time (Hr)**	**Axial (%)**	**Transverse (%)**	**Volume (mL)**	**Density (mg/mL)**
Variable	2	100	200	4.0	0.4

While the fabrication processes can be reliable, there was a yield issue when manufacturing actuators. Although many actuators were manufactured at varying temperatures, there were issues with films cured at the lower and higher end of the temperature range. The 100°C films were extremely soft and tore during manufacturing, so none could be tested. The 140°C cured films also seemed to have a low tear resistance, and the yield from 12 films was a single actuator. The fabrication yield increased above 160°C and was good until 200°C. At 200°C and 215°C, the films started to adhere to the glass substrate and posed great difficulty in removing them and fabricating actuators.

Determining the sensitivity of temperature on actuator performance required the characterization of the effect of curing temperature on the electrical and mechanical performance, which is a three-step process: The first step in testing is to shake down the actuator to remove one-time viscoelastic effects, followed by strain relaxation for the actuator to come to an equilibrium, followed by the active blocking force test to characterize the actuator's performance.

The initial step to shaking down the actuator is to make sure that the one-time viscoelastic effects have been eliminated. Actuator shakedown is done by cycling the actuator to a length greater than what will be tested for five cycles. The actuator is mounted into the force-displacement testing rig and then stretched by 10 mm at 1 mm/s using the computer-controlled interface. The testing is manually directed to move the actuator apart. Then, the actuator is manually directed to relax the actuator by bringing the chuck back together 10 mm at 1 mm/s. Typical results can be seen in Figure 44.

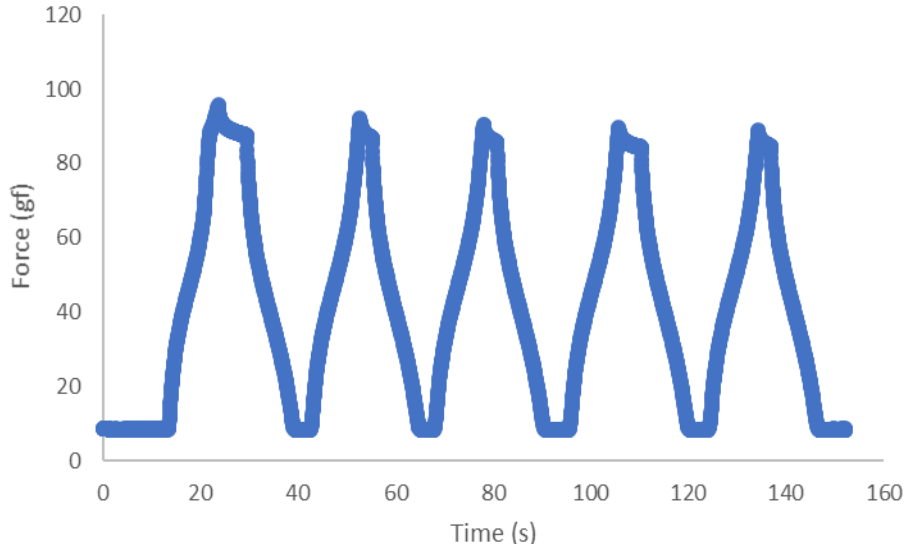

Figure 44. Shakedown Cycling Before Experimental Characterization.
Using automated testing setup.

The next step is to perform the active blocking force test. The blocking force consists of holding the actuator at a fixed displacement and measuring the force as the actuator is activated. The actuator has already achieved an equilibrium through the previous relaxation test. The active portion of the blocking force consists of applying a voltage differential to the actuator. The voltage is cycled ON and OFF for 10 s, and after each cycle, the ON voltage is increased by 50 V. The voltage rises from 0 V to 3000 V in increments of 50 V, with each cycle controlled by a 1/20 Hz square wave at 50% duty cycle. The force is then measured as the voltage increases, and the test is stopped when the actuator experiences an electrical or mechanical failure, which can be either a dielectric breakdown or a tearing of the actuator. The typical results for these tests can be seen in Figure 45.

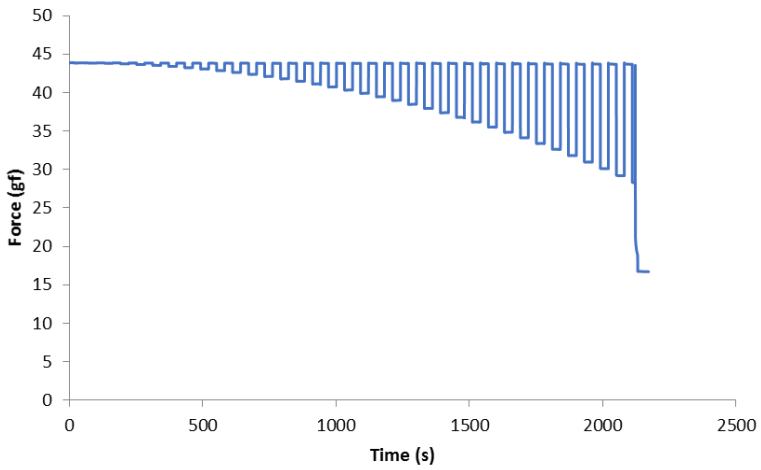

Figure 45. Active Blocking Force Experimental Characterization.

Using custom film characterization setup to derive material electronal properties experimentally.

The plot of the initial shakedown cycling of the actuator shows the force as a function of the time. Although the space is in the force-time space, the curves have the typical hyperplastic shape. Since the actuators are stretched at a constant rate, the curves, while under transition, are a scaled version of the force-displacement performance curves. The tension curves show an initial stiff region, a more softened stiffness, and increased stiffness as the actuator further lengthens. At each peak, before the actuator is cycled back, one can see the relaxation of the elastomer as some of the quick viscoelastic effects relax. The first cycle has a higher peak force than all subsequent cycles. The last two cycles have equivalent force levels. Since the cycles are all being directed manually, the time for relaxation at the stretched and unstretched configurations is not completely uniform. However, because the one-time viscoelastic effect is a function of the maximum stretch that the elastomer has experienced, the small inconsistencies in time do not impact the shakedown of the elastomer.

The typical strain relaxation results are shown in Figure 25. The test starts with the force at 0 and the actuator completely relaxed. Then, at a rate of 10 mm/s, the actuator is stretched to 12 mm, which appears as a vertical line, representing the stretching of the actuator to the blocking force length of 12 mm. The force is substantially changed as the actuator is initially held at 12 mm or lambda equals 3. Most of the strain relaxation occurs in the first 10 seconds. At the start, all the fast viscoelastic effects are relaxing. At longer time frames, the viscoelastic effects have longer time constants that are still active. Although the actuator will continue to relax as it is

held, the percentage change in the force decreases substantially the longer the actuator is held, and eventually, it can be thought of as having reached a transient creep -terminated equilibrium position.

The typical results for the blocking force experiment are shown in Figure 45. The typical result looks like a square wave, with each subsequent step having a lower force than the previous. The change in force is a quadratic function of the applied voltage. At all the OFF voltages, the force level returns to the relaxed force level where the voltage is OFF. If you zoom in on a single cycle, you can see some viscoelastic force drift on both the ON and the OFF sides. The change of force in the elastomer is a function of the applied voltage, as shown in Figure 45.

The constant parameter that relates to that change is the dielectric permittivity. The dielectric permittivity can be derived from Figure 46. The maximum sustained electric field at failure can also be evaluated because the voltage is stepped up until a maximum mechanical or electrical strength is reached. However, because the maximum electric field strength relies on a statistical process, this single data point can give only a rough estimation of the failure and only at the given strain field.

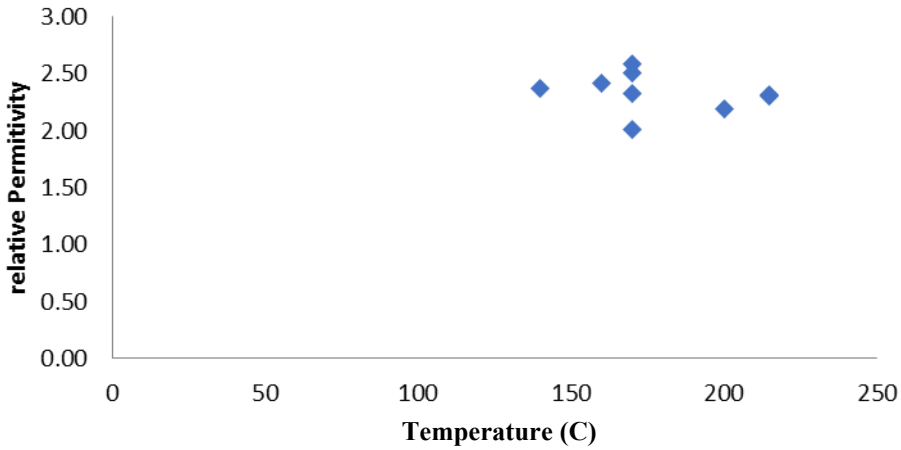

Figure 46. Relative Dielectric Permittivity Versus Curing Temperature Plot.

Relative dielectric permittivity derived from blocking force actuator characterization.

The dielectric permittivity can be plotted as a function of cure temperature. From the four samples at 170°C, there is a spread of over 25%in the calculated dielectric permittivity from the experimental results. The dielectric permittivity for the 140°C and the 160°C appears to be higher than the dielectric permittivity for the 200°C and the 220°C films. The four actuators at 170°C have a dielectric permittivity spread larger than the spread between the lower and higher

temperature data points. Therefore, the dielectric permittivity as a function of temperature remains relatively constant, while there is a spread due to the noise in the data. The dielectric permittivity is relevant for the actuator strain field tested.

Another way to evaluate the performance is to check the maximum electric field before failure occurs. The failure field can be derived by determining the maximum voltage the actuator sustained before a failure occurs, as shown in Figure 47. The lateral and axial stretch ratios are known along with the initial thickness; therefore, it is possible to derive the failure field from the voltage over the current thickness.

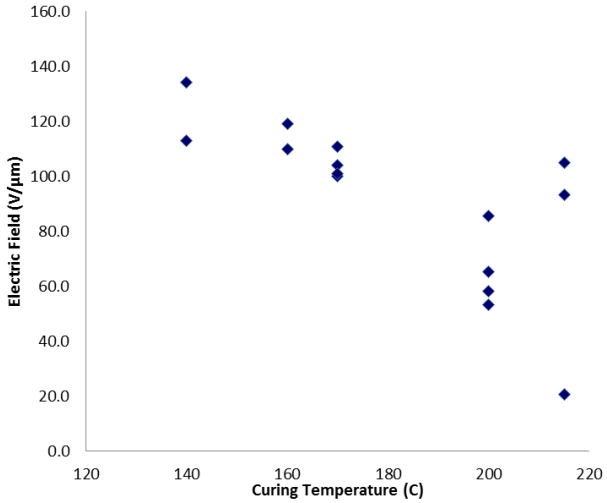

Figure 47. Maximum Electric Field Versus Film Curing Temperature.

Derived from custom film characterization setup.

Another way to analyze the impact on the performance is to plot the stress in the elastomer right before failure. In Figure 48, the film stress during the OFF voltage is plotted as orange squares, and the ON voltage stress in the film is plotted as blue diamonds. The film cured at 170°C shows a wide spread in the data. For the OFF voltage data in orange, there appears to be a trend where the elastomer cured at higher temperatures has a softer stiffness. Evaluating the ON stress level is challenging because the important aspect is the change in stress, not the absolute value. The change in stress under the maximum electric field is plotted in Figure 48.

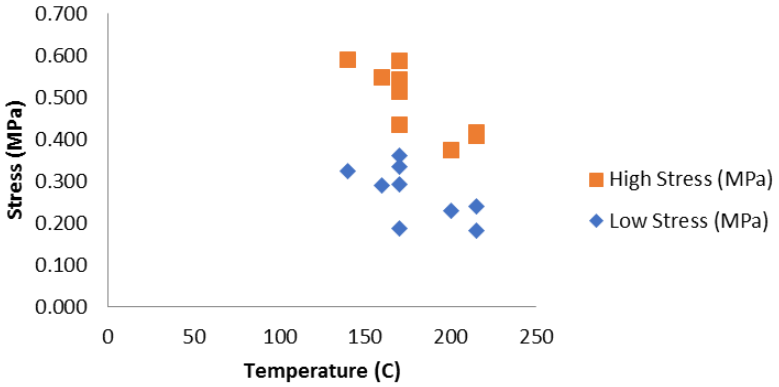

Figure 48. Stress at Maximum Electric Field.

Derived from custom film characterization setup.

The induced actuation stress is important because it impacts the elastomer's dielectric permittivity and stiffness. Including the induced actuation stress gives maximum stress achieved before failure, indicating the maximum achievable force levels. The maximum actuation stress as a function of the curing temperature is plotted in Figure 49. For the 175°C temperature data, there once again appears to be a sizable stress range induced at the maximum level. There seems to be a trend with a higher actuation strain at a lower curing temperature, but the noise in the data makes it difficult to confirm.

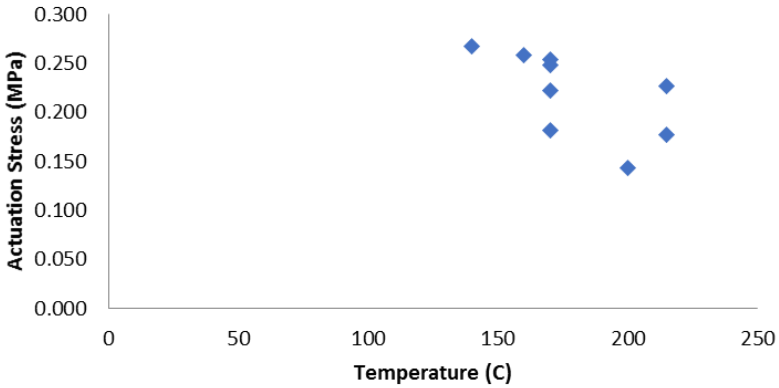

Figure 49. Actuation Stress at Maximum Electric Field.

Derived from custom film characterization setup.

This study aims to evaluate the effects of curing temperature on the performance of Silpuran films for use in dielectric elastomers. The dielectric permittivity for all the curing temperatures came about at similar levels. The stress level appears slightly higher for lower-temperature films, meaning the lower-temperature films are stiffer than higher-temperature films. However, the

actuation-induced stress in the elastomers is also higher at lower temperatures. Because of the noise in the manufacturing process, there is no curing temperature with optimal performance.

On the other hand, there is an optimal range under which the curing process produces films that can be made into actuators. At low temperatures, the elastomer tends to lose some of its toughness, resulting in many torn actuators during the fabrication process, which means the total fabrication of the actuator from film cured below 170°C has toughness issues. Consistent actuator fabrication below 170°C was unsuccessful. The probable cause of failure was insufficient energy to fully cure (cross-link) the elastomer, which is supported by the easy tearing of these elastomers. Conversely, curing temperatures above 180°C also appear to have yield problems during manufacturing. These films start to adhere to the glass substrate under which the films are drop-cast. This film adherence results in a low yield of film for fabricating actuators. There is no strong performance drop due to the curing temperature, but there is a yield drop when the actuators are cured outside a specific temperature range. Therefore, a temperature of 175°C was chosen to maximize the yield for the fabrication of dielectric elastomer actuators.

3.5.2.6. Performance Sensitivity to Electrode Density

Dielectric elastomer actuators must have compliant electrodes capable of maintaining conductivity over large strains. The SWNT electrodes enable large strain by allowing movement and flexing between carbon nanotubes that form a conductive mat. The electrode conductivity properties are proportional to the density of the SWNT electrodes, while the stiffness of the electrodes is inversely proportional to the density of the electrodes. Therefore, a trade-off exists for actuation strain between the larger density of SWNT electrodes for better conductivity and lower density electrodes for better flexibility and lower stiffness. The electrode density is determined by the fabrication parameters of the density of the solution of SWNT in isopropanol and the volume of the solution sprayed onto the actuator. A sensitivity study measures the actuation strain of a simple spot actuator with varying density electrodes to isolate the SWNT electrode density performance effect. A spot actuator is an elastomer stretched equally biaxially onto a fixed frame with a conductive circle in the middle that expands when a voltage is applied. These actuators are simple to fabricate, making them useful for exploring various parameters to determine general trends.

The spot-testing samples are made using the general fabrication process detailed in Section 2.3 but with a few modifications. The film is pre-stretched equally biaxially, a circular electrode spraying mask is used, and the test samples do not use the MTCs because they are not released from the fabrication frame. The actuator fabrication parameters are shown in Table 6. The mask has a diameter of 12.7 mm. The volume of the solution sprayed was chosen such that the surface density of the electrodes would match the surface density used for the tape actuators. The final step is to apply the reusable external electrical connections. This is done using a soft silicone adhesive conductive tape, 3M™ XYZ Axis Tape 9719, that connects to a conductive fabric tape, 3M™ Fabric Tape CN-4490, used for the external reusable electrical connection.

Table 6. Actuator Fabrication Parameters Electrode Density Study.

The same fabrication parameters were used to create all the samples for the study except for changing the density of the SWNT in isopropanol.

Actuator Parameters	Solvent Mixture					
	Material Preparation			Drop-Cast		
Silpuran ID	% Silicone in Isopar G	Part A (%)	Part B (%)	Area (in^2)	Volume (ml)	Evaporation (Hr)
6000/10	80	10	90	04.0	2.5	48

Film Preparation				Each Electrode	
Curing		Film Pre-Stretch		SWNT and Isopropanol	
Temp (°)	Time (Hr)	Axial (%)	Transverse (%)	Volume (mL)	Density (mg/mL)
175	2	125	125	4.0	0.03, 0.05, 0.1, 0.2, to 0.4

The purpose of the experimental setup is to measure the displacement of the spot actuator as a function of voltage. The setup consists of mounting a camera, a Canon S90, above a spot actuator directly down for optical measurements and using a custom-made LabView computer program to control and measure the applied voltage to the actuator. The computer generates a 0-5 volt signal amplified by a Trek 10/10B-HSA power amplifier to actuate the test sample. The amplifier also outputs the applied voltage and current through an output signal recorded by the same custom LabVIEW program that generates the output voltage signal. The spot actuators are tested by cycling the voltage level ON and OFF for five cycles, starting at a fixed voltage level, 500 V, and increasing the voltage level by 100 V until failure is reached. The voltage is cycled using a square wave at a frequency of 1/40 Hz with a duty cycle of 50%. At the end of each cycle, when the voltage is ON, the actuation strain is measured optically. The results of the study are shown in Figure 50.

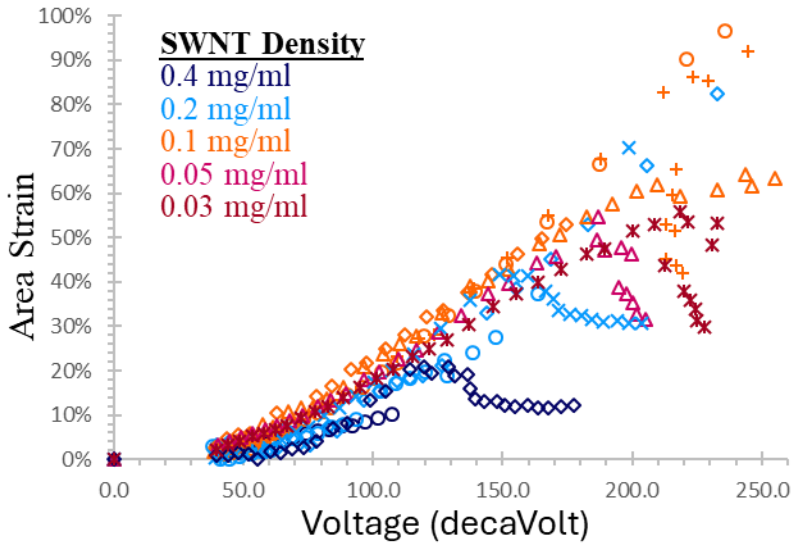

Figure 50. Spot Actuator Characterization with Variable SWNT Electrode Density.

The plot shows a study of the effects of SWNT electrode density on actuation strain when the applied voltage is increased in 100 V increments until failure.

The experiment aims to identify trends in the actuation performance relative to the electrode density. In Figure 50, the thick electrode densities, 0.2 and 0.4 mg/mL, increase the actuator's stiffness and substantially limit the actuation strain. With the thinner SWNT electrode densities, the actuator performs well initially but eventually reaches a point where it can no longer increase its strain. The performance limit is most likely caused by the electrodes reaching their percolation limit, meaning further stretching causes them to lose conductivity. Even though the actuator can support higher electric fields, it can no longer expand. The middle densities of electrodes are a good compromise between conductivity and stiffness, where they can achieve large actuation strain.

This experiment provides good guidance on the possible thickness of electrodes that will function for tape actuators. There is no need to explore the thick electrodes further because they significantly impact the performance, limit the actuator stroke, and cause early failure. The interesting densities to explore are those of the medium to thin electrodes. The thin electrodes could maintain conductivity only through a certain range of stretch before losing conductivity. In the fabrication of the DE tape actuators, pre-extended electrodes are used, which means that the electrodes might maintain conductivity through the full possible actuation range. The very thin electrodes in the extended configuration may not be extended farther than their percolation limit.

Thinner electrodes potentially save material cost and time because they use less material and are easier and faster to create. However, the medium electrodes also enable large performance. Therefore, a possible range of electrode densities provides reliable large-performance actuation. This range of electrode densities can be explored using the tape actuator architecture to see the impact of different electrode densities on a more complex actuation state.

3.5.2.7. Performance Sensitivity to Pre-Extended Electrodes

The compliant electrode for a dielectric elastomer actuator is a key component that can substantially impact the actuation performance. The challenge for the compliant electrode is that it must maintain conductivity through a larger stretch range without significantly increasing the stiffness. Using the minimum amount of material needed to maintain conductivity is one way to limit the stiffness. The percolation limit, the electrode density at which conductivity is lost, becomes a critical factor for low-density electrodes. The electrode density is a function of the initial electrode density and the amount the electrode is stretched. The electrode material distribution can significantly affect the percolation limit. Two electrodes with an equivalent mass of conductive material can reach their percolation limits at substantially different stretches depending on the material distribution. Dielectric elastomer tape actuators allow for the fabrication of pre-extended electrodes, which enables the formation of a compliant electrode with a new distribution of electrode material. Although there has been research on SWNTs for compliant electrodes for dielectric elastomers, pre-extended SWNT electrodes need to be explored for their ability to enhance actuation performance. Pre-extended electrodes are formed by creating the SWNT electrode mat in a stretched configuration. The electrode formation at a high axial strain state ensures that the electrodes are conductive in the extended state.

The electrodes will return to the fabrication state when actuated rather than stretched beyond their fabrication state. The pre-extended electrodes may provide better distribution of material and enable conductivity at lower electrode densities. The pre-extended electrodes have the potential to shift the trade-off between conductivity and stiffness, allowing larger strain ranges with lower-stiffness electrodes. This study explores actuation performance impacts on a tape actuator fabricated with pre-extended electrodes at two different strains when the electrode density changes. The study uses a steady-state cyclical actuation characterization technique to evaluate the actuation performance across various external forces. The tape actuator performance

is modeled using a Gent strain energy model to derive material parameters. Gent model parameters are used to determine the sensitivity of electrode density on actuation performance. The normalized performance is also evaluated for the different electrode densities.

The fabrication parameters of the DE actuators are shown in Table 7 and follow the steps detailed in Section 2.3, except for a variety of electrode density solutions. The 0.4 mg/mL solution has been discarded after the previous analysis with the spot actuators because of the poor performance. The experiment uses the custom-built force-displacement test setup that applies a constant force and measures the displacement as a voltage differential is applied to the actuator. The experimental setup is described in full detail in Section 3.2.3.

Table 7. Actuator Fabrication Parameters for the Pre-Extended Electrode Study.

The same fabrication parameters were used to create all the samples in the pre-extended electrode characterization study.

Actuator Parameters	**Solvent Mixture**					
	Material Preparation			**Drop-Cast**		
Silpuran ID	**% Silicone in Isopar G**	**Part A (%)**	**Part B (%)**	**Area (in^2)**	**Volume (ml)**	**Evaporation (Hr)**
6000/10	80	10	90	4	2.5	48

Film Preparation				**Each Electrode**	
Curing		**Film Pre-Stretch**		**SWNT and Isopropanol**	
Temp (°)	**Time (Hr)**	**Axial (%)**	**Transverse (%)**	**Volume (mL)**	**Density (mg/mL)**
175	2	110, 150	150	1.0	0.03, 0.05, 0.105, 0.2

The experiment uses the characterization methodology described in Section 3.4. The testing parameters are a 2300 V applied voltage at 1/40 Hz frequency and a 50% duty cycle square wave. The actuator is tested from 15 gf to 80 gf in 5 gf increments. The actuator is mounted and then shaken down with two cyclical tests to validate the actuator's general performance before the experiment's full characterization is performed. The actuator is cycled at 15 gf and then at 65 gf using an applied voltage of 2300 V. After the shakedown process; the actuator is characterized across its whole load range starting with 15 gf and increasing by 5 gf until the characterization is finished at 80 gf.

The characterization test data are in the form of displacement as a function of time. Typical results are shown below in Figure 51. The peaks in the data represent the times when the voltage is ON, and the valleys represent the data when the voltage is OFF.

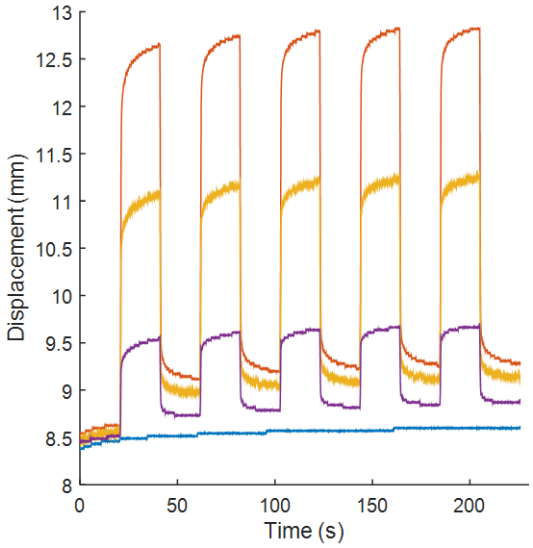

Figure 51. Typical Results from Cyclical Actuator Characterization.

Typical displacement over time from cyclical characterization at multiple voltage levels.

The data represent the five cycles of switching the voltage ON and OFF. The initial length is the shortest; after initiating voltage cycling, it never reaches that compressed length again. By the last cycle, the performance has reached steady-state cyclical performance, where the viscoelastic effects will be the same every cycle. After 20 seconds, the actuation has achieved most of the motion it will achieve, and it has reached a steady-state cyclical actuation. The cyclical experimental data are summarized as quasi-static performance in the force-displacement space by taking the maximum and minimum displacement during the last cycle to represent the cyclical data. The two data points become the length of the actuator at a constant force. All the cyclical experimental characterization data are shown in the force-displacement space in Figure 52.

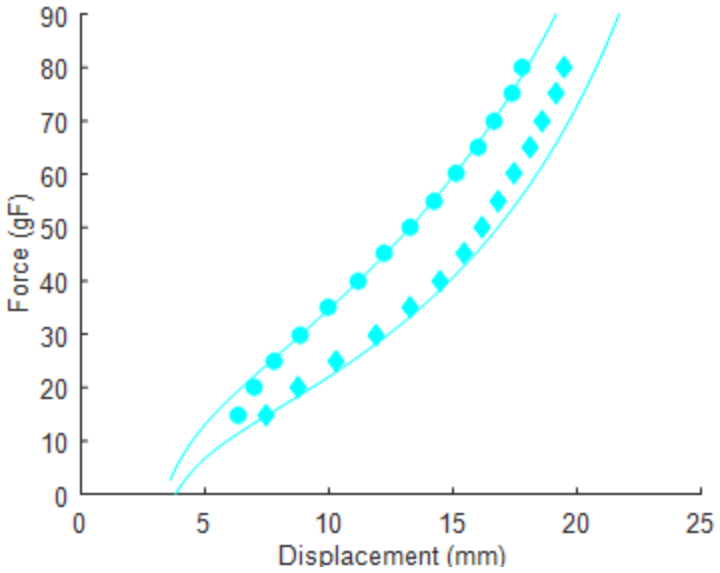

Figure 52. Cyclical Characterization Summarized in a Force-Displacement Plot.

The summarized data form the shape of a typical hyperelastic curve.

The data points in Figure 52 represent the experimental data, and the lines represent the data fitted to a Gent strain energy equation-based model of the actuator. The circles are the OFF voltage lengths of the actuator, and the diamonds are the ON voltage lengths of the actuator with an applied voltage of 2300 V. Both curves have the typical hyperelastic behavior, where they are initially stiff and then the stiffness decreases, or stress-softens, and finally the stiffness again increases as the actuator is stretched out toward its hyperelastic limit. The stiffening is much less apparent in the OFF voltage curve than in the ON voltage curve, which increases more rapidly at the higher force levels than the OFF voltage curve. The Gent strain energy equation is used to model the force-displacement profile of the OFF voltage curve. The Gent strain energy equation uses two parameters: Mu, the small shear strain modules, and J_m, the maximum stretch limit of the elastomer, to define the hyperelastic force-displacement curve. The material parameters for the OFF voltage experimental data are determined using a least-squares error fit. The derived material parameters are plotted in Figure 53.

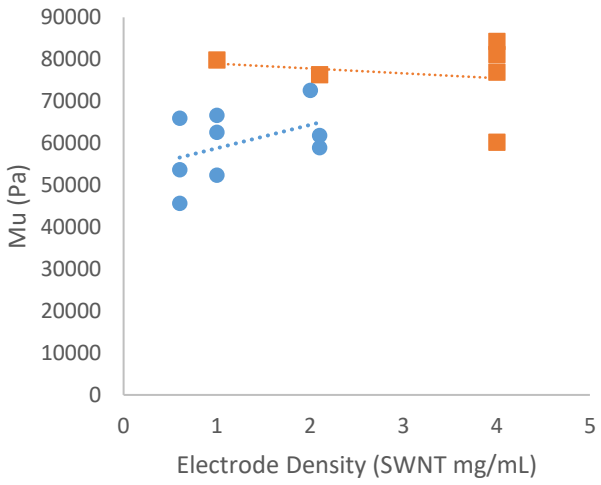

Figure 53. Derived Shear Modulus from Cyclic Characterization.

Actuators with electrodes fabricated with 100% and 150% pre-stretch and a range of electrode spray solutions from 0.5 to 4 mg/ml.

The derived shear constant as a function of the density of the electrodes is plotted in Figure 53. The blue circles represent the data from the actuators formed with a 100% axial pre-stretch, and the orange squares represent the actuators formed with a 150% axial stretch. Both data sets show a wide spread in the parameters, which makes drawing reliable conclusions challenging. For the actuators prepared with 150% axial pre-stretch, orange squares, the shear parameter is approximately 80 kPa, except for one actuator with a smaller shear modulus. The shear modulus for the actuators with 100% axial pre-stretch, blue circles, has a wide range, approximately 15 kPa, of performance. There is a slight trend toward a softer shear modulus at lower densities; however, this may be an artifact of the variability of the data and may not be significant.

The data in Figure 54 show the stretch limit property, J_m, as a function of electrode density. The blue circles represent the actuators fabricated with 100% axial strain, and the orange squares represent the actuators made with an axial pre-stretch of 150%. The Jm value varies between 30 and 50. Jm is a challenging parameter to derive because the actuators are not taken to their hyperelastic limit, so the model is predicting beyond the experimental data what the best possible Jm parameter would be for the data. The electrodes with the highest density have a very clustered maximum stretch limit, even including the outlier in the shear modulus. The electrodes with an SWNT solution density of 4 mg/mL have a lower J_m of around 30, which indicates that the increased electrode stiffness has the impact of decreasing the stretch range of the actuator.

Ultimately, the difference does not have a very large effect on the performance because the actuators are not used near their stretch limits, which decreases the impact of this parameter on the overall performance of a dielectric elastomer tape actuator.

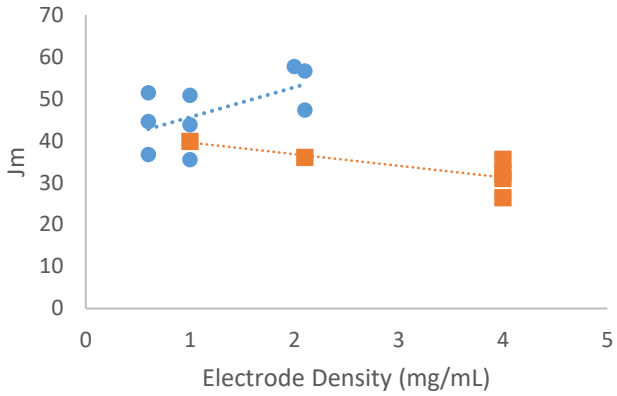

Figure 54. Stretch Limit as a Function of Electrode Density.

Actuators with electrodes fabricated with 100% and 150% pre-stretch and a range of electrode spray solutions from 0.5 to 4 mg/ml.

Having determined that there is not insignificant variability in the material model parameters from the density of the electrodes, the next step is to investigate whether there is a significant impact on the actuation performance as a function of the density of the electrodes. The most relevant metrics for the performance of a DE tape actuator are the stroke, shown in Figure 55, of the actuator and the work, shown in Figure 56, that the actuator produces.

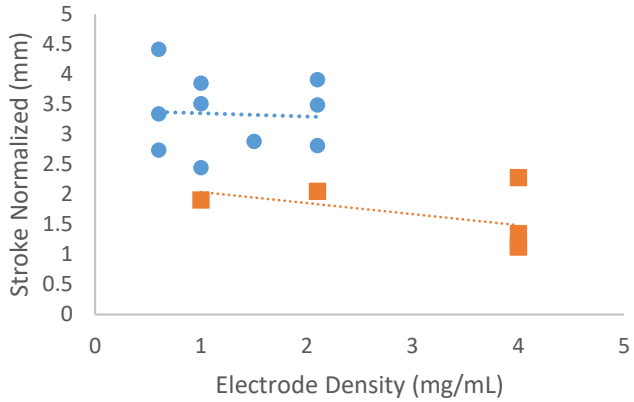

Figure 55. Stroke Normalized as a Function of Electrode Density.

Actuators with electrodes fabricated with 100% and 150% pre-stretch and a range of electrode spray solutions from 0.5 to 4 mg/ml.

An easy way to summarize the experimental data is to analyze the peak stroke location for each actuator and compare the performance as a function of the electrode density. The stroke of the actuator is normalized to the individual thicknesses. Because each actuation is evaluated at a fixed reference voltage, the different initial thicknesses of the films will cause them to have different electric fields. Therefore, the maximum stroke induced by the electric field caused by the applied 2300 V is normalized for each actuator to a reference geometry with a thickness of 134 um. The spread of the stroke data at a specific density shows substantial variability. However, the 4 mg/mL density of electrodes has a shorter stroke than the thinner densities. The normalized stroke performance of the actuator with a density between 0.6 mg/mL and 2 mg/mL is good and produces large strokes.

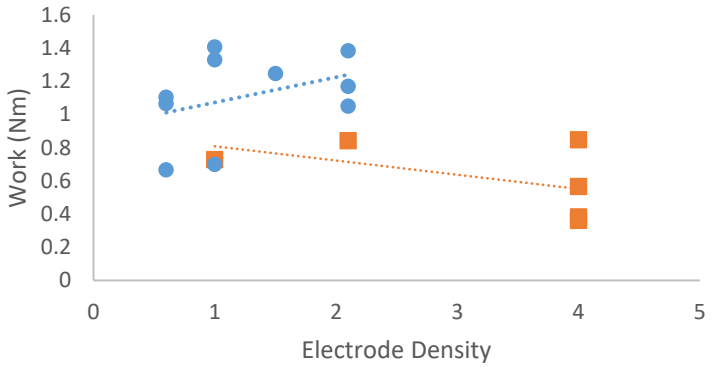

Figure 56. Work Normalized as a Function of Electrode Density.

Actuators with electrodes fabricated with 100% and 150% pre-stretch and a range of electrode spray solutions from 0.5 to 4 mg/ml.

The impact of the electrode density on actuation work is another useful metric. The work is normalized, using the same normalization as the actuation stroke, to ensure that the comparison provides relevant data, as shown in Figure 56. The peak work is plotted as a function of electrode density, with the blue dots representing electrodes fabricated at 150% pre-strain and orange squares at 100% pre-strain. The impact of electrode density is inconclusive because there is a wide range of performance at individual density levels that is similar in size compared to different electrode densities. The impact of the pre-extended fabrication strain length has a stronger trend regarding the effect on work. Actuators with the highest density electrodes produce less work than thinner density electrodes, which appear to create more work.

This study aims to determine the impact of pre-extended electrodes and SWNT electrode density on tape actuator performance. One problem with dielectric elastomers is the complexity of the behavior and the fact that the performance is a statistical result of the interaction of the individual polymers forming the elastomer. A large variation in performance can only be truly understood with a large statistically significant sample size. This study determined experimental techniques for measuring the impact of electrode density and the fabrication pre-extended strain length on performance. There are a few general conclusions that can be drawn from the data. For the spot actuators, light electrode densities could not match the strain performance of higher-density electrodes. However, with pre-extended electrodes, the performance of the lighter electrode is comparable to heavier electrodes. Therefore, the pre-extended electrodes change the inherent trade-off between thicker electrodes with better conductivity and thinner electrodes with less stiffness. Pre-extended electrodes enable lighter electrodes to match the actuation performance of thicker electrodes.

The comparison of actuation performance with different pre-strains, 100%, and 150%, provide inconclusive results due to the range of the results. The pre-extended electrode with 150% axial strain did not perform better than actuators with 100% axial pre-stretch during fabrication. The performance difference may be because of a difference in the mechanical properties of the elastomers themselves, or it could be how the electrodes are attached to the highly stretched elastomer, increasing the total stiffness of the elastomer, which negatively affects both the stroke and the work of the actuator. For the actuators fabricated with 100% axial prestretch, the stroke and work performance do not show a significant difference between the 0.6 mg and the 2 mg density of electrodes. The study concludes that 100% axial pre-stretch gives good actuation performance, while any lighter-density electrodes with 100% axial pre-stretch may have good DE actuators.

3.5.3. Performance Limits and Losses During Steady-State Cycling Actuation

Characterizing the limits and losses of DE tape actuator properties for the specific application context of steady-state cycling actuation is important for achieving robust and repeatable performance. The effectiveness of the self-healing electrodes is characterized to ensure that operation near dielectric breakdown will be unaffected by small fabrication errors. Establishing a safe voltage operating range for a DE tape actuator during steady-state cyclical

operation requires that the dielectric field breakdown strength be characterized during steady-state cyclical operation. Finally, the leakage current is measured to validate that a DE tape actuator requires low power to hold in the ON voltage state.

3.5.3.1. Dielectric Breakdown Strength Characterization

One of the main advantages of a dielectric elastomer tape actuator is that it is a large-strain actuator enabled by a large electric field. The magnitude of the electric field that the actuator supports controls the maximum actuation performance, given that no other limitations are reached. The maximum electric field is the elastomer's dielectric breakdown strength. Although there are standard ASTM tests, for example, ASTM D3755-14, to determine an elastomer's maximum electric field, they do not account for the complexities of a dielectric elastomer actuator, including the large stretch, stretching under an active electric field, and the interaction of the compliant electrode and elastomer, which have all been shown to affect breakdown strength. On top of the inherent complexities of DE actuators, a tape actuator uses SWNT electrodes capable of self-healing. This self-healing issue makes identifying the true electric field breakdown strength more complex.

A custom testing procedure was created to experimentally determine the maximum electric field supported by a cyclical actuating dielectric elastomer tape actuator working against a constant force. To account for the large pre-strain, the actuation under voltage, and the interaction of the compliant electrode and the silicon film, a dielectric elastomer actuator is used to determine the electric field breakdown limit. See Table 8 for the actuator fabrication parameters. With self-healing electrodes, the dielectric field breakdown strength test for a given voltage is repeated until no failures occur or until the actuator fails.

It can be challenging to distinguish temporary failure from total failure for a dielectric elastomer that self-heals. A temporary failure for a self-healing electrode occurs when the event eliminates the electrode material in the region of the fault, and the actuator proceeds to sustain a stronger electric field. An unsteady current draw typically identifies temporary failure events. The unsteady current is caused by an electrical short, conducting current through the film—the flowing current causes the local electrode material to self-heal self-healing. The electrode region around the short loses conductivity, eliminating the electrical short since there is no conductive path around the initial short in the film. This process may repeat rapidly for a single failure,

which causes an unsteady current draw. Total failure occurs when a tape actuator can no longer move. The easiest total failure to identify is a catastrophic failure, where the external load has torn the elastomer in two. Another type of total failure occurs when a steady current, significantly larger than the typical leakage current, is needed to maintain actuation. For this type of failure, an electrically conductive path has formed through the actuator, which can sustain the full current. Visually, this type of failure typically has minimal actuation, and there is either no visual evidence of self-healing or a strong spark at a fixed location. Total failure can also be identified when many self-healing events occur sequentially across the entire surface. In this case, the maximum electric field breakdown strength of the whole film has been reached, and as soon as one location self-heals, another location breaks down.

Table 8. Actuator Fabrication Parameters for Electric Field Breakdown Study.

The same fabrication parameters were used to create all the samples for the electric field breakdown study.

Actuator Parameters	Solvent Mixture					
	Material Preparation			Drop-Cast		
Silpuran ID	% Silicone in Isopar G	Part A (%)	Part B (%)	Area (in^2)	Volume (ml)	Evaporation (Hr)
6000/10	80	10	90	4	2.5	48

Film Preparation				Each Electrode	
Curing		Film Pre-Stretch		SWNT and Isopropanol	
Temp (°)	Time (Hr)	Axial (%)	Transverse (%)	Volume (mL)	Density (mg/mL)
175	2	150	100	1.0	0.05

The test setup uses a custom-built force-displacement setup that applies a constant force while measuring the displacement and can provide an applied voltage to the actuator. The test setup is detailed in Section 3.2.2. The test procedure consists of two initial shakedown tests and testing the actuator at increasing voltages until failure. The initial cycles are used to eliminate Mullins effects and are done at 15 gf and 65 gf at 2300 V. Each test consists of cycling the voltage applied to the actuator while loaded with a constant load. The voltage is cycled in a square wave pattern at a frequency of 1/40 Hz with a duty cycle of 50% for five cycles starting with the voltage off. A square wave is chosen for the test because it results in the fastest actuation, which is one of the advantages of dielectric elastomers—a square voltage input wave results in lower breakdown voltages than ramped voltages in literature. The testing frequency was chosen because the ASTM D3755-14 standard uses 20-second tests to validate that an elastomer can support a given electric field. The 20-second test also results in transient creep-

terminated actuation, where the viscoelastic effects have settled. The five cycles enable the actuator to achieve a steady-state cyclical actuation, repeatedly alternating between two states. The voltage steps for the breakdown strength tests start at 1500 V and proceed to 2000 V, followed by increases of 100 V until failure is reached anytime during the five actuation cycles. If the actuator self-heals, the test is repeated at the failure voltage until the test is completed without any electric field breakdowns or total failure. The last voltage fully supported for a full test is then determined to be the maximum electric field the actuator can support.

DE tape actuator samples at constant force levels of 30, 40, 45, 50, 60, and 65 gf were successfully tested for dielectric breakdown strength. The measured outcome of each test is the maximum voltage level for a given force level and actuator displacement. Using the initial length and thickness, it is then possible to calculate the electric field from the displacement and the applied voltage level. Determining the elastomer's stress and total material strain is also possible. The results of the test are plotted in Figure 57.

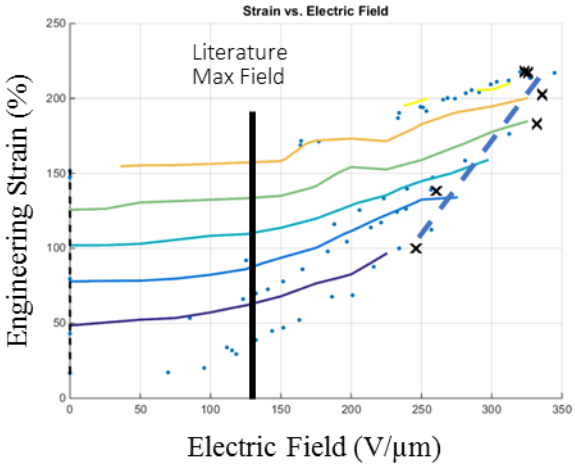

Figure 57. Maximum Electric Field Shown on a Strain versus Electric Field Plot.

The electric field and engineering strain are calculated from the initial conditions, applied voltage, and measured displacement. Each line represents a different constant force applied to the actuator while the applied voltage is increased.

The electric fields and engineering strains are calculated from the initial conditions, applied voltage, and measured displacement. Each line represents a constant force applied to the actuator while the voltage increases.

The results of this preliminary study indicate the trends and importance of the electric field breakdown of dielectric elastomer actuators. The engineering strain versus the electric field is plotted in Figure 57. The engineering strain is defined using the theoretical initial axial length of 5.3333 mm. This length corresponds to Lambda equals one for the axial stretch. The electric field is calculated using the initial thickness, the current strain state, and the incompressibility assumption for the elastomer. For each test of a different force level, the strain and the electric field increase with an increasing voltage. The total failure points are shown with black Xs. Although the data are noisy with the limited number of points, there is a strong trend of the maximum electric field increasing with increasing strain. The maximum supported electric field increased by 35% from 100% strain to 200% strain. These results demonstrate the importance of using a variable breakdown strength that is a function of strain rather than the traditional notion of a fixed breakdown strength. The high strains cause a substantial change in the maximum electric field supported.

This study demonstrated a new methodology for determining the electric field strength of an elastomer. A failure criteria for a DE actuator with self-healing electrodes was created to identify complete versus temporary failures. The self-healing electrodes enable the support of a larger electric field than for non-self-healing electrodes. The study shows a strong increase in electric field strength with strain. Determination of the maximum breakdown voltage of a dielectric elastomer is a complex process, but it is very important because the maximum supported electric fields control the limit of the actuation authority for a dielectric elastomer actuator.

3.5.3.2. Current Leakage Losses

An important aspect of dielectric elastomer actuators is that they are low-power actuators since they are fundamentally compliant capacitors. Energy is transferred from a source to the actuator to create the voltage differential that provides the actuation authority. The energy is stored while the actuator is ON and then can be transferred back to the source when the actuator is turned OFF. The actuator is not a perfect capacitor, which means that some of the electrical charge on the surface is lost as the actuator maintains the voltage differential. The power source must replace the lost electrical energy. This lost energy is known as the dielectric leakage current, and the power lost is the leakage current times the voltage differential. The strain state impacts the leakage current in elastomers. The purpose of the experiment is to evaluate the

current leakage of a tape actuator under actuation. See Table 9 for the actuator fabrication parameters. A dielectric elastomer tape actuator is cyclically actuated at a fixed voltage level against a constant external force while the displacement, applied voltage, and supplied current are measured. A tape actuator's leakage current and power loss data can be determined using the resulting data.

Table 9. Actuator Fabrication Parameters for Current Leakage Loss Study.

The same fabrication parameters were used to create all the samples for the current leakage loss characterization study.

Actuator Parameters	Solvent Mixture					
	Material Preparation			Drop-Cast		
Silpuran ID	% Silicone in Isopar G	Part A (%)	Part B (%)	Area (in^2)	Volume (ml)	Evaporation (Hr)
6000/10	80	10	90	4	2.5	48

Film Preparation				Each Electrode	
Curing		Film Pre-Stretch		SWNT and Isopropanol	
Temp (°)	Time (Hr)	Axial (%)	Transverse (%)	Volume (mL)	Density (mg/mL)
175	2	150	100	1.0	0.05

The leakage current experiment involves activating the tape actuator and measuring the resultant current. The test is performed by mounting an actuator to the force-displacement setup. A constant force, 35 gf, is then applied to the actuator. Immediately after the force is used, the initial length is captured optically, and the cyclical test is initiated. In this case, the cyclical test consists of cycling ON and OFF from a preset voltage level, 2300 V. The test frequency is at 1/20 Hz with a duty cycle of 50%. During the active test, the relative displacement of the actuator is measured along with the applied voltage and resultant current. The typical results of the current can be seen in Figure 58.

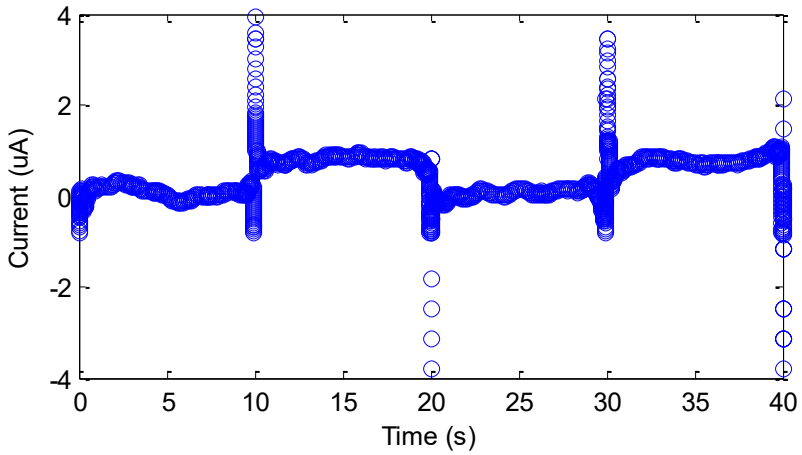

Figure 58. Measured Current During Voltage Cycling.

The supplied current is measured while a 35 gf is applied to the actuator and a 2300 voltage is cycled at 1/20 Hz with a 50% duty cycle.

The results show the expected behavior for the current with four regions: voltage OFF, actuator charging, voltage ON current draw, and sinking actuator charge. There is zero current drawn when the voltage is OFF. When the voltage is turned ON, the current draw has a vertical spike, representing the capacitor's charging. After the spike in current, the current draw settles into a relatively flat section, which is the leakage current of the actuator. At the end of the cycle, there is another spike in the negative direction, representing the current sinking back into the power supply. After the current has been sunk, the current draw returns to zero in the voltage OFF state. The leakage current is approximately $0.6\ \mu A$. Therefore, the power draw for the actuator is $1.4\ mW$ for a single tape actuator with an area of $0.0005\ m^2$. If the actuator is scaled to $1\ m^2$, then the actuator would lift 70 kg and would use $2.76\ W$. There is noise in the current data because the current being measured during the ON state is less than $1\ \mu A$, which is at the limit of what the power supply can measure. At such a low current draw, the electrical signal from the current sensor can be impacted by the high-voltage power supply or adjacent electrical signals. The low leakage current draw means the actuator will function well as a low-powered actuator.

3.5.3.3. Actuator Robustness and Repeatability with Self-Healing Electrodes

The extremely large actuation strain is one of the principal advantages of dielectric elastomer actuators. One limiting factor of large actuation strain is the maximum electric field

the elastomer can support before dielectric breakdown failure. Actuation strain is related to the square of the electric field, meaning that much of the total actuation will come from applying an electric field close to the breakdown limits. One issue with operating near the breakdown limit is that elastomers are complex materials that are hard to make and can easily include fabrication defects. These defects may have the effect of lowering the electric field breakdown strength in the defect region. Without a way to increase the lower local breakdown strength in the region of the defects, this breakdown strength becomes the effective breakdown strength of the whole film. With many types of compliant electrodes, the only way to avoid actuator failure around a local defect is to operate below the local breakdown field strength. However, this would result in an actuator with a reduced performance range. Another way to allow for local defects without compromising the performance range is to use a compliant electrode material capable of self-healing. Self-healing electrodes use the current that flows through the dielectric short to burn off the local conductive material. The reduced conductivity caused by the self-healing effect causes the electric field to be reduced below the local electric field breakdown strength in the defect region. Thus, the film can now support a higher maximum electric field with a local defect.

The SWNT electrodes used in the fabrication of the dielectric elastomer tape actuators have been shown to have a self-healing effect [55,179,269,270,286,290]. However, in Section 3.5.2.6, low-density electrodes had better strain performance but, at higher strain, would lose conductivity. In contrast, higher-density electrodes had worse comparative performance but could achieve high overall strains. Using pre-extended compliant electrodes is another complex factor yet to be explored. See Table 10 for the actuator fabrication parameters. This experiment aims to validate the self-healing ability of the pre-extended electrodes. The self-healing effectiveness will be evaluated by comparing the leakage current, actuation stroke, and actuation work between tape actuators that experience a fully cleared self-healing event and actuators that do not experience any self-healing events.

The setup uses the basic constant force setup detailed in Section 3.2.2. The general purpose of the setup is to apply a continuous force and an applied cyclical voltage to the actuator and measure the displacement. Both the supplied voltage and current are measured during the experiment. Self-healing electrodes require a resistor in series to limit the current draw when there is a short. The spike in current should be enough to burn off electrodes around the short

locally, but there should not be too much current. Too much current would cause a catastrophic failure of the actuator.

Table 10. Actuator Fabrication Parameters for the Self-Healing Electrodes Study.

The same fabrication parameters were used to create all the samples for self-healing electrodes under constant force loading study.

Actuator Parameters	Solvent Mixture					
	Material Preparation			Drop-Cast		
Silpuran ID	% Silicone in Isopar G	Part A (%)	Part B (%)	Area (in^2)	Volume (ml)	Evaporation (Hr)
6000/10	80	10	90	4	2.5	48

Film Preparation				Each Electrode	
Curing		Film Pre-Stretch		SWNT and Isopropanol	
Temp (°)	Time (Hr)	Axial (%)	Transverse (%)	Volume (mL)	Density (mg/mL)
180	2	150	100	4.0	0.4

The purpose of the experiment is to cyclically test an elastomer and measure the response before and after a short. The basic experimental procedure is to mount the actuator to the testing frame, add the external constant force, and, at the same time, take a photograph to measure the initial displacement and start the testing program. The testing program cyclically turns the voltage ON and OFF at a fixed frequency of 1/20 Hz with a 50% duty cycle. It has been shown that ramping the voltage increases the maximum electric field that can be supported [312]. Therefore, the square wave input ensures that the actuator has the most conservative result regarding electric field breakdown. The test program actuates a 1/20 Hz square wave and continues for 30 cycles. Typical results without any self-healing events are shown in Figure 59.

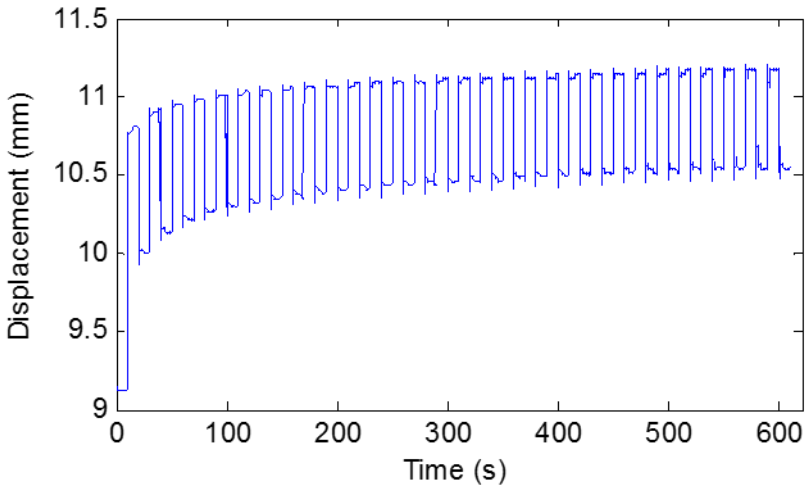

Figure 59. Typical Results from Cyclical Characterization.

Typical characterization results when there are no electrical shorts.

The data from each test are simplified and summarized by determining the displacement and actuation stroke for the final cycle when the actuator performance has reached a steady-state cyclical performance. The test applies a constant force to characterize the full performance envelope and is repeated at various force levels. This external force is varied from 10 gf to 50 gf by increments of 5 gf while cycling the 2300 V ON and OFF. A more detailed explanation of the procedure is given in Section 3.4. The DE tape actuator's relative displacement, the supplied voltage, and the resultant current are all measured for each test. The whole test must be completed without a short, or the experiment is repeated until a full iteration is completed. Eight actuators are tested and categorized into two groups: with and without self-healing events. Typical results of each category with and without self-healing are shown in Figure 60 below and Figure 59 above. Each experiment is then summarized by determining the peak stroke, work, and leakage current.

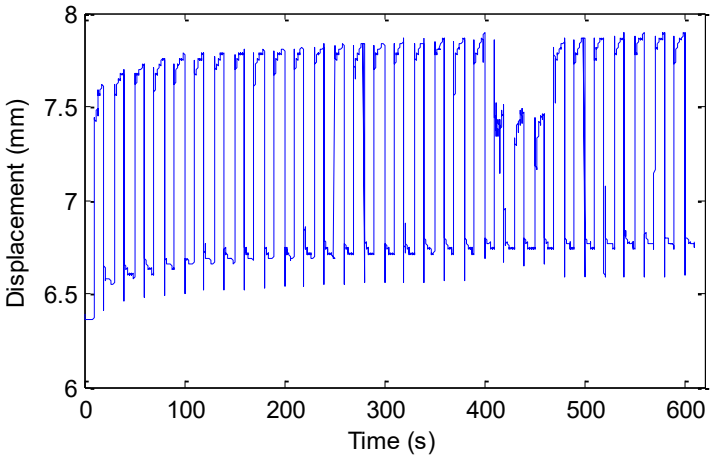

Figure 60. Full Performance After Electrode Self-healing.

Full performance after self-healing Silpuran 10% Part A 90% Part B lateral: 150% axial: 100% 0.4 mg/mL at 4 mL, 50 mm x 5.333 cyclical actuation 30 cycles at 1/20 Hz.

The typical results when a short has occurred look like Figure 60, and the typical results when there are no shorts are shown in Figure 59.

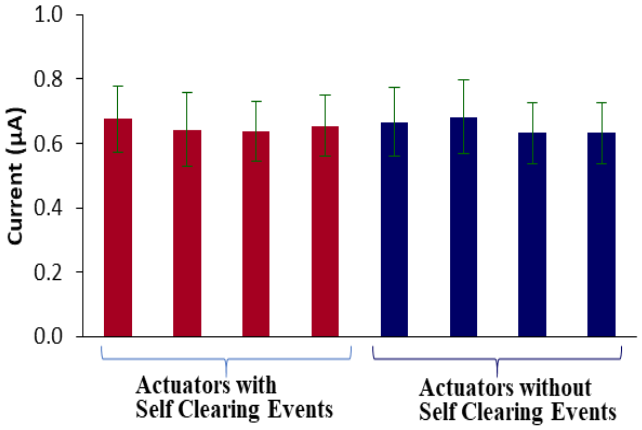

Figure 61. Actuator Leakage Current with and without Self-healing Events.

Low-leakage current Silpuran 10% Part A and 90% Part B, lateral: 150% axial: 100%, 0.4 mg/mL,50 mm x 5.333, cyclical actuation 30 cycles at 1/20 Hz.

The leakage data are summarized in Figure 61, with the average current across all cycles plotted along with the standard deviation for both actuators with and without self-healing events. The mean leakage current for both types of actuators, with and without self-healing events, is approximately the same. The differences in the averages are well within the standard deviation from the last five cycles of each actuator. The return to a low-leakage current after a self-healing

event is important because it indicates that the dielectric breakdown in the elastomer has been eliminated, as shown in Figure 62. The temporary electrical breakdown does not cause a residual power drain after self-healing. Thus, the actuator is returned to normal electrical performance.

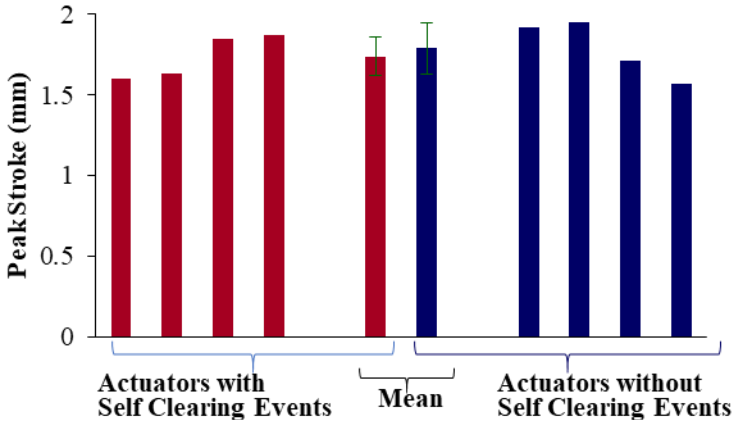

Figure 62. Actuator Peak Stroke with and without Self-healing Events.

Peak stroke recovered after burn-off, Silpuran 10% Part A and 90% Part B, lateral: 150% axial: 100%, 0.4 mg/mL, 50 mm x 5.333, cyclical actuation 30 cycles at 1/20 Hz.

Although the electrical performance has returned to baseline after a self-healing event, the actuator's stroke and work must be evaluated. The peak stroke from each of the eight actuators is plotted along with the average and the standard deviation. The average peak stroke of both categories of actuators is approximately the same, and the difference is within the standard deviation of the samples. Similar to the peak stroke, the peak work from each actuator is plotted along with the average and the standard deviation. The average maximum work of the actuators is approximately the same, and the difference is within the standard deviation of the samples, as shown in Figure 63.

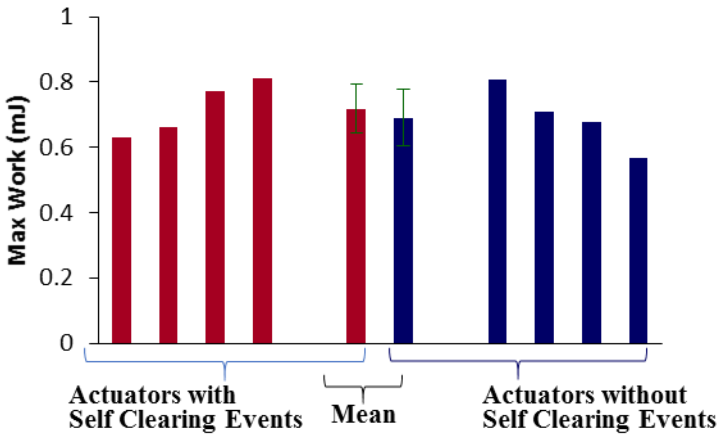

Figure 63. Actuator Peak Work with and without Self-healing Events.

Peak work recovered after burn-off, Silpuran 10% Part A and 90% Part B, lateral: 150% axial:100%, 0.4 mg/mL, 50 mm x 5.333, cyclical actuation 30 cycles at 1/20 Hz.

This experimental characterization evaluated the impact of self-healing events on DE tape actuators with pre-extended electrodes. The current leakage, peak stroke, and peak work analysis show that the actuator's performance remains approximately the same after self-healing events. Differences in the fabrication process may have caused the variation in the performance of the actuators without self-healing events. The impacts of fabrication variation appear larger than those due to self-healing events. Using SWNT as pre-extended electrodes enables the actuator to be exercised near its performance limits without having small defects compromising performance since the local defects are eliminated through self-healing electrodes. Pre-extended electrodes improve the actuation range and durability of DE tape actuators.

3.5.4. Summary and Conclusion for the Steady-State Cyclical Actuator Characterization

The technology developed through this research depends on new materials and fabrication processes. Validation tests are therefore necessary to ensure that the new actuator achieves performance expectations and that the fabrication process yields consistent results. This research required validation tests to verify the quality of the DE tape actuator's key components, namely the film and the electrode. In addition, an assessment of the DE tape actuator was required to determine which fabrication parameters are most critical to ensuring the actuator performs

reliably and effectively. Finally, the validation considered actuator performance properties under steady-state cyclic conditions to maximize performance. The key components of the DE tape actuator controlling its performance are the film and the electrode. The film thickness is a key indicator of film quality. Tests were conducted to evaluate the uniformity of thickness of an individual film, i.e., whether the film maintains its thickness across its entire area. The validation test found that the uniformity of the film thickness is adequate so that any thickness variation will not significantly affect actuation performance. The average standard deviation at each measurement location is 1 μm. Even at the worst thickness fabrication, the actuation performance was impacted by less than 4%. Therefore, the variance within the standard deviation will have negligible impacts on the actuator performance. In addition, film thickness across an entire batch of films was evaluated to verify that the film fabrication process produces similar films In terms of thickness. The validation test for batch consistency found that the films were virtually identical in thickness across the entire batch. The standard deviation of the thickness across the films was 1.1% of the thickness, which is an insignificant contribution to the variation in the performance of the actuator.

A compliant electrode must be repeatably and reliably fabricated on both elastomer surfaces to create a functional DE tape actuator. The fabrication process was evaluated by looking at the consistency of the electrode conductivity. Although the standard deviation of the electrode resistance varied up to 46% of the mean resistance, this variation is insignificant since several kilovolts are used to move the actuator. A higher resistance will potentially slow the actuation rate, but since the RC time constant is 4 μs and the actuation events of interest are in the tens of milliseconds, the impact on actuation speed is negligible. Measuring the capacitance will demonstrate whether the combination of film and electrode will result in a functional DE tape actuator. The capacitance measurement had a standard deviation of 2.8% of the average capacitance. Therefore, the validation tests showed that the film and compliant electrode fabrication process produces an actuator with consistent performance. Several fabrication parameters related to the film and electrodes impact actuator performance. The validation process requires understanding these parameters and their relative impact on the function of the actuator. Tests to determine the sensitivity of several parameters were conducted. The sensitivity of static mechanical material properties to elastomer cross-linking density was evaluated. The validation determined that cross-link density has a significant impact on film stiffness. When the

cross-link density of Part A was reduced from 50% to 10%, film stiffness dropped by 33%. The change does not necessarily lead to improved actuation performance. Similarly, the sensitivity of dynamic mechanical material properties to elastomer cross-linking density was evaluated. In this case, the cross-link density does not significantly affect the elastomer's viscoelastic properties, but the elastomer strain state significantly affects the elastomer's viscoelastic properties. Testing determined a correlation between the cross-link sensitivity and the dielectric permittivity, but the change from 50% Part A to 10% resulted in only a 10% reduction in the dielectric permittivity. Additional tests considered the sensitivity of DE tape actuator performance to three parameters: elastomer cross-linking density, film curing temperature, and electrode density. Regarding DE tape actuator performance sensitivity to elastomer cross-linking density, when cross-link density decreased from 50% Part A to 10%, the actuation stroke increased by 25%. The film reduction in stiffness caused by the change in cross-link density more than offset the reduced dielectric permittivity. As a result, 10% Part A was selected as the film that provides the largest actuation stroke without significantly compromising other properties. When looking at the sensitivity of DE tape actuator performance to film curing temperature, no significant actuation performance change was measured for different curing temperatures. However, actuator fabrication yield is significantly higher when the curing temperature is between 170C and 180C. As a result of these tests, 175C was selected as the standard curing temperature. The sensitivity of the DE tape actuator performance to electrode density was evaluated, and it was determined that the SWNT electrode density significantly affects actuation strain. Extremely high density electrodes, 0.4 mg/mL, substantially reduce actuation strain performance. High density electrodes, 0.2 mg/mL and 0.1 mg/mL, achieved the largest actuation strain. However, the performance of lower density electrodes matches that of high density electrodes until they reach a particular strain where they cannot expand further. The thinner electrodes may have reached their percolation limits when they stop expanding. Thinner electrodes are preferable if they achieve the same maximum actuation strain because they use less material and contribute less to the actuator stiffness.

Finally, the performance properties of the DE tape actuator in steady-state cyclic action were characterized in terms of electric field breakdown strength, current leakage, SWNT self-healing electrodes, and pre-extended electrodes. The characterization of DE tape actuators' electric field breakdown strength found that the maximum supported electric field increased by 35% when strain increased from 100% to 200%. The recorded dielectric breakdown strength is

approximately double what is currently found in the literature for Silpuran with a 50/50 component mix. The significant increase in dielectric breakdown strength with actuation strain indicates that dielectric breakdown strength should always be characterized in an application context. Otherwise, a substantial portion of the possible actuation strain will be unachievable by an artificially assumed dielectric breakdown strength. Characterization of DE tape actuator current leakage showed that when the actuator is scaled to 1 m2, the actuator would lift 70 kg and use 2.76 W power to hold ON the actuator. This very low leakage current means that this is an efficient actuator and will be well-suited for low power holding applications. In characterizing the DE tape actuator performance with SWNT self-healing electrodes, the current leakage, peak stroke, and peak work analysis demonstrated that the actuator's performance remains approximately the same post self-healing events. These are very effective electrodes, and even when defects exist in the fabrication process, they will allow the actuator to be used near the breakdown voltage. The self-healing electrodes mean that the quality control of fabrication does not need to be maintained at an extremely high level to produce high performance actuators, lowering the cost of producing DE tape actuators. The characterization of DE tape actuator performance from pre-extended electrodes found that the pre-extended electrodes made with 150% axial strain did not provide enhanced performance over actuators with 100% axial pre-stretch during fabrication. For the actuators fabricated with 100% axial pre-stretch, the stroke and work performance did not show a significant difference between the 0.6 mg and the 2 mg density of electrodes. The study concluded that an axial pre-stretch of 100% gives strong actuation performance, while any of the lower density electrodes with 100% axial pre-stretch may achieve good DE actuation. Using less material is less expensive, pointing to a lower density. However, these require more time to fabricate. Therefore, the 0.05 mg/mL density was selected since the fabrication time was approximately 50% less than 0.03 mg/mL.

3.6. Transient Creep-Terminated Steady-State Cyclical Actuation Characterization

Primary creep-terminated steady-state cycling is defined as steady-state cycling at a frequency such that the primary viscoelastic creep ends during each half period, as seen in Figure 27. The experimental characterization of the steady-state cyclical actuation required an experimental setup to identify the testing parameters. The experimental test setup was designed to control the external force and input voltage while measuring the length of the actuator. The

test setup was then used to identify the time required for transient creep-terminated actuation and to characterize the cyclical actuation performance. A testing procedure was then developed to characterize the transient creep-terminated steady-state cyclic performance. The dielectric tape actuators for the following test were fabricated using an early version of the fabrication method described in Section 2.3. The fabrication of the following actuator used a larger volume of SWNT, 8 ml versus 2 ml, to create the compliant electrodes compared to what is listed in Section 2.3.2.

3.6.1. Creep Displacement and Transient Creep-Terminated Characterization

Creep in hyperelastic elastomers has three phases: primary, secondary, and tertiary.

Primary Creep. Primary creep starts when stress is applied. The primary creep is a transient phenomenon that ends relatively quickly after the start of creep. The precise material will dictate the duration of the primary creep phase and can range from seconds and minutes to hours and days. The primary creep phase ends when the rapidly decreasing creep rate appears to reach a constant rate, which starts the secondary creep.

Secondary Creep. The secondary creep works on a very slow constant strain rate which is significantly smaller than the primary creep. The secondary creep may not affect the length of the elastomer. The lack of noticeable change in length is because the secondary constant strain rate is so slow that it causes insignificant changes in length in the time frame of the primary creep rate. The secondary creep phase ends when the elastomer has reached its elastic limit.

Tertiary Creep. Tertiary creep is a plastic deformation mostly caused by the slipping of the polymer chains and is also associated with necking and void forming. Secondary and tertiary creep are important phenomena to understand the long-term life but can also be on a time scale that they are irrelevant to the life of a dielectric elastomer actuator.

An active creep test determined the appropriate time frame for a transient creep-terminated cyclical actuation. The test consists of applying a constant external force and a Maxwell stress from an applied voltage differential and measuring the displacement as a function of time. The custom experimental characterization apparatus described in the previous section was used for this test. The external constant force was the median force level of the characterization range, 40 gf. The applied voltage differential was selected to match the characterization voltage level of 2300 V. This voltage level was chosen because it is approximately 90% of the lowest breakdown

voltage experimentally determined. The 90% level allowed the actuators to be consistently characterized without reaching the breakdown voltage limit. The typical results of one of the experimental runs are shown in Figure 64 below.

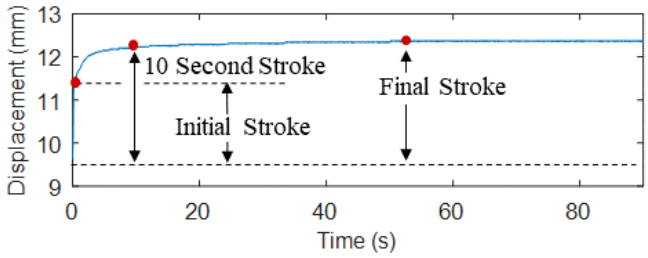

Figure 64. Creep Characterization with High Voltage Applied.

Active creep results showing displacement as a function of time. Different regions of the creep displacement are identified.

The results of the active creep test had three distinct regions: initial actuation, fast viscoelastic effects, and slow viscoelastic effects. The Maxwell stress caused The initial displacement within the first 50 ms, accounting for 62% of the actuation. At 10 seconds, the fast time constant viscoelastic effects had expired, and the displacement achieved 95% of the steady-state actuation. After 50 seconds, the actuation achieved a stable, steady-state displacement. There may be a much longer viscoelastic time constant that causes the actuator to continue to stretch; however, due to the desire for steady-state actuation over an intermediate time frame, the longer time constant does not matter. For intermediate time scales, the tape actuation can be assumed to have achieved transient creep-terminated displacement at 10 seconds when it has achieved 95% of the long-term displacement.

3.6.2. Experimental Determination of Characterization Process Parameters

The characterization procedure consisted of two initial shakedown tests followed by testing at discrete constant force levels across the actuator's whole operating range. The shakedown and the individual force level tests used the same procedure to characterize the actuator's steady-state cyclical performance. Each test consisted of the external cycling of the actuator for a fixed number of cycles at a constant frequency and external force.

The experimental procedure for a single test included applying the external load, documenting the initial displacement, and running the custom LabVIEW program that controlled

the experiment. In each test, the voltage was cycled in a square wave pattern at a frequency of 1/10 Hz with a duty cycle of 50% for 30 cycles, starting with the voltage off. A square wave was chosen for the test because it results in the fastest actuation, one of the advantages of dielectric elastomers. The square wave has also resulted in lower breakdown voltages than ramped voltages, making for a rigorous actuation[312]. The frequency was chosen because an experimental characterization showed that the tape actuation would achieve 95% of the complete actuation in under 10 seconds.

The shakedown tests eliminated the transient viscoelastic effects and ensured that the actuator could operate at the highest applied electric field and lowest film breakdown strength. The use of shakedown cycles to better achieve steady-state cyclical results was experimentally validated and is detailed in the Appendix. The shakedown tests were done at 15 gf and 65 gf at 2300 V, the minimum and maximum force range to be tested. The 15 gf cutoff is the lowest force that provides enough axial pre-stretch so that the applied 2300 V causes the actuator to have a useful displacement. The lowest force applies the lowest pre-stretch on the film, which correlates to the lowest breakdown field strength. The 65 gf level provides a large axial pre-stretch, which causes the elastomer to approach its hyperelastic limit before actuation. Therefore, the actuator's stroke is small because the applied Maxwell stress works against a highly stiffening film. The maximum force level also results in the largest applied electric field because the film has its lowest thickness.

After the actuator was mounted and the shakedown tests completed, the actuator was ready to be characterized. The general characterization of the actuator was done by characterizing the performance from 15 gf to 65 gf in increments of 5 gf at a fixed voltage of 2300 V. After each test, the applied external load was removed from the actuator and used again at the start of the next individual test. The typical inputs and outputs of the experimental test are shown in Figure 65.

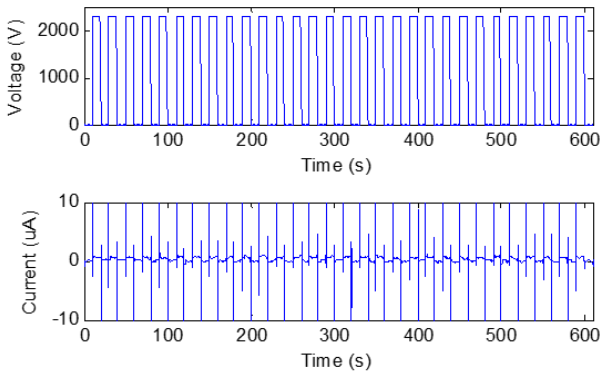

Figure 65. Typical Time Plots of Input Voltage and Current.

Voltage and current versus input voltage and current for cyclical actuation. The voltage is a square wave with a frequency of 1/10 Hz and a duty cycle of 50%. The peaks reach 2300 V while the valleys are at 0 V.

Figure 65 shows the measured electrical outputs of the voltage and current. The current plot shows a positive spike when the voltage is turned on and a negative spike when the voltage is turned off, which correlates to charging and discharging the actuator. The ON state current shifts from 0 A when the voltage is OFF to less than 1 μA when the voltage is ON. The small current level when the voltage is ON represents the leakage current of the actuator, which can be used to determine the holding power required to keep the actuator energized.

Figure 66 shows the displacement as a function of time. When the high voltage differential is applied, the actuator increases in length during the first cycle. During the subsequent cycles, the actuator continues to creep in length at the end of each LOW and HIGH voltage input. At around 400 seconds, the actuator appears to reach steady-state cyclical performance. By Zooming in on a single cycle, it is possible to see the bouncing that occurs as the actuator changes voltage state, which is the fast transient viscoelastic effect. The length at each state reaches a transient creep-terminated equilibrium length.

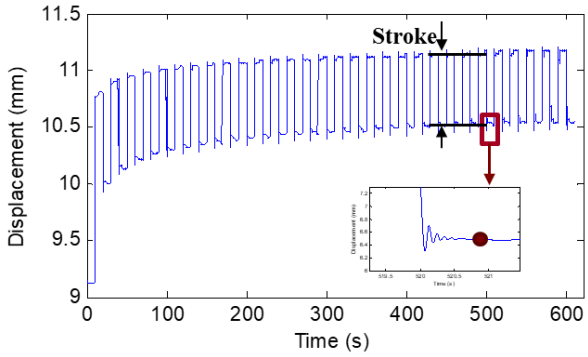

Figure 66. Cyclical Actuation Displacement.

Actuator length as a function of time during cyclical actuation.

The length results can be further analyzed determining the stroke of the actuator as a function of each cycle. The binary LOW and HIGH states can be extracted from the cyclical data by selecting the length at the end of each LOW and HIGH state. The difference between the two extracted lengths can be plotted for each cycle, which is the stroke. The stroke as a function of cycle number is plotted in Figure 67.

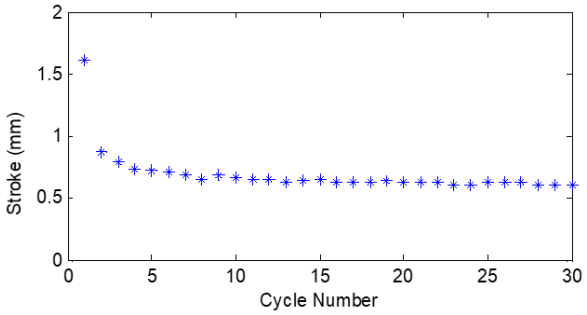

Figure 67. Cyclical Actuation Stroke.

The actuation stroke settles to approximately steady stroke after 5 cycles. Short-term viscoelastic effects have completed their processes.

The stroke of the first cycle is significantly larger than the subsequent cycles. The actuator continues to lose some strokes over the next few cycles. After five cycles, the actuator reaches a steady-state stroke. Even though the stroke becomes constant after five cycles, the actuator increases in length slightly. The impact of the change in length is highly dependent on the external application and can vary from insignificant to impactful.

3.6.3. Transient Creep-Terminated Steady-State Cyclical Actuator Performance

The actuation performance for different applications can have changing requirements. A pump may need to increase or decrease its pumping rate, or a flapping machine may need to increase the rate to go higher or decrease the rate to go lower, and finally, the walking pace may need to be sped up or slowed down. Therefore, knowing the steady-state cyclical performance across a wide performance range is desirable. One easy way to change the performance metrics for a DE actuator is to change the driving voltage. The performance of DE actuators is directly related to the driving voltage, which creates the electric field that drives the Maxwell stress, causing the actuation. To fully characterize the performance of a DE tape actuator, the performance should be evaluated across its entire range of possible voltages and loads. The steady-state cyclical characterization method, explained in Section 3.4, can be repeated at a range of fixed HIGH voltage levels to capture the whole performance.

The development of a consistent performance characterization methodology enabled the discovery of limitations of the existing fabrication process. The discovery of the fabrication limitations enabled modification of the fabrication process, resulting in the final fabrication parameters described in Section 2.3. The steady-state cyclical experimental methodology parameters, cycle time, and number of cycles to reach a steady-state changed from what is described in Section 3.3.1 because of the enhanced performance caused by the refined fabrication parameters. The experimental methodology described in Section 3.4.1.1 was repeated to determine the number of cycles and time to achieve steady-state cyclical actuation. The refined tape actuator test sample needed five cycles to achieve steady-state equilibrium, using 41 seconds to reach transient creep-terminated performance. Each cycle had a 50% duty cycle and included a 0.5-second ramp in each direction to eliminate transient bouncing, which is irrelevant to the steady-state performance. The actuator was tested with an external force from 15 gf to 65 gf in 5-gf increments.

The typical results of the displacement of the actuator as a function of time are shown in Figure 68 for a fixed-force level of 40 gf and four different ON voltage levels: 0 V, 1500 V, 2100 V, and 2500 V. There are two rates of viscoelasticity that the cycling testing allows to settle out: fast and slow. When Looking at a single cycle, it is possible to see that the 20-second characteristic time allows the settling out of 96% of the fast viscoelastic effects. A slower term viscoelastic effect settles out by the fifth voltage cycle, and displacement is achieved within 5%

of steady-state behavior. All voltages tested reached a steady-state cyclical length by the fifth cycle. The individual test for each voltage and load level is reduced to two data points: OFF state displacement and ON state displacement. Both data points are taken within the fifth cycle, one when the slow viscoelastic effects have settled out and one at the end of the cycle time when fast viscoelastic effects have settled out, as shown in Figure 68.

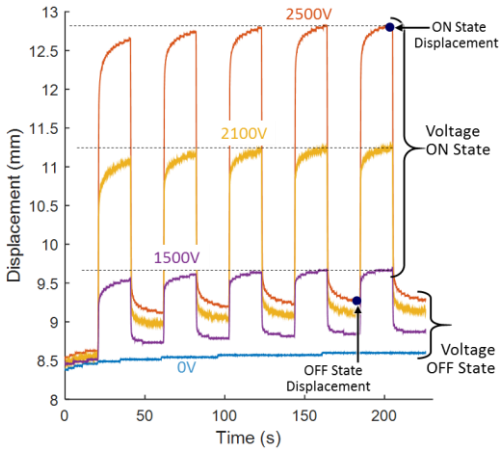

Figure 68. Typical Displacement Versus Time.

Typical displacement versus time for cyclically actuated tape actuators.

The 0 V test data represent a creep test that shows the long viscoelastic effects. The OFF voltage curves all end up at significantly different lengths after starting at the approximate same length. With the higher voltage, curves have a longer length. However, the difference between the OFF lengths decreases as the voltage increases. The small increase in length occurs at both the OFF and ON voltages, which means that the stroke remains relatively constant in each cycle.

The simplification of the performance characterization data into a force-displacement graph is shown in Figure 69 for a characteristic set of voltages. Each curve has the same basic hyperelastic shape; however, The displacement curves for the ON state move to the right (i.e., increase in length) with higher voltages. The largest separation between the OFF and ON curves occurs in the middle stretch range of the actuator. These performance curves represent the performance capabilities of a DE actuator across a wide range of external forces and voltages. A DE tape actuator can reliably actuate more than 25% strain for cyclical actuation. The stroke and work performance can be tailored to the desired performance by adjusting the external load and the applied voltage. The actuator can be easily adjusted by changing the driving voltage.

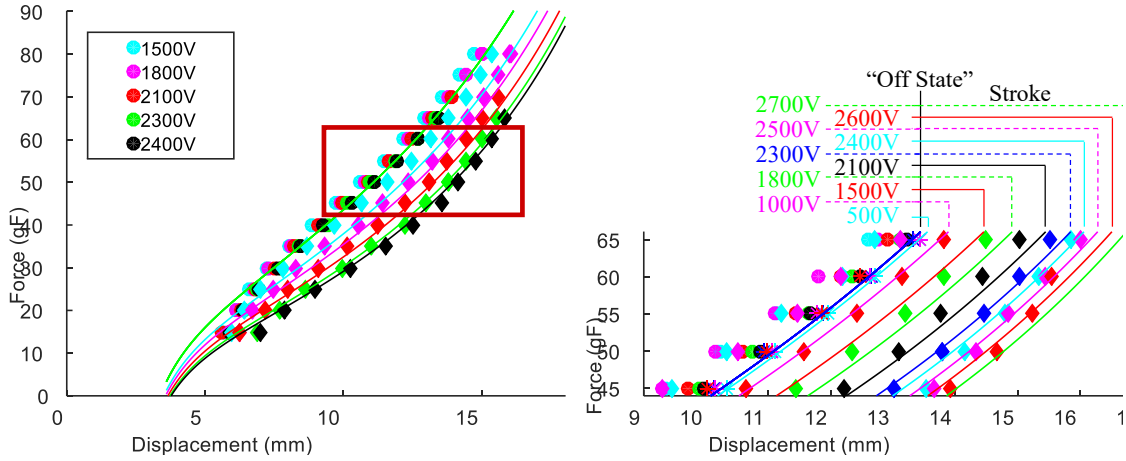

Figure 69. Summary of Cyclical Characterization Data.

Summary of cyclical characterization data into a force-displacement graph. The left figure show the full data set range and the right figure shows an expanded view of the red square region of the graph

3.7. Tape Actuator Modules in a Stack Architecture with Performance Characterized for Transient Creep-Terminated Steady-State Cyclical Actuation

The final step in the application context characterization methodology is Step 5: thoroughly characterizing the actuator performance. A significant attribute of dielectric elastomer tape actuators is their compact package and modularity. To fully comprehend these benefits, multiple modules must be assembled into a larger architecture and characterized using the process previously employed for steady-state cyclical actuation.

A notable challenge for dielectric elastomer (DE) actuators is their low force output. One solution is to use multiple actuators to improve performance. This study investigates the performance scaling of multilayer DE tape actuators and explores the losses associated with the assembly and use of multiple modules. It also highlights the capabilities of the multifunctional tape connectors in enabling modularity. Stacking DE tape actuators can enhance actuation performance by increasing the external force output without enlarging the footprint.

The experimental characterization must capture the information required to determine actuation losses from the architecture assembly process to evaluate the modular scaling effectively. It should also demonstrate the efficiency of the multifunctional tape connectors when stacked.

DE tape actuators are modular and when stacked, the force output should scale with the number of layers. The stroke of the actuators should stay constant as the number of layers increases, although some losses from stacking are anticipated. The stroke should not alter with additional layers if the alignment is perfect. Misalignments are inevitable, but dielectric elastomers should handle these well owing to their compliant nature. Consequently, the force and work are expected to scale with the number of layers, and the stroke will slightly decrease as the number of layers increases.

3.7.1. Stack Actuator Experimental Characterization Procedure

The experimental characterization of the multilayer tape actuator performance used the steady-state cyclical actuation characterization method, described in Section 3.4, to determine the actuator performance as individual elements and then combine these into a stack. Each actuator was created following the methods described in Section 2.3. The multilayer actuators were created by assembling individual actuators on top of each other. Subsequently, the multilayer actuators are layered on each other to produce a larger stack actuator.

The initial set of actuators started with eight single-layer actuators, producing four 2-layer actuators. The four 2-layer actuators led to the creation of two 4-layer actuators. The two 4-layer actuators were then assembled into a larger stack. However, a single actuator was torn and removed during stacking, leaving a final 7-layer stack actuator for testing. The individual actuators were randomly paired to assemble the multilayer actuators. At each assembly stage, each actuator was experimentally characterized.

A constant external stress was applied to each actuator for easy performance comparison. The external force applied to each actuator was scaled by the number of layers, which resulted in each actuator reacting against a constant force per layer. The external force parameters for the test varied from 10 gf x (number of layers) to 60 gf x (number of layers) by increments of 5 gf x (number of layers) while cycling the voltage ON and OFF at 2300 V.

3.7.2. Quasi-Static Stack Actuator Performance Results Simplified from Transient Creep-Terminated Steady-State Cyclical Actuation

The steady-state cyclical actuation experimental results are summarized into a single force-stroke graph, as shown in Figure 70. The results from the testing show the typical shape for the force-stroke curves for each multilayer actuator. The blue circle represents the single-layer

actuator performance, the red triangles represent the 2-layer actuators; the green squares represent the 4-layer actuators, and the black circles represent the 7-layer actuators. The performance curves all have the same characteristic shape, a rotated parabola, as seen in the typical force stroke in the previous section, as shown in Figure 31. The stroke is initially small at low loads and grows with the external force as the electric field grows from the constant applied voltage. After the peak stroke level, the stroke decreases until the maximum load is reached.

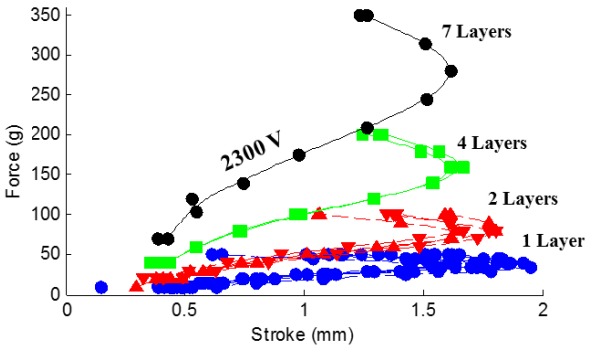

Figure 70. Multilayer Force-Stroke Comparison.

Force-stroke for 1, 2, 4, and 7 layers. The peak stroke decreases as the number of layers in the actuator increases. As more layers are added, the loss of stroke decreases.

These results demonstrate that the force roughly scales linearly with the number of layers, as expected. The multifunctional tape connectors can maintain electrical and mechanical connections in a stack actuator. The bond between the frame and the film had sufficient strength to support at least 7 times the maximum force level for a single actuator. The stroke of the actuators at the maximum force level increases from the 1-layer actuators to 2-layer actuators and from the 2-layer actuators to the 4- and 7-layer actuators. By distributing the load among multiple layers, each film may not stretch as far toward its hyperelastic limit. Limiting the stretch would cause the total actuator stroke to increase at higher loads because the film is not constraining the higher electric field as much. There appears to be a decrease in the peak stroke as the number of layers increases, which may be caused by misalignment of the actuators when stacked; this would mean that the films are not as fully stressed in actuators with fewer layers.

These same data can also be replotted into the force-work plot to verify the scaling of the work performance, as shown in Figure 71. The shapes of the curves are similar except scaled. The work is small at low forces because the actuator has a low force and a small stroke. As the

force is increased, the stroke also increases, which causes the work to increase until a peak is reached. At peak work, the stroke has decreased faster than the corresponding increase in force levels. The peak work level has shifted higher toward the maximum load of the actuator. When compared, the force-stroke and force-work graphs have different peaks, so a trade-off must be made when selecting the level to operate a DE tape actuator. The scaling of the work and the force levels with a DE tape actuator demonstrate how to compensate for the low-force challenge inherent in dielectric elastomer actuators.

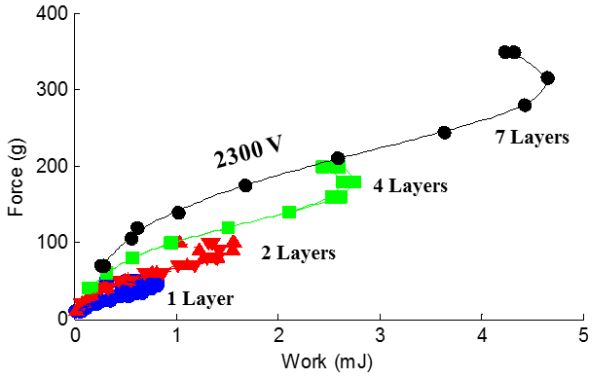

Figure 71. Multilayer Force-Work Results.

Force-work of 1, 2, 4, and 7 layers. The force and the work of the actuator both increase as the number of layers increases.

Although these two charts exemplify multiplying the performance by the number of layers, it is difficult to analyze the performance losses caused by the layering of the actuators. Another way to present the same data is to analyze the performance on a per-layer basis. The force-displacement and force-stroke performance normalized by the number of layers is shown in Figure 72 and Figure 73.

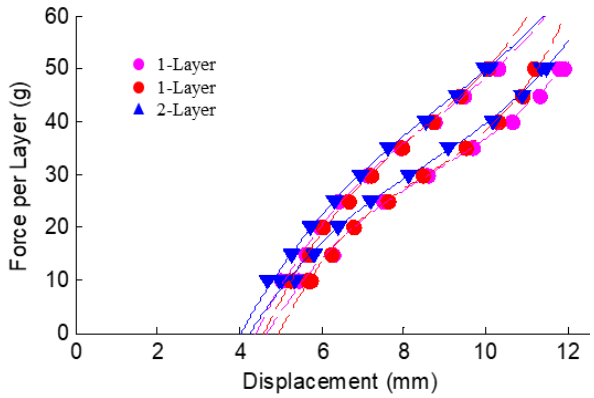

Figure 72. Force-Displacement Performance Curve per Layer.

Force-displacement per layer at 0 V and 2300 V. When the force-displacement is normalized by the number of layers, the actuation performance is similar.

The pink circle data represent the 2-layer actuators, the blue triangle data represent the 4-layer actuators, and the red circles represent the 7-layer actuators. The normalized performance for the force-displacement curves all exhibit the typical force-displacement curve for a DE actuator's voltage OFF and voltage ON curves. They all have an initially stiff region followed by a strain-softening region until the material stiffens as the hyperelastic limit approaches. The normalized force-stroke data also show that the stroke performance is similar; however, there is a noticeable drop in the peak stroke from the 2-layer actuators to the 4-layer actuators. There is a smaller drop in performance between the 4-layer actuators and the 7-layer actuators.

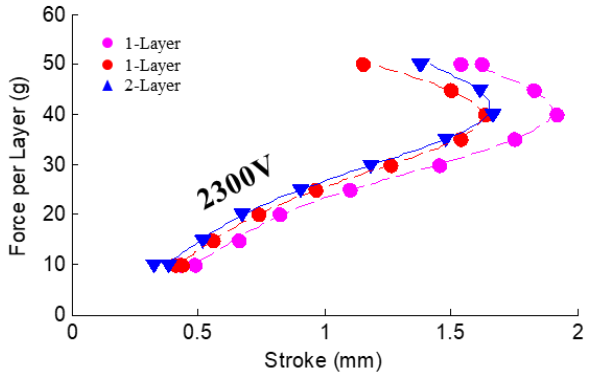

Figure 73. Force-Stroke per Layer at 2300 V.

Force-stroke per layer at 2300 V. When the force-displacement is normalized by the number of layers, the actuation performance is similar.

Quantifying the drop in performance for stroke and work should be done numerically per-layer basis. The average performance level and the deviation are plotted in Figure 74. There is an 8% loss in the average stroke, from 1.76 mm to 1.62 mm, between the single-layer actuators and the 7-layer actuators. The average work lost from the single-layer actuators to the 7-layer actuator is 6%, from 0.70 mJ to 0.66 mJ.

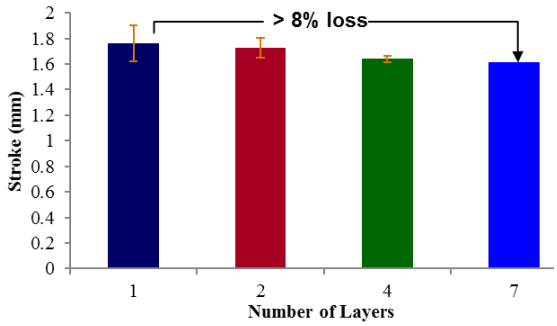

Figure 74. Dielectric Elastomer Actuator Work Loss per Layer.

Dielectric elastomer actuator work loss per layer in a stack architecture.

This qualitative study of multilayer dielectric elastomers demonstrates the advantages of larger architectures to mitigate the challenge of DEs being low-force actuators. The fabrication of the stacked actuators demonstrates The capabilities of the multifunctional tape connectors without any additional materials required besides multiple tape actuators. Since only a limited number of stacked actuators was used to verify the scaling of the performance and measurement of the losses, the performance and losses presented here are a qualitative representation or a very rough quantitative representation of the stacking potential of tape actuators. Elastomers are inherently variable in their performance because they comprise an enormous number of polymer chains, and their macro performance level is based on the statistical average of all the polymer chain interactions. Therefore, there is some statistical variation in the performance of DE tape actuators. A much larger study is required to completely validate the performance losses to determine a statistical variation in the performance levels. The theory is that DE actuators can be scaled through stacking, which is proven by the results of this study. The general scaling has been validated, and the losses have been characterized, with the results being limited to losses in stroke and work caused by the stacking. Fundamentally, DEs are thin and flat, and the whole package remains thin and flat with multifunctional tape connectors. Therefore, stacking actuators

increases the performance without increasing the footprint of the package, and the package remains thin and flat.

3.8. Conclusion for Application Context Approach to Dielectric Elastomer Actuator Characterization

Following the creation of the new DE tape actuator architecture, it became imperative to develop an accompanying characterization methodology. Fundamentally, this new methodological approach uses application context to characterize DE actuators. The power of this new characterization process was demonstrated using the steady-state cyclic application context. The elegance of this methodology is that it simplifies the characterization data using a binary paradigm to easily present it as force-displacement information to predict the performance for binary actuation. The new characterization methodology was demonstrated with two versions of the DE tape actuators possessing different performance properties.

In addition, the methodology displays the conformal, compact, and distributive properties of the DE tape actuator while verifying the actuator's large-strain actuation performance. The DE tape actuators have demonstrated that it is possible to take full advantage of the unique properties of DEs while at the same time minimizing the challenges of working with soft polymers. The multifunctional tape connectors were robust, thin, conformal, and capable of creating larger, multilayer architectures. While a significant potential drawback for DE actuators is that they are low in force, this research revealed that the challenge of low-force actuation can be overcome using a multilayer actuator, and it illustrated the potential for these multilayer actuators to enhance actuation force while maintaining a compact package. Finally, the research demonstrated that the performance of DE tape actuators can be easily tailored by varying the external force and the applied voltage.

The outcomes of this work creating a characterization methodology, ascertaining that steady-state cyclical actuation can be portrayed as binary actuation, determining that DE tape actuators can be used in multilayer configurations, and identifying how external force and applied voltage impact DE tape actuators are significant contributions that promise to simplify the task of understanding DE tape actuation performance as it pertains to industrial applications.

Chapter 4 Modeling of Cyclical Dielectric Elastomer Actuation

The advancement of dielectric actuator technology calls for the creation of analytical models capable of predicting an actuator's performance and aiding in actuator, device, and system design. These models should allow for easy identification of calibration data points and accurately predict actuation performance. An effective design model will also help develop an intuitive understanding of how model parameters influence performance.

Effective material parameters are often used to encapsulate complex behavior and properties In modeling smart material actuators, which frequently exhibit complex behaviors like hysteresis and viscoelasticity. The performance of a dielectric elastomer actuator depends on its base elastomer's material properties, including its hyperelastic curves, viscoelastic effects, and history-dependent properties.

Creating analytical models for dielectric actuators can be challenging due to their inherent viscoelastic nature, often necessitating complex, time-dependent models. However, this complexity can potentially be mitigated by adopting the application context methodological approach outlined in the previous chapter, Chapter 4. focusing on the desired actuation performance can simplify complex viscoelastic performance data into quasi-static Force-Length space. Viewing the actuation performance data through the lens of a binary actuator is one way to achieve this simplification which then allows the capturing of complex viscoelastic actuation performance using a simple, time-independent model.

The initial decision in modeling dielectric elastomer actuators involves choosing between a hyperelastic, time-invariant model and a viscoelastic model. This choice represents a trade-off between prediction accuracy over a broad performance range and model simplicity. While easier to understand and accurate at their calibration points, time-invariant models lose significant accuracy when variables and parameters change from the calibration point. Conversely, viscoelastic models, although more accurate and complex, require more calibration data and expertise to use effectively.

A system-based modeling approach that considers the application context can simplify model development. Developing simple, time-invariant models that accurately predict actuation performance across a broad actuation range is possible. The application context encompasses the actuator's usage, the type of actuation required, and the actuator architecture, thereby controlling and limiting actuation performance.

Once an application context has been defined, the selected actuator should be fully characterized, as outlined in chapter 3. The process of model development commences with application context characterization data. If the performance data has been simplified into the quasi-static Force-Length space, identify an existing time-invariant model that aligns with the actuation performance characterization data. All parameters and variable combinations should be plotted, focusing on identifying patterns. If no patterns or trends are found or simplification is possible, alternative models may be necessary.

4.1. Review of Dielectric Elastomers and Elastomer Mechanics Modeling

This section contains a basic review of the operation of DE actuators, elastomer material modeling, and DE actuator modeling. The operation section covers how a DE actuator functions and how it can be represented graphically. The elastomer modeling covers both simple quasi-static hyperelastic material models and full transient viscoelastic models, including the limitations of both models. The DE modeling covers the advantages and disadvantages of using each model to represent steady-state cyclical actuation.

4.1.1. Overview of Dielectric Elastomer Modeling Approaches

Dielectric elastomer actuator models are based on elastomer material behavior models on top of which the effects of the electric field are added. The basic models use a hyperelastic constitutive model to represent the quasi-static stress-stretch behavior of the elastomer and a Maxwell stress boundary to define the impacts of the electric field [33,35]. More complex models add more time-dependent elements than hyperelastic models to capture the viscoelastic effects. The Standard Linear Model is one such model that can capture the full transient properties. However, many transient effects have settled out in steady-state cyclical actuation and are unnecessary to predict the binary actuating states. For binary actuation, switching between two states using a simple hyperelastic material model to represent the performance is possible.

The simple modeling approach using hyperelastic material models is most accurate when the binary states are steady-state and not changing between cycles. However, if the operating voltage changes for the same operating frequency, the steady-state viscoelastic effects will also change, causing this simple model to lose accuracy. Another simple hyperelastic model can be calibrated to the new operating condition, but this limits the utility of a simple model if it needs to be recalibrated for many operating voltages. This change in actuation performance can be captured with a fully transient model and a single set of parameters. However, the increased complexity of a fully transient model increases the number of needed parameters over a simple model and increases the difficulty of using the model for design. Therefore, current models have limitations when trying to represent the performance of a steady-state cyclical operation of a DE actuator. It would be preferable to have a simple, non-transient model that could accurately represent the steady-state cyclical actuation when operating at different actuation authorities.

This chapter derives a simple quasi-static model that captures the steady-state cyclical performance operating at a fixed frequency and the changing viscoelastic effects of operating at different driving voltages. The DE actuator model predicts the steady-state cyclical actuation performance using a single additional term, variable shear, in the Gent strain energy equation. The new term captures the impacts of the steady-state viscoelastic effects of being cyclically driven at a range of fixed forces and voltages. A general variable shear Gent DE actuator model is derived from the first principles under steady-state cyclic operation. The model is applied to a particular actuator architecture with appropriate assumptions and boundary conditions. The new parameter in the Gent model is derived from the phenomenological effects. Therefore, every parameter has phenomenological meaning. The steady-state cyclical characterization methodology at two ON voltage levels is used to characterize the actuator's performance and identify the mechanical model parameters. A different experimental test is required to determine the electrical model parameter. Minimizing the required number of parameters in the model to capture all the relevant features enables a simple parameter identification process and reduces the number of experimental test results needed for parameter identification. Simple model validation is done to validate the performance at a single voltage level, after which the model with a single set of model parameters is used to compare the performance to experimental data across a wide range of forces and voltages. Finally, the assumption of a variable shear term is validated, and the complete model's performance is shown to significantly increase the model's accuracy across

a wide range of operating conditions compared to a standard Gent model. The result is a model and characterization methodology that captures all the salient behaviors of steady-state cycling with minimal complexity.

4.1.2. Elastomer Material Models

Dielectric elastomer modeling typically uses the stress-stretch performance of the elastomer as the basis for determining the actuator's performance. A hyperelastic curve defines The stress-stretch behavior of an elastomer. Elastomer materials are intrinsically viscoelastic but can have a wide range of viscoelastic properties, from mostly elastic to very viscous. Depending on the type of actuation, the model accuracy desired, and the viscoelastic behavior of the elastomer, it is possible to model the elastomer performance using either a quasi-static hyperelastic material model or a fully transient viscoelastic model. Dielectric elastomer actuator modeling adds the impacts of the applied voltage difference, Maxwell stress, the actuator configuration, and the type of actuation. While both types of models can be used to demonstrate steady-state cyclical actuation, they each have trade-offs of accuracy versus complexity that need to be balanced for the desired application.

4.1.2.1. Hyperelastic Material Properties

Elastomers are formed from many long polymer chains. The connections and interactions between these polymer chains enable the large elastic stretching of elastomers. The polymer chains' base materials are monomers typically made of silicone, oxygen, carbon, or hydrogen. The monomers are combined in a polymerization process to create polymer chains. Elastomers are formed by creating chemical cross-links between the individual polymer chains. The length of the polymer chains and the number of chemical cross-links between the chains are the factors that control the behavior of the elastomers. The macro behavior of the elastomer is an average of the individual interactions between polymer chains. The elastic properties of the polymer are due to the changes in the configuration of the polymer chains. They are initially configured in some amorphous, non-straight shape where the polymer chains can be considered coiled. As the polymer chains are stretched, they straighten out, and upon relaxation, they return to an amorphous coiled state. Since chemical bonds are not being broken in the stretching process, it is possible to return to the initial configuration without any permanent changes. The mechanical

properties of the elastomer are related to the forces needed to stretch the polymer chains. As an elastomer is initially stretched, the material's stiffness is correlated to the required forces to uncoil the polymers. The stiffness decreases Upon further stretching because the forces needed for stretching correlate to the straightening of the non-straight polymer chains. The ultimate stiffness of the elastomer is reached when the polymer chains have been fully straightened and can no longer be stretched without breaking chemical bonds [217,313,314].

4.1.2.2. Hyperelastic Material Models

Hyperelastic material models capture the essential quasi-static elastomer material behavior. Three classifications of models are used to represent elastomer materials: phenomenological, mechanistic, and hybrid. Phenomenological models statistically describe the behavior of a hyperelastic curve and often use many parameters to capture the essential behavior. Mechanistic models use the underlying behavior and interaction of the polymer chains to describe the behavior. The hybrid models combine the properties of the other two model types. Three phenomenological models often used in DE models are the Ogden, Mooney-Rivlin, and Yeoh [52,249,314–316]. Polynomials enable these models to represent the hyperelastic curve of any elastomer accurately. The earliest DE models used a Neo-Hookean mechanistic model [33,195,317] These models captured the initial and strain-softened stiffness but could not represent the increase in stiffness as an elastomer approached its hyperelastic limits. The Gent strain energy equation is A common hybrid model used for elastomer modeling [318]. A simple two-parameter model captures the full basic hyperelastic material profile. The parameters also have phenomenological meaning, which aids in the intuitive understanding of the model. All these models are used to represent the elastic behavior of polymers but are incapable of representing the more complex time-dependent elastomer behavior, which includes viscoelasticity.

4.1.2.3. Viscoelastic Properties

Polymer chains, the base of all elastomers, form a viscous fluid before cross-linking. The resulting polymers' viscosity depends on the length of the individual polymer chains. Longer polymer chains form a more viscous fluid, and shorter polymer chains form a less viscous fluid. After cross-linking, the elastomer material will retain some viscous properties. For an elastomer,

viscoelasticity is defined by the change in performance as a function of time. Viscolasticity presents itself in two main ways when dealing with elastomers in DEs. A simple manifestation is the elastomer creep response to increased stress on the elastomer. A change in stress causes the elastomer to change length. Initially, there is an instantaneous response, the elastic response, after which the elastomer will keep lengthening at a decreasing strain rate, which is the viscous response. A position-controlled experiment also exhibits the viscoelastic response, increasing the material stiffness as the strain stretching rate increases [319].

4.1.2.4. Viscoelastic Material Models

Capturing an elastomer's full transient viscoelastic behavior requires a more complicated model than the basic hyperelastic material models. The Standard Linear Model is a relatively simple transient model that can capture the viscoelastic behavior of an elastomer. This model comprises a hyperelastic spring in parallel with a spring and dashpot in series. The spring and dashpot in series is called a Maxwell material model. The simplest Standard Linear Model uses linear elements in the Maxwell material model to capture the viscoelastic effects. When dealing with multiple time scales, it is required to increase the complexity of the model further. The additional time scales can incorporate nonlinear viscoelastic elements or add additional terms. A more generalized model that can capture the transient properties in any time frame is the Generalized Maxwell Model, also known as the Maxwell–Wiechert model. The Maxwell–Wiechert model adds more Maxwell material elements in parallel to capture the viscoelastic effects at different time scales. DE actuator models have used the Standard Linear Model and Maxwell–Wiechert models [58]. These models can be used with control algorithms to create fully transient control of a DE actuator [320–324].

4.1.3. Quasi-Static Design Modeling Using Steady-State Cyclical Actuation Performance

When modeling this cyclical steady-state performance, defining the critical point during a cycle where the performance will be evaluated is first necessary. The essential points of interest for binary actuation are the force and displacement values at the end of each half-cycle. Figure 75 shows the HIGH -state points as squares and triangles, while circles and stars represent the LOW -state points. The points can only be measured for transient creep-terminated steady-state actuation after the actuator has achieved steady-state actuation. In the example in Figure 75, this

occurs after the start of the third cycle. Limiting the data that needs to be predicted simplifies and limits the performance data that the model predicts. The steady-state force-displacement positions at the end of each half-cycle can be replotted in the force-displacement space shown in Figure 76. If this experiment is repeated at a range of force levels, then a HIGH and LOW state force-displacement curve can be derived for each operating voltage. A quasi-static zero voltage line, V_o, is also plotted. This line represents the steady-state performance when there is no actuation. The curves' separation depends on the viscoelastic properties of the base elastomer material and the characteristic time scale of interest. For a fixed external force level, the steady-state cyclical length of the actuator for each of the two binary states lengthens as the applied cyclical voltage increases.

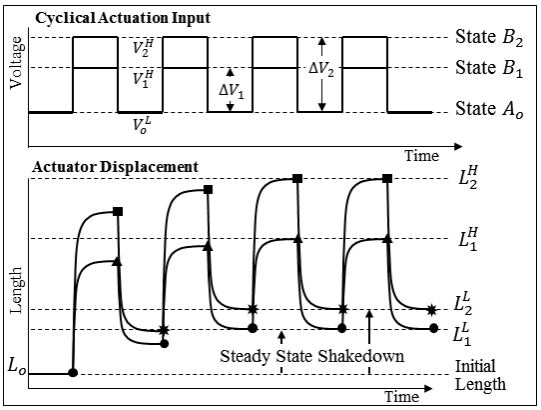

Figure 75. Schematic Graphs of Cyclical Actuation.

Schematic graphs of cyclical actuation results at multiple voltages with maximum and minimum locations for each cycle identified and marked.

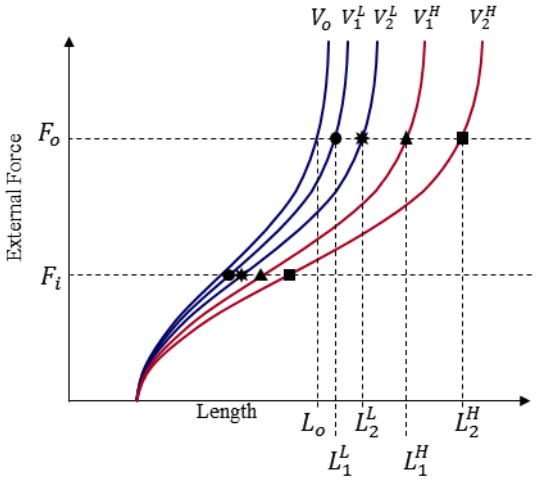

Figure 76. Steady-State Cyclical Actuation Force-Displacement Curves.

Steady-state cyclical actuation force-displacement curves at multiple voltage differences.

Hyperelastic material models can accurately capture the performance of the LOW and HIGH force-displacement curves at a single voltage level. The advantage of using a simple hyperelastic material model is that it is possible to capture the behavior using a simple low-term model. One of the simplest and most often used in DE modeling is the Gent strain energy model, a hybrid hyperelastic model. This model uses only two terms to capture the essential properties of the hyperelastic stress-stretch curve. Another advantage of the Gent model is that there is phenomenological meaning to the two terms: one represents the small-strain shear modulus, and the other represents the hyperelastic limit of the material. The model parameters can be identified from a single force-displacement curve. However, any hyperelastic material model will have an

increasing error the farther it is used from the calibration voltage. The error is caused by the shifting curves, which are caused by the viscoelastic properties of the elastomer. Because the actuation of a DE is a coupled system between the base elastomer force-displacement curve and the Maxwell stress from the electrodes, this increasing error can limit the usefulness of a simple hyperelastic-based model.

If more accuracy is required than a hyperelastic material curve model can achieve, then a viscoelastic material model must be used. A viscoelastic model such as the Standard Linear Model can accurately model all the viscoelastic properties. However, a viscoelastic model significantly increases the complexity because time dependency is in the model and additional parameters are introduced. A full viscoelastic model can capture the performance at any time scale, but these models require a complicated process to determine the parameters' values. Deriving the model parameters for the Standard Linear Model requires the force-displacement profile and creep or frequency tests to derive the viscoelastic model parameters within the Maxwell material model. Full transient models are very powerful and can accurately capture all the actuator's features and predict the performance at any time frame, initial condition, and history, but the power comes at the cost of complexity. Although the fully transient model can capture the behavior, the ultimate force-displacement curves are for a single time frame, so the time complexity will be eliminated once the material effects are determined. Therefore, a significant model and parameters identification complexity are introduced to capture the viscoelastic effects of steady-state cyclical operation, which are then simplified to a single force-displacement curve. It would be desirable if a simple hyperelastic model included an additional parameter that could account for the change in performance as a function of operating at different voltages.

4.2. Variable Shear Gent Strain Energy Model

The goal of the variable shear Gent model is to predict the force-displacement performance of an actuator for steady-state cyclical actuation with the minimum number of parameters. The model is based on the Gent strain energy equation, which uses two parameters to represent a hyperelastic material curve: μ, the small-shear strain, and J_m, the hyperelastic stretch limit. The variable shear Gent model is developed by introducing a new variable shear term to replace the fixed shear term in the standard Gent model. The new variable shear term is a function of the

driving voltage and is added to capture the viscoelastic effects on the transient creep-terminated steady-state cycling behavior. This model captures the essential behavior of the entire stress-stretch curve of a hyperelastic material for steady-state cyclic actuation. The Gent material model has been previously applied to represent differential elements of dielectric elastomer actuators [12–14]. The new model is developed from first engineering principles with appropriate assumptions and then applied to a particular actuator architecture with the correct boundary conditions.

When modeling DE actuators, there are assumptions based on the fundamental properties of a DE, the geometric properties of the actuator architecture, and the fabrication materials and methods. The variable shear Gent model adds an assumption that the steady-state viscoelastic effects can be modeled as a function of the driving voltage of a DE actuator.

4.2.1. Gent Strain Energy Equation

While there are many advanced models for elastomeric materials [20] to predict the force-displacement performance of the dielectric elastomer actuator, a simple two-parameter Gent strain energy model is used to represent the stress-stretch behavior of the actuator:

$$U(\lambda_1, \lambda_2, \lambda_3) = \frac{-\mu J_m}{2} \ln\left(1 - \frac{{\lambda_1}^2 + {\lambda_2}^2 + {\lambda_3}^2 - 3}{J_m}\right) \quad (1)$$

Where U is the strain energy of the elastomer, μ is the small-strain shear modulus, J_m is the asymptotic stretching limit, and $\lambda_1, \lambda_2,$ and λ_3 represent the principal stretch ratios, as shown in Equation 1. The stretch ratios are identified in Figure 77, repeated from Chapter 1, where it is fully defined.

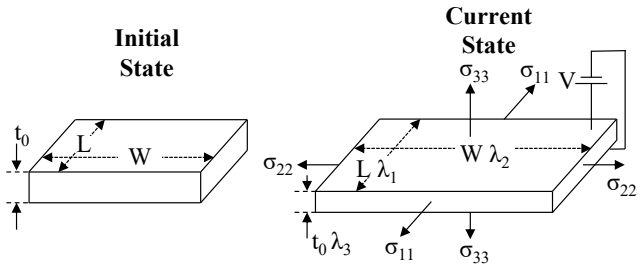

Figure 77. Dielectric Elastomer in the Initial and Current States.

Dielectric elastomer in the initial state and the current state with a differential voltage applied.

4.2.2. Constitutive Law for Incompressible Materials

A basic assumption in modeling DE actuators is that the elastomer itself is assumed to be incompressible, which is equivalent to a Poisson's ratio, v, of $1/2$ [13]. The constitutive law relating the principal Cauchy stress of an incompressible material to the strain energy is:

$$\sigma_i = \lambda_i \frac{\partial U}{\partial \lambda_i} + P^*, \text{No sum} \quad (2)$$

where σ_i is stress in the principal directions and P^* is a hydrostatic pressure applied to the elastomer, which can be determined from boundary conditions.

4.2.3. Electrical Boundary Condition

Two basic assumptions are typically made regarding the elastomer's electrical behavior when modeling DEs. One is that the elastomer dielectric permittivity is assumed to be constant [13]. Another assumption is that the Maxwell stress applied to the film by the electric field can be represented as a simple Maxwell stress in a single direction. The result of the applied electric field is to create a stress on the dielectric material as defined by Maxwell's equation [15-16]:

$$\sigma_{ij}^{(elec)} = \varepsilon E_i E_j - \frac{1}{2}\varepsilon E^2 \delta_{ij} \quad (3)$$

where $\sigma^{(elec)}$ is the Maxwell stress tensor, ε is the elastomer dielectric permittivity, E is the electric field, and δ is the Kronecker delta function.

Since DE actuators have an electric field in only the 3-direction, the Maxwell stress tensor is reduced to $\sigma_{11}^{(elec)} = -1/2\,\varepsilon E^2$, $\sigma_{22}^{(elec)} = -1/2\,\varepsilon E^2$, and $\sigma_{33}^{(elec)} = 1/2\,\varepsilon E^2$. By adding an external stress of $1/2\,\varepsilon E^2$ to all components, it is assumed that this tri-axial stress state for an incompressible elastomer is equivalent to and can be represented by a Maxwell stress [13,17] only in the 3-direction by

$$\sigma_{33}^{(elec)} = \varepsilon E^2. \quad (4)$$

This single boundary condition representing the electrified field's complete impact simplifies the derivation of the DE actuator models. Using the assumption that the electric field effects can be represented by a Maxwell pressure in the 3-direction, as shown in Equation (4), then the boundary condition on the three surfaces results in

$$\sigma_3 = -\varepsilon E^2. \quad (5)$$

Using the stress-strain constitutive relationship for an incompressible material, Equation (5), in the 3-direction, and the boundary constraint, Equation (4), it is possible to determine that the hydrostatic pressure, P^*, is

$$P^* = -\lambda_3 \frac{\partial U(\lambda_1, \lambda_2, \lambda_3)}{\partial \lambda_3} - \varepsilon E^2. \tag{6}$$

4.2.4. Principal Stress Derivation

Once the hydrostatic pressure is determined, the true Cauchy stress, shown in Equation (2), in the 1- direction, σ_1, which is correlated to the external load, F_a, can be derived by substituting in the hydrostatic pressure equations derived from the boundary conditions, as shown in Equation (6). The result is an equation that relates the principal true Cauchy stress in the 1-direction, σ_1, to the principal stretches, λ_i, and the electric field, E, resulting in

$$\sigma_1 = \lambda_1 \frac{\partial U(\lambda_1, \lambda_2, \lambda_3)}{\partial \lambda_1} - \lambda_3 \frac{\partial U(\lambda_1, \lambda_2, \lambda_3)}{\partial \lambda_3} - \varepsilon E^2. \tag{7}$$

using the isochoric assumption,

$$\lambda_1 \lambda_2 \lambda_3 = 1, \tag{8}$$

and substituting the Gent strain energy equation, Equation (1), into the Cauchy stress equation, Equation (7), it is then possible to derive the principal stress, σ_1, as a function of the principal stretches in terms of only $\lambda_1, \lambda_2,$ and the electric field, E, such that

$$\sigma_1 = \frac{\mu\left({\lambda_1}^2 - {\lambda_1}^{-2}{\lambda_2}^{-2}\right)}{1 - \frac{{\lambda_1}^2 + {\lambda_2}^2 + {\lambda_1}^{-2}{\lambda_2}^{-2} - 3}{J_m}} - \varepsilon E^2, \tag{9}$$

which is equivalent to the results of previous work [12,14].

4.2.5. Phenomenological Derived Variable Shear Parameter

Since the literature shows that DE materials cyclically actuated have repeated displacement performance for a fixed performance [269,310,325], the shear modulus term is modified to account for the actuator actuating at different voltages, which leads to different displacements.

The shakedown of elastomers is known to vary with the length the materials have been stretched and is often referred to as a Mullins effect [203,218,219,309,326–328]. When an elastomer is initially stretched and then allowed to return to an unstretched length, it returns to

some length longer than the initial length [133]. This change in length is caused by the polymer chains in the elastomer uncoiling and recoiling to some new configuration. With cyclical stretching, the performance eventually settles down to a consistent force-displacement profile. Because of Maxwell's equation, a DE actuator's actuation stroke depends on the driving voltage's square. Therefore, it can be assumed that the form of the variable shear is a function of the voltage squared,

$$\frac{1}{\mu(\mathrm{V})} = \frac{1}{\mu_0} + \mu_{\mathrm{V}}\mathrm{V}^2, \tag{10}$$

where $\mu(\mathrm{V})$ is the variable shear parameter, μ_0 is the shear parameter at 0 volts, μ_{V} is the variable shear constant, and V is the applied voltage.

The assumed form of this relationship will later be validated using experimental data. The final step in deriving the variable shear Gent actuator equation is to introduce the variable shear parameter term that accounts for the viscoelastic effects as a function of the driving voltage. Substituting the variable shear term, $\mu(\mathrm{V})$, into the standard DE Gent equation, Equation (10), to replace the fixed shear term, μ, results in the final variable shear Gent actuator equation:

$$\sigma_1 = \frac{\mu(V)\left({\lambda_1}^2 - {\lambda_1}^{-2}{\lambda_2}^{-2}\right)}{1 - \frac{{\lambda_1}^2 + {\lambda_2}^2 + {\lambda_1}^{-2}{\lambda_2}^{-2} - 3}{J_m}} - \varepsilon E^2, \tag{11}$$

4.2.6. Application Model for Released Frame Actuator

Extending the stress-stretch equation, Equation (9), into an equation that represents the force-displacement of an actuator requires a change of variables. For DE actuators, the free variables are the axial stretch, λ_a, the external axial load, F_a, and the applied voltage, V. It is assumed that the transverse pre-stretch, λ_2, is a constant called λ_t. The axial stretch, λ_a, is equal to the stretch in the 1-direction,

$$\lambda_1 = \lambda_a. \tag{12}$$

The axial load, F_a, is equal to the Cauchy stress in the 1-direction, σ_1, times the current width, $W\lambda_t$, and current thickness, $\frac{t_0}{\lambda_a\lambda_t}$, with t_0 defined as the initial thickness, which results in

$$F_a = \sigma_1\left(W\lambda_t\frac{t_0}{\lambda_a\lambda_t}\right). \tag{13}$$

The electric field, E, is the applied voltage, V, over the current thickness, $\frac{t_0}{\lambda_a \lambda_t}$, which results in

$$E = \frac{V}{\frac{t_0}{\lambda_a \lambda_t}}. \tag{14}$$

Performing a change of variable to the axial stretch, as well as substituting in the stress to force and electric field to voltage, Equations (12), (13), and (14), into the true Cauchy stress equation, Equation (11), results in an equation that relates the axial force, F_a, to the axial deformation, λ_a, and the applied voltage, V, such that

$$F_a = \frac{W \frac{t_0}{\lambda_a} \mu(V) \left({\lambda_a}^2 - {\lambda_a}^{-2} {\lambda_t}^{-2} \right)}{1 - \frac{{\lambda_a}^2 + {\lambda_t}^2 + {\lambda_a}^{-2} {\lambda_t}^{-2} - 3}{J_m}} - \frac{W \lambda_a \lambda_t}{t_0} \varepsilon V^2. \tag{15}$$

This final equation has three mechanical parameters, μ_0, μ_V, J_m, and a single electrical parameter, ε, that must all be determined experimentally and that are the minimum data needed to capture the essential behavior of an actuator in an analytical model. Knowing the force as a function of displacement and voltage for an actuator enables the design of actuators for systems where the force-displacement curves of the system are known.

4.3. Parameter Identification for Variable Shear Gent Strain Energy Model

The performance of any actuator depends on the base material properties, and an analytical model prediction of this performance will enable a faster, more robust device design. Although performance can be fully characterized experientially over a complete range of forces and voltages, it is more efficient to use a minimal set of experimental tests to identify the model parameters to do analytical prediction. The variable shear cyclical Gent actuator model allows the prediction of performance, but it requires the experimental identification of three mechanical parameters: two for the shear as a function of voltage (μ_0 and μ_V) and one for the maximum stretch limit (J_m). The model uses one electrical parameter, dielectric permittivity (ε), which must also be experimentally determined. Since the variable shear is a function of the voltage, the actuator must be characterized at two voltage levels across the whole load range, which allows for the determination of μ_0 and μ_V, while the maximum stretch limit parameter, J_m, can be derived from data for a single voltage level. The dielectric permittivity of elastomers is known to

change with the stretch ratio [29,198,203], so a separate electrical test is required to determine the parameters in the range of tape stretch utilized.

The experimental characterization is based on the need of applications and the test sample and will always have two components: the experimental test setup and the characterization methodology. The model has three variables: length, force, and applied voltage, and the experimental setup needs to control two while measuring the third. The desired use as an actuator and the complexity of the viscoelastic effects lead to a choice of displacement as the dependent variable in the testing setup. The cyclical actuation characterization methodology is designed to represent the actual use the actuator will see when used in the steady-state cyclical configuration when performance has become repeatable.

4.3.1. Mechanical Model Parameters Identification

The mechanical parameter identification requires the LOW state force-displacement curve for two voltage levels. The test sample's force-displacement curves are captured by testing the sample in 5 gf increments from 15 gf to 65 gf, using the transient creep-terminated steady-state cyclical procedure described in Section 3.6. The two voltage levels selected are 2500 V and 0 V. The 0 V voltage cyclical test is, in fact, just a creep test where the summarized data are extracted at the standard times for the transient creep-terminated cyclical testing procedure. The experimental LOW force-displacement data are plotted in Figure 78, where dark blue circles represent the 0 V cyclic data, and the 2500 V cyclic data are represented as light blue diamonds. These two experimental data curves are generally parallel and show the typical hyperelastic behavior with an initial stiff region followed by a strain-softened region and finally with a stiffening caused by approaching the hyperelastic stretch limit. The LOW 2500 V data (light blue diamonds) are longer than the 0 V data (dark blue circles). This difference in length can be seen as a shift to the right of the higher voltage curve. The 2500 V data are increasingly shifted to the right as loads are increased, which is expected from the variable shear Gent tape actuator model's μ, which softens under increasing applied voltage.

The least squares method is used to identify the variable shear Gent tape actuator model mechanical parameters. The experimental LOW 2500 V data are fit with the model to determine the mechanical parameters, $\mu(2500\ V)$ and J_m, while a second least squares fit is used to identify the $\mu(0\ V)$ from the 0 V LOW experimental data. The μ identified at the two voltages (2500 V

and 0 V) is used in the variable shear equation, Equation (10), to determine the constants μ_0 and μ_V algebraically. Finally, the two model calibration curves, using the parameters identified, are plotted with the experimental data in Figure 78.

Using the following parameters in the model, $J_m = 38.9$, $\mu_0 = 84{,}049\ Pa$, and $\mu_V = 1.6038 * 10^{-13}\ Pa$ results in a model prediction with an average error of 4.74% across the whole load range. The model does not predict the low force-displacement as well as it does at higher loads because of the wrinkling of the actuator. The out-of-plane wrinkles form on the two free edges and are caused by the high lateral pre-stretch. The wrinkles reduce the actuator's effective width and increase the film axial stress. The increased stress causes the actuator to achieve equilibrium at a longer length than the model predicts. This phenomenon is eliminated at loads above 25 g, where the load causes the actuator to become flat. The low load inaccuracy is relatively unimportant because the tape actuator does more useful work at higher loads. For the load region above 25 gf, where the actuator is without wrinkles, the average error between the model calibration curves and the experimental data is 1%.

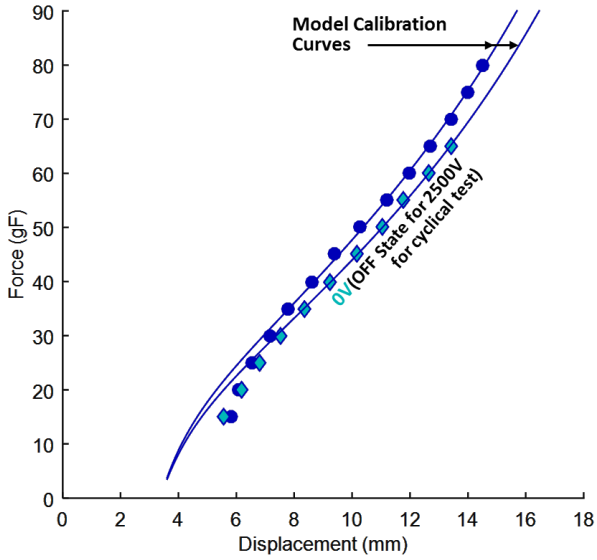

Figure 78. Model Calibration Plots.

Model calibration at cyclical voltage of 2500 V.

4.3.2. Electrical Model Parameters Identification

The standard test for measuring dielectric permittivity, ε_r, uses a capacitance measurement of a relaxed film sandwiched by two metal plates with a known separation distance [216].

However, the standard test requires modification because the dielectric permittivity for many elastomers is known to decrease as a function of stretch. Instead, the capacitance of a pre-stretched film must be measured. The film stretch ratios of a DE actuator change as it actuates. Therefore, useful pre-stretch ratios that represent the regime where the actuator functions best should be chosen for the dielectric permittivity test. The capacitance, C, is directly related to the dielectric permittivity, or the relative dielectric permittivity times the dielectric permittivity of vacuum, $\varepsilon_r * \varepsilon_0$, the area of the overlap of two conductive electrodes, A, and inversely proportional to the distance between the two plates, d:

$$C = \varepsilon \frac{A}{d} = \varepsilon_r \varepsilon_0 \frac{A}{d} \tag{16}$$

A separate simple capacitor was fabricated using the thin film fabrication and pre-stretching steps described in Section 2.3.1 and carbon grease electrodes. The transverse pre-stretch, λ_t, was chosen to be 150% strain, and an axial pre-stretch, λ_a, was chosen to be 200% strain because the tape actuators are most useful at high forces, which correlate to high strains. The thickness separating the conductive electrodes is controlled by the thickness of the pre-stretched film, which can be related to the unstretched measured thickness through

$$d = \frac{t_0}{\lambda_a \lambda_t}. \tag{17}$$

Carbon grease rather than SWNT was used as a conductor because it forms electrodes with low resistance, which is required for high-frequency capacitance measurement. The carbon grease electrodes are brushed onto both sides of the stretched film through a circular mask with a diameter of 35 mm to control the area. The capacitance was measured by an LCR meter, AMPROBE LCR55A. Since the initial thickness, $t_0 = 125\ \mu m$, the stretching ratios, $\lambda_t = 2.5$ and $\lambda_a = 3$, and the diameter, $d = 35\ mm$, are known, as is the dielectric permittivity of vacuum, $\varepsilon_0 = 8.8510^{-12}\ F/m$, it was possible to use Equation (16) to compute the relative dielectric permittivity, ε_r, from the measured capacitance. A test sample's capacitance is measured, resulting in a capacitance of 0.625 nF. The measured capacitance is used to derive the relative dielectric permittivity, ε_r, of 1.4.

4.4. Validation of Variable Shear Gent Strain Energy Model

The accuracy and utility of the variable shear Gent DE actuator model are validated and proven against a larger set of experimental data. A simple model validation evaluates how well the model captures the basic behavior of the HIGH voltage curve at a single voltage level and enables the evaluation of the basic limitation of model assumptions to capture the actual configuration of the experimental prototype. The model's power is derived from its ability to predict the performance over a wide range of voltages and forces from a minimum of model calibration data, shown over the full operating range. From the experimental data, it is possible to identify the optimal shear parameter for each voltage level, which can then be used to validate how well the variable shear equation assumption does at capturing the effects of the actuator being driven at different voltages. To evaluate the improvements of the variable shear Gent DE equation and determine whether added parameters significantly improve the accuracy, the variable shear Gent model is compared to the standard Gent model.

4.4.1. Simple Actuation Model Validation

A simple validation is performed by comparing the model prediction for the 2500 V HIGH-voltage force-displacement curve from the variable shear Gent tape actuator model using the previously identified parameter values with the experimental data, as shown in Figure 79. Although the 2500 V HIGH voltage was gathered in the previous experiment to get the 2500 V LOW-voltage data, it was not used in the parameter identification and calibration, allowing its use in model validation. The model prediction performance accurately matches the experiential values within 4% across all loads. Contrary to the problem of model fit of the LOW curves in the low-force region, the model accurately predicts the HIGH displacement because the high voltage causes the actuator to become planar such that the model accurately predicts the displacement. Because of the shape of the force-displacement curves and the tight performance envelope, an accurate design of the external force-displacement profile will allow the design of devices to take the best advantage of the dielectric elastomer tape performance.

As loads become very large, the experiential results become overpredicted. This length over prediction could be due to an inaccuracy in the stretch limit parameter, J_m, because the mechanical model parameters are identified without taking the sample near this limit. A secondary edge effect could also cause inaccuracy at high loads. The model assumes the film

edges are straight, but the experimental sample has edges curved inward in arcs and reaches the narrowest point in the middle of the actuator length, as shown in Figure 79. These curved edges change the effective electrode area and the thickness near the curved regions. For the LOW-voltage curves, this discrepancy between the model and the test sample is accommodated in the parameter identification process because the process fits the experimental data from the LOW-voltage curves. This accommodation no longer applies to the HIGH voltages because the edges become less curved. For the HIGH voltage, the length of the actuator depends on the dielectric permittivity, the electric field, which is a function of the voltage and film thickness, and the force-displacement of the elastomer material. The effect of any thickness discrepancies is magnified for the HIGH-voltage curves because there is an inverse square relationship to the thickness. A second source of error is the dielectric permittivity, which is assumed to be fixed but is known to vary with stretch.

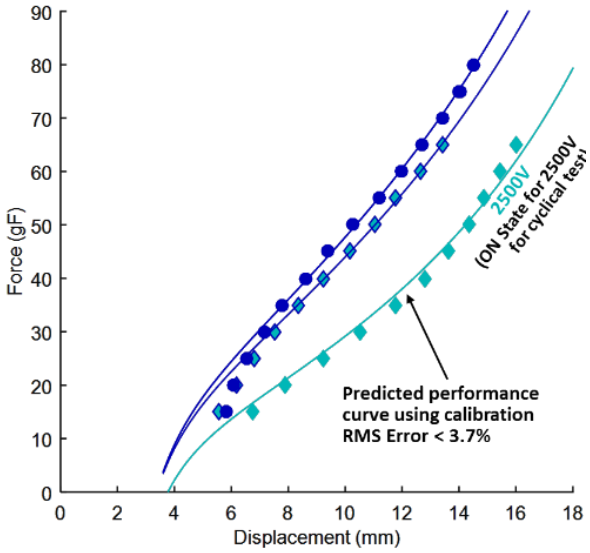

Figure 79. Variable Shear Gent Model Validation.

Variable shear Gent model validation at 2500 V with model calibration curves at two LOW voltage levels, 0 V and 2500 V.

4.4.2. Model Validation over the Whole Operating Range

Analytical models are most efficient if they can predict the performance across the entire actuation range from minimal experimental data. The experimental characterization of the tape actuator's force-displacement performance was validated across a range of voltages, 0 V to 2700

V, and forces, 15 gf to 80 gf. This experimental data and the tape actuator model predictions using the previously identified parameters are plotted together in Figure 80. The model accurately predicts the force-displacement profile with an average error of 4% across all voltage and force levels above 25 gf. The out-of-plane folding of the dielectric elastomer actuator caused by the high lateral pre-stretch causes the displacement to be underpredicted below 30 gf. However, the LOW-force performance is not matched for the OFF curves; the HIGH displacement is once again much better represented by the model because the electric field causes the actuator to flatten and become planar, matching the model's assumption. The new variable shear terms are validated using all the LOW curve experimental data to calculate best fit shear terms. A comparison of the best-fit shear values and the shear values predicted from the new variable shear term resulted in a match within 3%. The full experimental data are plotted along with the model parameters identified. The average error across all loads and voltages for the LOW-voltage curves is 1.6%, and the HIGH-voltage error is 3.0%. The efficiency of the tape model comes from the necessity of experimental characterization data from only two voltage experiments to identify the model parameters. The effectiveness of the new model was additionally proven by using all pairs of voltages as calibration voltages to derive the required model parameters. The result of the study is that if any two voltage curves are selected, with at least one being higher than 1000 V, then the average error for any pair of voltages is 4.0%. The

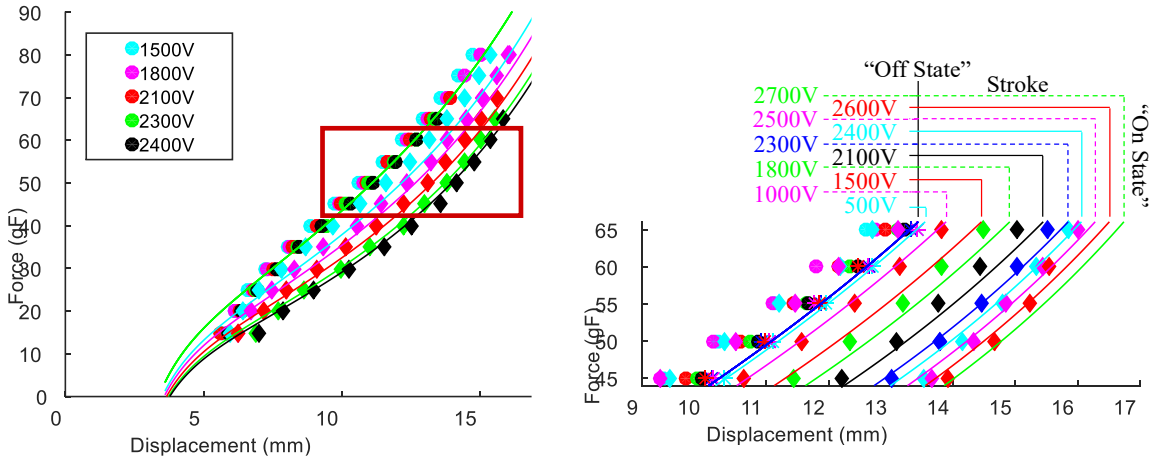

Figure 80. Steady-State Cyclical Actuation Data with Magnification.

Steady-state cyclical actuation data summarized in force-displacement space with variable shear Gent model predictions.

variable shear Gent model assumed that the shear term in the Gent strain energy equation

changes with the maximum length of the actuator, which is related to the square of the applied voltage, as seen in Equation (15). The complete set of experimental data can be used to validate this assumed relationship. An independent least squares fit parameter identification analysis is done on each experimental LOW-voltage force-displacement curve to identify the best possible shear parameter at that voltage level. These best-fit shear parameter values are the points plotted in Figure 81. The predicted shear parameters as a function of voltage, which use the $\mu(0\ V)$ and $\mu(2500\ V)$ for calibration, are shown as a solid pink parabolic curve. The individually identified shear values form a strong parabolic shape with an average error of 1% to the model's prediction. This small error in the shear values derived from the variable shear term demonstrates that the assumption of a variable shear term is valid and can be used to predict actuation performance accurately.

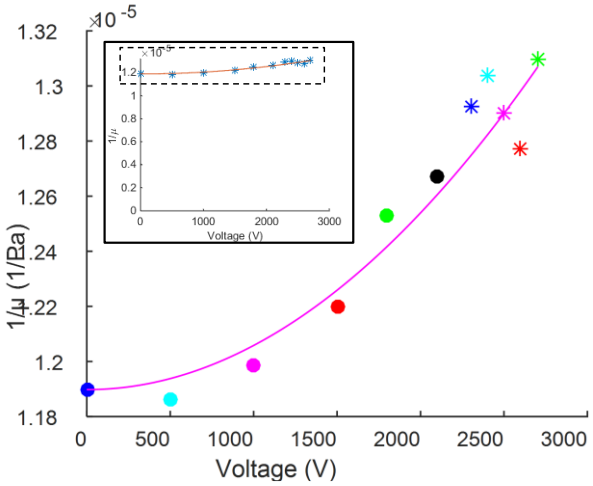

Figure 81. Variable Shear Experimentally Determined Results.

Variable shear experimentally determined results plotted with the model prediction of the equivalent values.

4.4.3. Comparison to Standard Gent Strain Energy Equation

The root mean square error (RMSE) average was plotted for each cyclical voltage test to quantify the accuracy of the model's fit. The RMSE is lowest around where the model is calibrated at 2500 V. The model predictions at other voltage levels have significantly increased errors and are a maximum RMSE of 4 gf and 8% error concerning a 50-gf reference force at 1500 volts. The Gent model predicts the performance within a 4% error between 2100 V and 2500 V, but accuracy degrades to less than 5% outside that range.

The Gent model and the variable shear Gent model accuracy are compared by calculating the RMSE for the HIGH and LOW state for each cyclical voltage level, as shown in Figure 82. All percentages are evaluated against a mean load of 50 gf. The Gent model has a maximum error of 11.2% (5.6 gf) and a mean error for the OFF state and ON state curves of 3.9% (2.0 gf) and 5.6% (2.8 gf), respectively. The modified Gent model has a maximum error of 4.6% (2.28 gf) and a mean error for the OFF state and ON state of 1.7% (0.85 gf) and 3.0% (1.5 gf), respectively.

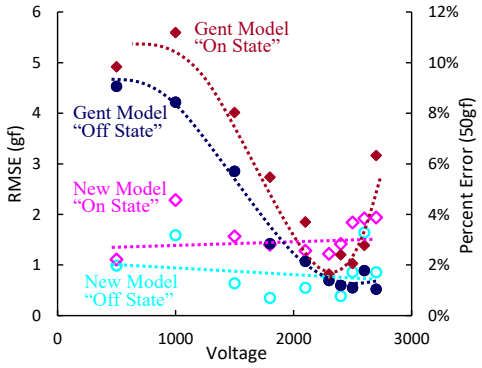

Figure 82. Variable Shear Gent Model Accuracy.

The plot shows the accuracy of the variable shear Gent model compared to a Gent only model.

If a voltage level other than 2500 V is used to identify the model parameters, the model still does a good job predicting the actuator performance. For any voltage between 1500 and 2600 (1500, 1800, 2100, 2300, 2400, 2500, 2600), the modified Gent model has a maximum error of 8.8% (4.4 gf) and a maximum mean error for the OFF state and ON state of 2.0% (1.0 gf) and 4.8% (2.4 gf), respectively.

4.5. Analytical Model Limitations and Future Work

The general new variable shear Gent model needs to be validated using a particular architecture and actuator. The architecture used for validation is a released-frame architecture that uses two parallel plates that hold the elastomer film and leave the edges free. A geometric simplification is that the width, W, in Figure 79, is assumed to be constant. While the end plates hold the width constant where they are affixed to the elastomer membrane, the side edges between the plates may bow inward when there is a transverse pre-stretch, or the actuator is

stretched. The bowing inward edge effects are considered negligible if the width-to-length ratio exceeds 10:1. However, the transverse pre-stretch may also cause the film to buckle out of the plane, increasing the edge effects by decreasing the effective width of the elastomer. For these types of actuators with a width-to-length ratio smaller than 10:1, the negligible edge effects assumption can remain valid under an electric field if the actuation extends the side edges of the elastomers and unbuckles the film, thereby making the edges better conform to the fixed width assumption.

Although the compliant electrodes for dielectric elastomers are typically assumed to have negligible stiffness, DE actuators have used electrode materials that can have a significant stiffness, such as conductive polymers or single-wall carbon nanotubes (SWNT) [18, 19]. If the electrode stiffness is not modeled, which avoids adding complexity to the design model, then another method to capture the impact of the increased stiffness must be used. The experimental method can capture the stiffness effect by which the analytical model material parameters are derived for actuators. Capturing the increased stiffness with the model parameters is possible because the composite structure acts as one unit, and the electrodes have long chains with similar stress-stretch material behavior compared to a polymer. SWNTs have been modeled using hyperelastic materials models [329,330]. Therefore, it is assumed that the analytical model does not need to be modified to include electrode stiffness if the experimental identification of the model material parameters includes both the elastomer and the compliant electrode stiffness.

4.6. Conclusion for Modeling Cyclic Dielectric Elastomer Actuation

This chapter outlines the methodological approach to using an application context in analytical modeling. This approach facilitated the development of the new variable shear Gent model, which predicts the steady-state cyclical actuation of dielectric elastomer actuators. The new variable shear Gent dielectric elastomer actuator model significantly contributes to DE actuator modeling. It accurately predicts the steady-state cyclical actuation performance. This model bridges the gap between simple material models without viscoelastic effects and complex full transient viscoelastic models. The new variable shear gent model is simpler than any viscoelastic model. It requires less calibration data, provides insights into the effects of variables and parameter modification on actuation performance, and can be easily incorporated into a quasi-static design process. The phenomenological origin of the new variable shear term can help

improve our understanding of the role of viscoelasticity in steady-state cyclical actuation in DE actuators.

The new model was established from first principles and calibrated using a minimal set of experimental cyclical actuation data; this simple quasi-static analytical model relies on a low number of terms to accurately predict the steady-state cyclic performance of DE tape actuators. The accuracy of the calibrated model for predicting performance was validated against a larger set of experimental data. The experimental analysis determined that the new variable shear Gent model cuts the maximum error in half over the standard Gent model, from 11.2% to 4.6%. Furthermore, the variable Gent model maintains accuracy over the actuator's entire force and voltage range, while the Gent model is reasonably accurate only at the calibrated voltage and force levels.

The general form of the new variable shear model that links the length of the actuator to the driving voltage was validated with experimental data. The new model predicts two curves for each actuation voltage level: the LOW-voltage curve and the HIGH-voltage curve, which are seen in the data as pairs of separately identifiable curves for each voltage level. The experimental cyclical actuation characterization data also show that for each operating voltage, the LOW-voltage force-displacement curves shift to the right, lengthening as the operating voltage level increases, even though all the LOW curves have a zero operating voltage. The new model predicts this increase in length and is the property that the variable shear term is intended to capture. The variable shear Gent model cuts the maximum percent error by 59% compared with the standard Gent model. The experimental data validate the model accuracy, ranging from 0 to 2600 V and 30 to 65 gf. The average prediction error for the Gent model is 3.9% and 5.6% for the LOW-voltage and HIGH-voltage. The Gent model's maximum error is 11.2%. For a single set of model parameters, the average experimental error for the new variable shear Gent actuator model for the LOW-voltage, HIGH-voltage, and maximum error is 1.7%, 3.0%, and 4.6%, respectively. The assumption of an inverse quadratic relationship between the variable shear term, μ_V, and the voltage for steady-state cyclical actuation is validated from the experimental data. Shear terms for each voltage level were determined separately from the experimental data for each voltage level. A comparison of the individually identified shear terms to the variable shear model's prediction of the variable shear term, $\mu(V)$, evaluated at each voltage level,

showed that they both formed strong parabolic curves, and the predicted values are within 1% of the individually identified values.

The mechanical model parameters can be derived from the experimental force-displacement characterization data at two operating voltages. To further prove the model's accuracy beyond the two calibration voltages chosen for most of this analysis, a study of the new model's accuracy when any two particular voltage levels are chosen was performed. If any two operating voltage curves are selected with at least one higher than 1000 V, then the average error for any pair of voltages is 4.0% over all possible pairs.

This analysis confirms that the variable shear Gent model is accurate and predictive outside the voltage levels used for parameter identification. Even though this model is validated with a single architecture and actuator materials, a released frame with silicone film, and single-wall carbon nanotube electrodes, the variable shear ent model can potentially be used for any DE actuator in a steady-state cyclical operation.

The variable shear Gent cyclical DE model accurately predicts the DE actuator performance over the complete range of voltages and forces. With its limited parameters, the need for experimental data for model calibration is significantly reduced. The calibrated model remains accurate across all loads and driving voltages. Additionally, the phenomenological meaning of the parameters aids in the intuitive understanding of the performance characteristics of DE actuators. A notable gap exists in dielectric elastomer modeling between hyperelastic-based material models and fully complex viscoelastic models. This model bridges the gap between simple material models that ignore viscoelastic effects and complex full transient viscoelastic models that may be overly complex for modeling steady-state cyclical operation.

Dielectric elastomer actuators can be challenging for non-experts due to the complexity of elastomers' viscoelastic properties. For straightforward actuator applications with fixed architecture parameters and actuator variables, it is feasible to experimentally characterize all behavior for the specified actuation situation. In such cases, a hyperelastic material model can serve as the basis for the actuator model. However, gathering all necessary information for quasi-static model-based design becomes significantly harder and more time-consuming for more complex applications with unknown model or device parameters or a wide range of desired actuation performance. These complex applications necessitate a viscoelastic model.

Comprehensive viscoelastic characterization of a dielectric elastomer actuator requires more experimental equipment, a more complicated characterization process, a deep understanding of viscoelastic materials' analytical modeling, and significant expertise in using the information in a model-based design process. The complexity of dielectric elastomer actuators and their viscoelastic effects, hysteresis, and complex material interactions pose a significant barrier to their broader use and adoption. Therefore, while dielectric elastomer actuators are easy to use for simple applications, they become significantly more challenging for more complex applications. This gap can be bridged by developing models between simple hyperelastic material base actuation models and more universally accurate complex viscoelastic models.

The new variable shear gent strain energy model is crucial in bridging this modeling gap by accurately modeling full viscoelastic behavior in the quasi-static Force-Length space. This new model allows for simpler quasi-static model-based design for a wide range of applications. The model achieves this by encompassing all the viscoelastic behavior for steady-state cyclical actuation inside a variable shear parameter dependent only on the applied voltage.

This new model demonstrates the feasibility of discovering and creating time-invariant models that effectively capture all the critical viscoelastic behavior. Such models could significantly decrease the knowledge needed to use dielectric elastomer actuators, making dielectric elastomers a more practical and useful actuator technology.

Chapter 5 Quasi-Static Model-Based Design Applied to Dielectric

Dielectric elastomer tape actuator performance depends on many factors, and these actuators possess inherent limitations based on their frame configuration and materials, making them challenging to use in applications. These challenges underscore the importance of utilizing a model-based methodology to develop a framework for understanding and designing DE actuator devices/systems. For this research, the framework will address the following objectives: develop a simple method for designing quasi-static DE actuator systems; understand the limitations of DE actuators; identify ways to minimize or compensate for these limitations; create a categorization of common and useful DE actuation devices/systems; and develop a methodology for evaluating the advantages and disadvantages of a particular device/system.

The capabilities of DE actuators are closely tied to materials and design. As previously discussed, basic materials significantly impact overall performance. However, the performance of a DE actuator is heavily influenced by the design of the actuator and the way it is used. The maximum performance can be garnered when all the elements are designed together. The materials are extremely complex, which makes design challenging. The keys to simplifying and improving the ease of DE actuator design are identifying the critical elements that drive performance and understanding which elements can be simplified. The specifics of any design will depend on the requirements of the system. For steady-state cyclical actuation, a useful simplification is considering the performance quasi-static. While there exist many techniques and methodologies for designing with quasi-static actuators, this research will adopt a graphical technique to demonstrate the process and advantages of using a quasi-static design process with DEs to enhance performance and aid in the fundamental understating of the characteristics of DE tape actuators.

5.1. Quasi-Static Design Process Applied to Released Frame Actuator Architecture

Although the inherent properties of DE elastomers make them an exciting option for actuation opportunities that are not viable with conventional actuators, there are many challenges

to using DEs because of the complexity associated with maximizing their performance [24,29,113,198]. One of the principal challenges lies in designing a system that takes advantage of the DE properties. This section first reviews a quasi-static design process [324,331–334] applied to DE actuators and then explores the insights gathered about DE actuators using this quasi-static design process. The insights are categorized into three areas: overall actuator performance, design sensitivity of a system to parameter variations, and finally, implementation complexity of fabricating the design.

The actuator's performance can be categorized into actuation stroke, force, and external work. Design sensitivity refers to the variation in performance due to slight variations in design parameters, including offsets, load levels, external system force-displacement profile changes, and actuation voltage. Implementation complexity concerns the difficulty of fabricating the total system, the number of parts required, and the introduction of bearing surfaces or other moving parts. In any design, trade-offs are necessary in making design choices: understanding the impact of those trade-offs enables the selection of properties that are most relevant or important to an application. One approach that assists in design is categorizing the external system into different types of families and analyzing the trade-off(s) required when selecting a particular external system. If an actuation system is being designed from scratch, design choices can be made to work well with DE actuation. When a DE actuator is being integrated into an existing system, the trade-off analysis allows designers to know the potential range of performance and how the system can be modified to enhance the total system by making modifications that will make the system performance better match the capabilities of DE actuators.

Dielectric elastomers are complex materials whose performance is coupled with external systems. This coupling leads to the need for a simple methodology for system design. For quasi-static actuation, design complexity can be minimized by using the force-length design space. This design space allows for the force-length performance of each component to be individually characterized without coupling. A system design is determined in a common design space. The force-length space of DE actuators' performance at different voltage levels typically has hyperelastic performance curves. These curves enable highly variable performance, depending on the design of the system interactions.

The general process for a quasi-static design consists of four steps: characterization of both the actuator and target system in the force-length design space, determination of the

transformation from one coordinate frame into the other system, the combination of the two performance curves in one design space, and determination of the actuator stroke. The force-length characterization of the system can be done experimentally or analytically. While any coordinate frame can be used for the design space, a coordinate frame that is relevant to the system design and improves an intuitive understanding of the system's performance and limitations is preferable. The second coordinate frame needs to be transformed into the primary coordinate frame. Such a transformation depends on the geometry of the system configurations and is adjustable by system parameters. With the coordinate offsets, it is then possible to plot both force-length characterization curves on a single axis. Finally, the location of the two-system characterizations overlaps determines the equilibria of the final system.

5.1.1. Force-Displacement System Characterization

The first step in the force-displacement system characterization is to break down the system into its components, after which each element can be individually characterized in the force-displacement space. The modular system evaluation simplifies the process of characterizing the whole system. Binary systems, where the components are broken into two subcomponents, are often simple, practical, and useful as example systems. A two-component example system is shown in Figure 83. The system consists of a DE tape actuator connected to a non-deformable lever, shown by the green line, free to rotate around a pivot. The gold lines represent the multifunctional tape connectors (MTCs), excluded from the length calculations since they are inextensible. A tension spring is attached to the lever On the opposite side of the pivot from the DE tape actuator. Both attachments to the lever are on pivots and allowed to rotate freely. Both the DE tape actuator and the spring are fixed to a wall but allowed to move vertically. These pinned and rolling constraints ensure that only horizontal tension forces exist in the subcomponents, the DE tape actuator, and the spring. This example will be used for the rest of this analysis to demonstrate the force-displacement process, although, with a few modifications, the process can be utilized for a system that has more components.

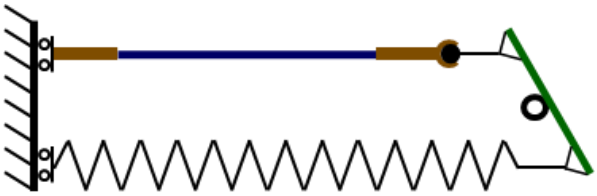

Figure 83. Two-Component System.

Schematic of a two-component system with a spring and actuator connected through a lever.

Identifying and breaking down the system into components is very important. There are always different layers and levels into which a system can be broken down into smaller subsystems. The complexity of the individual components can affect the difficulty of characterizing the system. The characterization process should isolate the simplest systems that can be identified as a separate system or components with fixed and not easily changed parameters. The purpose of the breakdown is to simplify the characterization process, which should be considered when selecting the components. In the example, Figure 83, the system comprises three components: the DE tape actuator, the spring, and the pivot. Although there are three components, only the DE tape actuator and the spring have a force-displacement profile. The pivot is assumed to be frictionless and contributes insignificantly to the system's performance. If this assumption turns out to be incorrect, the influences can be incorporated later. For the first-order analysis, the pivot will be assumed not significantly to contribute to the system performance. Therefore, only the DE tape actuator and the spring must be characterized in the force-displacement space.

After each component has been broken down into its most basic components or architecture that is not easily changeable, a coordinate frame must be selected for each element. The coordinate frame for the subsystem should make the characterization of the system the easiest possible. The coordinate frame should track the macro behavior of the subsystem, which is of interest and will impact the performance of a larger structure. The subcomponent coordinate frame can be linear, polar, or any other frame that makes sense for the application and characterization. A Cartesian coordinate frame that defines the active area of the DE tape actuator is chosen, as shown in Figure 84. With the selected coordinate frame, the DE actuator at zero force has a defined length. The defined length is the relaxed length of the actuator when there is no load on it. The relaxed length will be less than the original one because the lateral

stretch causes compression in the axial direction due to the Poisson effect. The Cartesian coordinate frame is also used to model the spring, as shown in Figure 85, which starts at the end of the spring when it is fully relaxed. This coordinate frame allows for the simple calculation of the spring constant. The final step is to characterize the force-displacement performance in the designated coordinate frame fully.

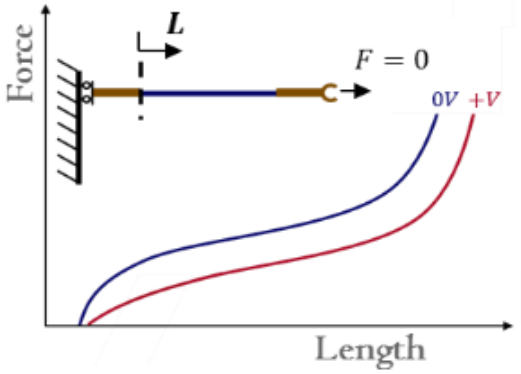

Figure 84. Coordinates Frame for DE Actuator.

Cartesian coordinates used to model a DE actuator performance.

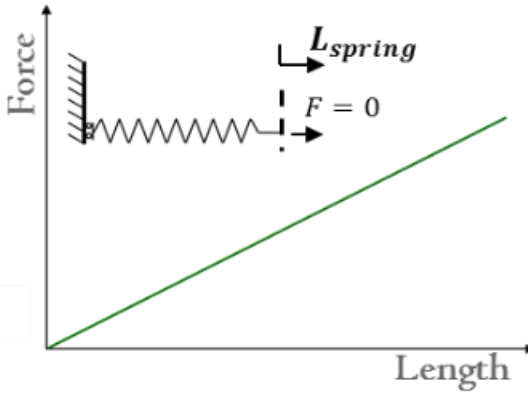

Figure 85. Coordinates Frame for Spring.

Cartesian coordinates used to model the spring.

5.1.2. Coordinate Frame Transformation between Systems

Many factors go into the coordinate transformation step. The first step is to select a coordinate frame that best fits the final system. For this example, there are three possible categories of coordinate frames to choose from: the two-coordinate frames defined for the subcomponent characterization process and the intermediate coordinate frame representing the pivot. After selecting the primary coordinate frame, there needs to be a coordinate transformation of the characterization data into the chosen coordinate frame. The transformation can include leveraging elements or scaling, offsets, transformation from linear to polar coordinates, or combining all three scaling features.

Selection of the primary coordinate frame will depend on what makes the most intuitive sense to aid in the system's design. Suppose the actuator is being added to an existing design of a system. In that case, any modifications relate to how the actuator will be implemented or integrated into the system. In this type of case, for integration into a fixed system, the different performances available from the actuator will best be interpreted using the actuator coordinate frame as the primary coordinate frame. The tape actuator's primary coordinate frame enables an

understanding of how the DE's actuation performance changes with variable adjustments. When a system is designed around a leverage point or the performance is symmetrical, it makes more sense to use the symmetrical performance coordinate frame instead of the force-displacement coordinate frames from the characterization step. The performance requirements can also be a guiding force when selecting the primary coordinate frame. If an application requires a minimum amount of rotation, it would make sense for the primary coordinate frame to correlate to the system's requirements.

Dielectric elastomers have complex performance so, in most situations, it is more advantageous to use the DE actuator's coordinate frame to allow for the building of an intuitive understanding of how best to use a DE. In this case, due to the complex behavior of the DE tape actuator and the high interest in its capabilities, the coordinate frame for the DE tape actuator will be chosen as the primary coordinate frame, as shown in Figure 86.

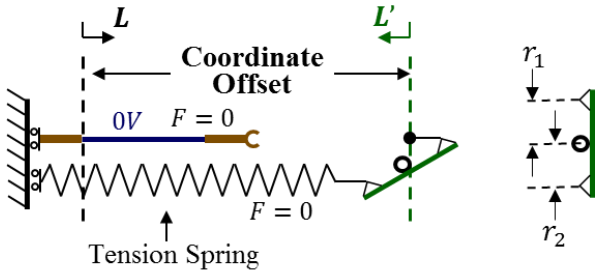

Figure 86. Primary Coordinate Frame Selection.

The schematic shows the primary coordinate frame, L, representing the basic DE actuator coordinate frame. A secondary coordinate frame, L', represents the tension spring. The coordinate offset is defined as the distance between the two coordinate frames.

5.1.3. Combining Systems

The system combination is a simple process that uses the characterization data in the first section combined with the coordinate frame transformations determined in the second. As shown in Figure 87, both characterization data sets are transferred into the primary coordinate frame using the coordinate frame chosen to represent the system. This transformation includes any scaling and offsets needed for the baseline configuration.

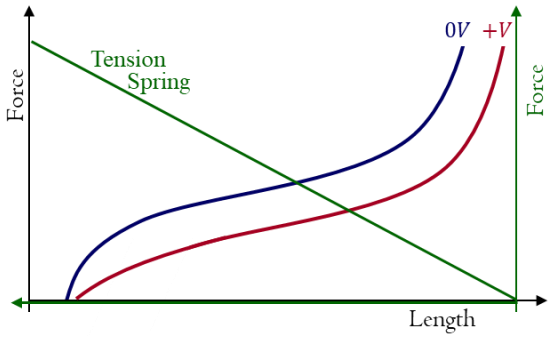

Figure 87. Design Plot with Actuator and Spring Performance Curves.

The DE actuator performacne curves and the transformed spring force into the primay coordinate frame all graphed together. Combined data set.

5.1.4. Stroke Determination

The final step in the process is to determine the stroke of the actuator. The stroke is the x-coordinate distance between the intersections of the two characterization curves in the primary coordinate frame. The stroke determination and the work of the actuator will depend on design parameters. The visualization of the performance can also enable the adjusting of parameters to get better performance.

5.1.5. Designing with Dielectric Elastomers – Design Performance and Sensitivity

Designing well with DE tape actuators is complex and challenging because of the unique force-displacement performance curves. A free-clearance variable defines The connection between the external system and the DE tape actuator. This variable is used to modify the interactions of the two systems. The offset controls the axial pre-stretch and prestress on the tape actuator. For a fixed external system and DE tape actuator, the free-clearance also controls the stroke and work performance of the whole device by controlling where the two curves intersect. The location of the intersection also controls the sensitivity of the design. The sensitivity of the design for DE tape actuators is caused by the hyperelastic shape of the tape actuator's ON and OFF performance curves. System friction can significantly impact the performance of a DE tape actuator system because of the typical low-force actuation authority. Understanding the impacts of varying the free-clearance on both the performance and the sensitivity enables better designs while explaining how friction will impact the total performance.

5.1.5.1. Free-Clearance

In the final combined graph in the previous example, the DE tape actuator and external system performance curves are fixed, creating a fixed equilibrium point. However, the equilibrium location of the system can be changed by translating the external system laterally. This lateral translation in the graphical space is equivalent in the hardware to changing the pre-stretch required for the actuator to achieve equilibrium. A free-clearance variable will create a repeatable standard for controlling the offset between the two systems. The free-clearance is the length the actuator must stretch to be attached to the external system when both systems are relaxed with zero forces. The free-clearance is defined as the total distance between the coordinate offsets minus the amount of passive material between the coordinate frames. In the previous example, the external system, a tension spring, is transformed into a parallel coordinate frame but offset from the tape actuator coordinate frame through a leverage mechanism. The free-clearance is shown schematically and graphically in Figure 88 and Figure 89, respectively. The two systems will reach equilibrium after connecting the tape actuator and the external system. This equilibrium position also defines the axial pre-stretch and the axial preload of the tape actuator, as shown in Figure 89. The axial pre-stretch is the length of the actuator in the OFF voltage equilibrium position. The preload is the corresponding tension in the film at the OFF voltage equilibrium position.

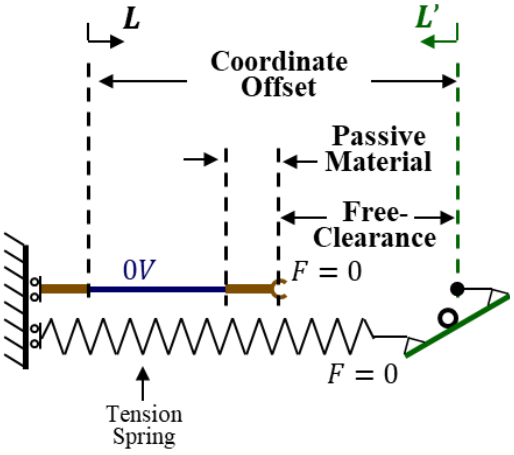

Figure 88. Schematic Showing Free-Clearance and Coordinate Offset.

Schematic showing critical design parameters.

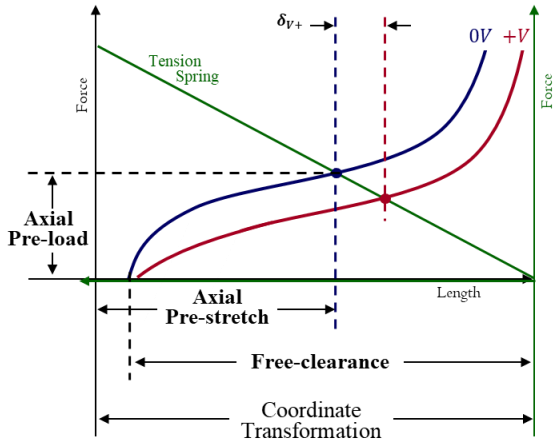

Figure 89. Graphical Representation of Free-Clearance.

The plot shows critical design variables and parameters.

5.1.5.2. Performance and Sensitivity

The quasi-static design process aids in the design of systems for both novice and expert designers. The quasi-static design process helps visualize the performance and allows an analysis of the trade-offs between performance and the design sensitivity to parameter changes. Visualizing the performance allows for the growth of an intuitive understanding of the system's performance. The impact of changing the design parameters can be seen in the force-displacement space. For example, the DE tape system and spring, through a lever system shown in Figure 90, has several design parameters that can be changed to modify system performance. The actuator free-clearance is the most useful parameter because it can alter the performance and the design sensitivity.

The basic force-displacement profile for a DE tape actuator is equivalent to a hyperelastic material curve. The OFF voltage force-displacement curve has an initial stiff region, followed by a strain-softened region, where the curve becomes flatter, and finally, the curve stiffens again as it approaches the hyperelastic limit of the elastomer. The ON force-displacement curve is generally parallel to the OFF curve with an offset. With the spring lever example in the previous section, the external system curves cross the force-displacement curves in the middle of the strain-softened region. There is low design sensitivity to the actuator offset in this region, where the curves are locally parallel and approximately straight. If the free-clearance changes slightly, the external curve will shift slightly to the left or right. This slight shift would cause insignificant changes in the actuator's stroke or the total work performed because the system performance curves are locally parallel and approximately straight. If the free-clearance is decreased significantly, there would be significant impacts with the actuation stroke decreasing and the total work decreasing. The stroke will also decrease If the free-clearance increases significantly, causing the equilibrium position to enter the hyperelastic stretch limit region. With a longer free-clearance, there will be a trade-off with the amount of work performed because as the actuation stroke decreases, the force increases. In the extreme of both free-clearances, small or large, the overall design becomes more sensitive, as shown in Figure 90. Small changes in the free-clearance can cause the stroke to change significantly. The changes in stroke are because both the ON and OFF voltage curves are curved, representing a changing stiffness, so a small change in the offset can cause the intersection between the performance curves and the system curves to change significantly.

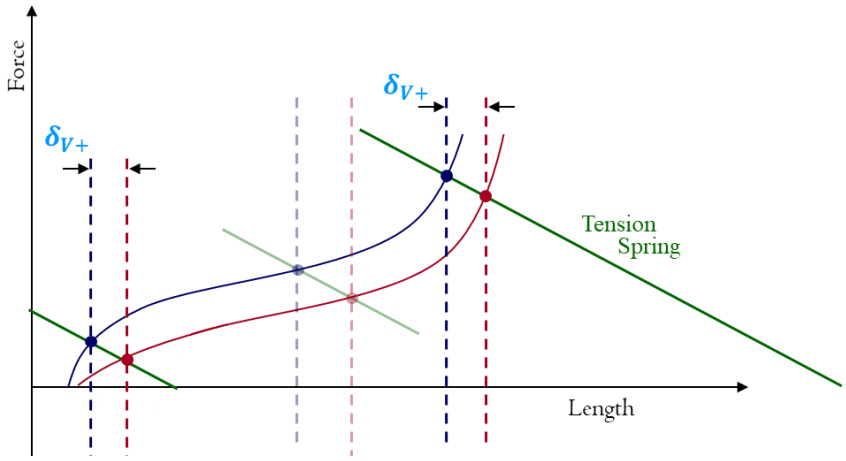

Figure 90. Actuation Stroke Changes with Free-Clearance Modification.

The actuation stroke changes as the free-clearance is changed to modify the equilibrium positions. Both large and small free-clearances cause smaller actuation strokes compared to a medium free-clearance, which causes the equilibrium to occur in the middle of the strain-softened region on the hyperelastic curves.

The system design impacts both the performance and the sensitivity of the design. One of the unique aspects is that dielectric elastomers have a large stretch range. This large stretch range allows for significant variability in the performance, which is seen by the change of performance simply by changing the free-clearance in the example above, as shown in Figure 90. All the designs in the previous example use only a small portion of the entire stretch range of the DE actuator. Therefore, there is significant potential to enhance the actuation stroke of the actuator by using more of the force-displacement profile. By decreasing the spring stiffness of the external system, the actuator stroke can be increased.

5.1.5.3. Friction Effects

Friction can have a substantial detrimental effect on the performance of a DE actuation system. To evaluate the effects of friction, we can use the same simple spring and lever system discussed in the previous section and shown in Figure 83. Friction always works against a system and requires additional force to move. The effects of friction on the force-displacement profile of the external spring system are shown in Figure 91. When the spring is extended, as indicated by the blue line, the force-displacement of the real system is offset above the basic spring system by the force of friction. When the spring is compressed, as shown by the orange line, the force of friction takes away the spring force, and it appears the force level is reduced.

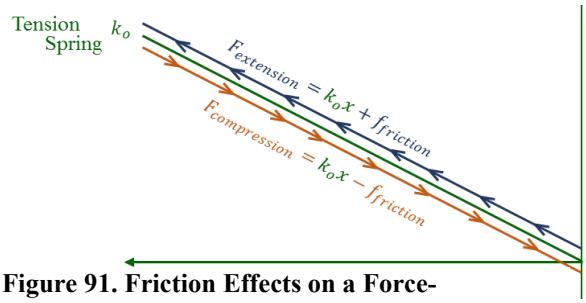

Figure 91. Friction Effects on a Force-Displacement Profile.

Friction effects on a force-displacement profile of an external spring system. In extension and contraction, a friction force always works against the system's performance.

The impact of friction on the performance of the actuator and the system is displayed graphically in Figure 92. As the spring is extended, shown by the light blue curve with arrows, the spring with the friction curve crosses the OFF voltage curve to the right of where the spring is with no friction equilibrium. When the tape actuator is energized, the ON equilibrium occurs where the compression spring force-displacement line, shown by the orange curve with arrows, crosses the ON voltage curve, shown by the red line. The new ON equilibrium with the spring with friction is to the left, where the equilibrium would have been for a spring without friction. The difference between the two equilibrium positions is the stroke for the system with friction. The system's stroke with friction is lower than when friction is not included. Friction adversely effects both the OFF and ON equilibrium positions and substantially affects DE systems.

The performance curves are parallel and close together, which magnifies the impact of friction on the system. The actuation authority of a DE is typically low, as seen in the small separation between the parallel voltage OFF and ON curves, which causes the new equilibrium positions with friction included to eliminate a significant part of the actuator stroke. If the separation between the OFF and ON performance curves were greater or the curves were not parallel, then the friction would have substantially less effect on the total performance.

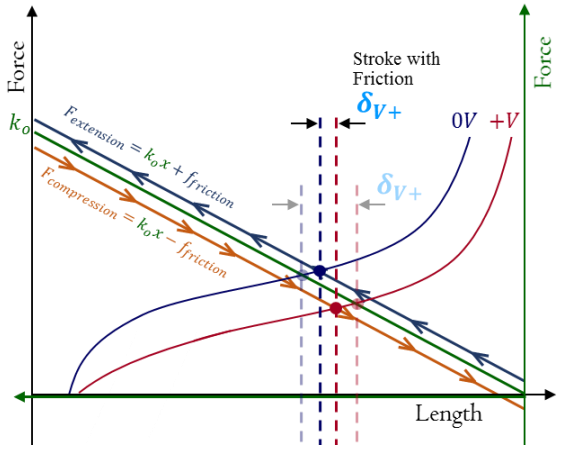

Figure 92. Impact of Friction on Design Performance.

The impact of friction on performance. The actuation stroke without friction effects is shown as faded blue and red lines. The actuation stroke with friction is marked by the solid blue and red lines.

Dielectric elastomer tape actuators do not lend themselves to innately intuitive designs because they are a reverse actuation that relaxes when energized; they are based on hyperelastic films that control the actuation performance and sensitivity, and changing the implementation of the design parameters can lead to countering the desired performance. The physical implementation of the actuation system, friction, and other real-world forces (gravity, inertia, etc.) can significantly reduce the total actuation performance. Using the quasi-static design process with DE tape actuators allows a designer to predict the impact of changing system parameters, free-clearance, and potential sensitivity of a particular design to miss assembly or real-world effects of friction in the system. a trade-off must be made between design performance, design sensitivity, and implementation complexity when using DE tape actuators.

5.2. Scaling Performance with Dielectric Elastomer Actuators

One significant challenge with large-stroke DE tape actuators is that they are limited in their total actuation authority because they use a soft elastomer to achieve their large stroke. Sometimes, larger actuation performance, force, or stroke is required than what is achievable by the design parameters for the basic modular tape actuator. In these cases, scaled performance can be achieved by changing the geometric parameters (the actuator size) or using the modular capabilities of DE tape actuators to create a larger architecture scaling. Geometric scaling is a process in which the intrinsic fabrication parameters of the tape actuator, actuator width, axial

length, and film thickness are modified. Modular tape actuators can be aligned in parallel or in series to increase the actuation performance. Changing the geometry or the larger architecture can have similar effects in improving the actuator force or the stroke, with a trade-off coming from increased packaging size or complexity.

The impact on the actuation system's performance depends on the scaling type. There are fundamentally two types of scaling: parallel and series. Parallel scaling has the result of amplifying the force capabilities of the system. Series scaling has the impact of increasing the stroke of the system. Selecting the performance scaling method, either modifying geometric parameters or using multiple actuator modules, determines the difficulty in improving performance. Depending on the situation, either choice could be the easiest solution. The following section will first define the different types of scaling, including how they can be made and the potential challenges with each type. The next subsection will cover in the design space how scaling impacts the quasi-static design process and how one can determine which type of scaling should be used based on the system's requirements.

5.2.1. Parameter Scaling

The following subsection will cover the creation and limits of both geometric and architectural scaling. The geometry of a tape actuator comprises three primary parameters: width, length, and thickness. These parameters are variables that can be modified in the fabrication process. Each parameter influences the performance and necessarily has both negative and positive effects. The architecture scaling uses multiple DE tape actuator modules combined in series or parallel. The most significant macro effect from scaling is a change in the force levels, the displacement, the driving voltage required, and the packaging size. Modular scaling uses multiple actuators in either parallel or series to increase the actuator performance.

5.2.1.1. Width

The width of a tape actuator is directly linked to the force of the actuator. There are no physical limits on the maximum width of a tape actuator except those constrained by the application requirements and manufacturing complexity. Increasing the width will linearly increase the amount of active material, resulting in the actuator's force scaling linearly. The width of the packaging size will also increase linearly, with an increase in the width of the tape

actuator. There are physical limits to how narrow the width can become before the changing width affects the actuator's performance. The ratio between the height and width is critical because a tape actuator requires a lateral pre-stretch. The lateral pre-stretch enables the actuator to achieve large strains by thinning the actuator and allowing the surface pressure to be translated into an axial displacement rather than stretching the actuator biaxially. At some point, a low width will result in the complete loss of the lateral pre-stretch. Because the pre-stretch enables large linear actuation, a low ratio of width to height of the actuator will have a very limited actuation stroke.

5.2.1.2. Axial Length

The axial length of the actuator directly affects the total stroke of the actuator. The stroke of the actuator will scale linearly with the axial length of the actuator as long as the lateral pre-stretch in the actuator is maintained. There is no defined limit for the axial length of a dielectric elastomer, but it must maintain a sufficient width-to-length ratio such that the actuator can maintain the lateral pre-stretch in the film. Lengthening the actuator adds more active material, responding to applied voltage similarly to the original actuator. There is no limit to how short the actuator can be. The length of the actuator will change the packaging size of the actuator.

5.2.1.3. Thickness

An increase in the thickness of the film of a DE will scale force performance by increasing the stiffness of the complete actuator. The actuation stroke will be maintained if the increased thickness is linked to an increased voltage such that the applied electric field is maintained. The negative impact of increasing the thickness is that the required applied voltage to create actuation is scaled with the thickness square. The package size does not significantly change as the film thickness is increased.

5.2.1.4. Series Architecture

A scaled architecture with multiple tape actuator modules aims to increase the actuation force or stroke. An architecture with actuators in parallel will increase the total actuation force while maintaining the actuator stroke. An architecture with series actuators will increase the stroke while keeping the force level. These larger architectures increase actuation performance with a trade-off of increased complexity.

Series architecture scaling increases the total stroke of the actuator while also increasing the total length of the actuator. The multifunctional tape connectors in the DE tape actuator allow for easy connection between two actuators. The multifunctional connectors carry the embedded electrical connectors and the tape aspect, creating a secure mechanical bond. The modular actuator in-plane alignment maintains the thin packaging while increasing the total stroke. Two actuators in a series will double the stroke but double the total length because the multifunctional tape connector is nonactive. As the number of actuators connected in series becomes large, there will be a delay in actuation because of the resistance of the compliant conductors.

5.2.1.5. Parallel Architecture

Architecture scaling in parallel can be accomplished in two manners, but the result of either method is to maintain the stroke while increasing the actuation force. Tape actuators can be combined in a stack or parallel. The advantage of the stack actuator is that the force increases while the packaging space remains approximately the same. The minimal thickness of the tape actuators with the multifunctional tape connectors allows the actuator to be stacked without taking up significantly more packaging space. The actuators can be stacked until the attachment strength of the MTC connection to the external system is weaker than the stack of actuators. In the parallel case, the total width of the combined actuator has doubled, and the force has doubled. Both parallel architectures increase the force linearly with the number of actuators while maintaining the same stroke, provided the pre-stretch in each actuator is kept at the same level. An unlimited number of actuators can be combined side to side if there is space and a way to connect them electrically. The electrical connection will have to be done externally for adjacent actuators.

5.2.2. Architecture Scaling with Multiple Modules

One simple way to understand the impact of scaling is to look at performance changes in the force-displacement space. The two main effects of scaling in the force-displacement space are scaling the force while the displacement is maintained and scaling the displacement while the force is maintained. Scaling the performance will also impact the package size, complexity, or driving voltage. The effects of scaling a tape actuator are shown using three force-displacement curve pairs in Figure 93; each pair is a different line type. The OFF voltage curves are plotted in

blue, and the ON voltage curves are in red. For a nominal DE tape actuator, scaling the width, adding parallel actuators, stacking actuators, and increasing the film thickness all have the same effect in the force-displacement space of increasing the force levels without impacting the feasible displacement. The results of force scaling are plotted in dashed lines. Increasing the axial length of the actuator has the same effect as adding actuators in series, which is that the displacement is scaled without changing the force capabilities of the actuator. The results of displacement scaling are plotted in dotted lines.

The effect of scaling the force level in the force-displacement space is to increase both the force level for a given displacement and the vertical separation force level of the OFF and ON voltage curves. The impact of scaling the force on the design will depend on the type of external force. A constant force and a spring force external load will be explored to explain the impacts of scaling.

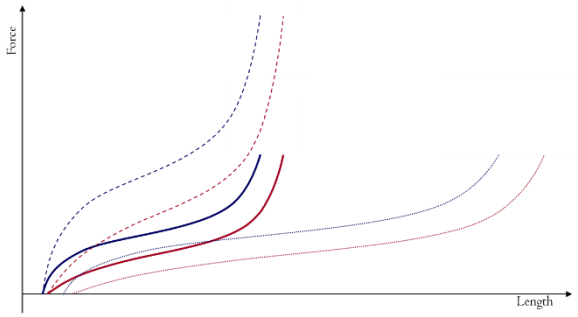

Figure 93. Scaling Effects on DE Tape Actuators.

The effects of scaling a tape actuator. Dashed lines represent parallel scaling, and dotted lines represent series scaling.

In the case of constant force, the impact of load scaling will depend on the interaction of the constant force level of the force-displacement curves. As a first -case example, let us assume that the external force is scaled directly with the increased actuation authority of the tape actuator, shown in Figure 94. The original system is plotted in solid lines with a thick green line.

In the case of constant force, the impact of load scaling will depend on the interaction of the constant force level of the force-displacement curves. As a first -case example, let us assume that the external force is scaled directly with the increased actuation authority of the tape actuator, shown in Figure 93. The original system is plotted in solid lines with a thick green constant force system line, and the scaled system is plotted in dashed lines with a thin green constant force system line. In this case, the stroke for the two systems is equivalent. In a second case, let us

assume that the force level is fixed with the original constant force level, shown by a thick green line, then scaling of the force will cause the external system to cross the force-displacement curves in the lower range of the curves, where there is low separation between the OFF and ON performance. Scaling the actuator's performance then reduces the stroke of the total system for the scaled load system compared to the original system. As another case study, let us assume the fixed load of the system is the higher constant force load, shown by the thin green line. In this case, the scaled load system will have an increased stroke compared to the original system. These examples show the importance of matching the external system and the tape actuator performance to achieve a good design.

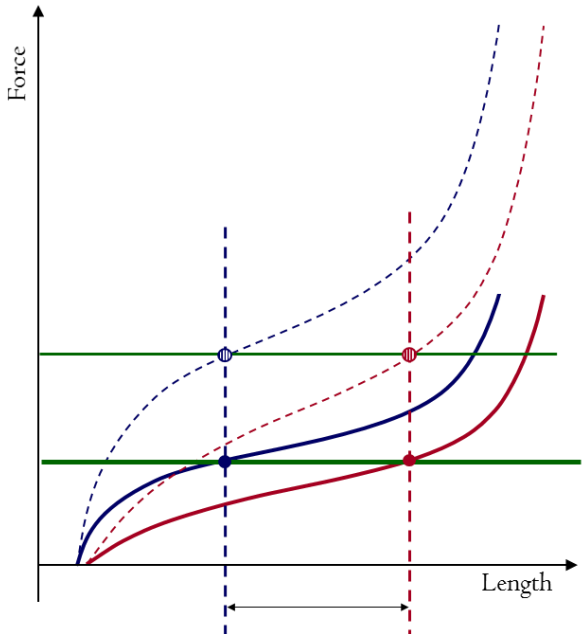

Figure 94. Impact of Parallel Scaling.

Impact of parallel scaling with a constant force in the force-length space.

In the case of a spring, the scaling of the force performance will typically have a substantial impact. In Figure 95, the original system is plotted in solid blue (OFF) and red (ON) lines, the scaled system is plotted in dashed blue (OFF) and red (ON) lines, and the spring system is plotted as a green line. The stroke of the system increases substantially for the scaled-force system as opposed to the original system. The actuation stroke increases because the scaled system has a larger force separation between the OFF and ON voltage curves. The new performance curves cause the system's equilibrium points to increase in force, resulting in an increased actuation stroke. For this case, the free-clearance is unchanged for the two systems.

Even though the free-clearance may not be in the optimal length for the largest stroke for each actuator curve, the spring system crosses both the performance curves in the middle parallel range close to the optimal stroke location. Intersecting the actuator performance curves in this parallel region provides good performance and has low design sensitivity because the OFF and ON voltage curves are close to parallel.

The increased stroke will depend on the stiffness of the external system. Softer springs, in general, will receive less stroke performance gains than stiffer springs. At the limit of low stiffness, which is equivalent to a constant force, the system will not have any improved stroke as long as shown in the previous example. The maximum increase in stroke for a system with a fixed spring stiffness will be equivalent to the actuator performance scaling. If the actuator is scaled by a factor of two, then the stroke can be scaled by a maximum factor of two. The maximum stroke scaling will occur only for very stiff systems. In general, for a spring system, the stroke gains for scaling the actuator performance curves will be linked directly to the stiffness of the spring system.

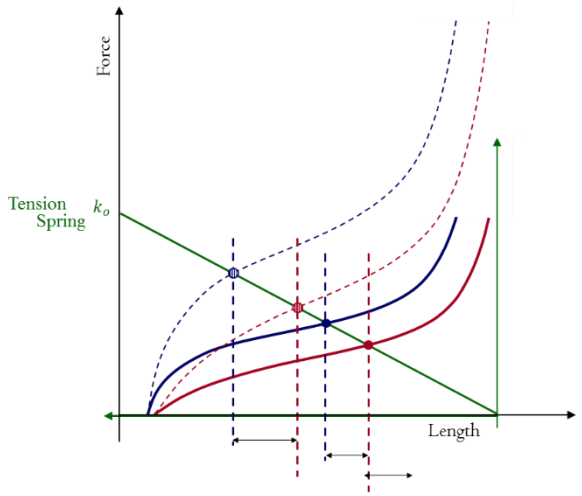

Figure 95. Impact of Parallel Scaling with an External Spring Force.

Impact of parallel scaling with an external spring force in the force-length space. The scaled performance curves are shown as dashed lines.

Scaling the displacement levels in the force-displacement space increases the total displacement range and the horizontal separation, or displacement length, of the OFF and ON voltage curves. The impact of scaling the displacement on the design will depend on the type of

external force. A constant force and a spring force external load will be explored to explain the impacts of scaling.

In the case of constant force, the impact of displacement scaling will result in a direct scaling of the stroke by the same factor. In Figure 96, the original tape actuator performance curves, shown as solid thick lines, are scaled by a factor of two as dotted thin lines and a constant force curve plotted as a green line. The stroke for a constant force is shown to double, which is the same as the displacement scaling factor. The actuation stroke will scale directly with the displacement scale factor for any external constant force level.

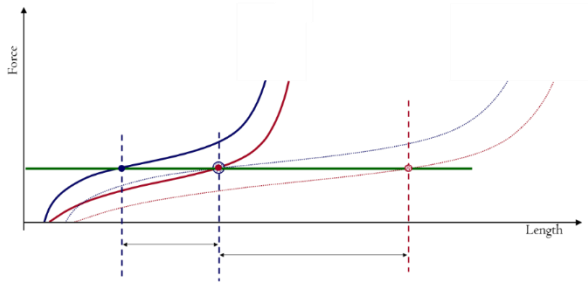

Figure 96. Performance Impact of Series Scaling.

Performance impact of series scaling of DE tape actuators when the biasing force is a constant force. The increased stroke is scaled by the number of actuators in series.

In the case of spring force, the displacement scaling will increase the stroke. However, the increase in stroke will depend on the spring stiffness and the actuator performance curves. In Figure 97, the original tape actuator performance curves, shown as solid thick lines, are displacement scaled by a factor of two, shown as dotted thin lines and a spring force curve is plotted as a green line. The stroke for a spring force is shown to increase marginally after displacement scaling. The same free-clearance is used for both sets of performance curves. Even though an optimized free-clearance is not used for each case, the spring force crosses the performance curves in the parallel region, where the performance level is approximately equal regardless of the free-clearance. For an extremely stiff spring system, displacement scaling will not change the actuation stroke because the vertical spacing between the performance curves has not changed with the series actuators.

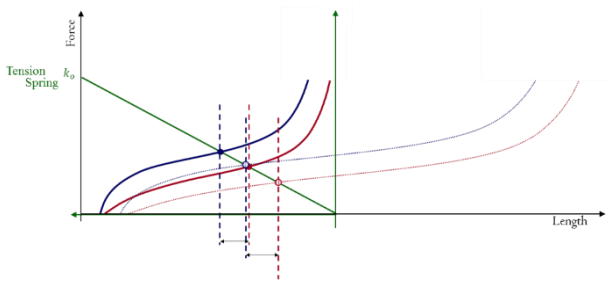

Figure 97. Series Scaling with a Constant Force Spring.

Series scaling with a constant force spring. The location of the graph intersection changes, but since the intersection points are in the middle plateau region, the actuation stroke remains approximately the same.

In summary, architecture scaling can be used to increase the actuation performance of a system and can be achieved in several ways, with the most common ways summarized in the previous subsections. Both force scaling and displacement scaling can increase the performance of a system. The type of performance scaling that can best be used to improve a system will depend on the type of external system. For softer spring and constant force systems, displacement scaling will substantially enhance the actuation stroke. For stiffer spring systems, a greater performance gain can be had using force scaling versus displacement scaling.

Force scaling can be achieved in many ways, each with advantages and disadvantages. Force scaling can be achieved through either geometric changes or a larger architecture. Increasing the width or thickness of a single actuator causes a force scaling for geometric changes. An advantage of geometric changes is that the scaling is infinitely adjustable, and an actuator can be precisely tailored for the application. Changing the thickness or the length will have different advantages. The advantage of changing the thickness is that the force is scaled within the same packaging size. The disadvantage of a thickness change is that the required driving voltage is increased. The advantage of scaling the length and width is that the driving voltage will remain the same. The disadvantage of increasing the width is that the overall package size will increase. There is also a geometric constraint such that the width-to-length ratio must remain large. A custom geometry actuator can be tailored for a specific design; however, this will require a custom fabrication process, adding to the overall complexity. The main advantage of using a modular system is the simplification of the fabrication process and the ability to change the scaling at any time easily. Stacking tape actuators scale the force in whole increments. A disadvantage of stacking actuators is that multiple actuators make the implementation slightly

more complex. Adding actuators in parallel has the same effects as adding width, except an additional electrical connection will be required for the additional actuator. Adding actuators in parallel also increases the width.

In the case of series scaling, there is a significant limit to the amount of geometric scaling that can be achieved compared to architectural scaling. The length of the actuator can be increased during the fabrication process, which will result in larger displacement. However, there are significant limits to the amount of the possible increase. When the length is increased, the length-to-width ratio decreases, which can reduce the pre-stretch, which provides a large actuation. A greater length can be achieved only by maintaining the length-to-width ratio, resulting in a larger package size and stiffer actuation performance curves. Architecture series scaling does not suffer this limitation of increasing the length because each tape actuator is supported by its multifunctional tape connector. The actuator can be connected in series without increasing the width. The disadvantage of architecture scaling is that the MTC introduces inactive material to the length so that the actuator will be made longer by the number of actuators used. The other advantage of using a modular architecture in series rather than a geometric lengthening is that the manufacturing process does not need to change. Standardizing the fabrication process leads to more repeatable results and robustness.

5.3. Actuator System Categorization for Common or Useful Actuator Situations

There are many ways to approach the external systems to understand their relevance to dielectric elastomers. One approach used here is categorizing the systems in the context of actuator design for DEs.

There are many different types of external systems, and to aid in understanding them, six categories of systems and system architectures relevant to DE tape actuators will be identified: constant force, spring force, leverage designs, reverse bias designs, antagonistic designs, and reverse bias antagonistic designs. To further enhance the usefulness of these categories, each identified system can be evaluated on the actuation performance stroke, the design sensitivity, design complexity, and implementation complexity.

The actuation performance could be related to many different variables, depending on the situation. The possible variables include actuation strain, force, speed of actuation, dampening, specific force, and specific energy. A large-strain actuation stroke is the performance property

that sets dielectric elastomers apart from other technologies, so To simplify the performance evaluation, the stroke will be used to evaluate performance. The performance stroke of the actuator will then be assessed against the total stretch range of the tape actuator.

The sensitivity of the design is a measurement of how much the performance stroke will change as a function of the design changing. In the previous section, it was described how scaling the actuation could impact the performance. Under some circumstances, the performance would not change under scaling. The design is not sensitive in these situations because the scaling does not change the performance. On the other hand, some actuators experience extreme changes in stroke with scaling. These systems have a sensitive design.

Design complexity is related to the number of design variables and the impact of changing the variables on performance. The theoretical design controls The overall performance and sensitivity of the design. Design parameters are completely under the designer's control, and the number of these variables increases the complexity of the design and possibly the performance. With more variables, the possible peak performance is harder to identify.

The implementation complexity is the number of parts, the challenge in fabrication and assembly, and the types of interfaces. The implementation complexity requires a trade-off that will have to be made with the design in general. More intricate external system designs that use the entire dielectric elastomer stretch range will require a more complex implementation than a constant force or simple spring. One of the primary advantages of DEs over conventional technologies is the simplicity of the actuation and the lack of moving parts. As implementation complexity increases and additional complexity is introduced, the advantage of a dielectric elastomer actuator over other technologies will be reduced. It also introduces more failure points.

A trade-off among the four categories, actuation performance, sensitivity of the design, design complexity, and implementation complexity, is required when designing a DE to work with a system. The trade-off needed is illustrated with six identified systems that will be evaluated on the key parameters.

5.3.1. Constant Force

Constant force systems demonstrate the advantage of dielectric elastomers' ability to create large actuation strokes. Constant force systems are also relevant because they are easily used and can be easily replicated for experimental validation.

A simple constant force system with the coordinate frame defined is schematically shown in Figure 98. The system performance can be evaluated using the quasi-static design process described in Section 5.1. The typical coordinate starts at the interface of the active material and the MTC, with a positive direction toward the active material. A constant force is independent of all coordinate frames; therefore, the second coordinate frame can be defined as the primary coordinate frame without a coordinate transformation. The system equilibrium and actuation are schematically shown in Figure 99, with both the ON, $0V$, and OFF, $+V$, equilibrium lengths. The actuator length without the force applied, as shown in Figure 98, is shorter than the OFF equilibrium length shown in Figure 99 because the elastomer must stretch to balance the external force.

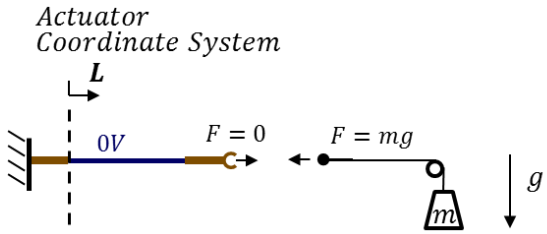

Figure 98. Simple Constant Force System with Coordinate Systems Defined.

Simple constant force system with coordinate systems defined.

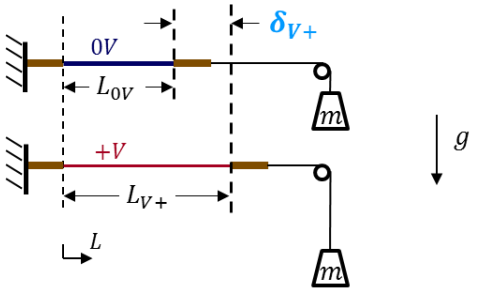

Figure 99. Constant Force System in Equilibrium Positions.

Simple constant force system shown in the equilibrium OFF and ON states.

The force-displacement design space is plotted in the coordinate frame of the DE tape actuator, as shown in Figure 100. There is only a single design variable for a constant force system: the force level. There is no free-clearance because the external system does not change as a function of position. Therefore, the final design space is plotted with the green horizontal line representing the constant force, the blue line representing the OFF voltage curve, and the RED line representing the ON voltage curve. System stroke is the length between the two equilibrium locations, where the green line crosses the OFF and ON voltage curves, the vertical blue dashed line, and the vertical red dashed line. The horizontal force line is nearly the same slope as the actuation curves, which allows the constant force systems to have a high actuator stroke. The actuator stroke depends on the force level, but it can be large when selected correctly.

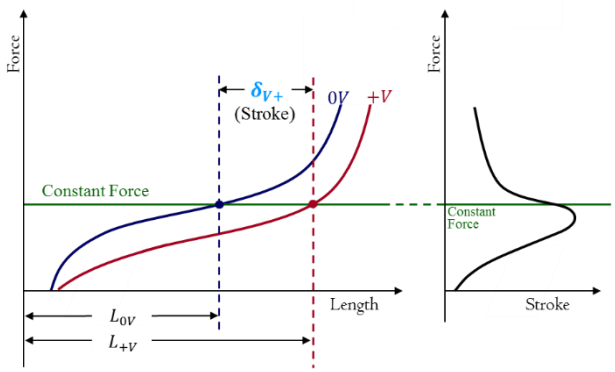

Figure 100. Constant Force System Design Plots.

Constant force system represented in the force-length space and force versus stroke.

The constant force systems contain two regions of low sensitivity where the stroke is relatively stable: near the peak stroke and at high loads. Directly around the peak stroke region for the OFF and ON performance, the curves are relatively parallel, so the stroke will be insensitive to small system changes. However, a small decrease in the actuator stroke will occur if the peak is not hit exactly. Farther from the peak stroke location, the actuation stroke changes substantially. At high loads, the actuation stroke decreases with an increasing load, but the slope is small, so the system will not be extremely sensitive to small changes in the configuration. At high loads, any increase in load will decrease the actuation stroke, while a reduction in load will increase the stroke.

The simplest form of a constant force is generated by gravity. Gravity times the mass results in a constant force. Another way to produce a constant force is to use a constant force spring element, which can be a helical spring, a spool, or a superelastic SMA wire. There are also many more complex methods for producing a constant force; however, the performance of any constant force system will be the same.

There are multiple challenges when using constant force systems, depending on the source of the constant external force. If a system depends on gravity for the origin of the force, then the system will be severely limited in its application because it must maintain a constant orientation to gravity; otherwise, the force in the system will change. This dependence on orientation to gravity limits the applications. The mass of gravity-driven constant forces also generates inertial forces. The inertial forces increase at a faster rate than the applied force. Therefore, higher inertial forces will be seen in applications that require higher forces. Using a constant force spring as a biasing element minimizes the inertia and eliminates the challenges associated with

using gravity as a constant force. Typically, constant force springs will come in form factor, which will significantly increase the packaging space of the total system. Any rotation elements increase the system's complexity and eliminate the simplicity advantage of dielectric elastomer actuators. The need for a rotating system introduces the need for bearings and other system requirements, which increases the system's complexity and detracts from the simplicity advantage of DEs. Overall, the implementation complexity is low for a large actuation stroke. If gravity generates a constant force, then the system will be limited to its orientation to gravity, while systems that use springs will have added complexity without increasing the performance.

5.3.2. Spring Force

The stroke is highly dependent on the type of system configuration. A spring system, which is very common in the real world, can be characterized in its coordinate frame, where the force is zero at the origin and increases as the spring is elongated, as shown by the green line in Figure 103. A schematic of a basic spring system is shown in Figure 101, where the spring coordinate frame is reversed and offset from the coordinate frame of the DE actuator coordinate frame. The coordinate offset is the distance between the two coordinate frames minus the length of any passive material, which is the multifunctional tape connector. Schematically, the two systems are shown combined in Figure 102 when the voltage is OFF and ON. Also, the two equilibria are shown in the force-length design space, and the difference in these two locations is the stroke of the actuator, which is smaller than the stroke for a constant-force system.

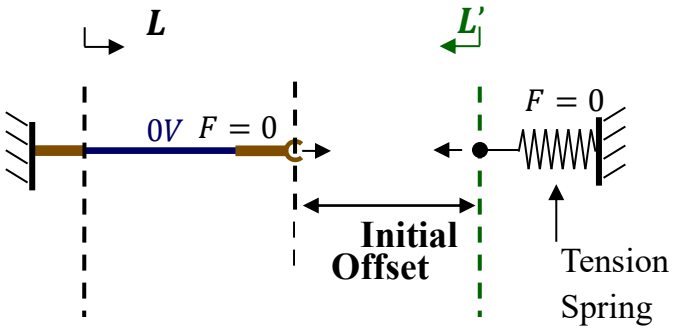

Figure 101. Schematic of Antagonistic System Showing Free-Clearance.

Schematic of a dielectric system with a second actuator as a biasing force forming an antagonistic system.

A spring is a mechanism that stores strain energy through elastic mechanical deformation. The spring constant typically defines a spring, k (n/m), which is the force required to move the element over a distance. The simplest representation of a spring system is a constant spring where the constant, k, is the same as the length changes. These systems can also exist in tension or compression. A more complicated spring would be used in a system with a nonlinear spring constant where the slope of the force-length curve changes as a function of position. Nonlinear springs are quite common in the real world; they can take any shape and have a spring constant from almost flat and constant to very stiff and vertical. They may also have negative slopes where the stiffness increases as a function of length.

A common biasing element in DE actuators is a spring force. All elastic forces can be represented by some spring. Although the definition of a spring is very broad, this section will be limited to linear springs with constant stiffness that does not change with position. Limiting the systems to a constant force spring is to exemplify the characteristics of a spring system in a simple system. Even within constant springs, there is a large range of stiffnesses. A constant force is an infinitely soft spring, while a blocking force is an infinitely strong spring. There are many methods for producing a constant stiffness spring, but the most common type of linear spring is a coiled spring.

A schematic of a DE with a spring biasing force is shown in Figure 102. The system identification system discussed in the previous section will again be used to characterize the system. The coordinate frame, L, for the DE, is the previously identified standard one that starts with the active material. The coordinate frame for the spring, L', is in line with the spring and the L coordinate frame but with an inverted primary axis that starts at the end of the spring when there is no force on the spring. Each element is characterized in these two systems. The two systems are combined into one, shown schematically in Figure 102, indicating the equilibrium with the voltage. The two coordinate frames are joined into a single coordinate frame by multiplying the spring constant by a negative one and using the distance between the two coordinate frames as the coordinate offset. The coordinate, or initial, offset is the distance between the two coordinate frames with any inactive material removed, which has been previously defined in Section 5.1. The free-clearance and the coordinate transformation are then used to plot both performance curves on a single force-displacement plot, as shown in Figure 103.

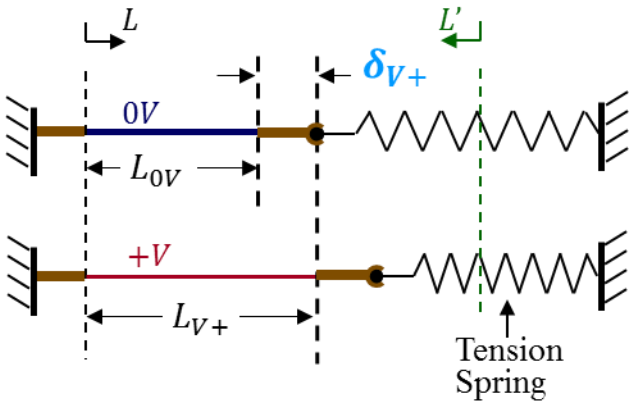

Figure 102. System in Equilibrium with the Applied Spring Biasing Force.

The schematic of a dielectric elastomer spring system in equilibrium with the applied biasing force.

The sensitivity of a dielectric elastomer actuator stroke working in conjunction with a spring will depend on the performance curves of the two elements and also on how they are combined, which is dictated by the free-clearance. In Figure 103, the DE performance is plotted for the low-voltage curves in blue and the high-voltage curves in red, while the spring in the transformed coordinate system is plotted in green. The plot also contains the total length of the OFF voltage DE and equilibrium and the total length of the DE with the ON voltage equilibrium. The difference between these two lengths is the stroke of the actuator. The coordinate offset is also shown in Figure 103. The coordinate offset also contains within it the free-clearance. Therefore, changing the free-clearance will change the coordinate offset, which is how the free-clearance is used to change the performance stroke of the combined system.

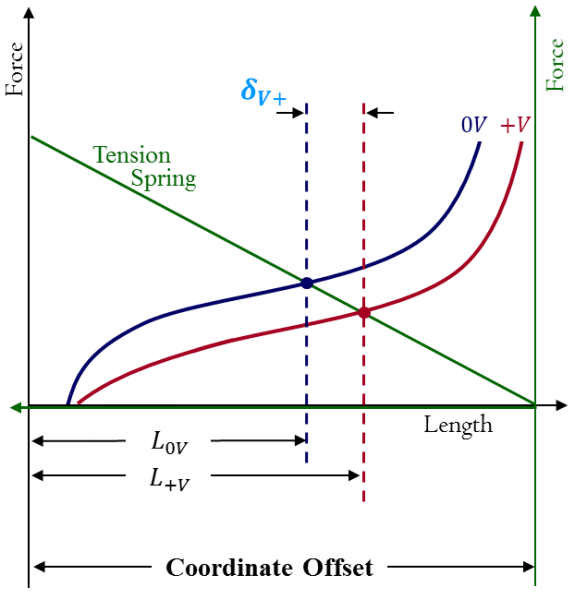

Figure 103. Design Graph Showing Force-Displacement Performance Curves.

The force-displacement performance curves of the dielectric elastomer and spring are plotted on a common coordinate system using the coordinate offset. From these data, it is then possible to determine the actuator stroke between the low-voltage and high-voltage states.

Dealing with quasi-static actuation and more complex initial settings, such as the free-clearance of the force-displacement plot, is very useful for determining performance. This example shows the tension spring crossing through the middle plateau of the DE. Slight perturbations of the coordinate offset would not significantly impact the stroke of the actuator because the lines are parallel in this region. However, as the coordinate offset is shifted substantially left or right, the stroke will decrease and, at certain locations, will start to decrease dramatically when the dielectric elastomer curves are in the initial stiffness zone or approaching the high-stiffness range and the asymptotic stretch limit.

The design complexity of a spring system is relatively straightforward because only two principal design variables need to be adjusted: the stiffness of the spring and the free-clearance. The impact of changing the free-clearance is to shift left or right the locations where the spring crosses the actuation curves of the DE. Shifting the preload left or right will allow the spring to interact with different regions of the DE and can be moved to where the optimum performance is possible. The stiffness of the spring controls the slope of the external system, which then provides for the maximum possible actuation stroke. Modest changes to either of these variables

will produce modest changes in the performance; therefore, it is fairly simple to design systems with a spring force.

The implementation complexity of spring systems is relatively low. Springs are very common elements and easy to understand and integrate into systems. Purchasing a spring to use as a constant force is very easy. Springs do not have moving parts and are very simple systems, which makes them good options for biasing elements. When purchasing springs, getting different spring constants varying from tension to compression forces is easy. Springs are cheap because they are made by altering the bending stiffness of the materials.

Springs are a challenge because they depend on their bending stiffness, which is not fully understood, although if the actuation is limited to certain stretches, the force-displacement is constant. When functioning with a DE, the problem with spring systems is that they do get a decreased stroke performance because of the nature of the force-displacement profiles of the curves. Attaching a spring can be challenging because it needs to be anchored so that the metal spring anchor place pulls in a certain direction. The most common springs are linear and pull at a focused point, which takes away from the advantage of distributed actuation. There is a need to look for alternative types of springs, such as the bending of flexible plates or their materials, that do a better job of providing the bias force and taking advantage of the distributed conformal advantages of DE actuators.

5.3.3. Leveraged Force

This transformation is important as it can enhance fixed system-actuator performance or transform actuator work to match the system's needs. The mechanism transforms the shape of the force-displacement curve into another shape at the end of the mechanism.

Leverage systems are relevant because they are a way to increase the performance of a DE actuator or to change a system’s force-displacement profile so that it can be used to a better degree, as shown in Figure 104. Some systems are complex and have multiple components, or because there is no easy way to attach to a system directly, it is necessary to use a mechanism to facilitate the attachment. Leverage systems enable a system to change its force-displacement profile. Leverage is a tool that can be used to enhance actuation.

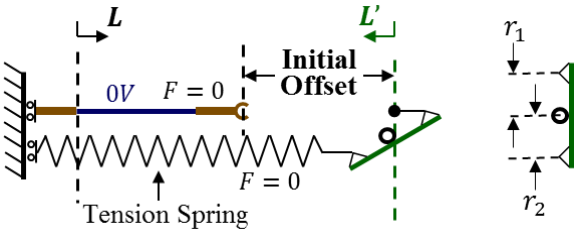

Figure 104. Leverage System Schematic with Initial Offset.

Leverage system shown with a spring acting through an infinitely stiff beam on a frictionless pivot and always pulling in line.

To explore the capabilities of a leverage system, a simple symmetrical beam connected to a DE tape actuator and spring is shown in Figure 105. The free-clearance is defined as the length the tape actuator needs to stretch to reach the attachment point on the lever arm when the arm is connected to the biasing spring and internal forces on the spring are minimized. If the system allows, the internal force will be zero when the free-clearance is measured. The system schematic is shown in Figure 105 and the voltage OFF and ON equilibria.

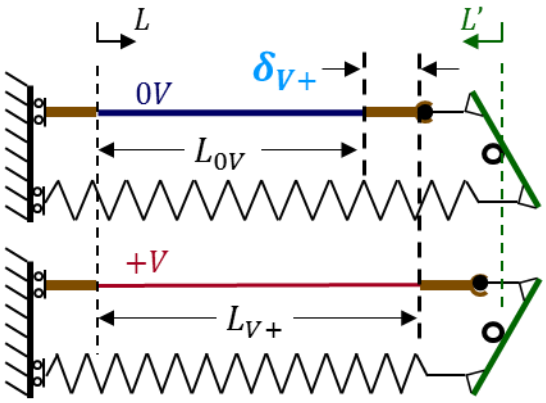

Figure 105. Leverage System Equilibria Points.

Voltage equilibria ON and OFF schematic of a single-pivot system.

Using a quasi-static design process for a leverage system enables easy design and understanding of performance impact with parameter modifications. The basic components that must be characterized are the tape actuator and the spring. The primary coordinate frame will be selected as the tape actuator coordinate frame. The coordinate transformation encompasses the leverage system and transforms the spring into a reversed and offset coordinate frame from the tape actuator. as in Figure 106, the system appears equivalent to the spring-biased system when combined into a single graph.

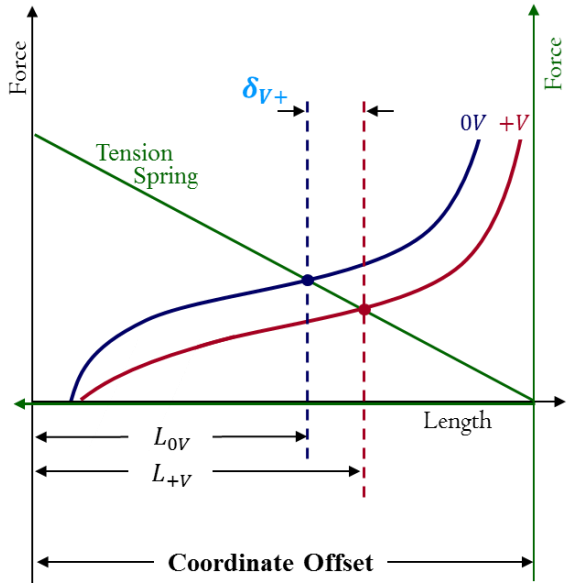

Figure 106. Primary Coordinate Frame Design Graph with Performance Curves.

DE actuator and pivot biasing force plotted in the primary coordinate frame.

The resulting system in the force-displacement space is the same as the spring force system. Two design parameters can change the system: the free-clearance and the leverage ratio between the two lever arms. The free-clearance has the same capability to shift the equilibrium positions of the system as shown in the previous spring example. For a more detailed explanation, please see Section 5.1.

The design parameter easily modified in the spring lever system is the ratio of the lever arms. The impact of changing only the lever arm ratio is shown in Figure 107.

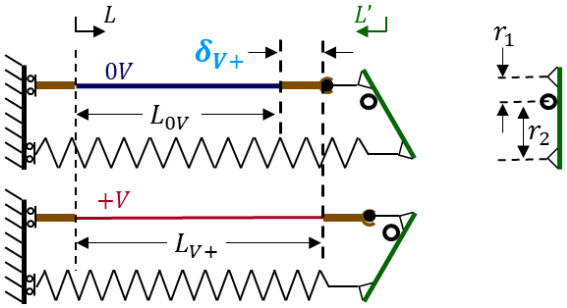

Figure 107. Unequal Leverage Equilibrium Positions Schematic.

Schematic of leverage equilibrium positions when the pivot point has moved and the moment arms are of different lengths.

The original ratio of the lever arms is $k_0 = 1$, shown by the solid green line, where the two arms are the same length. If the leverage ratio is raised, as shown by k_3, then the impact would be to increase the apparent stiffness of the external system in the actuator coordinate frame, as shown by the green dashed line in Figure 108. The result of the increased stiffness is that the stroke of the actuator is reduced, while the total work will most likely decrease because the stroke has decreased and the force level is approximately the same. On the other hand, if the leverage ratio is reduced, as shown by k_2, then the apparent stiffness of the external system will decrease in the primary coordinate frame, as shown by the dotted green line in Figure 108. The softer system has a larger actuation stroke, and the total work is greater because the force level is approximately the same.

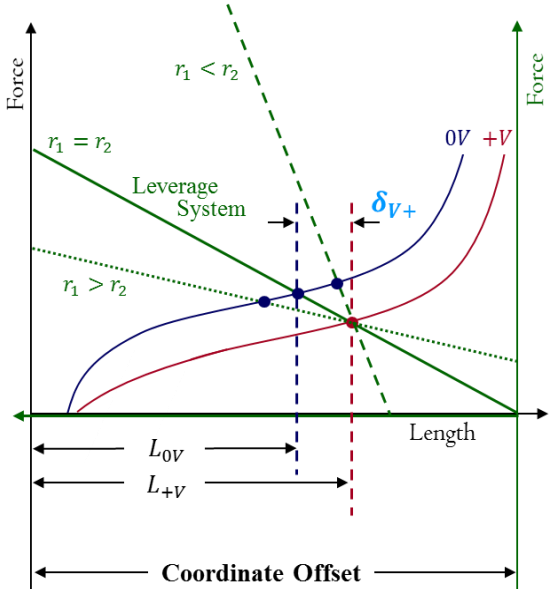

Figure 108. Transformed System Performance into the Design Graph Plot.

Forced-displacement graphs showing the transformed system in the coordinate frame of the dielectric elastomer when the ratio of the moment arms around the pivot is modified.

The design complexity of a leverage system will depend on the complexity of the leverage mechanism. as shown in the previous example, the system's slope will depend on the moment arms' ratio and the free-clearance change for simple leverage mechanisms. The coupling of the changing ratio and the change in the free-clearance makes the system of medium complexity. However, it is possible to vary the geometry to maintain the same free-clearance, thus simplifying the design. It is also possible to use much more complex leverage systems to produce

the desired performance; however, this example is limited to a very straightforward, simple leveraging mechanism.

The advantage of a leveraged system is that it is possible to tailor the performance to exactly what is needed. Leverage can transform a linear system into rotary motion and vice versa. Leverage can also convert a surface actuator into a point actuator or a point actuator into a surface actuator. The challenge with a leverage system is that more complexity is introduced. There are more moving parts, and that means more potential failure points. Leverage can also have the effect of changing the packaging shape, which can hurt the performance of the system. Commonly, some leveraging mechanism will be required due to packaging constraints, which provides the opportunity to tailor the performance to match the performance of the DE actuator. The stiffness appearance of the external system can be changed to better match the performance of the tape actuator.

5.3.4. Reverse Bias Force

Reverse bias systems are relevant to DE tape actuators because they are one way to use the full range of performance. A reverse bias force has a high force at small displacement and a low force at high displacement, which is the opposite of typical springs, which have a low force at low displacement and a high force at high displacement. Reverse bias forces are great for dielectric elastomers because the hyperelastic curve in the large stretch range, where the ON-and-OFF occurrences are approximately parallel, has the approximate shape of a reverse bias spring. Therefore, the performance of a reverse bias spring can closely match the force-displacement of a DE and use the full stretch of a DE actuator.

A simple reverse bias system is an inverse pendulum. An example of this type of system is a mass at the end of a beam that pivots with an actuator attached along the beam, as shown in Figure 109.

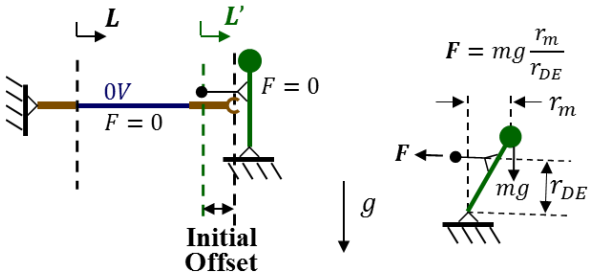

Figure 109. Schematic of an Inverted Pendulum.

Schematic of an inverted pendulum attached to a dielectric elastomer, which creates a reverse bias system for the dielectric elastomer.

When the mass is vertical, the torque caused by the mass around the pivot location is zero. As the beam rotates, the torque increases as the horizontal distance between the mass and the pivot location increases. The maximum torque occurs when the arm is horizontal or perpendicular to gravity. The opposing torque is provided by the actuator attached to the beam. The torque supplied by the actuator is a function of both the actuator force as well as the moment arm of the actuator. The moment arm is the perpendicular distance between the rotating actuator coordinate frame, which is aligned with the actuator, and the pivot location. This moment arm length decreases as the mass pivots to the horizontal. The result is that the force on the actuator appears as a ratio of the two moment arms, which increases as the mass pivots. (See Figure 110.) The final result is a system characterization curve where the force increases as the DE actuator lengthens, as opposed to remaining constant as it would have without the reverse bias leverage.

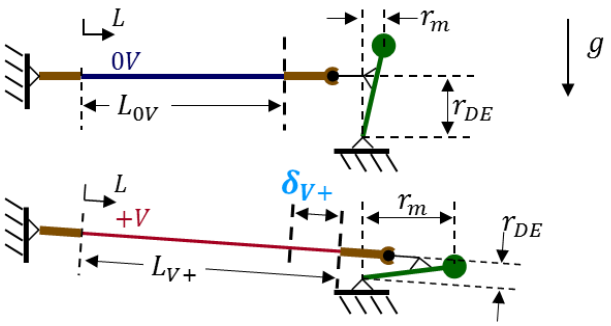

Figure 110. Pendulum Equilibrium Positions.

Schematic of the ON and OFF voltage equilibrium positions of a reverse bias system using a pendulum.

For an inverted pendulum supported by a DE, as shown in the schematic in Figure 109, the resultant external system will have a reverse bias. The system's two components are the tape actuator and the inverted pendulum. The DE will be characterized in its primary coordinate frame. The inverted pendulum can be described with the moment as a function of the angle, with a zero angle being the unstable equilibrium. The tape actuator's primary coordinate frame is always aligned with the DE. In this case, that coordinate system will rotate so that it is always directly in line with the fixed anchor and the attachment point to the pendulum. The force angle characterization of the inverted pendulum is then transformed into the primary DE coordinate system. Setting the second coordinate frame for the pendulum to be zero when the force of the pendulum is zero simplifies the free-clearance since it, too, will be zero. The two systems can then be combined, as shown in Figure 111, and the stroke determined for the two systems.

The free-clearance for this combined system is extremely important to enable the reverse bias to match up with the tape actuator's performance curves. One interesting aspect of the free-clearance is that it is negative, meaning that rather than being stretched to reach the zero-force location of the external system, it will need to be compressed. This negative free-clearance is because the inverted pendulum is inherently unstable and needs to be rotated away from the fixed anchor to achieve equilibrium. This results in a system that uses the DE actuator's full stroke, exploiting the actuator curves' parallel characteristics and providing much more motion. Using the whole length of the hyperelastic curve increases the strain of the actuator and the amount of work that can be performed.

The force-displacement graph in Figure 111 shows the advantages and challenges of a reverse bias system. The green line represents the reverse bias force in a DE coordinate system. The green line starts at the origin, then crosses the DE OFF curve in the initial stretch region, and crosses the DE ON curve at the end of the middle plateau region of the elastomer. This results in an extremely large stroke for the actuator. The challenge of reverse bias systems is that they are extremely sensitive to slight changes in the design parameters. If the parameters are off, such that the reverse bias system shifts slightly, the result will be that the stroke is significantly decreased because it will cross both DE curves at the end of the plateau region. On the other hand, if the reverse bias system shifts down, the reverse bias curve will cross both the DE curves in the initial stretch region, resulting in a much -reduced actuation stroke. It is also extremely possible to have

a system where the reverse bias does not cross both performance curves, resulting in an actuation system that would not function.

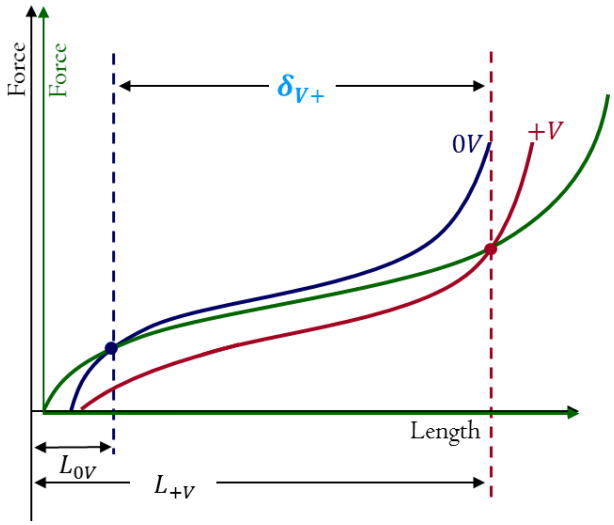

Figure 111. Profile of a Reverse Bias System.

Force-displacement profile of a reverse bias system where an extremely large actuation stroke is achieved by matching the external system to the shape of the dielectric elastomer performance curves.

Design complexity will depend on how little reverse bias system is created. In this case, a limited number of variables are used: the ratio of the moment arms, the mass of the pendulum, and the free-clearance. Even with this limited number of variables, producing systems that would not function with the dielectric elastomer is extremely easy. The shape of the reverse bias force in the primary coordinate system depends on all the variables, but each will have a different effect. The free-clearance will generally shift the transformation coordinate frame to the left or right relative to the primary coordinate system. The location of the DE attached to the pendulum relative to the center of the mass will generally control the overall shape of the reverse bias system. The mass of the pendulum will, in general, affect the slope of the reverse bias curve. A heavier mass increases the slope of the transformed performance curve, while a lighter mass decreases the slope of the transformed performance curve. The design complexity of the system is moderate because it is possible to understand the impacts of changes to the design parameters intuitively.

The challenges of working with a reverse bias system with dielectric elastomers are that they are hard to produce, and the design space for good performance between the two DE actuation curves is a small window. Achieving the tolerances needed actually to produce the desired

actuation is challenging. It is also possible that upon implementing the design, enough tolerance errors can lead to catastrophic failure: either a runaway electric field event or the mass overcomes the maximum stretch limit of the dielectric elastomer. The system can also have infinite leverage, which would cause the system to cascade until failure. Potential dielectric limits can also be reached, where the provided voltage will need to be scaled as the elastomer stretches because the dielectric field strength of the material changes with stretching, and dielectric strength also changes.

A further limitation of the system is that an unstable pendulum requires a physical orientation relative to gravity to function, which will limit its applications. Dynamic configurations introduce added complexity because inertial effects affect the system's performance. There are limited methods to achieve reverse bias; therefore, the actuation system has to be designed specifically with reverse bias in mind. The limited and complex means required to achieve a reverse bias spring means that the whole design must be tailored to the situation.

5.3.5. Antagonistic Force

One way to achieve large strokes with DE actuators independent of gravity is to use them in an antagonistic configuration. An antagonistic actuator system involves multiple actuators, each providing the bias force required to produce actuation. The simplest antagonistic system involves two directly opposite actuators, which is seen schematically in Figure 112.

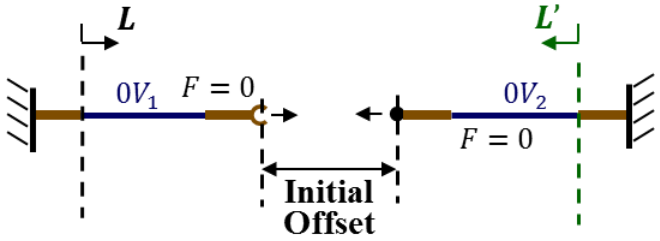

Figure 112. Simple Antagonistic System.

A schematic of a simple antagonistic system where the dielectric elastomers are used to produce the biasing force for each other.

This system configuration results in four equilibrium points, shown schematically in Figure 113:the first, where both actuators are OFF; one when the first actuator is ON and the second is

OFF; one where the second actuator is ON and the first is OFF, and finally when both actuators are ON.

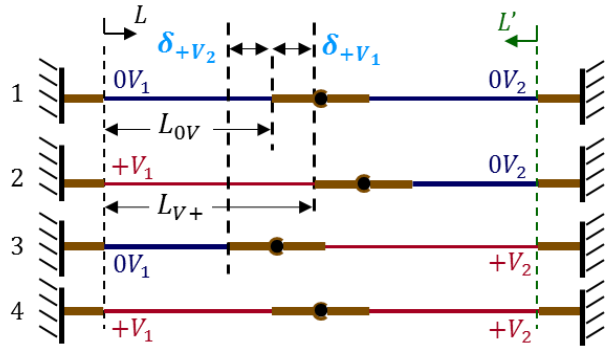

Figure 113. Schematic of the Four Equilibrium Positions.

A schematic of the four equilibrium positions possible for an antagonistic system using two dielectric elastomers.

The two components of an antagonist system are the two actuators. Each actuator can be characterized in its coordinate frame. The coordinate transformation involves flipping the axial direction of the one actuator and setting the offset of the anchor locations. The two systems are combined in Figure 114. The maximum stroke achievable is equivalent to a constant force when the system is alternated between the ON/OFF and OFF/ON states. This design also allows the system to come to equilibrium anywhere inside the diamond by applying partial voltages to the actuators. The free-clearance of the system will control the magnitude of the stroke of the actuator. It is also possible to achieve a range of actuation strokes at different force levels and create different force levels for a given stroke.

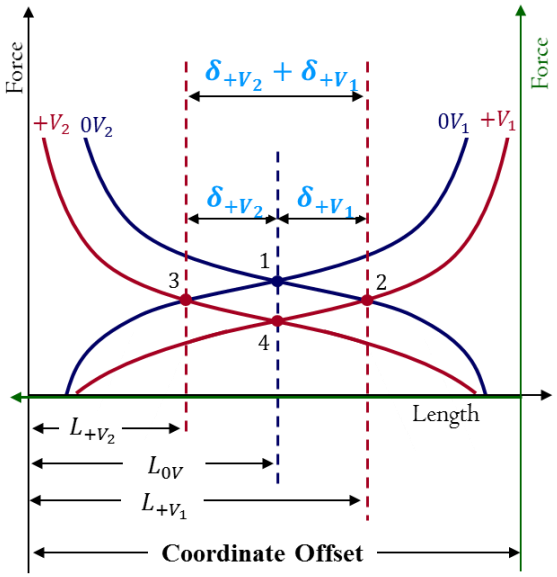

Figure 114. Antagonistic System Force-Displacement Design Graph.

Force-displacement graph showing the dielectric elastomer performance curve for an antagonistic system using two dielectric elastomers. Possible performance is described by the approximate diamond shape in the center of the graph.

The design sensitivity of this antagonistic configuration is low. The only significant design parameter is the free-clearance, which controls the equipment offset. Free-clearance controls where all equilibrium positions appear on the hyperelastic curves. For the larger stroke design, the curves will be arranged such that the two curves cross the plateau region of the hyperelastic curve. Since the performance curves are relatively parallel in this region, slight parameter variations will not significantly affect the maximum performance. The system also allows for any stroke and force within the area defined by the four equilibrium points. This flexibility simplifies the design process if the system is designed to enclose the target performance within the performance space.

In terms of design complexity, the technical system is simple. The free-clearance controls the location of the four equilibrium points. Increasing the free-clearance will shift both equilibrium points up the highlighted hyperelastic curve, while decreasing the free-clearance will shift the equilibrium points down the hyperelastic curve.

The implementation complexity of an antagonistic system is low and has many potential benefits. The actuation performance is equivalent to a constant-force mechanism and has the

same advantages of a large stroke, but it is independent of gravity and significant inertial effects. Using a second DE actuator as the biasing element enables the whole actuation system to consist of soft and conformal materials. Another advantage is that an antagonistic configuration uses completely distributed actuation, which can lead to decreased requirements for support material at the interfaces. With the second actuator comes an additional set of force requirements and a second control system. Coordination of the control systems is necessary to achieve the desired performance.

There is an increased packaging size because the actuators are offset from each other. It will be challenging to align the actuators precisely, and offset moments may need to be accounted for in the design by artificially reducing the possible actuation performance from the model predictions. Although an antagonistic design gives the equivalent stroke of a constant-force system, which is better than what can be achieved by a spring system, it is not nearly as beneficial in terms of stroke as the reverse bias gravity system, but it can be physically orientated independent of gravity.

5.3.6. Reverse Bias Antagonistic Force

In general, as the system's complexity is increased, it is possible to fine-tune performance curves to achieve the greatest performance by a DE tape actuation system. However, the system's complexity also leads to a more complex design process and a more sensitive design. One way to achieve this increased complexity is to use multiple design configurations. As discussed in Section 5.3.4, A gravity-driven reverse bias system5.3.4 achieves great performance but at the cost of high design sensitivity and significantly challenging implementation complexity. Alternatively, the direct antagonistic configuration, discussed in Section 5.3.5, is a relatively simple design, with design insensitivity and low implementation complexity while still providing significant performance benefits. Leveraging mechanisms, discussed in Section 5.3.3, are a useful way to adjust the performance of biasing elements in an actuation configuration setup. Combining three configurations makes it possible to create a reverse bias antagonistic system. This reverse bias antagonistic configuration can have many advantages over individual configurations while reducing some negative implementation and sensitivity aspects of different designs.

A reverse bias antagonistic design is shown in Figure 115. The design uses dielectric elastomers acting against each other through a leverage mechanism. In this case, both actuators are identical; therefore, they can be characterized in the standard force-displacement space. Two coordinate frames are identified to be used for the system: L, the standard coordinate frame for a DE actuator, and L', which is the second dielectric elastomer actuator transformed through the leverage mechanism. The key variables for the setup are the free-clearance, defined below, the length of r_2 and r_1, and the ratio of these two distances.

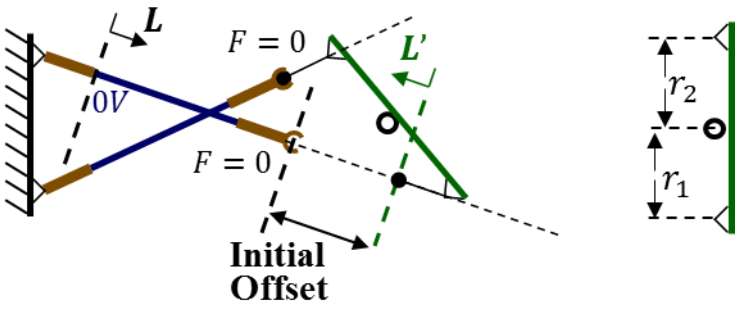

Figure 115. Reverse Bias Coordinate Systems.

A schematic of a reverse bias system with the primary and secondary coordinate systems defined along with the critical variables r_2 and r_1 and the free-clearance.

Figure 116 shows the schematic of how the reverse actuation system works. In the figure, the secondary DE extends during activation, and the primary DE contracts. As the system rotates, the leveraging changes as a function of l_2 and l_1.

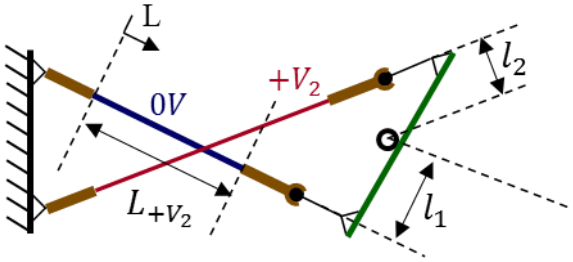

Figure 116. Reverse Bias Antagonistic System Equilibrium Positions.

Reverse bias antagonistic system connected with one dielectric actuator activated, showing the moment arms used for calculating the torque around the pivot.

The next step is transforming the secondary coordinate system into the primary one. The result of this transformation is that it is possible to see how the moment arms of the system affect

the transformation. The ratio of the two moment arms is the key variable that controls the transformation from the primary coordinate system into the secondary coordinate system. Figure 117 shows the standard force-displacement curve in the L prime coordinate system, the faded red and blue curves, and the force-displacement after the coordinate transformation of the dark red and blue curves has transformed it. The ratio of the two moment arms controls the magnitude of the transformation. When the primary actuator is activated, the length of the first actuator increases, which causes the l_1 moment arm to decrease and the l_2 moment arm to increase. Therefore, the ratio of the two variables is large, which causes the apparent stiffness of the secondary actuator to be large when the primary actuator is extended. This is shown on the right side of the figure, where the low stiffness of the secondary actuator increases substantially to have a much higher stiffness. Conversely, when the secondary actuator is activated, and in an extended length, the ratio of the two variables becomes small, such that the apparent force in the primary coordinate system is small. The result of these transformations is that the secondary actuator is transformed into a reverse bias slope in the coordinate system of the primary actuator.

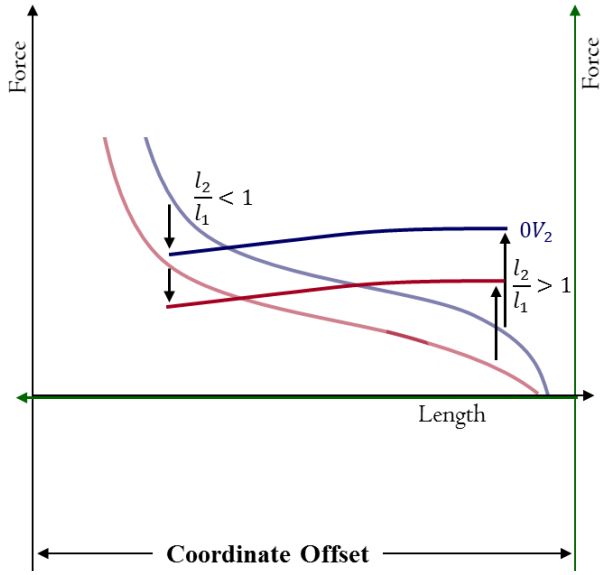

Figure 117 Transformation Plot of Performance Curve.

The force-displacement profile of the secondary actuator in the L prime coordinate system, faded red and blue lines, and the transformed coordinate system in the primary coordinate system, dark red and blue lines. The graph also shows how the ratio of the moment arms of l_2 and l_1 affect the transformation of the performance curve during the coordinate transformation.

The primary DE force-displacement curve and the secondary DE force-displacement curve in the transformed coordinate system are plotted in Figure 118. Like the previous antagonistic design, this system has four equilibrium points that bound a region of achievable force-displacement. In the graph, intersection 1 represents the point when both actuators are voltage OFF, intersection 2 denotes when the primary actuator is voltage ON, and the secondary actuator is voltage OFF, intersection 3 occurs when the primary actuator is voltage OFF, and the secondary actuator is voltage ON and intersection 4 signifies when both actuators have ON. Achieving particular points in the region can be challenging because the system is highly nonlinear.

In Figure 118, the system appears nonsymmetric; however, this is an artifact of the secondary actuation system being transformed into the L' coordinate system. The L prime coordinate system is highly transformed and compressed. At equilibrium point 1, the primary actuator is activated, voltage ON, and a new equilibrium point, 2, is reached. Actuator 1 has increased in length, δ_{+V_1}, while actuator 2 has decreased, δ_{+V_1}, in the L' coordinate system. δ_{+V_1} in the L' coordinate system is equivalent to $-\delta_{+V_2}$ in the primary coordinate system. If the actuation is reversed, the primary actuator will be displaced $-\delta_{+V_2}$, and actuator two will displace $-\delta_{+V_2}$but in the L' coordinate system. $-\delta_{+V_2}$, transformed into its base coordinate system, will be equivalent to δ_{+V_1}. Therefore, the system is, in fact, symmetric.

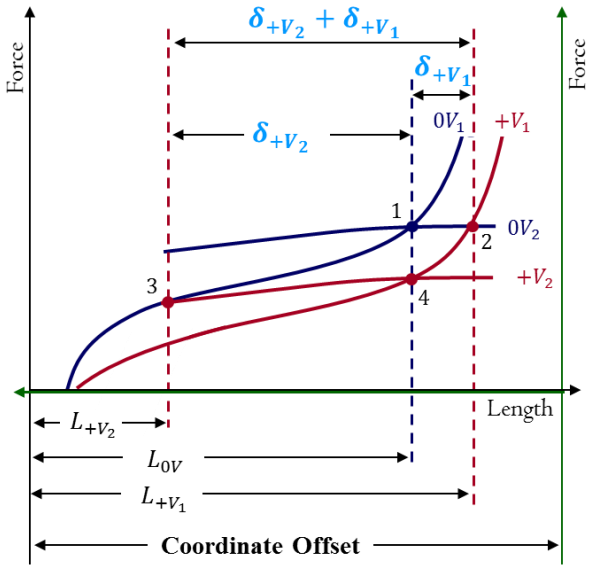

Figure 118. Performance Curves of a Reverse Bias Antagonistic System.

Force-displacement diagram showing the performance curves of a reverse bias antagonistic system design on a common coordinate system. There are four equilibrium positions that encapsulate the entire region, which is achievable by this particular design.

The sensitivity of the reverse bias antagonistic design will depend highly on how aggressively the system is antagonistic, directly related to how much actuation performance is achieved. More actuation performance is achieved for dielectric elastomers by using a larger percentage of hyperelastic curves. To use a higher percentage of the elastic curve requires that the reverse bias curve split the difference between the OFF and ON actuation curves for a large percentage of the force-displacement performance. Because of the closeness of the OFF and ON actuation curves, a large reverse bias antagonistic system will have a very high sensitivity. Slight changes in the input parameters can significantly impact the achieved performance. Alternatively, a reverse bias antagonistic system can be designed to use the force-displacement curve, leading to a more robust design with less sensitivity. The purpose of the configuration is to achieve higher performance; therefore, a reverse bias antagonistic design will have a sensitive design.

The reverse bias antagonistic configuration shown in Figure 118 is a simple example of this type of system. The system has many different variables that go into its configuration. These variables necessitate an analytical design for the performance prediction. Plotting the system on a

single force-displacement graph is a good way to estimate system performance. The substantial transformation of the secondary coordinate system makes it difficult to predict the performance change from modifying the parameter input. If the desired performance level requires a tight tolerance, an analytical design will be needed to achieve the desired performance level. Although performance changes caused by parameter modifications cannot be precisely predicted from the forced-displacement performance graph, it is possible to simplify the variables to aid an intuitive understanding of how performance can change when the input parameters are varied.

Implementation complexity for any reverse bias antagonistic configuration is high. Many design parameters can be off due to manufacturing tolerances, misassembly, or misalignment. Therefore, any reverse bias antagonistic system will need to have the capability of micro-adjustments for the parameter input so that the as-built system can achieve the desired performance level. The high number of variables enables the option of many micro-adjustments that can significantly change the actuation performance. The high number of parameters also makes it difficult to identify which parameter must be modified when the actuation levels are not reaching the expected performance level. In an actual implementation, all the variables must be remeasured if the performance is off to allow for the analytical deduction of which parameters must be modified to meet the expected performance levels. The real advantage of the reverse bias antagonistic system is that it has numerous practical applications and can use the full range of the actuation performance of a DE. During the design process, it is also possible to design a system with a robust performance level and higher tolerances for manufacturing errors. The trade-off is that any increase in robustness will come at the cost of maximum performance achievable.

5.4. Conclusions for Quasi-Static Actuator Design Process Used for Dielectric Elastomer Actuators

Developing a framework to use in understanding and designing DE actuator devices/systems is fundamental to this research as it lays the groundwork for expanding the reach of DE tape actuators in industrial applications. A framework was developed to meet industrial application needs for a simple method to design quasi-static DE tape actuator systems, understand the limitations of DE tape actuators, identify ways to minimize or compensate for these limitations, create a categorization of common and useful DE tape actuation devices/systems; and develop a methodology for evaluating the advantages and disadvantages of a particular device/system.

The challenge of designing with DE tape actuators arises from the complexity of the DE materials in combination with being joined with external systems. A quasi-static design process addresses these complexities by using the force-length design space and applying it to DE actuator architectures to simplify designing. Scaling performance with DE tape actuators was also explored. Due to the modularity of DE tape actuators, architecture scaling can be used to increase the actuation performance of a system and can be achieved in several ways, with the most common ways summarized in the previous subsections. Both force scaling and displacement scaling can increase the performance of a system. The type of performance scaling that can best be used to improve a system will depend on the type of external system.

Finally, this research considered system identification and categorization in the context of actuator design for DEs. A trade-off approach was employed by categorizing external systems into different types and analyzing the trade-offs required when selecting a particular external system. Six categories of systems and system architectures relevant to DE tape actuators were identified: constant force, spring force, leverage designs, reverse bias designs, antagonistic designs, and reverse bias antagonistic designs. As shown in Table 11, each of these systems was evaluated on the actuation performance stroke, the design sensitivity, the design complexity, and the implementation complexity.

Table 11. System Categorization and Comparison with Qualitative Evaluation.

Categorization of actuation systems that are relevant or useful for use with dielectric elastomer tape actuators. The qualitative evaluation is based on the actuation performance, sensitivity, design complexity, and implementation complexity of each system.

System Categorization	Performance	Sensitivity	Design Complexity/ # of Variables	Implementation Complexity
Constant Force	Large	Low	Low	Low
Spring Force	Low	Low	Low	Low
Leverage Force	Medium	Low	Medium	Medium
Rverese Bias	Very Large	High	Medium	High
Antagonistic	Large	Low	Low	Low
Antogonistic Reverse Bias	Very Large	High	High	High

The trade-off approach validates new design and redesign scenarios where a DE tape actuator is integrated into an existing system. The trade-off analysis allows designers to know the potential range of performance and how the system can be modified to enhance the total system by making modifications that will make the system performance better match the capabilities of DE tape actuators. The technique enables an easy and intuitive understanding of designing with

DE tape actuators. Furthermore, this design process can be adapted for any system configuration, and it allows a designer to maximize the possible performance for a given configuration without the need for extensive trial-and-error experimentation.

Chapter 6 Dielectric Elastomer Tape Actuator Architecture and Application Context Approach to Characterization, Modeling, and Design Advantage Validation with Case Studies

The final element of this dissertation consists of validating the research goals while moving the technology toward industrial applications. Three design cases confirm the previously derived design elements and processes. The configurations to be explored include a spring configuration, a reverse bias gravity-driven configuration, and a reverse bias antagonistic configuration. While these case studies demonstrate the advantages of the DE tape actuator, including large and conformal actuation with compact multilayer architectures, they also display the simplicity of integrating DE tape actuators into existing applications.

Each of the case studies illustrates significant attributes of a DE tape actuator. One encompasses a large distributed conformal strain in a compact package and design utilization to achieve a desired performance level. Another study demonstrates the performance capability of a DE system when it is developed from the beginning rather than as an ad hoc addition to an existing system. The final example uses all the findings in this dissertation: the DE tape actuator and its material and actuation properties utilizing architecture scaling; device categorization to demonstrate the capabilities of a DE tape actuator; the new variable shear Gent model for use in design; and the design methodology. These case studies illustrate how DE tape actuators can achieve fast, large-strain actuation while performing external work in a conformable and compact package with the ability to scale modularly and still be easily integrated with a device/system. They also demonstrate the ease of using the design approach (including characterization, modeling and design) based on application context. The final two case studies included in this dissertation were conducted by students who lacked expertise in DE actuators. These students could design functional actuation systems.

6.1. Active Automotive Weather Stripping

The automotive industry is extremely competitive. One common complaint concerns door seals. Currently, car door seals are made of passive rubber and are designed to achieve multiple

conflicting functions. The primary purpose of a car door seal is to act as a barrier to the external environment. The purposes include road and wind noise, and water intrusion. These sealing purposes would strengthen the seal to provide a strong barrier. However, a stiff seal prevents the door from closing properly. People want the door to close easily. The door-closing process involves more than simply shutting it because people also want to feel they have closed it properly. There must be some feedback from the door-closing process to assure the user that the door has closed. On top of feeling that the door has shut properly, there is also an experience, both tactile and audible, associated with closing the door.[128–132]

Moreover, people want this experience to be as pleasant as possible. These conflicting requirements mean that trade-offs must be made in door seal design to achieve a compromise behavior. The trade-offs required for the design of a seal could be part of why there are so many complaints about car door seals [128–132]. Since the rubber is completely passive, the design is forced to be a compromise. However, if there were a way to make the seal adaptable, it would be possible to eliminate some of the trade-offs required when designing a seal. a DE tape actuator was chosen to be integrated into a car door seal to explore the feasibility of creating an active seal.

6.1.1. Proposed Active-Seal Concept

The proposed concept is to adjust the tension in a seal with a DE tape actuator. A car door seal in the shape of a C is selected. Many types of seals are used on cars, and a C shape was chosen from a high-end luxury vehicle. The shape of the seal allows for simple integration of the DE tape actuator across the seal gap. The spring system is one of the simplest systems to integrate a DE. By bridging the gap, it will be possible to control the amount of compression in the seal.

6.1.2. Seal Force-Displacement

The first step in the quasi-static design process is to measure the force-displacement profile of both systems: the DE tape actuator and the seal. A custom-built seal compression load deflection (CLD) tester was used to derive the force-displacement profile. The resultant force-displacement profile can be seen in Figure 119. The raw data can be reduced to three force-displacement regions. The horizontal line represents the region before the test is in contact with

the spring. The second region with a constant slope represents the compression of the seal. Eventually, the seal becomes fully closed, and at that point, further compression compacts only the rubber itself. This region has a steep slope because we have fully compressed the seal. The rubber is still compressible, but the seal is fully shut.

The quasi-static design process will be used to create the design of the active seal. The tape actuator will have one system component, and the external system will be the seal. The tape actuator will be characterized experimentally for the force-displacement profile of a single-layer actuator. The tape actuator characterization will use the process identified in Section 3.6. The parameters used in the characterization are as follows: The tape actuator is characterized at three voltage levels: 0 V, 2300 V, and 2800 V. The force levels for the 2300 V were 15 gf to 80 gf in 5 gf increments. The 2800 V force levels were 15 gf to 65 gf in 5-gf increments. The test used 10 cycles at 1/20 Hz for each load level. The results of the characterization data are shown in Figure 119.

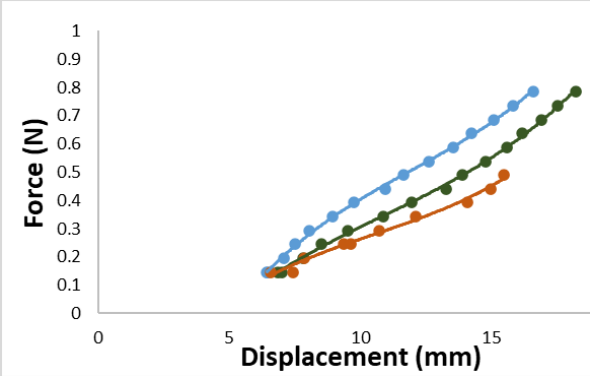

Figure 119. Three Activation Voltages Performance Plots.

DE tape actuator force-displacement curves for three activation voltages.

The next step in the design process is to choose a coordinate frame for each subcomponent of the proposed system: the DE tape actuator and the seal. The coordinate frame for the actuator represents the tape actuator and uses the default coordinate frame of the actuator. The DE tape actuator's default coordinate frame starts at the active material. This joint is between the multifunctional tape connector and the silicone film and is the tape actuator's zero length. The coordinate frame for the seal is correlated to the seal tester. The seal tester has a single degree of freedom where a slider moves up and down, and the seal is mounted on a lower plate that includes a force sensor. The seal is then mounted on the lower flange. The seal contains a C

channel to mount the seal onto the car. This same C channel mounts the seal onto the seal tester. The seal is then tested by raising the top bar above it so it is not in contact with it. This location is defined as the zero force location for the seal. The seal tester measures the displacement as the bar is lowered and, at the same time, measures the force on the seal. As the top of the seal tester contacts the seal, the load required to compress the seal increases. The raw data for the force - displacement performance curve of the seal are shown in Figure 120. The coordinate frame for the seal is defined as zero at some height above the seal, and then, as the top bar is lowered, the displacement is measured as negative length. The seal measures the pressure from a bar across the top of the seal. The proposed concept puts the tape actuator across the front of the seal. The tape actuator will be attached to the seal at the top of the mounting C channel and the other end at the edge of the seal. In the initial configuration, the seal tester measures the force-displacement profile of the seal by pressing down on the whole top surface. However, the tape actuator will pull down on the seal's front edge, not the top surface. An angle adaptor was fabricated and attached to the upper half of the CLD tester to ensure that the pressure from the top plate would contact only the front edge of the seal. The force-displacement measurement and how the tape actuator works are not precisely the same because the seal tester compresses the seal while the actuator pulls the seal closed. Even though the applied force comes from different directions, the same force is exerted on the rest of the seal system. Therefore, it is assumed that the force-displacement profile of the seal is the same if the seal compression is caused by compression from above or pull from below.

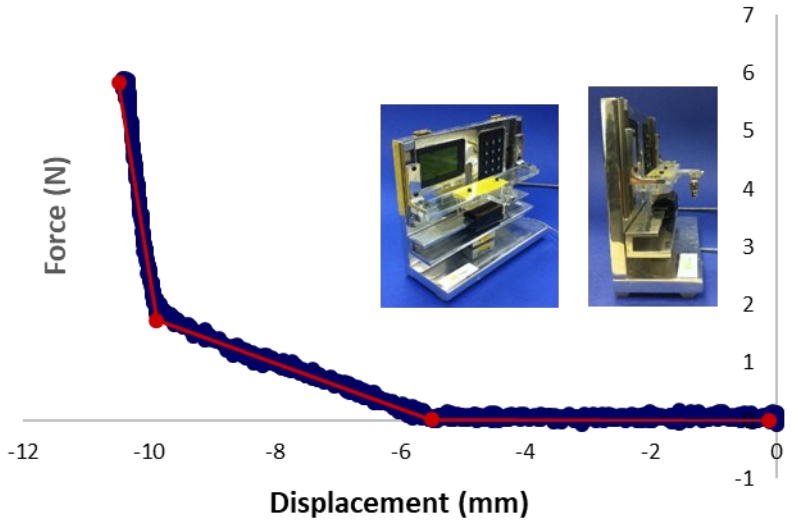

Figure 120. Seal Closing Force Characterization.

Measuring the force-displacement curve of the unmodified seal, using a custom-built test setup.

6.1.3. Seal Design Process with Single-Layer Actuator

The design process requires the two force-displacement curves to be brought into a single coordinate frame for the axis. The coordinate frame for the actuator and seal are parallel, so there is a single free-clearance between the subsystems. A single DE tape actuator forms the simplest system possible. The purpose is first to validate the concept and use only a single layer to simplify the design process. The result is that a single variable, the free-clearance, can be varied in the design. A single-layer design also limits the implementation complexity and enables the determination of attachments and other practical concerns with integration.

The systems are plotted together in Figure 121. The seal system is plotted twice with two 9 mm and 16 mm free-clearances. The force-displacement profile of the spring is approximately linear, making it simple to understand the impact of changing the free-clearance. The maximum stroke for the system will occur in the location with the maximum offset between the OFF and ON voltage curves. In the range of the experimental data, the separation between the OFF and ON curves increases as the actuator is stretched. The maximum free-clearance is restricted by the geometry of the seal and the attachment points. Therefore, the best design will be one where the free-clearance is set to the maximum the seal allows. The free-clearance is set to 9 mm. The proposed design will theoretically have a stroke of 0.4 mm.

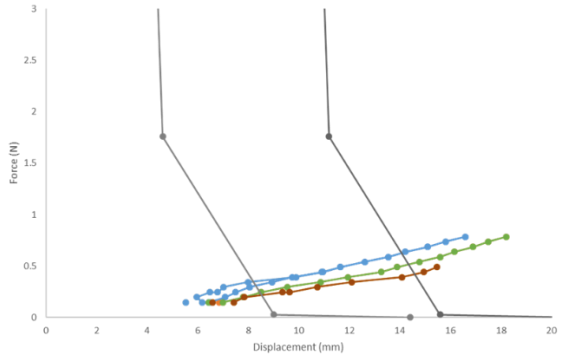

Figure 121. Seal System Performance Curves Plotted.

The systems force-displacement curves plotted in the primary coordinate frame. The seal force-displacement is plotted twice with different free-clearances.

6.1.4. Prototype

The final phase is to build a prototype using the design process. The tape actuator is already built from the process explained in Section 2.3. The tape actuator will be directly attached to the seal on the top compression surface of the seal and connected to a mounting plate that fits in the gap for the C channel used to mount the seal to a frame, as shown in Figure 122. The top connection is further enhanced by attaching a double-sided Kapton tape to the top surface of the seal. On top of the actuator, a piece of black electrical tape is used to isolate and hide the top of the tape actuator. The edge of the multifunctional tape connector extends slightly beyond the top surface of the seal so that none of the active area is touching the rubber seal. This location will ensure that the entire active region is used for actuating the seal. The C channel of the seal contains fins that allow the C channel to adhere to the vehicle's frame. Therefore, The fins require a mounting plate to provide a solid surface to which the MTC can attach. The mounting plates are thin aluminum rectangles that are electrically isolated using electrical tape. Two mounting plates isolate the MTC from the fins on both sides of the C channel. The mounting plates also provide a slight space that increases the free-clearance, which results in a larger stroke. The mounting plates also add a second degree of freedom where the anchor point of the actuator can be moved horizontally in the C channel. The second degree of freedom allows the active area of the tape actuator to be vertical and pull straight down, similar to how the seal CLD was tested in the earlier section. The external electrical connections are made by connecting

wires to the electrical connection of the MTC. The two mounting plates still allow the seal to be mounted onto a vehicle flange, as seen in Figure 123. An advantage of tape actuators is that they are distributed actuators.

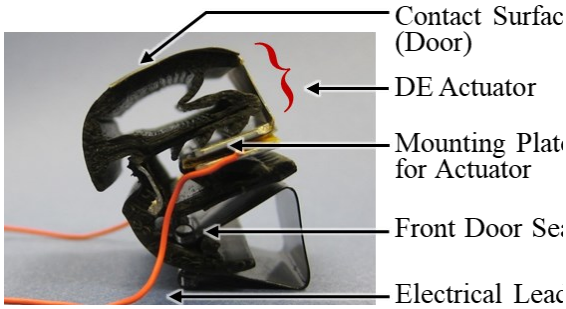

Figure 122. Integrated DE Tape Actuator.

Car door seal with integrated DE tape actuator with components labeled.

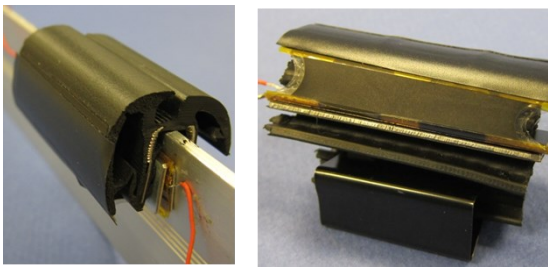

Figure 123. Active Seal Mounted.

Active seal mounted on simulated car frame. Direct view of DE tape actuator.

The seal was then experimentally tested with a custom test that uses a custom LabVIEW program that, through a DAQ, controls a power amplifier that supplies the regulated voltage and current to the DE tape actuator. The seal is mounted on a simulated car door flange and held in a horizontal configuration, which is parallel to how the force-displacement profile of the seal is tested. A camera, Canon SD 90, is used to capture the actuation of the unmodified seal optically. The experimental prototype demonstrates some of the advantages of a tape actuator. The actuator is conformable and sticks well to the curved seal contact surface without removing the seal's ability to deform. The distributed actuation pulls the whole surface of the actuator down equally as opposed to discrete actuation technology, which requires the underlying structure to distribute the force. The distribution of the force requires a stiff material, which takes away from the purpose of the seal, which is to provide a seal between the car frame and the door. The rubber offers a deformable material to create a tight seal. By being conformable, the tape actuator does not take away from the inherent purpose of the seal, which is seen in the single-layer demonstration.

Although a single-layer actuator proves the raw feasibility of creating an active seal, it is limited in its capabilities because it has limited actuation authority to modify the seal. A larger actuation authority is required to match the force-displacement profile of the seal better. One of the easiest ways to improve the stroke is to increase the number of layers of the tape actuators. Suppose the external system has a greater force capability than a single-layer tape actuator. In that case, one simple way to increase the stroke of a combined system is to increase the number

of layers of actuators. DE tape actuators working in a stack configuration increase the vertical force for the same displacement. The result of stacking actuators in parallel is to improve the force levels while the stroke remains the same. Using the MTC of the tape actuators, it is easy to stack actuators in parallel and scale the performance.

The separation between the OFF and ON actuation curves allows an increased stroke. In the seal configuration, the external system, the seal force-displacement profile is approximately constant until the seal has been fully compressed when the stiffness of the seal increases almost vertically. The maximum seal compression is then limited to the combined system's free-clearance set. Therefore, the number of actuators in the stack of tape actuators should be set so that the maximum offset is used and the equilibrium stretch position closes the seal. The OFF equilibrium position will occur right before the stiffness of the external system increases vertically.

In Figure 124, the force-displacement profile of a three-layer actuator is shown. The force-displacement profile of the tape actuator is scaled algebraically from the experimental characterization data. The stroke of the final configuration at a voltage level of 2800 V is 1.2 mm. Although a stacked actuator does increase the load levels, the separation between the ON and OFF performance curves, the design stroke, is still highly dependent on the free-clearance. If the free-clearance is decreased to 9 mm, as shown in Figure 124, then the stroke of the combined system would be substantially reduced to 0.4 mm. Because the external system force-displacement curves and the tape actuator curves cross each other close to perpendicular and the tape actuator curves are parallel, the system will not have substantial sensitivity. If the free-clearance is slightly adjusted, the performance will not change dramatically. The one exception is if the actuator is placed such that it pulls the seal past fully closed and starts to compress the rubber, which is the vertical part of the external system curve. In this case, actuation authority will be used to uncompress the seal and the result is that the stroke will be reduced. Therefore, the free-clearance must be set during construction to ensure the seal does not go past the fully closed position, where the seal CLD becomes vertical.

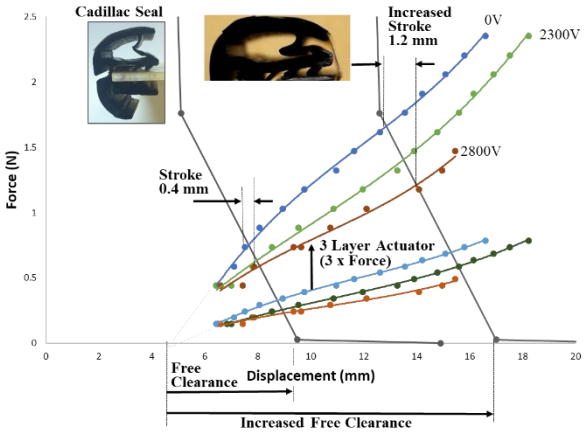

Figure 124. Theoretical Combined System Plots on Design Graph.

Theoretical performance curves of 3-layer stacked actuator added to the combined system plot and the new increased achievable actuation stroke.

The active seal was created the same as the single-layer active seal except that three actuators stacked in parallel were used. The resultant seal was tested using the same experimental setup. The active seal had a travel of 1.1 mm. The actuator matched the designed performance well with a small error of 8.3%. The error in the stroke can result from losses caused by stacking.

6.1.5. Seal Design Process Using Bias Spring

The previous design assumed that the force-displacement profile of the seal was fixed. However, modifying the external system to change the force-displacement profile is possible. A super-elastic SMA wire was bent in half and added to the interior of the seal to modify the force-displacement profile. Two 15-mil super-elastic SMA wires were bent in half and placed inside the seal to increase the force-displacement profile. The CLD of the new modified seal was measured using the custom CLD tester. The new force-displacement profile is shown in Figure 125. There are three approximately linear regions. The maximum stroke will occur again when the OFF equilibrium position is approximately closed, and the maximum free-clearance is used. The increased force levels, caused by the biased spring, have increased the load levels. The first-step section of the external system curve, the seal plus bias springs, has a steep slope resulting from the stiffness of the SMA wire and the seal. The slope of the curve changes and becomes approximately parallel to the old CLD. The SMA wires have reached their stress plateau at this load level, where the force change becomes constant. The result of the SMA wires is that they have shifted the force-displacement curve vertically, increasing the force level while not

changing the stiffness in the region where the seal is mostly closed. A 7-layer stacked tape actuator makes it possible to design a system to achieve a stroke of 2 mm. A 7-layer stack actuator increases the actuation authority by 133%, from 3 layers to 7 layers, while the designed stroke is increased by 67%, from 1.2 mm to 2 mm. The increased actuation stroke from the 7-layer actuator results in a smaller percent increase in the total system length compared to earlier designs. A larger number of layers in the stack and using an additional biasing element to the seal structure increases the implementation complexity. The scaled actuation authority, created by significantly increasing complexity, does not correspond to a commensurate increase in displacement. There are diminishing returns to increasing the basic complexity of the bare seal in terms of increased system performance. To substantially improve the system, a custom seal with a force-displacement performance curve that better matches the performance of the tape actuator should be selected. With a small free-clearance, the complex implementation of the 7-layer tape actuator with a biasing element inside the seal would result in a stroke of 0.6 mm, which is similar to what is possible with a single-layer actuator and a good design with the correct free-clearance.

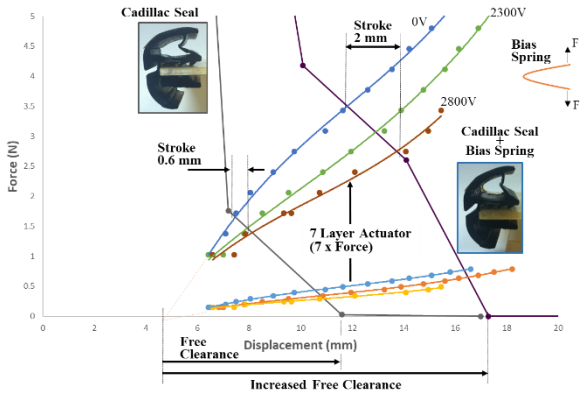

Figure 125. Theoretical Architectural Scaling .

Theoretical architectual scaling of the actuator by stacking multiple models to increase the system performance using a 7-layer stacked architecture.

6.1.6. Active Seal Conclusions

This case study demonstrates the feasibility of integrating a DE tape actuator into a seal. The example shows the ability of the quasi-static design process to be used to design a complete system. The seal showed the advantage of a soft distributed actuator: the tape actuator pulled down the whole seal line equally. Evenly pulling the seal allowed the seal to maintain its

conformable properties. The ability of the tape actuator to be easily stacked to better match the performance levels of the external system was demonstrated. The MTC made it easy to connect the seal to the top surface. A mounting plate was used to anchor the other end, but the thinness of the MTC still allowed the seal to be mounted on a frame without interfering.

6.2. Gravity Reverse Bias Rotating Panel

The proposed concept for the gravity reverse bias rotating panel uses an inverse pendulum to create a reverse bias force so that the entire force-displacement profile of a DE tape actuator is used. Creating a reverse bias force that splits the force-displacement curve is challenging because the force must be very precise [335–344]. The idea is to create a panel that rotates on a center axis with a slightly off-center mass. As seen in Section 5.3.4, one way to make a reverse bias force is to use an inverse pendulum with the center of the mass above the rotation axis. The center of the mass above the axis provides the force to the external system. When the mass is offset from the center of the axis, there is a torque on the axis that is a function of the force of the mass, mg, and the moment arm perpendicular to gravity to the center of the mass. The force of the mass is fixed, but the moment arm changes as the mass pivots around the axis. In a vertical position, the moment is zero, and the mass exerts zero torque. As the pendulum rotates, the center of the mass will move farther from the axis, causing the moment arm to increase. The increased moment arm results in increased torque around the centerline axis. The torque will continue to grow until the mass reaches a horizontal level equal to the centerline axis. As the pendulum continues to rotate, the moment arm decreases again. The stable equilibrium for the pendulum is the center of the mass hanging below the centerline axis. For this example, the center of the mass will be constrained to be above the axis, thereby providing an external load with a reverse bias. The tape actuator will counteract the torque from the pendulum's mass. The tape actuator will be anchored to the ground and attached to the rotating panel. As the panel rotates, the moment arm for the tape actuator will change the torque.

A reverse bias system is a complex system that can achieve a very large performance and use the force-displacement profile of a DE tape actuator. Since the design will require an external force-displacement curve that splits the ON and OFF parallel curves, the design will be very sensitive. The implementation complexity is intermediate. Using a rotating panel is not complicated; the anchor for the tape actuator is fixed, which limits the challenges. However, the

requirements for precision for the sensitive design performance increase the implementation complexity.

6.2.1. Quasi-Static Design Process Using Simplified Viscoelastic Actuator Performance

The standard quasi-static design process will be used again to design the reverse bias device. The proposed reverse bias can be simplified to a two-dimensional plane problem. There are three locations of interest: the panel's centerline axis, the panel's center of gravity (CG) of the panel, and the anchor point of the tape actuator. The three locations are important relative to each other. Another critical variable is the total mass represented at the CG.

The first step in the design process is system identification. The system's two components are the DE tape actuator and the rotating panel. Although the tape actuator can be made to any geometric proportions, the standard tape actuator model that has been identified will be used. The characterization process for the tape actuator will use the experimental method identified in Section 3.6. The coordinate frame for the tape actuator will use the standard coordinate frame for the tape actuator, where the zero length represents the beginning of the active material. In this case, The rotating panel is a theoretical design and can be calculated analytically. The coordinate frame for the panel that makes the most intuitive sense is a polar coordinate frame, with the origin being the center of rotation of the panel. The torque as a function of the rotation can then be determined from the initial angle and radius of the center of the mass.

The coordinate frame of the DE tape actuator was chosen as the primary coordinate frame. Using the tape actuator coordinate frame allows for understanding how much of the total performance can be attained by fitting the gravity reverse bias system between the ON and OFF performance force-displacement curves of the tape actuator.

The transformation from the panel coordinate frame into the tape coordinate frame is related by using the torque of the two systems. Vector math makes it possible to set the two torques equal and solve for the force in the tape actuator coordinate frame required to keep the panel in equilibrium. The torque provided on the panel by the center of the mass of the panel can be derived from the dot product of the radius and the force vector at the CG.

The two systems are now in the same coordinate frame. However, they are not yet attached. The free-clearance will link the tape actuator and the rotating panel. With the location of the axis and tape actuator anchor point fixed, the change of the angle of the panel can be directly related

to the change in length of the distance between the tape actuator anchor point and the location where the tape actuator attaches to the panel.

The actuator stroke can be determined from where the external system crosses the OFF and ON performance curves. Some hard restraints limit the viable geometric position for the anchor of the tape actuator and where the actuator attaches to the panel. Assuming the geometry is fixed, a change in the applied load will change the slope of the reverse bias. Figure 126 plots a 50.22 gf force-displacement curve and the actuator performance curves. The maximum travel for the tape actuator is approximately 8.00 mm to 15 mm. For the 2300 V ON performance curve, the change in force level is approximately 40 gf to 60 gf.

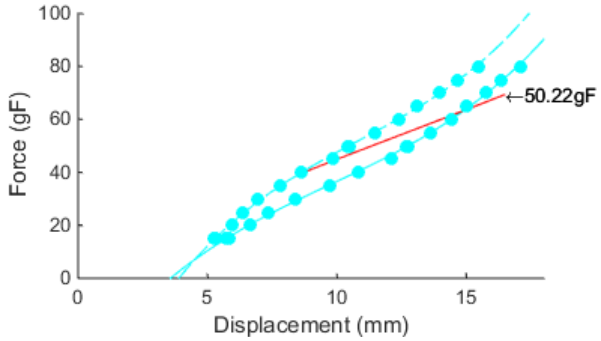

Figure 126. Inverted Pendulum Performance Curve.

A reverse bias stroke from an inverted pendulum with a 50.22 gf force-displacement curve and DE tape actuator performance curves plotted for 0 V and 2300 V.

* THE AUTHOR CREATED THIS FIGURE AND IT APPEARS IN THE DOCUMENTATION OF A COLLABORATIVE PROJECT WITH ADAM ROSE KELLY.

The changing angles of the moment arms enable the rotating panel to achieve a large reverse bias. The total travel of the actuator is geometrically fixed by the axis's geometry and the tape actuator's two anchor points. The shape of the stiffness and shape of the force-displacement curve of the external system are completely controlled by the geometry. The force of the system is scalable by adjusting the total mass of the system.

6.2.2. Prototype

As a feasibility study of constructing a gravity-driven reverse bias device, the prototype is built from materials that can be easily modified and adjusted to create the precise design required. (See Figure 127.) Fabrication precision is necessary in the locations that are explicitly designed. These are the panel axis, the tape actuator anchor points, and the CG of the panel. The model assumes a frictionless bearing at the axis and a normal direction to gravity. The support

for the device is built using T-slot 1" 80-20 aluminum extrusions. The slotted connection enables simple modification of the support frame. The frame will support both the axis of the panel and the fixed anchor of the DE tape actuator, as shown in Figure 127.

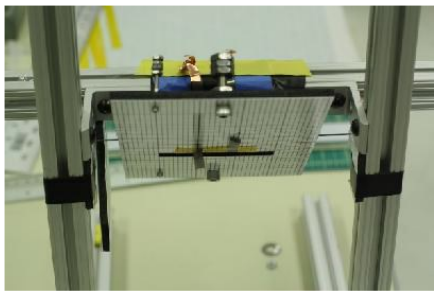

Figure 127. Prototype Reverse Bias Panel.

Reverse bias panel showing 10-24 nuts and 4-40 nuts, which control the mass and the center of gravity location vertically.

* THE AUTHOR CREATED THIS FIGURE AND IT APPEARS IN THE DOCUMENTATION OF A COLLABORATIVE PROJECT WITH ADAM ROSE KELLY.

The rotating panel is made from a 3/16" foam core and is 4" x 6". The hinge, located at the center of the panel, is made by piercing the foam core with a piece of thin steel wire. The axle is then connected to the T-slots using additional foam core pieces. Two foam core squares are attached to the T-slots. The support squares are pierced by the steel wire, which is the axis of the panel. This simple configuration allows for a nearly frictionless joint. The small diameter of the wire causes the force due to friction at the joint to be negligible. The force from friction is insignificant because the friction coefficient between the steel and the foam is low. Also, the moment arm of the axis is half the wire diameter, which is small, causing the torque on the axis to be negligible. A hole is cut in the rotating panel to attach the tape actuator to the panel. The second anchor of the tape actuator is affixed to the T-slots support beams through an adjustable acrylic support. The height of the acrylic is fixed to the support frame with bolts. However, the horizontal distance from the axis is adjustable using slots in the acrylic support, which enables the sliding in and out of the acrylic support. A tailorable implementation is used To achieve the necessary accuracy of the center and make it adjustable. The panel itself is balanced with the CG at the axis. The adjustable CG is created by having adjustable weights on the top and bottom of the panel. The adjustability is accomplished by using bolts, nuts, and washers. A 1.5" 10-24 bolt and a 1.5" 4-40 bolt are placed on both the top and bottom of the panel, as shown in Figure 128.

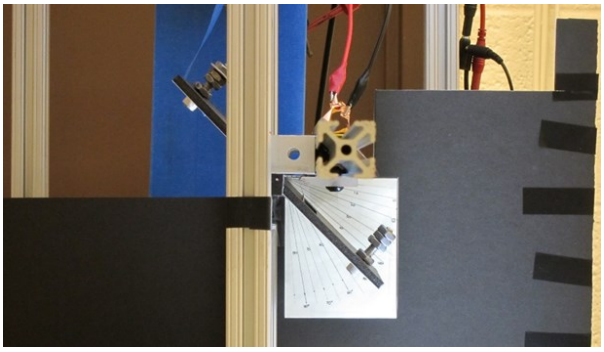

Figure 128. Reverse Bias Panel Angle Measurement.

Side view of the reverse bias panel showing the applied math along with the optical measurement of the angle.

* THE AUTHOR CREATED THIS FIGURE AND IT APPEARS IN THE DOCUMENTATION OF A COLLABORATIVE PROJECT WITH ADAM ROSE KELLY.

The 10-24 bolts are placed on the centerline and the 4-40 bolts are offset to the side but in line with each other. The CG of the panel can then be moved vertically by adding nuts to either the top or bottom bolts. The horizontal distance of the CG can be adjusted by screwing the nuts in or out on the bolts. The 10-24 nuts allow general control of the mass and CG, and the 4-40 nuts allow fine-tuning the CG. The DE tape actuator is anchored to the supports such that the induced force from the actuation does not provide any peeling force. Preventing any peeling force is accomplished by attaching the actuator to the panel through the cut hole and on the opposite side of the CG. The fixed anchor of the DE tape actuator is attached to the top side of the acrylic support, which is above the rotational axis, as shown in Figure 129.

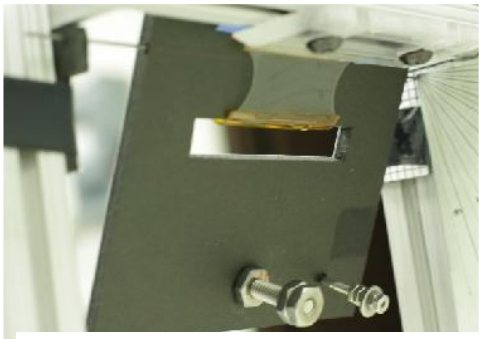

Figure 129. Rear View of Connected DE Tape Actuator.

Rear view of the DE tape actuator connected through a pass-through so that there is no peel force applied to the system.

* THE AUTHOR CREATED THIS FIGURE AND IT APPEARS IN THE DOCUMENTATION OF A COLLABORATIVE PROJECT WITH ADAM ROSE KELLY.

Figure 130. Magnified View of Upper Bolts.

Magnification of the upper bolts, which shows how the nuts can be adjusted in and out to change the center of the mass.

* THE AUTHOR CREATED THIS FIGURE AND IT APPEARS IN THE DOCUMENTATION OF A COLLABORATIVE PROJECT WITH ADAM ROSE KELLY.

Attaching the prepared DE with leads assembled was the next step. Typically, the bottom of the DE was easiest to attach through the slot in the panel, and then the top could be connected to the adjustable Plexiglass piece. The critical step was to provide proper pre-stretch to the DE by maintaining exposure of the 8 mm non-DE material between the two attachment locations. Typically, 2 mm was exposed at the bottom edge and 6 mm at the Plexiglass edge. The last step is to connect the leads to the voltage supply, one positive and one negative. A side view of the reverse bias panel shows the applied math and the angle's optical measurement. The reverse bias panel showing 10-24 nuts and 4-40 nuts controlling the mass and the CG location vertically is shown above in Figure 130.

6.2.3. Experimental Validation of Design and Actuation Performance

The experimental setup is designed to supply voltage to the reverse bias gravity-driven panel and measure the rotation. The voltage supply is provided through a Trek high-voltage amplifier and controlled through a NI DAQ and a custom LabVIEW program. The rotational measurement of the panel is measured optically with a digital camera, Canon S90.

The experimental process consists of a cyclical voltage application, with each cycle increasing the voltage. The test is done at a frequency of 1/40 Hz with a duty cycle of 50% and using a square wave. The test starts at 1400 V and increases by 100 V each cycle to 2500 V. The rotational displacement is measured at the end of each cycle just before switching the voltage from ON to OFF or OFF to ON, as shown in Figure 131. The whole voltage range was experimentally tested three times. The results of the test are shown in Figure 132.

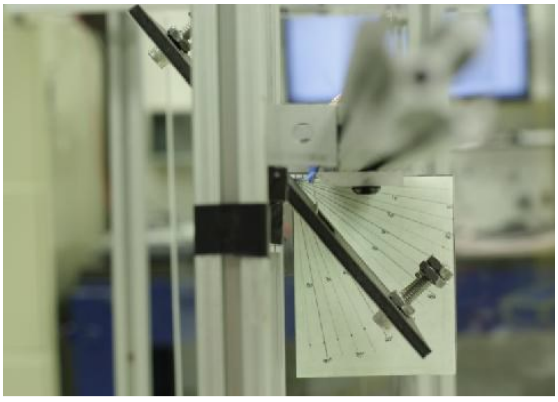

Figure 131. Side View Showing Panel Angle.

Side view of the system showing the angle of the panel. The DE actuator is also in view but difficult to see because of the thinness of the actuat

* THE AUTHOR CREATED THIS FIGURE AND IT APPEARS IN THE DOCUMENTATION OF A COLLABORATIVE PROJECT WITH ADAM ROSE KELLY.

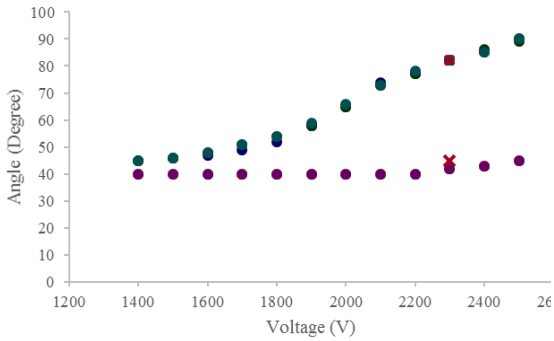

Figure 132. Plotted Theoretical and Experimenta Results.

Theoretical performance of the system as a function of applied voltage shown as circles. The experimental results at 2300 volts are shown as red

* THE AUTHOR CREATED THIS FIGURE AND IT APPEARS IN THE DOCUMENTATION OF A COLLABORATIVE PROJECT WITH ADAM RO KELLY.

The experimental results of the testing are shown above in Figure 132. The results show two lines representing when the panel is OFF and ON and the voltage rotation angle as a function of the applied voltage. The bottom data points represent the OFF voltage rotation angle, and the upper data set represents the ON voltage rotation angle. Although three data sets are being graphed simultaneously, the results are almost identical, demonstrating the device's repeatability and controllability. The OFF voltage rotation angle is mostly flat from 1400 V to 2200 V. After 2200 V, the OFF voltage rotation angle increases slightly and does not return as far as compared to lower voltages. The ON voltage rotation angle varies from 47° at 1400 V to 89° at 2500 V. The ON voltage data have an S-shaped curve where the rotation angle changes slightly for lower voltage and the slope increases for the middle voltages and then decreases again at higher voltages. The shape of the curve is due to the interaction between the actuation authority of the tape actuator and the changing leverage of the system. The leverage does not change significantly at lower voltages, and the tape actuator has lower actuation authority. At intermediate voltages, the system's leverage increases as the panel rotates, and the actuation authority of the tape actuator increases. At high voltages, the leverage starts to change less while the actuation authority of the tape is at its largest. Figure 133 shows the 0 V length, 8 mm, and the fully extended length, 19.7 mm, right before failure at 2500 V. This delicate elastomer tape actuator extended 146% linearly. Although the pendulum rotates as the actuator moves, the dielectric elastomer only stretches linearly as a panel.

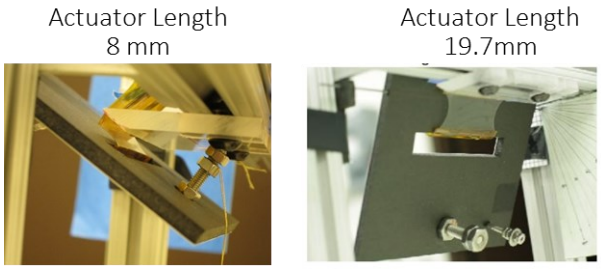

Figure 133. Panel with Voltage ON And OFF.

Reverse biased actuator configuration shown in the voltage OFF and fully extended with the voltage ON.

* THE AUTHOR CREATED THIS FIGURE, AND IT APPEARS IN THE DOCUMENTATION OF A COLLABORATIVE PROJECT WITH ADAM ROSE KELLY.

6.2.4. Conclusions for Gravity Reverse Bias Rotating Panel

The reverse bias gravity-driven panel is an opportunity for a silent acoustic panel. The DE tape actuator is scalable, and the panel achieves large strokes. The panel shows that using the entire stroke of a DE tape actuator is possible. The design process achieves an accurate and precise design. This design requires a very sensitive design. The implementation complexity is medium. The system requires a rotational axis, which increases the complexity. The anchor point is fixed to the axis, which minimizes the complexity. The precision required is necessary to achieve the reverse bias design.

The panel's actuation is limited to the inertial force of the mass of the panel. The force applied to the tape actuator by the external system changes substantially as the panel rotates. The separation between the two ON and OFF voltage curves for a single-layer actuator is small, so the actuation authority to move the panel is low. A DE- actuated panel is viable for uses where smooth motion and slow actuation are acceptable. The intermediate control allows unlimited rotation angle control within a specified range.

Overall, this case study demonstrates the viability of the DE tape actuator design process, the performance possible from a DE tape actuator, the ease of integration into a system, the distributed lightweight intermediate actuation, and the viability of using a reverse bias to create an extremely large linear stroke performance.

6.3. Active Louvers for Architecture

A case study is performed on a fluttering panel actuated by a series of antagonistic DE tape actuators operating with reverse-biased leveraging for greatly enhanced actuation performance. A

kinematic model of the fluttering panel is presented and used in the design process to provide a desired panel rotation given a desired maximum material use in terms of the forces and strains employed. A hardware prototype is fabricated and used to validate the practicality of the design process. This model-based analytical design process enables designers to fully exploit the benefits of the DE tape actuator configuration to create compact and lightweight actuation applications and a larger architecture to increase performance with minimal complexity.

There is great potential for using rotating panels in an architectural setting. The rotating panels could cause visual and acoustic effects that could change the impact of a building on people, as shown in Figure 134. One problem with this is that each panel must be independently controlled. Using a DE would provide large-stroke, silent actuation. The large gravity reverse bias example demonstrated that large rotational motions could be provided. However, a significant issue with a gravity-driven panel is that it is limited regarding the panel rotation to gravity without extra levers to change the rotation concerning gravity. One way to eliminate the need for the orientation to gravity is to use another external system to work against it. One way to further increase the stroke and controllability of DE tape actuators is to use them antagonistically. When using a standard DE tape actuator, the precision required to achieve the reverse bias design is challenging to implement correctly. One way to decrease the sensitivity of the design is to scale the dimension so that small implementation errors will be a smaller percentage of the desired length. This case study presents a rotating panel with antagonistic reverse bias DE tape actuators. A pair of actuators are used in series to increase the actuation stroke. The reverse bias antagonistic design is achieved by increasing the implementation complexity and using an offset design that requires the panel to link the two actuators and reach the induced offset moment. The antagonist design doubles the amount of rotation possible from the device compared to the gravity-driven design. The design achieves a large performance with a large stroke from the tape actuators in series. The design sensitivity required is high because both actuators provide the restoring force for the other actuators. The restoring force must also split the difference between the parallel ON and OFF performance curves. This design shows the ability of the DE tape actuators to be used in a reverse bias antagonistic design to achieve large-panel rotation with intermediate control.

Figure 134. Industrial Uses of Louvers.

Possible louver options that could be used with an antagonistic reverse bias actuator configuration.

6.3.1. Quasi-Static Design Process Using Simplification Enabled by the Actuation Context

The antagonistic reverse bias panel has three components: the two actuators and the panel. The critical locations that determine the design are the four anchor points of the two actuators relative to the panel rotation center and the free-clearance of the two actuators, as shown in Figure 135. The attachment points will be designed to be symmetrical. The symmetry requirement halves the number of variables needed for the design.

The critical design variables become the tape actuator's anchor points and the actuator's free-clearance, drawn schematically in Figure 136. The panel will be assumed to be rotating on a frictionless axle. The mass of the panel will be ignored because the panel will be aligned to be normal to gravity. The panel is assumed to be infinitely rigid. The design aims to achieve +/- 30 degrees of rotation from a vertical panel.

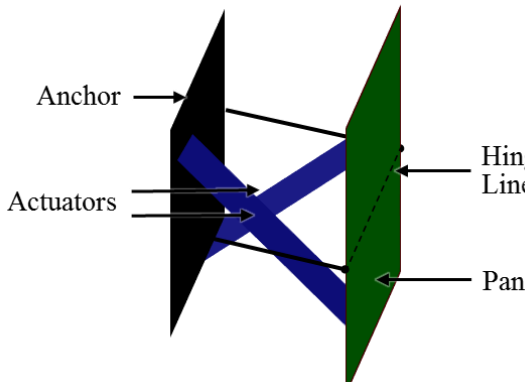

Figure 135. Panel with Antagonistic Reverse Bias Configuration.

Schematic of an antagonistic reverse bias configuration with the components labeled.

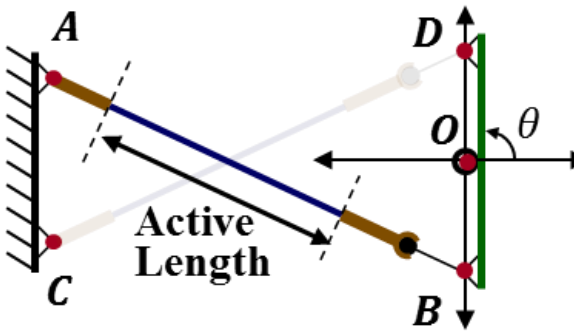

Figure 136. Schematic of Reverse Bias Antagonistic Configuration.

Schematic of tape actuators used in the reverse bias antagonistic configuration.

The three components of the system, the two actuators, and the panel, can be characterized separately. The tape actuators will be experimentally characterized to derive the parameters required to use the Gent variable shear dielectric actuator model, which will be used for all actuators because of symmetry. The characterization of the mechanical system, the rotating panel, is represented by a simple geometric formula due to the assumptions put into the system. These assumptions include that the mechanism is symmetric, the panel rotates around a fixed joint and does not deflect the transient creep-terminated motion, and frictional forces are ignored because of the cone hinges. The characterization of the tape actuator is described in detail in 0$\mu_0 = 84{,}049\ Pa, \mu_V = 1.6038 * 10^{-13}\ Pa$ $J_m = 38.9$, $\varepsilon = 1.4$.

Each component has its coordinate frame. The panel coordinate frame is polar, with the rotation center being the origin. The tape actuators each have a rotating Cartesian coordinate frame. The primary axis of the coordinate frame is a vector between the fixed anchor location and the panel attachment point, as shown in Figure 137. The primary coordinate frame for the design will be one of the tape actuators. The two actuators are connected through the panel and must be in equilibrium. The actuation force for each actuator can be derived by setting the total torques applied to the panel equal to zero. The torques are derived from the actuators' geometric relationship and force. A torque balance, the leverage ratio, and vector mathematics transform the second actuator into the primary tape actuator coordinate frame, as shown in Figure 137 and Figure 138.

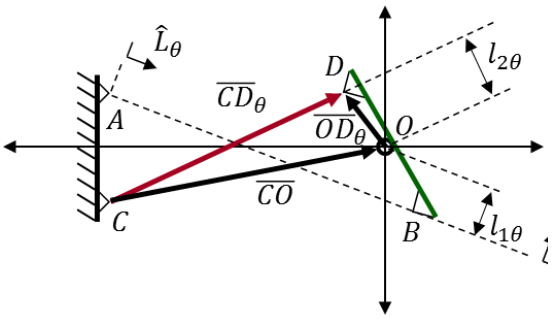

Figure 137. Geometry Schematic with Critical variables.

Schematic of the geometry with critical variables and parameters labled. The vectors show are used for the derivation of the geometric relationships.

$$\overline{AB}_\theta = \overline{AO}+\overline{OB}_\theta \qquad \overline{CD}_\theta = \overline{CO}+\overline{OD}_\theta$$

$$\hat{L}_\theta = \frac{\overline{AB}_\theta}{|\overline{AB}_\theta|} \qquad \hat{L}_\theta^2 = \frac{\overline{CD}_\theta}{|\overline{CD}_\theta|}$$

$$\hat{L}_\theta^\perp = \hat{L}_\theta * \begin{bmatrix} 0 & 1 \\ -1 & 0 \end{bmatrix} \qquad \hat{L}_\theta^{2\perp} = \hat{L}_\theta^2 * \begin{bmatrix} 0 & \\ -1 & \end{bmatrix}$$

$$l_{1\theta} = \hat{L}_\theta^\perp \cdot \overline{OB}_\theta \qquad l_{2\theta} = \hat{L}_\theta^{2\perp} \cdot \overline{OB}_\theta$$

$$\tau_1 = \tau_2$$

$$F_{1\theta} l_{1\theta} = F_{2\theta} l_{2\theta}$$

$$F_{1\theta} = F_{2\theta} \frac{l_{2\theta}}{l_{1\theta}}$$

Figure 138. Derivation of Algebraic Equations.

VThe vector math needed to derive the algebraic equations relating the actuation torques, controlling the angle of the pivoting panel, to the panel angle.

The systems are combined into the primary coordinate frame. The stroke of an equilibrium position of an antagonistic design will have infinite variability. This reverse bias antagonistic design transfers the two force-displacement curves from the primary and the two performance curves from the secondary actuator into the primary frame coordinate system. Because the rotating panel is set up symmetrically, the panel will not rotate if the same voltage is applied to both actuators. If a different voltage is applied to the actuators, the panel will rotate while the actuator with the higher voltage level extends and the lower voltage actuator contracts. The largest panel rotation will occur when one actuator is ON and the other is OFF. If the actuators' energy levels are switched, the panel will reach its maximum rotation again but in the opposite direction. With a fixed desired rotation angle and symmetrical design, it is possible to create a plot showing the maximum torque ratio as a function of the anchor position points.

The design aims to achieve +/- 30 degrees of rotation in the panel. A wide range of anchor points can be used to achieve the +/- 30-degree rotation. Because there are many solutions to the problem, the next step is to choose a solution from the other crucial factors, including the design sensitivity and the implementation complexity. The sensitivity of the design plays a key role in the minimum precision required to achieve the desired performance. A very precise design will need a very precise implementation. Therefore, a good design will be one where the performance levels do not change if there are small errors in the implementation. One way to improve the sensitivity is through scale. If the device requires an implementation of 1 mm and a 10% error is

acceptable, then the error in the implementation will be 0.1 mm, which is very precise on the scale of the panel, which is ~100 nm. If the implementation calls for 10 mm, then the error of 10% results in a 1 mm tolerance.

The tape actuator attachment to the panel is designed with this limitation in mind. If the panel is assumed to be solid, then the attachment to the panel will have to occur at a minimum of half the thickness of the panel away from the axis. Although there are techniques that can be used to implement the attachment that is in line with the axis or even on the opposite side of the axis from the fixed anchors, these techniques will require greater complexity in the design and further increase the implementation complexity. The panel attachment will be fixed at 10.7 mm length and 2.6 mm height from the axis to make the device simpler to manufacture and simplify the implementation complexity. It is possible to explore the sensitivity of the torque ratio at the maximum panel rotation by plotting the ratio as a function of the *X* and *Y* coordinates using the fixed attachment to the panel and the desire for +/- 30-degree rotation, as seen in Figure 139.

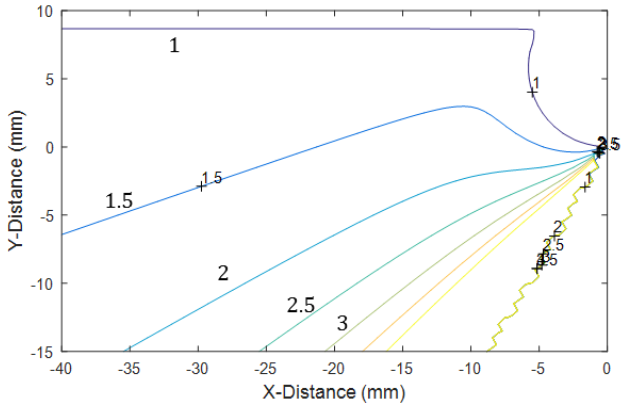

Figure 139. Ratio of Reverse Lever Arms Plotted.

Maximum ratio of the reverse lever arms of the bias system as a function of the anchor points.

The torque ratios in Figure 139 provide insight into the sensitivity of different designs. The contour lines represent the torque ratio at 30 degrees for the actuator with a panel connection at 10.7 mm and 2.1 mm. Each contour represents a 0.5 increase in the torque ratio. The contour line with a 1 is equivalent to a constant-force system. One way to interpret the graph is that the distance between the lines indicates the sensitivity of the design. When the lines are close together, the torque ratio changes significantly with small variations in the geometric implementation. When there is a large space between the contour lines, the design is relatively insensitive because small changes in the position do not substantially change the torque ratio. For

the design To achieve a large reverse bias, it is necessary for the fixed anchor on the opposite side of the panel axis from the attachment to the panel. When the fixed attachment point crosses the *X*-axis, the implementation complexity must increase substantially because both actuators cannot be in the same plane. In this configuration, the limit for how close the fixed anchor points can get to the *X*-axis will be limited by the material used as the anchor. If the two actuators are offset, they will induce an additional moment, increasing the reaction force at the axis. The packaging of the device must also increase because of the offset.

The final design selected is shown in Figure 140. two tape actuators connected in series are used for actuation to achieve the required large-stroke performance. The coordinate frame of the system is in the primary tape actuator rotating Cartesian coordinate frame. The coordinate transformation has transformed The second actuator's force-displacement curve into the primary coordinate frame. The primary tape actuator force-displacement curve has the typical hyperelastic force-displacement profile. The secondary tape actuator is shown as a reverse bias in the primary coordinate frame. The secondary curves contain only a slight reverse bias. The OFF curve of the secondary curve, the blue horizontal curve at the top of the graph, has a slight reverse bias where the force increases as the actuator is shortened, moving right. When both actuators are OFF, the equilibrium position occurs where the two blue lines intersect, and the panel is at 90 degrees. The other two equilibrium points represent the panel rotating +/- 30 degrees.

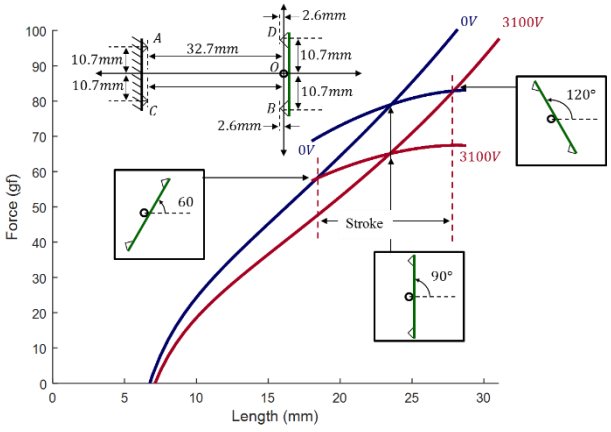

Figure 140. Design Plot with Performance Curves.

Force-displacement profile of both sub-component systems plotted in the primary coordinate frame. The proposed parameters for the dimensions are shown along with the corresponding equilibrium points.

The performance sensitivity for this reverse bias antagonistic design is shown in the force-displacement graph by the angle between the intersecting curves. If the curves continue without a high level of curvature, then the angle between the curves where they intersect can provide information about the sensitivity of the design. A shallow intercept angle between the curves represents a higher level of sensitivity. Small errors in the final design, caused by errors in implementation, fabrication parameters, or friction, can result in large shifts in the intersection and substantially degrade the performance.

6.3.2. Prototype

The prototype's construction materials and fabrication method must enable high dimensional accuracy because small dimensional errors can significantly affect the performance of the antagonistic reverse bias actuation system. A laser cutter, Universal Laser Systems X-660, was selected as the primary fabrication tool to achieve the tight tolerances required for the prototype. Acrylic panels with a thickness of 1/8 inch were chosen as the primary material for their strength and ease of use with a laser cutter. The wall panel prototype was designed in SOLIDWORKS and constructed from acrylic sheets, which can be connected using adhesive or bolts.

The design for the prototype must be carefully considered. The precision of the design will drive fabrication decisions on materials and methods. The inherent issues with friction will drive the design toward a low-friction solution. The sensitivity and accuracy of the reverse bias design indicate that the prototype should have easy adjustability with high precision and accuracy. The prototype is shown schematically in Figure 141.

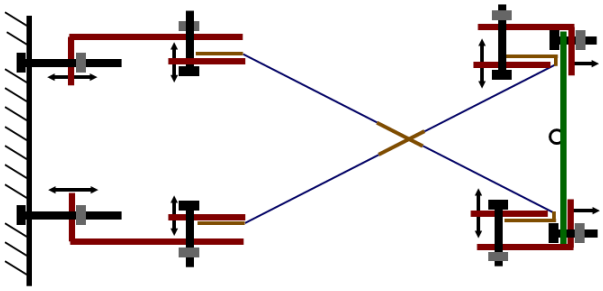

Figure 141. Schematic Overhead View of an Active Louver.

Overhead view of the louver reverse bias antagonistic configuration.

Fundamentally, the choice of materials is driven by the system's requirements. The panels must support the actuator's load and maintain their shape without deforming. Because of the low

actuation authority, there is an advantage to low-mass materials because they will have less inertia. Since dielectric elastomers are low force, the material stiffness is low. Therefore, acrylic plastic was chosen as the base material. The acrylic allows a laser cutter to cut the individual components to any design specifications accurately.

Friction can significantly impact the device's performance and should be avoided. The bearing joint must resist the forces caused by the actuators pulling on the panel. The axis will react to the moment introduced by the offset actuators. The low forces required for the bearing surface allow for less conventional bearing surfaces. The friction on the bearing surface is a function of the system's diameter and friction coefficient. One way to minimize the impact of the bearing friction is to reduce the contact surfaces of the axle and panel. A cone was selected as the bearing surface for the pin. The bearing surface becomes the point of the cone and the acrylic plastic. The cone's small head and contact area enable a very low friction joint. This type of joint is limited to low-force applications with low side loads.

One aspect of the reverse bias design is a requirement for precise implementation. The precision can come from the assembly and design or can be allowed through the device's ability to adjust easily. A design that enabled adjustment was selected to allow for design modification if required. The adjustment was accomplished using the same technique for the X and Y coordinates of the fixed anchor position of the tape actuator and the Y coordinate of the attachment to the panel. The attachments are adjustable using two pins to allow motion in a single direction, as shown in Figure 142. The anchors have close-fit holes that slide along the pins, which restricts the movement to a single axis. The actual location of the anchors is controlled using springs, bolts, and nuts. The springs are mounted on the pins and provide a force to push the anchor points. A clearance hole is cut in the anchor plates to allow the plate to slide freely over the bolt. A nut is then attached to the bolt and used to control the position of the plates. Screwing the nut down or up the shaft of the bolt allows for fine control of the position of the anchor location. The X position of the panel attachment is adjustable by adding shims between the panel attachment's L-bracket and the panel. The additional hardware on the panel enables adjustment and adds mass to the rotating panel. This extra mass increases inertia in the system, which has the effect of slowing the actuation speed.

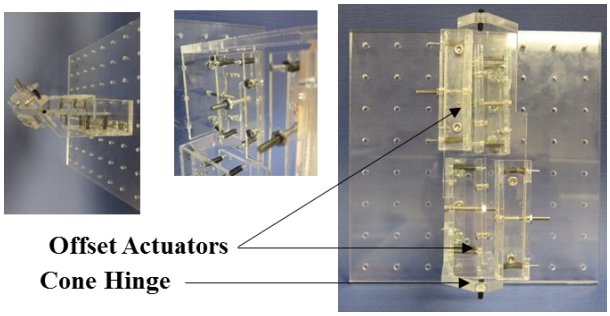

Figure 142. Prototype of Reverse Bias Antagonistic System.

Physical construction of the reverse bias antagonistic system.

6.3.3. Experimental Validation of Design and Viscoelastic Actuation Performance

The experimental setup is designed to supply a voltage to the reverse bias gravity-driven panel and measure the rotation. The voltage supply is provided through a Trek high-voltage amplifier and controlled through a NI DAQ and a custom LabVIEW program. The custom LabVIEW program also measures the applied voltage and current to the system. The rotational measurement of the panel is measured optically with a digital camera, Canon S90.

The experimental process involves cyclically applying a voltage five times to one set of actuators while the second set is OFF. The tests were done at a frequency of 1/40 Hz with a duty cycle of 50% and using a square wave. The tests started at 1500 V and increased by 100 V until 3100 V. At each voltage level, the system is cycled five times. The panel's rotational displacement was measured just before each 50% duty cycle ended. The experimental validation test setup is shown in Figure 143. The panel axis is aligned with gravity so that the panel’s motion is perpendicular to gravity. The camera is aligned directly with the axis, using an adjustable tripod.

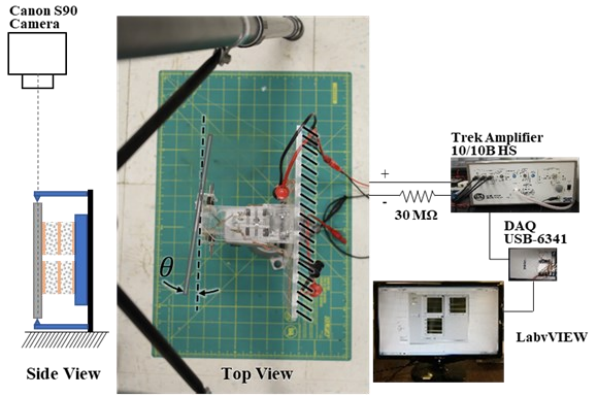

Figure 143. Active Louver Experimental Test Setup.

Experimental test setup for the panel test article, which shows both the side and top views. Included in the image are the optical measurement setup and the high-voltage amplifier driven by a custom LabVIEW control program.

The panel aims to change orientations; therefore, the critical relationship is between the rotation angle and the applied voltage. The experimental results, shown as red dots, are plotted in Figure 144 on a rotation-versus-voltage graph. The graph also contains a blue line, the predicted rotation as a function of applied voltage derived from the analytical model. The dielectric elastomer tape actuator had a premature failure at 3000 V and broke. The experimental results fall within 1.13 degrees of the model prediction, shown in Figure 144, and the percent error of the designed panel rotation, 30 degrees, is a maximum of 4%, which is shown in Figure 145. The actuators prematurely failed at 3000 V even though they had been previously exercised to 3100 V many times. The cause of the failure is unknown.

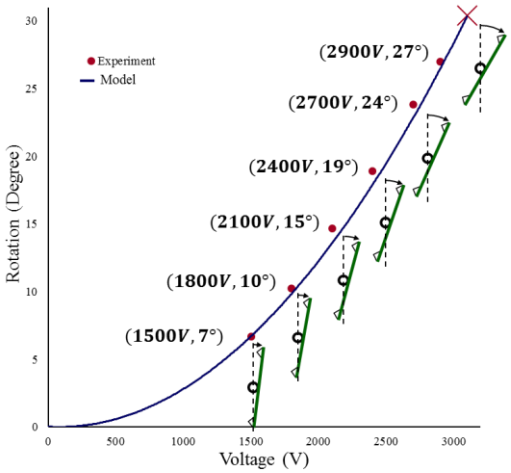

Figure 144. Predicted and Experimental Results Plotted Together.

The theoretical system performance is plotted (the thick blue line, and the experimental results are plotted as red dots.

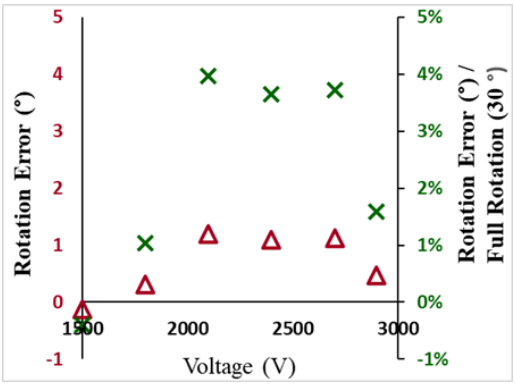

Figure 145. Panel Rotation Error.

The panel rotation error in degrees and the percent error as a function of the full panel rotation 30 degrees.

The error graph shows that the experimental results match the predicted rotation to within 4%. The error in degrees is displayed with the red triangles, while the green Xs show the percent error. There is no consistent trend in the error.

6.3.4. Conclusions for Active Louvers Actuation System

Applying the research findings developed through this dissertation to relevant case studies validates the scientific conclusions while demonstrating their ease of use and value in meeting current industrial needs. Each case study utilizes a different configuration and illustrates different attributes of DE tape actuators. In combination, they offer a broad view of the possible applications of DE tape actuators while confirming the functionality of the characterization methodology, the variable shear Gent model, and the design process in this dissertation.

Findings from the dissertation coalesce and culminate in the third and final case study, where the information, procedures, and processes developed for quasi-static design with DE tape actuators are applied to solve a problem of a rotating panel that potentially requires cyclical rotation at different angles. An antagonistic reverse bias design was proposed to create the desired rotation. The quasi-static design process was used to design a system to meet the specified goals of rotating a panel 30° in both directions from flat. The design further required architecture scaling performance using DE tape actuators in series to achieve actuation strains and displacement needed for the analytical design. Finally, a prototype of the proposed solution

was built. Experimental characterization of the prototype matched predicted performance to within 4% across a range of inputs. Achieving this accuracy required that each subcomponent perform correctly and accurately since slight inaccuracies in the expected performance characterization or tolerances would result in a non-functional antagonistic reverse bias design. The prototype functioned as designed, validating the various design elements, including the new information and technology developed through this research. While the prototype has additional complexity to allow for fine adjustments, this example demonstrates the feasibility of making a lightweight modular system that can be simplified and mass-produced to cover a whole wall system. This case study builds confidence that this new technology and design process can be expanded to other industrial applications.

Chapter 7 Conclusion

Rapid and revolutionary developments in miniaturization combined with the expanding capabilities of electronics and batteries have opened the floodgates to new applications for actuators in transportation and medical technologies, as well as in consumer products. Specifically, there is a mounting need for actuators that achieve fast, large-strain actuation while performing external work in a conformable and compact package with the ability to scale modularly, exhibiting robust and repeatable actions throughout the life of the device. Equally pressing is the need for research to facilitate the move from investigative findings to industrial applications of these devices, which will require a simplified design process that enables predictable and controllable variable performance. Motivated by these imperatives, this research is to create a new dielectric elastomer (DE) actuator architecture and develop a foundation for the systematic, model-based design of DE actuators for industrial applications. This goal was achieved by meeting the following objectives:

1. **Dielectric Elastomer Tape Actuator:** Identify a DE actuator frame configuration, elastomer and compliant electrode materials, and electrical and mechanical connections that enable a fast, large-strain actuator that performs external work in a conformable and compact package that can scale modularly and meet requirements for industrial applications. Those requirements include exhibiting robust and repeatable action over the life of the device while offering the design qualities of having predictable and controllable variable performance.
2. **Application Context Approach and Steady-State Cyclical Characterization:** Develop an approach for characterizing dielectric elastomer actuators for applications that use DE's inherent advantages, support actuator modeling, and a simple design process.
3. **Variable Shear Gent Strain Energy Equation:** Develop an analytical model that predicts a DE actuator's performance, which is useful for designing actuation systems. The model should utilize a minimum number of parameters to predict performance, require a minimum number of calibration data points, and finally, aid in the intuitive

understanding of how modification of parameters and variables impact the performance of a dielectric elastomer actuator.

4. **Quasi-Static Model-Based Design Applied to DE Actuators:** Create a framework for understanding and designing dielectric elastomer actuators in device and actuation systems. Identify the limitations of a dielectric elastomer actuator's performance and methods to minimize or compensate for the disadvantages; finally, identify common or useful actuator systems for the DE actuators and methods or processes that can be utilized to generate the best performance from a dielectric elastomer actuator.
5. **Automotive and Architectural Case Studies:** Demonstrate the validity of the research findings. Case studies are needed to validate the potential of dielectric elastomer actuators for industrial applications and to validate new characterization processes, models, and design approaches.

7.1. Research Overview

This dissertation focuses on developing an actuator technology that fully harnesses the advantages of dielectric elastomers and a new methodology approach to DE actuators that simplifies many of the challenges encountered when integrating them into new and existing applications.

The aim is to create an actuator that offers fast, large-strain actuation, the ability to perform external work in a conformable and compact package that can also scale with multiple modules, robust and repeatable action over its lifetime, and provides predictable and controllable performance over a wide actuation variable range. Current state-of-the-art dielectric elastomer actuator technology has demonstrated these characteristics separately; this research integrates all the advantageous properties into a single architecture, progressing DE technology down the path for industrial applications.

The new methodological approach focuses on the characterization of dielectric elastomer actuators. It significantly impacts analytical modeling and streamlines the model-based design process for DE actuators. The new methodological approach identifies that sometimes much of the complexity within dielectric elastomer actuators can be simplified by defining an application context, which outlines the actuator architecture, actuation requirements, and any additional

information needed to account for the complexity of dielectric elastomer technology, primarily viscoelasticity.

This approach negates the need for broad characterizations of an actuator for every conceivable situation, which is particularly challenging due to dielectric elastomers' viscoelastic properties. Instead, the application context narrows down the information required for accurate performance prediction, allowing for a limited characterization process that captures all essential information. Identifying and isolating the critical performance data needed for the application context makes simplifying the viscoelastic actuation performance behavior into the quasi-static Force-Length domain possible. Then, an existing time-invariant actuator model can be used to match the experimental results. The critical viscoelastic performance can be successfully simplified into the quasi-static Force-Length domain. In that case, creating a new model based on known phenomenological properties and the hyperelastic material model that captures the full viscoelastic actuation performance but remains time invariant is possible. The new model will have parameters that effectively embed all the critical viscoelastic information inside them. A simple quasi-static model-based design process can use the new model to accurately predict the actuation performance for modifying the architecture parameters and actuation variables. Thus, utilizing the application context methodological approach simplifies the characterization process, enables the time-invariant model to predict full viscoelastic performance, and makes the whole design process easier.

The application context methodological approach simplifies the characterization process, can enable a time-invariant model to predict full viscoelastic performance, and eases the design process. Both the new actuator architecture technology and the application context methodological approach are validated through case studies.

Identifying steady-state cyclical actuation as a useful situation for dielectric elastomers was critical in developing the new methodological approach. A new characterization process was designed to capture the essential actuation information for steady-state cyclical actuation. This approach viewed steady-state cyclical actuation through a binary actuation paradigm, simplifying complex viscoelastic performance data into the quasi-static Force-Length space. Extensive experimental results provided the data to develop the new variable shear Gent strain energy equation. Finally, novice dielectric elastomer researchers used the application context

characterization process and the new equation to fully design complex dielectric elastomer actuator devices, demonstrating the benefits of dielectric elastomer actuator technology.

7.1.1. Dielectric Elastomer Tape Actuator Architecture

In light of emerging technologies, A review of existing DE actuator architecture exposed a critical and growing need: a compact actuator that was conformable under large movements while maintaining robustness and high replicability. This research focused on creating a new DE actuator architecture that met the identified need while exhibiting modular scalability, with a long-term goal of satisfying industrial application requirements. Elements to be considered in the new architecture included a DE actuator frame configuration, elastomer material, compliant electrode material, and electrical and mechanical connections.

Frame Configuration. Before this research, a paradigm for categorizing frame configurations did not exist. Therefore, the initial step in determining which frame configuration to utilize was to create a frame categorization paradigm. Existing frame configurations were reviewed, sorted into categories, and evaluated for their ability to exploit the advantages of DE actuators. The frame configurations were a frameless configuration (i.e., actuators without an external frame), a flexible full frame that uses a flexible material around the perimeter of the active material, a rigid full frame configuration where a rigid frame is completely attached to the perimeter of the film; and a rigid release frame configuration in which a rigid external frame is attached to two opposing ends of a dielectric elastomer while the remaining edges are unattached. While each of these configurations has value in certain applications, none fully captures the fundamental advantage of DE actuators: the ability to enable fast, large-strain actuation while performing external work in a conformable and compact package with the ability to scale modularly. The following needs were identified: a DE actuator that uses moderate force levels and can be used in large architecture for enhanced force capabilities while performing external work and maintaining conformance.

A new configuration was designed to satisfy these needs: the flexible release frame that uses two thin, inextensible, and flexible frames to connect two separate edges of a rectangular, active DE region while the other two edges remain free. The flexible release frame configuration enhances the fundamental advantages of DE technology: it is large and conformal while having distributed actuation in a compact package with moderate forces.

Elastomer Material. The research considered the following key properties of elastomer film for these applications: force-displacement profile, viscoelasticity, dielectric permittivity, and dielectric breakdown strength. The benefits and limitations of acrylics, silicones, and, to a lesser extent, polyurethanes were evaluated for use as a large-strain actuator for industrial applications. Silicone was selected as the film material for this dissertation because it exhibits low viscoelasticity, low environmental sensitivity, and high actuation strain performance.

Compliant Electrodes. DE actuators rely on compliant electrodes to enable large-strain performance. Success depends on two critical yet often competing properties: conductivity and robustness, i.e., the electrode's adherence to the elastomer. In general, over repeated use, the conductivity of electrodes will vary inversely with their robustness. For this research, identifying compliant electrodes that provide conductivity under large strain while maintaining their robustness was essential. This dissertation reviewed carbon-based electrodes, including powders, viscous fluids, polymers, carbon nanotubes, and metallic electrodes, to determine the best configuration for the new DE actuator architecture. Because of the dual needs for conductivity and robustness, self-healing carbon nanotube electrodes were identified as the superior option for the new DE actuator. Specifically, the criss-crossing pattern of the carbon nanotubes promotes conductivity with very low stiffness when stretched.

Multifunctional Tape Connectors. Mechanical and electrical connections, linking the actuator's active area to the external world, comprise the final element of the DE actuator. Before this dissertation, mechanical and electrical connections were accomplished separately. A critical breakthrough was realized in this DE actuator research, which enhanced the conformal and compact package properties, creating a multifunctional tape connector (MTC) that combines mechanical and electrical connections. The MTC addresses the electrical connection needs of conductivity and conformity by using a combination of conductive silicone adhesive tape and conductive fabric tape. The mechanical connections are made with double-sided polyimide tape (Kapton), silicone adhesive, and windows cut out for the external electrical connection.

New DE Tape Architecture. The first element of this research resulted in the creation of a new DE tape actuator that extends the benefits of existing architectures by utilizing a new flexible release frame and new multifunctional tape connectors in combination with silicone film and single-wall carbon nanotube (SWNT) electrodes. After considering various materials, the DE tape actuator created with this dissertation employed a silicone film with multi-walled carbon

nanotube electrodes to make the active portion of the actuator. Kapton, adhesives, and conductive materials were used to create the MTCs. This new tape actuator exhibits the advantage of DEs by being a large-strain actuator that is conformable and compact. The MTC design enables modular expansion of the DE tape actuator so that it can be expanded by stacking and in parallel or series.

7.1.2. Cohesive and Integrated Application Context Methodological Approach to Dielectric Elastomer Actuator Design

This research addresses the methodological challenges present in existing characterization, modeling, and design processes related to DE actuators, this research used a system-based approach predicated on the application context of the actuation. This approach recognizes that the selected application context will drive the characterization, modeling, and design. Furthermore, each element of this process needs to consider the system's actuation behavior rather than each component's behavior to identify key effective material parameters that will capture the dynamics embedded in the entire system to simplify the design process.

7.1.2.1. Steady-State Cyclical Actuation Characterization Process

The purpose and results of this research extended beyond creating a new DE actuator architecture to address the accompanying needs for characterization and predictability. A five-step process was developed that can be used as a template to characterize DE actuators in various contexts beyond the limits of this dissertation:

1. Identify a specific application context.
2. Identify physics or performance metrics that are not fully characterized.
3. Develop initial characterization process.
4. Evaluate the characterization process and modify parameters or variables to improve performance.
5. Characterize the actuator performance for the application context using the new characterization process.

Bonus Step: Identify additional application contexts that may be able to use the characterization process.

The focus of this research objective was to develop a methodology for characterizing steady-state cyclical actuation that captures the key mechanical and electrical actuation properties that drive performance. Two primary factors led to selecting steady-state cyclical actuation as a focal point of the characterization efforts. First, it applies to the technologies where DE tape actuators would be employed, i.e., large-strain, repeatable motion. The intended purpose of DE tape actuators is for use in steady-state cyclical actuation performing external work. Second, steady-state cyclical actuation provides the considerable advantage of enabling simplification: the amount of data required to predict actuation performance under these conditions is much less than for other actuation methods. This research defines steady-state cyclical actuation as the repeated actuation performance level reached after several cycles when the long-term transient viscoelastic properties, Mullins effect, or actuator shakedown have settled out. The focused experimental investigations on this one type of actuation, steady-state cyclical actuation, allowed for simplifying the requirements for advancing DE actuator technology for this application sphere.

Both displacement control and force control testing methods were considered in this dissertation. Ultimately, the force control method was selected due to its advantages in capturing viscoelastic complexities presented by the DE tape actuator. Performance data were presented using force-length graphs for varying force levels when applying the same high and low voltage levels. Curves developed for the low voltage levels exhibited the same hyperelastic shape as those designed for the high voltage levels, with the curves for the high voltage shifted to the right, reflecting the additional displacement caused by the higher voltage.

After creating a custom experimental setup to characterize the steady-state cyclical actuation of a DE tape actuator, an active creep test was used to determine the appropriate time frame for the transient creep-terminated cyclical actuation. The characterization process used two initial shakedown tests followed by testing at discrete constant force levels across the actuator's operating range. The shakedown tests achieved better steady-state results by eliminating transient viscoelastic effects and ensuring that the actuator could operate at the highest applied electric field and lowest film breakdown strength.

7.1.2.2. Quasi-Static Analytical Design Model Capturing Full Viscoelastic Performance

With a steady-state cyclical actuation characterization model identified, the next task was to develop a simple analytical model to predict a DE tape actuator's quasi-static force and length during steady-state cyclical actuation for an applied driving voltage. The research objective was to develop an analytical model that uses a minimum number of parameters to predict performance, requires a minimum number of calibration data points, aids in the intuitive understanding of how the parameters impact the performance of a dielectric elastomer tape actuator, and identifies the accuracy and limitations of the model.

The variable shear Gent strain energy model for quasi-static actuation was created from first principles and an assumed relationship between the driving voltage and the shear parameter in the Gent model. The new model predicts two curves for each actuation voltage level: the LOW-voltage and HIGH-voltage curves. These are seen in the data as pairs of separately identifiable curves for each voltage level. The experimental characterization data also show that for each operating voltage, the LOW-voltage force-displacement curves shift to the right as the operating voltage level increases, albeit the LOW curves have zero operating voltage. This increase in length, predicted by the model, is the property that the variable shear term is intended to capture. The new model reduces the maximum error rate by 59% compared to the standard Gent model. Experimental data to validate the model accuracy ranged from 0 to 2600 V and 30 to 65 gf. Average error rates using the standard Gent model average error for the LOW-voltage, HIGH-voltage, and maximum error are 3.9%, 5.6%, and 11.2%, respectively. With the new variable shear Gent model, those rates drop to 1.7%, 3.0%, and 4.6% for the LOW-voltage, HIGH-voltage, and maximum error for a single set of model parameters. In addition to improved accuracy at the model calibration points, the new variable shear Gent model was shown to improve accuracy across the entire array of driving voltages and loads. The experimental data validated the assumption of an inverse quadratic relationship between the variable shear term, $\mu(V)$, and the voltage for steady-state cyclical actuation. Shear terms for each voltage level were separately determined from the experimental data. A comparison of the individually identified shear terms to the variable shear model's prediction of the variable shear term, $\mu(V)$, evaluated at each voltage level, showed that they both formed strong parabolic curves, and the predicted values are within 1% of the individually identified values. Further analysis confirmed that the

variable shear Gent model is accurate and predictive outside the voltage levels used for parameter identification.

While simple, this new variable shear Gent cyclical DE model accurately predicts the DE tape actuator performance over a wide range of voltages and forces. Since it relies on limited parameters, the amount of experimental data required for model calibration is greatly reduced. The calibrated model remained accurate across the full range of loads and driving voltages. Furthermore, the phenomenological meaning of the parameters enables this model to aid in the intuitive understanding of the performance characteristics of DE tape actuators. This model fills an important gap between simple material models that do not capture viscoelastic effects and complex full transient viscoelastic models that are overly complex for steady-state cyclical operation.

7.1.2.3. Quasi-Static Model-Based Design Process for Predicting Essential Viscoelastic Actuation

Due to the complexity of DE actuators, creating a framework to assist in understanding and designing DE actuator systems is necessary to facilitate their adoption for industrial applications. This dissertation addressed this need by developing a framework that provides a simple method for designing quasi-static dielectric elastomer actuator systems. This framework identifies the limitations of dielectric elastomer actuators, considers ways to minimize or compensate for these limitations, categorizes common and useful dielectric elastomer actuation devices/systems, and presents a methodology for evaluating the advantages and disadvantages of a particular device/system.

Designing with DE actuators must address the DE materials' complexity and the joining with external systems. This research applied a quasi-static design process using the force-length design space to DE actuators with a release frame configuration. In the force-length design space, it is possible to identify the principal variable and the free-clearance, which can be used to adjust the actuator's performance in an application. The design space performance and sensitivity impacts of changing the free-clearance and friction impacts are demonstrated in the quasi-static force-length design space.

One of the principal challenges of using DE actuators is their limited force authority because they are based on thin elastomers. This limitation can be overcome by scaling the performance, parameter changes, and employing a larger architecture using multiple modules. The advantages

of scaling with both methods were explored, and the disadvantages of each method were introduced.

This dissertation explored six different actuation systems that can be advantageous to DEs. To further enhance the usefulness of these categories, each identified system was evaluated on the actuation performance stroke, the design sensitivity, design complexity, and implementation complexity. Suppose designers are integrating a DE actuator into an existing system. In that case, this cataloging will allow them to identify the system they are using and the potential performance and challenges with integration. The categorization also allows for selecting the appropriate design system when designing DEs into a fully newly developed system.

Finally, system identification and categorization in the context of actuator design for DE actuators was considered. A trade-off approach was employed by categorizing external systems into different types and analyzing the trade-offs required when selecting a particular external system. Six categories of systems and system architectures relevant to DE actuators were identified: constant force, spring force, leverage designs, reverse bias designs, antagonistic designs, and reverse bias antagonistic designs. These systems were evaluated on the actuation performance stroke, the sensitivity of the design, the design complexity, and finally, the implementation complexity. The trade-off analysis allows designers to know the potential range of performance and how the system can be modified to enhance the total system by making modifications that will make the system performance better match the capabilities of DE actuators. The technique enables an easy and intuitive understanding of designing with DE actuators, can be adapted for any system configuration, and allows designers to maximize the possible performance for a given configuration without extensive trial-and-error experimentation.

7.1.3. Architecture and Methodological Validation Through Case Studies

To conclude this research, these advancements of DE actuators were integrated into three case studies that exemplify some potential advantages of using DEs. The first example, using an active seal for a vehicle, demonstrated the conformal properties and packaging of the DE tape actuator. It also exemplified the modular properties and architectural scaling by multilayer actuators to enhance the force-displacement performance of the actuation system.

The second case study utilized a gravity-driven reverse bias panel to demonstrate DE tape actuators' very large strain actuation potential. This example relied heavily on accurate characterization and modeling to achieve the extremely large-strain reverse bias leverage performance.

The third case study employed an antagonistic reverse bias acoustic panel. The rotating acoustic panel prototype demonstrated many of the techniques developed during the creation of this dissertation. First, it showcased the performance enabled by the flexible release frame configuration, the modular properties facilitated by the multifunctional tape connector, and the properties of the materials developed for this tape actuator. It exemplified a use-case where the steady-state cyclical actuation is relevant, and therefore, the steady-state cyclical actuation characterization methodology is critical for characterizing performance. Finally, the new variable shear Gent strain energy model accurately reflected the actuation performance while the quasi-static design process was applied to achieve the desired performance.

7.2. Future Work

This research has made significant strides in DE actuator technology through a new tape architecture and a novel methodological approach. This new approach can streamline the characterization, modeling, and design of dielectric elastomer actuators. However, this dissertation has created many new research questions. The full potential of the dielectric elastomer tape actuator is yet to be explored, and the limitations of the application context methodology need to be identified. The variable shear Gent model has only been validated at a frequency where transient creep has concluded during each half cycle.

Future research should consider applying the application context approach from this dissertation to more applications with varying actuation types. New application contexts will require creating new targeted characterization processes, new opportunities in simplifying critical viscoelastic performance data into quasi-static Force-Length domain, creating new models that bridge the gap between hyperelastic material models and full transient viscoelastic models, applying the quasi-static design methodology to more applications, and enabling other researchers to use these ideas. Investigating alternative DE tape actuator architectures is also vital, along with validating whether the characterization process and the new variable shear Gent

model function as anticipated when applied to other steady-state frequencies, not just those where transient creep has concluded.

A substantial product of this dissertation was the creation of the new DE tape actuator architecture. While the focus and result of the research was an actuator architecture, for the specific purposes and applications considered in this dissertation, material selection was limited to a single type of silicone film. The effects of pre-extended electrodes need to be further explored with different types of carbon nanotubes and other electrode materials. Future research into using other elastomer materials, particularly materials of varying stiffnesses, will build on the base understanding established here. Similarly, the application of the new actuator architecture was limited. Although this dissertation focused primarily on flat actuation surfaces, it did determine that some performance loss occurred when the surface was not flat. Investigating and characterizing performance losses when applying this architecture to conformable and bending conditions is another important avenue for future research.

For this dissertation, transient creep-terminated steady-state cyclical actuation was selected because it has many potential applications and avoids complications introduced by transient creep. Confirming that the steady-state cyclical characterization process and the new model also apply to applications with transient creep conditions could vastly expand the uses of these advances in the field of dielectric elastomer. Validating that this methodology works with different architectures will also significantly increase its usefulness. The new variable shear gent model may also have potential applicability to other fields of research that require modeling of long interacting chains.

7.3. Contributions

Embedded within this dissertation are multiple findings that will significantly advance the field of dielectric elastomer actuators. While the primary achievements directly relate to the research objectives outlined previously, other innovations were generated while advancing the research. The contributions can be broadly grouped into technological contributions associated with the new DE tape actuator architecture and methodological contributions deriving from the system-based approach.

Technological Contributions. The novel DE tape actuator architecture created through this research transforms the DE actuator landscape by meeting the critical need for a DE actuator that

performs fast, large-strain actuation while doing external work and maintaining conformance. Additionally, this innovative DE tape actuator is compact and modular. Its modularity enables architectural scaling, which ameliorates the low force limits of actuation due to being based on a soft elastomer. This pioneering actuator was made possible by developing two new facets of the architecture: the flexible release frame and the multifunction tape connector. The new flexible release frame configuration exploits the inherent advantages of DE actuator technology by facilitating large strain and conformal actuation. The new multifunctional tape connector uses Kapton, adhesives, and conducting materials, enabling easy electrical and mechanical connections in a flat, compact package while maintaining a transverse pre-strain in the elastomer film. These new elements, in combination with a silicone film and pre-extended single-wall carbon nanotube (SWNT) electrodes, result in an actuator architecture that exhibits robust and repeatable performance over extended use. Its robustness is demonstrated in its insensitivity to environmental factors such as heat and light. Robustness is also shown with the ability to overcome minor material flaws through self-healing, which extends the actuator's failure limits. This new DE tape actuator architecture promises to meet the ever-growing need for conformal, lightweight actuation under large strain critical in medical technology, transportation technologies, and consumer products. Several building block contributions were realized before and during the development of the new actuator. A fundamental outcome of this dissertation was to demonstrate the demand for a DE actuator to satisfy the requirements of new and evolving technologies. Similarly, before this research, existing frame configurations had not been categorized. By identifying and grouping frames into distinct types that were then evaluated according to their different characteristics, the author could envision a new kind of configuration: the flexible release frame, which draws from the strengths of both the flexible and rigid release frames. Developing a system to categorize frame types will facilitate future research and actuator development by providing a structure to evaluate frame types based on desired characteristics.

Methodological Contributions. A defining and substantial contribution is the determination that DE actuator technology requires a system-based design methodology. Due to the complexity of the elastomer materials in combination with the various elements of an actuator, a system-based design approach based on the selected application context is utilized to determine the appropriate characterization methodologies and identify key performance parameters. Based on modeling, the key effective material parameters that capture the dynamics embedded in the

system can be identified and incorporated to simplify the design process. This dissertation articulates and validates the need for and the elements of a system-based design methodology in designing DE actuator technology.

Two contributions resulted from the characterization process of the research: a template for characterizing DE actuators was created, and the experimental process for characterizing the DE tape actuator for steady-state cyclical actuation was established. The five-step template detailed in Section 3.1 provides a roadmap for characterizing DE actuators. The crux of the process is understanding that DE actuator characterization hinges on the application context which encompasses the actuator situation, the actuation requirements, and the identification of a specific DE actuator. Once these elements are established, the template outlines a straightforward path to characterizing DE actuators. Establishing the new experimental method to characterize a dielectric elastomer for steady-state cyclical actuation that captures the essential information to be used in applications comprises another impactful result of this research. The novel steady-state cyclical actuation characterization methodology allows for accurate, repeatable characterization of DE tape actuators for systems that use transient creep-terminated cyclical actuation. It also simplifies characterization data so that the information can be easily presented as force-displacement information to predict the performance of binary actuation. The initial finding that led to developing the actuation characterization methodology was determining that cyclical actuation could be represented as binary actuation in a quasi-static framework.

Developing a model to predict DE tape actuator performance is a notable contribution of this research. The variable strain Gent model developed through this research simplifies and accurately models the performance of DE tape actuators used in transient creep-terminated steady-state cycling situations over the full range of applied voltages and forces from a limited set of experimental data. This pioneering model cuts the error approximately in half against a Gent-only based model for the characterization of voltages and forces where the Gent model is most accurate, while the variable Gent model maintains its accuracy over the entire force and voltage range of the actuator. While the accuracy is impressive, the more significant contribution is model simplification arising from using effective material parameters made possible by the system-based approach centered on the application context. This model fills an important gap between simple material models that do not capture viscoelastic effects and complex full transient viscoelastic models that are overly complex for steady-state cyclical operation.

This dissertation identifies and demonstrates the application of a quasi-static design process using DE tape actuators to six actuation systems relevant to dielectric elastomers. The quasi-static design process simplifies the knowledge required to design with tape actuators that have complex actuation performance. The technique enables an easy and intuitive understanding of designing with DE tape actuators. The process was categorized and applied to the six actuation systems that were then evaluated for advantages and disadvantages.

Finally, the dissertation demonstrates and validates the relevance and advantages of the new DE tape actuator hierarchy and the system-based design approach, using the characterization methodology and the innovative variable strain Gent model for real-world applications. The final two case studies included in this dissertation were conducted by students who lacked expertise in DE actuators. Using the new DE tape actuator and the system-based design approach, including the steady-state cyclical actuation characterization and the variable shear Gent model in conjunction with the developed design process, these students were able to design functional actuation systems.

In summary, this dissertation establishes a DE tape actuator architecture with the demonstrated advantages of having conformal and compact properties, easy mechanical and electrical connections, parallel and series architectures, and very large strain while also providing a methodology for designing DE tape actuator systems that non-experts can employ to relevant applications. These accomplishments lay the groundwork for future DE tape actuators research, development, and application.

7.4. Closing

This research was conceived and driven by a desire to address the exploding demand for actuators in developing industrial applications, specifically consumer products, transportation, and medical technologies. Requirements arising from these technologies dictated the need for actuators that achieve fast, large strain actuation while performing external work; retain conformal and compact packaging while being able to scale modularly; maintain repeatable and robust functionality throughout the life of the device; and support a simplified design process offering predictable and controllable variable performance. Likewise, considering these needs from an industrial perspective required the development of a characterization methodology and a predictive design model. The outcomes of this research, a new DE actuator architecture, a

characterization paradigm, and a predictive design model, along with a design methodology accompanied by supporting case studies, provide a foundation for future progress to enable wider adoption and advancement of these actuators.

References

[1] Liu, J., Yang, C., Wu, H., Lin, Z., Zhang, Z., Wang, R., Li, B., Kang, F., Shi, L., and Wong, C. P., 2014, "Future Paper Based Printed Circuit Boards for Green Electronics: Fabrication and Life Cycle Assessment," Energy Environ Sci.

[2] Yuan, L., Xu, X., Ding, T., Zhong, J., Zhang, X., Shen, Y., Hu, B., Huang, Y., Zhou, J., and Wang, Z. L., 2012, "Paper-Based Supercapacitors for Self-Powered Nanosystems," Angewandte Chemie.

[3] Zeng, W., Shu, L., Qiao, L., Chen, S., Wang, F., and Tao, X., 2014, "Fiber-Based Wearable Electronics: A Review of Materials, Fabrication, Devices, and Applications," Advanced Materials.

[4] Blaabjerg, F., Yang, Y., Ma, K., and Wang, X., 2015, "Power Electronics - The Key Technology for Renewable Energy System Integration."

[5] Blaabjerg, F., Yang, Y., Kim, K. A., and Rodríguez, J., 2023, "Power Electronics Technology for Large-Scale Renewable Energy Generation," Proceedings of the Ieee.

[6] Pomilio, J. A., Canesin, C. A., Marcelo Antunes, F. L., Reis, F. S. Dos, and Sampaio, L. P., 2011, "Power Electronics Courses for the New Paradigms of the Electrical System."

[7] Roccaforte, F., Greco, G., Fiorenza, P., and Iucolano, F., 2019, "An Overview of Normally-Off GaN-Based High Electron Mobility Transistors," Materials.

[8] Carrasco, J. M., Franquelo, L. G., Bialasiewicz, J. T., Galván, E., Guisado, R. C. P., Prats, Ma. A. M., Leon, J. I., and Moreno-Alfonso, N., 2006, "Power-Electronic Systems for the Grid Integration of Renewable Energy Sources: A Survey," Ieee Transactions on Industrial Electronics.

[9] Jiya, I. N., and Gouws, R., 2020, "Overview of Power Electronic Switches: A Summary of the Past, State-of-the-Art and Illumination of the Future," Micromachines (Basel).

[10] Trivedi, D., Rahn, C. D., Kier, W. M., and Walker, I. D., 2008, "Soft Robotics: Biological Inspiration, State of the Art, and Future Research," Appl Bionics Biomech, **5**(3), pp. 99–117.

[11] Koca, K., Genç, M. S., and Ertürk, S., 2022, "Impact of Local Flexible Membrane on Power Efficiency Stability at Wind Turbine Blade," Renew Energy, **197**, pp. 1163–1173.

[12] Bruce, P. J. K., and Colliss, S. P., 2015, "Review of Research into Shock Control Bumps," Shock Waves, **25**(5), pp. 451–471.

[13] Reich, G., and Sanders, B., 2012, "Introduction to Morphing Aircraft Research," https://doi-org.proxy.lib.umich.edu/10.2514/1.28287, **44**(4), p. 1059.

[14] Biddiss, E., and Chau, T., 2008, "Dielectric Elastomers as Actuators for Upper Limb Prosthetics: Challenges and Opportunities," Med Eng Phys, **30**(4), pp. 403–418.

[15] Costa, J., Ghilardi, M., Mamone, V., Ferrari, V., Busfield, J. J. C., Ahluwalia, A., and Carpi, F., 2020, "Bioreactor With Electrically Deformable Curved Membranes for Mechanical Stimulation of Cell Cultures," Front Bioeng Biotechnol, **8**, p. 505964.

[16] Swan, M. C., Bucknall, D. G., Goodacre, T. E. E., and Czernuszka, J. T., 2011, "Synthesis and Properties of a Novel Anisotropic Self-Inflating Hydrogel Tissue Expander," Acta Biomater, **7**(3), pp. 1126–1132.

[17] Marchese, A. D., and Rus, D., 2015, "Design, Kinematics, and Control of a Soft Spatial Fluidic Elastomer Manipulator," https://doi.org/10.1177/0278364915587925, **35**(7), pp. 840–869.

[18] Shepherd, R. F., Ilievski, F., Choi, W., Morin, S. A., Stokes, A. A., Mazzeo, A. D., Chen, X., Wang, M., and Whitesides, G. M., 2011, "Multigait Soft Robot," Proc Natl Acad Sci U S A, **108**(51), pp. 20400–20403.

[19] Gu, G. Y., Gupta, U., Zhu, J., Zhu, L. M., and Zhu, X., 2017, "Modeling of Viscoelastic Electromechanical Behavior in a Soft Dielectric Elastomer Actuator," IEEE Transactions on Robotics, **33**(5), pp. 1263–1271.

[20] Wang, L., Yang, Y., Chen, Y., Majidi, C., Iida, F., Askounis, E., and Pei, Q., 2018, "Controllable and Reversible Tuning of Material Rigidity for Robot Applications," Materials Today, **21**(5), pp. 563–576.

[21] Pelrine, R., Sommer-Larsen, P., Kornbluh, R., Heydt, R., Kofod, G., Pei, Q., and Gravesen, P., 2001, "Applications of Dielectric Elastomer Actuators," https://doi.org/10.1117/12.432665, **4329**, pp. 335–349.

[22] Shintake, J., Rosset, S., Schubert, B., Floreano, D., and Shea, H., 2016, "Versatile Soft Grippers with Intrinsic Electroadhesion Based on Multifunctional Polymer Actuators," Advanced Materials, **28**(2), pp. 231–238.

[23] Rosset, S., and Shea, H., 2016, "Small, Fast, and Tough: Shrinking down Integrated Elastomer Transducers," Appl Phys Rev, **3**(3).

[24] Guo, Y., Qin, Q., Han, Z., Plamthottam, R., Possinger, M., and Pei, Q., 2023, "Dielectric Elastomer Artificial Muscle Materials Advancement and Soft Robotic Applications," SmartMat, **4**(4), p. e1203.

[25] Rodriguez, A. R., 2007, "Morphing Aircraft Technology Survey," Collection of Technical Papers - 45th AIAA Aerospace Sciences Meeting, **21**, pp. 15064–15079.

[26] Apsite, I., Salehi, S., and Ionov, L., 2022, "Materials for Smart Soft Actuator Systems," Chem Rev, **122**(1), pp. 1349–1415.

[27] Rus, D., and Tolley, M. T., 2015, "Design, Fabrication and Control of Soft Robots," Nature 2015 521:7553, **521**(7553), pp. 467–475.

[28] Majidi, C., 2014, "Soft Robotics: A Perspective - Current Trends and Prospects for the Future," Soft Robot, **1**(1), pp. 5–11.

[29] Gu, G. Y., Zhu, J., Zhu, L. M., and Zhu, X., 2017, "A Survey on Dielectric Elastomer Actuators for Soft Robots," Bioinspir Biomim, **12**(1), p. 011003.

[30] Li, Z., Gao, C., Fan, S., Zou, J., Gu, G., Dong, M., and Song, J., 2019, "Cell Nanomechanics Based on Dielectric Elastomer Actuator Device," Nano-Micro Letters 2019 11:1, **11**(1), pp. 1–19.

[31] Gu, J., Zhou, Z., Zhu, Z., Huang, G., and Zhang, Z., 2023, "Mechanical Stimulation of Cells with Electroactive Polymer-Based Soft Actuators," The European Physical Journal Special Topics 2023, pp. 1–14.

[32] Kauffman, G., 1997, "The Story of Nitinol: The Serendipitous Discovery of the Memory Metal and Its Applications," The chemical educator, **2**(2), pp. 1–21.

[33] Pelrine, R. E., Kornbluh, R. D., and Joseph, J. P., 1998, "Electrostriction of Polymer Dielectrics with Compliant Electrodes as a Means of Actuation," Sens Actuators A Phys, **64**(1), pp. 77–85.

[34] Kornbluh, R., Pelrine, R., Joseph, J., Heydt, R., Pei, Q., and Chiba, S., 1999, "High-Field Electrostriction of Elastomeric Polymer Dielectrics for Actuation," https://doi.org/10.1117/12.349672, **3669**, pp. 149–161.

[35] Kornbluh, R., Pelrine, R., and Joseph, J., 1995, "Elastomeric Dielectric Artificial Muscle Actuators for Small Robots," Proceedings of the Third IASTED International Conference on Robotics and Manufacturing, pp. 14–16.

[36] Pelrine, R., Kornbluh, R., Joseph, J., and Chiba, S., 1997, "Electrostriction of Polymer Films for Microactuators," Proceedings of the IEEE Micro Electro Mechanical Systems (MEMS), pp. 238–243.

[37] Pelrine, R. E., Kornbluh, R. D., and Joseph, J. P., 1998, "Electrostriction of Polymer Dielectrics with Compliant Electrodes as a Means of Actuation," Sens Actuators A Phys, **64**(1), pp. 77–85.

[38] Kornbluh, R., Pelrine, R., Joseph, J., Pei, Q., and Chiba, S., 2000, "Ultra-High Strain Response of Elastomeric Polymer Dielectrics," Materials Research Society Symposium - Proceedings, **600**, pp. 119–130.

[39] Kofod, G., Kornbluh, R., Pelrine, R., and Sommer-Larsen, P., 2001, "Actuation Response of Polyacrylate Dielectric Elastomers," Smart Structures and Materials 2001: Electroactive Polymer Actuators and Devices, **4329**, p. 141.

[40] Heydt, R., Pelrine, R., Joseph, J., Eckerle, J., and Kornbluh, R., 2000, "Acoustical Performance of an Electrostrictive Polymer Film Loudspeaker," J Acoust Soc Am, **107**(2), pp. 833–839.

[41] Heydt, R., Kornbluh, R., Pelrine, R., and Mason, V., 1998, "Design and Performance of an Electrostrictive-Polymer-Fllm Acoustic Actuator," J Sound Vib, **215**(2), pp. 297–311.

[42] Pelrine, R., Kornbluh, R., Pei, Q., Stanford, S., Oh, S., Eckerle, J., Full, R. J., Rosenthal, M. A., and Meijer, K., 2002, "Dielectric Elastomer Artificial Muscle Actuators: Toward Biomimetic Motion," Proceedings of SPIE, **4695**, pp. 126–137.

[43] Petralia, M. T., and Wood, R. J., 2010, "Fabrication and Analysis of Dielectric-Elastomer Minimum-Energy Structures for Highly-Deformable Soft Robotic Systems," IEEE/RSJ 2010 International Conference on Intelligent Robots and Systems, IROS 2010 - Conference Proceedings, pp. 2357–2363.

[44] Balakrisnan, B., and Smela, E., 2010, "Challenges in the Microfabrication of Dielectric Elastomer Actuators," Electroactive Polymer Actuators and Devices, **7642**, pp. 76420K-76420K–10.

[45] Fox, J. W., and Goulbourne, N. C., 2007, "An Experimental Study on the Dynamic Response of Dielectric Elastomer Membranes," Proceedings of SPIE, **6524**, pp. 65241Z-65241Z–12.

[46] Kofod, G., 2008, "The Static Actuation of Dielectric Elastomer Actuators: How Does Pre-Stretch Improve Actuation?," J Phys D Appl Phys, **41**(21), p. 215405.

[47] Lucking Bigue, J.-P., Chouinard, P., Denninger, M., Proulx, S., and Plante, J.-S., 2010, "Thermodynamic Model Using Experimental Loss Factors for Dielectric Elastomer Actuators Design," San Diego, CA, USA, pp. 76420T-76420T–12.

[48] Lochmatter, P., Kovacs, G., and Michel, S., 2007, "Characterization of Dielectric Elastomer Actuators Based on a Hyperelastic Film Model," Sens Actuators A Phys, **135**, pp. 748–757.

[49] York, A., Dunn, J., and Seelecke, S., 2010, "Experimental Characterization of the Hysteretic and Rate-Dependent Electromechanical of Dielectric Electro-Active Polymer Actuators," Smart Mater Struct, **19**(9), p. 094014.

[50] Zhu, J., Cai, S., and Suo, Z., 2010, "Resonant Behavior of a Membrane of a Dielectric Elastomer," Int J Solids Struct, **47**(24), pp. 3254–3262.

[51] Matysek, M., and Lotz, P., 2008, "High-Precision Characterization of Dielectric Elastomer Stack Actuators and Their Material Parameters," … and Materials …, **6927**, pp. 692722-692722–10.

[52] Plante, J.-S., and Dubowsky, S., 2006, "Large-Scale Failure Modes of Dielectric Elastomer Actuators," Int J Solids Struct, **43**(25–26), pp. 7727–7751.

[53] Moscardo, M., Zhao, X., Suo, Z., and Lapusta, Y., 2008, "On Designing Dielectric Elastomer Actuators," J Appl Phys, **104**(9), pp. 1–7.

[54] Yuan, W., Brochu, P., Ha, S. M., and Pei, Q., 2009, "Dielectric Oil Coated Single-Walled Carbon Nanotube Electrodes for Stable, Large-Strain Actuation with Dielectric Elastomers," Sens Actuators A Phys, **155**, pp. 278–284.

[55] Yuan, W., Brochu, P., Zhang, H., Jan, A., and Pei, Q., 2009, "Long Lifetime Dielectric Elastomer Actuators under Continuous High Strain Actuation," Carbon N Y, **7287**, pp. 1–8.

[56] Bigué, J. L., Chouinard, P., Denninger, M., Proulx, S., and Plante, J., 2010, "A Thermodynamic Model Using Experimental Loss Factors For Dielectric Elastomer Actuator Design," **7642**(1), pp. 819–821.

[57] Proulx, S., Chouinard, P., Denninger, M., Plante, J.-S., and Lucking Bigué, J.-P., 2010, "Thermodynamic Model Using Experimental Loss Factors for Dielectric Elastomer Actuator Design," Electroactive Polymer Actuators and Devices (EAPAD) 2010, **7642**(1), p. 76420T.

[58] Tianhu He, Leilei Cui, Cheng Chen, and Suo, Z., 2010, "Nonlinear Deformation Analysis of a Dielectric Elastomer Membrane-Spring System," Smart Mater Struct, **19**(8), p. 085017 (7 pp.).

[59] Suo, Z., 2010, "Theory of Dielectric Elastomers," Acta Mechanica Solida Sinica, **23**(6), pp. 549–578.

[60] Lotz, P., Matysek, M., Flittner, K., and Schlaak, H. F., 2010, "Modeling of Non Ideal Dielectric Elastomer Stack Actuators," **7642**, pp. 764214-764214–9.

[61] McKay, T. G., Calius, E., and Anderson, I. A., 2007, "Modelling a Dielectric Elastomer Actuator Based on the McKibben Muscle," Proceedings of SPIE, **6524**, pp. 65241W-65241W–8.

[62] Goulbourne, N. C., 2009, "A Mathematical Model for Cylindrical, Fiber Reinforced Electro-Pneumatic Actuators," Int J Solids Struct, **46**(5), pp. 1043–1052.

[63] Goulbourne, N. C., 2004, "Electro-Elastic Modeling of a Dielectric Elastomer Diaphragm for a Prosthetic Blood Pump," Proceedings of SPIE, **5385**, pp. 122–133.

[64] Wissler, M., and Mazza, E., 2005, "Modeling of a Pre-Strained Circular Actuator Made of Dielectric Elastomers," Sens Actuators A Phys, **120**(1), pp. 184–192.

[65] Carpi, F., and De Rossi, D., 2004, "Dielectric Elastomer Cylindrical Actuators: Electromechanical Modelling and Experimental Evaluation," Materials Science and Engineering: C, **24**(4), pp. 555–562.

[66] Xuanhe Zhao, Wei Hong, and Zhigang Suo, 2007, "Electromechanical Hysteresis and Coexistent States in Dielectric Elastomers," Phys Rev B Condens Matter Mater Phys, **76**(13), pp. 134113–1.

[67] Goulbourne, N. C., Frecker, M., Mockensturm, E., and Snyder, A., 2003, "Modeling of a Dielectric Elastomer Diaphragm for a Prosthetic Blood Pump," **5051**, pp. 319–331.

[68] Suo, Z., Zhao, X., Hong, W., Zhou, J., and Greene, W. H., 2008, "A Theory of Large Deformation in Soft Active Materials," **6927**, pp. 692710–1.

[69] Son, S., and Goulbourne, N. C., 2009, "Finite Deformations of Tubular Dielectric Elastomer Sensors," J Intell Mater Syst Struct, **20**(18), pp. 2187–2199.

[70] Patrick, L., Gabor, K., and Silvain, M., 2007, "Characterization of Dielectric Elastomer Actuators Based on a Hyperelastic Film Model," Sens Actuators A Phys, **135**(2), pp. 748–757.

[71] Zhao, X., and Suo, Z., 2010, "Theory of Dielectric Elastomers Capable of Giant Deformation of Actuation," Phys Rev Lett, **104**(17), p. 178302 (4 pp.).

[72] Lochmatter, P., Michel, S., and Kovacs, G., 2006, "Electromechanical Model for Static and Dynamic Activation of Elementary Dielectric Elastomer Actuators," Smart Structures and Materials 2006 Electroactive Polymer Actuators and Devices EAPAD, **6168**(section 5), pp. F1680–F1680.

[73] Kofod, G., and Sommer-Larsen, P., 2005, "Silicone Dielectric Elastomer Actuators: Finite-Elasticity Model of Actuation," Sens Actuators A Phys, **122**, pp. 273–283.

[74] Son, S., and Goulbourne, N. C., 2009, "Finite Deformations of Tubular Dielectric Elastomer Sensors," J Intell Mater Syst Struct, **20**, pp. 2187–2199.

[75] Zhao, X., and Suo, Z., 2008, "Method to Analyze Programmable Deformation of Dielectric Elastomer Layers," Appl Phys Lett, **93**, pp. 2008–2010.

[76] Kaal, W., Herold, S., and Melz, T., 2010, "Modeling Approaches for Electroactive Polymers," Polymer (Guildf), **7642**, pp. 764211-764211–11.

[77] Carpi, F., Migliore, A., Serra, G., and De Rossi, D., 2005, "Helical Dielectric Elastomer Actuators," Smart Mater Struct, **14**(6), pp. 1210–16.

[78] Prahlad, H., 2005, "Programmable Surface Deformation: Thickness-Mode Electroactive Polymer Actuators and Their Applications," Proceedings of SPIE, **5759**, pp. 102–113.

[79] Zhang, R., Lochmatter, P., Kunzb, A., and Kovacs, G., 2006, "Spring Roll Dielectric Elastomer Actuators for a Portable Force Feedback Glove," Proceedings of SPIE, **6168**, pp. 61681T-61681T–12.

[80] Zhao, X., and Suo, Z., 2008, "Electrostriction in Elastic Dielectrics Undergoing Large Deformation," J Appl Phys, **104**(12), p. 123530.

[81] Wingert, A., Lichter, M. D., and Dubowsky, S., 2006, "On the Design of Large Degree-of-Freedom Digital Mechatronic Devices Based on Bistable Dielectric Elastomer Actuators," IEEE/ASME Transactions on Mechatronics, **11**(4), pp. 448–456.

[82] Zhu, J., Cai, S., and Suo, Z., 2010, "Nonlinear Oscillation of a Dielectric Elastomer Balloon," Polym Int, **59**(3), pp. 378–383.

[83] Jordi, C., Michel, S., Durager, C., Bormann, A., Gebhardt, C., and Kovacs, G., 2010, "Large Planar Dielectric Elastomer Actuators for Fish-like Propulsion of an Airship," **7642**, p. The Society of Photo-Optical Instrumentation Engin.

[84] Kovacs, G., Lochmatter, P., and Wissler, M., 2007, "An Arm Wrestling Robot Driven by Dielectric Elastomer Actuators," Smart Mater Struct, **16**(2), pp. S306–S317.

[85] Menon, C., Carpi, F., and De Rossi, D., 2009, "Concept Design of Novel Bio-Inspired Distributed Actuators for Space Applications," Acta Astronaut, **65**, pp. 825–833.

[86] Zhang, R., Wegener, K., Kunz, A., and Kovacs, G., 2007, "Development of Dielectric Elastomer Actuators and Their Implementation in a Force Feedback Interface," D-Mavt, **PhD**(17584), p. 224.

[87] Plante, J.-S., Devita, L., Tadakuma, K., and Dubowsky, S., 2009, "MRI Compatible Device for Robotic Assisted Interventions to Prostate Cancer," Biomedical Applications of Electroactive Polymer Actuators, pp. 411–425.

[88] Jordi, C., Michel, S., and Fink, E., 2010, "Fish-like Propulsion of an Airship with Planar Membrane Dielectric Elastomer Actuators.," Bioinspir Biomim, **5**(2), p. 026007.

[89] Sîrbu, I.-D., Moretti, G., Dirè, S., Fambri, L., Vertechy, R., Meniglio, D., and Fontana, M., 2019, "Electrostatic Actuator for Tactile Display Based on Hydraulically Coupled Dielectric Fluids and Soft Structures," https://doi-org.proxy.lib.umich.edu/10.1117/12.2514279, **10966**, pp. 334–339.

[90] Pece, F., Zarate, J. J., Vechev, V., Besse, N., Gudozhnik, O., Shea, H., and Hilliges, O., 2017, "MagTics: Flexible and Thin Form Factor Magnetic Actuators for Dynamic and Wearable Haptic Feedback," UIST 2017 - Proceedings of the 30th Annual ACM Symposium on User Interface Software and Technology, pp. 143–154.

[91] Qiu, Y., Ma, S., Pei, Q., and Holbery, J. D., 2019, "A Self-Conformable Smart Skin with Sensing and Variable Stiffness Functions," Advanced Intelligent Systems, **1**(5), p. 1900054.

[92] Peng, Z., Qiu, Y., Shi, Y., Zhang, Z., Alwen, A., Yin, H., Plamthottam, R., Ren, Z., and Pei, Q., 2019, "Bistable Electroactive Polymers for Refreshable Tactile Displays," https://doi.org/10.1117/12.2513780, **10966**, pp. 327–333.

[93] Ren, Z., Niu, X., Chen, D., Hu, W., and Pei, Q., 2014, "A New Bistable Electroactive Polymer for Prolonged Cycle Lifetime of Refreshable Braille Displays," https://doi.org/10.1117/12.2044978, **9056**, pp. 511–519.

[94] Niu, X., Brochu, P., Stoyanov, H., Yun, S. R., and Pei, Q., 2012, "Bistable Electroactive Polymer for Refreshable Braille Display with Improved Actuation Stability," https://doi.org/10.1117/12.915069, **8340**, pp. 203–210.

[95] Yun, S., Yu, Z., Niu, X., Hu, W., Li, L., Brochu, P., and Pei, Q., 2012, "Compliant Composite Electrodes and Large Strain Bistable Actuation," Proceedings of SPIE, **8340**(1), pp. 834012-834012–11.

[96] Lotz, P., Matysek, M., and Schlaak, H. F., 2011, "Fabrication and Application of Miniaturized Dielectric Elastomer Stack Actuators," IEEE/ASME Transactions on Mechatronics, **16**(1), pp. 58–66.

[97] Matysek, M., Haus, H., Moessinger, H., Brokken, D., Lotz, P., and Schlaak, H. F., 2011, "Combined Driving and Sensing Circuitry for Dielectric Elastomer Actuators in Mobile Applications," **7976**, pp. 797612-797612–11.

[98] Yun, S., Niu, X., Yu, Z., Hu, W., Brochu, P., and Pei, Q., 2012, "Compliant Silver Nanowire-Polymer Composite Electrodes for Bistable Large Strain Actuation," Advanced Materials, **24**, pp. 1321–1327.

[99] Lau, G. K., Tan, D. D. T., and La, T. G., 2015, "Large Axial Actuation of Pre-Stretched Tubular Dielectric Elastomer and Use of Oil Encapsulation to Enhance Dielectric Breakdown Strength," Smart Mater Struct, **24**(4), p. 045025.

[100] Christianson, C., Bayag, C., Li, G., Jadhav, S., Giri, A., Agba, C., Li, T., and Tolley, M. T., 2019, "Jellyfish-Inspired Soft Robot Driven by Fluid Electrode Dielectric Organic Robotic Actuators," Front Robot AI, **6**, p. 486295.

[101] Poulin, A., Rosset, S., and Shea, H., 2014, "Toward Compression of Small Cell Population: Harnessing Stress in Passive Regions of Dielectric Elastomer Actuators," https://doi-org.proxy.lib.umich.edu/10.1117/12.2044784, **9056**, pp. 419–427.

[102] Poulin, A., Saygili Demir, C., Rosset, S., Petrova, T. V., and Shea, H., 2016, "Dielectric Elastomer Actuator for Mechanical Loading of 2D Cell Cultures," Lab Chip, **16**(19), pp. 3788–3794.

[103] Akbari, S., Niklaus, M., and Shea, H., 2010, "Arrays of EAP Micro-Actuators for Single-Cell Stretching Applications," https://doi.org/10.1117/12.847125, **7642**, pp. 107–116.

[104] Araromi, O., Poulin, A., Rosset, S., Favre, M., Giazzon, M., Martin-Olmos, C., Liley, M., and Shea, H., 2015, "Thin-Film Dielectric Elastomer Sensors to Measure the Contraction Force of Smooth Muscle Cells," Electroactive Polymer Actuators and Devices (eapad) 2015, **9430**(Figure 1), p. 94300Z.

[105] Akbari, S., Rosset, S., and Shea, H., 2012, "Stretching Cells with DEAs," Proc. SPIE, **8340**, pp. 83401R--83401R--9.

[106] Imboden, M., Poulin, A., de Coulon, E., Rosset, S., and Shea, H., 2016, "Electrically Shielded Dielectric Elastomer Actuators for the Study of the Mechanical Perturbation of Cardiomyocytes," EuroEAP 2016 - Sixth international conference on Electromechanically Active Polymer (EAP) transducers & artificial muscles, (June), p. 701614.

[107] Akbari, S., and Shea, H., 2012, "Microfabrication and Characterization of an Array of Dielectric Elastomer Actuators Generating Uniaxial Strain to Stretch Individual Cells," Journal of Micromechanics and Microengineering, **22**, p. 045020.

[108] Carpi, F., Coppola, M., Di Franco, R., Rosi, E., and Vizzarro, V., 2020, "Bioinspired Electromechanically Active Polymer-Based Robotics," Encyclopedia of Robotics, pp. 1–19.

[109] Seelecke, S., 2018, "Dielectric Elastomer Actuator-/Sensor Systems - From Basic Science to Application Ideas | VDE Conference Publication | IEEE Xplore," 16th International Conference on New Actuators.

[110] Gu, G., Shea, H., Seelecke, S., Alici, G., and Rizzello, G., 2021, "Editorial: Soft Robotics Based on Electroactive Polymers," Front Robot AI, **8**, p. 676406.

[111] Pelrine, R., Kornbluh, R., and Pei, Q., 2018, "Dielectric Elastomers: Past, Present, and Potential Future," https://doi-org.proxy.lib.umich.edu/10.1117/12.2302815, **10594**, pp. 15–22.

[112] Qiu, Y., Zhang, E., Plamthottam, R., and Pei, Q., 2019, "Dielectric Elastomer Artificial Muscle: Materials Innovations and Device Explorations," Acc Chem Res.

[113] Madsen, F. B., Daugaard, A. E., Hvilsted, S., and Skov, A. L., 2016, "The Current State of Silicone-Based Dieletric Elastomer Transducers," Macromol Rapid Commun, **37**, pp. 378–413.

[114] Carpi, F., Bauer, S., and De Rossi, D., 2010, "Stretching Dielectric Elastomer Performance.," Science, **330**(6012), pp. 1759–61.

[115] McLean, D., 1966, "The Physics of High Temperature Creep in Metals," Reports on Progress in Physics, **29**(1), p. 1.

[116] Siebenbürger, M., Ballauff, M., and Voigtmann, T., 2012, "Creep in Colloidal Glasses," Phys Rev Lett, **108**(25), p. 255701.

[117] Weiss, J., and Amitrano, D., 2023, "Logarithmic versus Andrade's Transient Creep: Role of Elastic Stress Redistribution," Phys Rev Mater, **7**(3), p. 033601.

[118] Dowling, N. E., 2013, "Mechanical Behavior of Materials : Engineering Methods for Deformation, Fracture, and Fatigue," p. 936.

[119] Ward, I. M., and Pinnock, P. R., 1966, "The Mechanical Properties of Solid Polymers," British Journal of Applied Physics, **17**(1), pp. 3–32.

[120] Sperling, L., 2005, *Introduction to Physical Polymer Science*.

[121] Zhang, J., Ru, J., Chen, H., Li, D., and Lu, J., 2017, "Viscoelastic Creep and Relaxation of Dielectric Elastomers Characterized by a Kelvin-Voigt-Maxwell Model," Appl Phys Lett, **110**(4).

[122] Gao, C., Li, Z., Zou, J., Cheng, J., Jiang, K., Liu, C., Gu, G., Tao, W., and Song, J., 2020, "Mechanical Effect on Gene Transfection Based on Dielectric Elastomer Actuator," ACS Appl Bio Mater, **3**(5), pp. 2617–2625.

[123] Dennis, M., 2013, "Effectiveness of Intermittent Pneumatic Compression in Reduction of Risk of Deep Vein Thrombosis in Patients Who Have Had a Stroke (CLOTS 3): A Multicentre Randomised Controlled Trial," The Lancet, **382**(9891), pp. 516–524.

[124] Li, Y., and Goulbourne, N. C., 2023, "Methods for Numerical Simulation of Soft Actively Contractile Materials," Scientific Reports 2023 13:1, **13**(1), pp. 1–11.

[125] Skulborstad, A. J., Wang, Y., Davidson, J. D., Swartz, S. M., and Goulbourne, N. C., 2013, "Polarized Image Correlation for Large Deformation Fiber Kinematics," Exp Mech, **53**(8), pp. 1405–1413.

[126] Skulborstad, A. J., and Goulbourne, N. C., 2014, "Biaxial Mechanical Characterization of Bat Wing Skin and Development of Biomimetic Constructs," ASME 2013 Conference on Smart Materials, Adaptive Structures and Intelligent Systems, SMASIS 2013, **1**.

[127] Leo, D., Weddle, C., Naganathan, G., Buckley Donald Leo, S. J., Buckley, S. J., and Leo Craig Weddle Stephen J Buckley Nagi Naganathan, D. J., 1998, "Vehicular Applications of Smart Material Systems," https://doi-org.proxy.lib.umich.edu/10.1117/12.310625, **3326**(16), pp. 106–116.

[128] Movahed, S. O., Ansarifar, A., and Estagy, S., 2016, "Review of the Reclaiming of Rubber Waste and Recent Work on the Recycling of Ethylene–Propylene–Diene Rubber Waste," Rubber Chemistry and Technology.

[129] Keiningham, T. L., Morgeson, F. V, Aksoy, L., and Williams, L., 2014, "Service Failure Severity, Customer Satisfaction, and Market Share," J Serv Res.

[130] Stenti, A., Moens, D., Sas, P., and Desmet, W., 2008, "Low-Frequency Dynamic Analysis of Automotive Door Weather-Strip Seals," Mech Syst Signal Process.

[131] Cho, J.-R., Han, K., Kim, J. S., Lee, S. B., and Lim, O.-K., 2012, "Fatigue Life Prediction and Optimum Topology Design of EPDM Weather Strip," Finite Elements in Analysis and Design.

[132] Li, Q., Zhu, W., Zhang, L., and Yuan, M., 2019, "Analysis and Structure Optimization on Buckling Destabilization and Wrinkling of an Automobile Weather-Strip Seal in Assemblage," Proceedings of the Institution of Mechanical Engineers Part D Journal of Automobile Engineering.

[133] Rosset, S., Poulin, A., Shea, H., and Anderson, I. A., 2019, "Taming the Viscoelastic Creep of Dielectric Elastomer Actuators," https://doi-org.proxy.lib.umich.edu/10.1117/12.2513981, **10966**, pp. 149–157.

[134] Poulin, A., Shea, H., and Rosset, S., 2018, "Fabrication and Characterization of Silicone-Based Dielectric Elastomer Actuators for Mechanical Stimulation of Living Cells," https://doi-org.proxy.lib.umich.edu/10.1117/12.2295687, **10594**, pp. 133–141.

[135] Cacucciolo, V., Nabae, H., Suzumori, K., and Shea, H., 2020, "Electrically-Driven Soft Fluidic Actuators Combining Stretchable Pumps With Thin McKibben Muscles," Front Robot AI, **6**, p. 504552.

[136] Pei, Q., Pelrine, R., Stanford, S., Kornbluh, R., Rosenthal, M. S., Meijer, K., and Full, R. J., 2002, "Multifunctional Electroelastomer Rolls and Their Application for Biomimetic Walking Robots," https://doi.org/10.1117/12.475071, **4698**, pp. 246–253.

[137] Illenberger, P. K., Madawala, U. K., and Anderson, I. A., 2016, "Big Power from Walking," https://doi-org.proxy.lib.umich.edu/10.1117/12.2218986, **9798**, pp. 112–121.

[138] Nguyen, C. T., Phung, H., Nguyen, T. D., Lee, C., Kim, U., Lee, D., Moon, H., Koo, J., Nam, J., and Choi, H. R., 2014, "A Small Biomimetic Quadruped Robot Driven by Multistacked Dielectric Elastomer Actuators," Smart Mater Struct, **23**(6), p. 065005.

[139] Lichter, M. D., Sujan, V. a., and Dubowsky, S., 2002, "Computational Issues in the Planning and Kinematics of Binary Robots," Proceedings 2002 IEEE International Conference on Robotics and Automation (Cat. No.02CH37292), **1**(May), pp. 341–346.

[140] Kesner, S., Plante, J.-S., Dubowsky, S., and Boston, P., 2007, "A HOPPING MOBILITY CONCEPT FOR A ROUGH TERRAIN SEARCH AND RESCUE ROBOT," ADVANCES IN CLIMBING AND WALKING ROBOTS, PROCEEDINGS, pp. 271–280.

[141] Pei, Q., Pelrine, R., Stanford, S., Kornbluh, R., and Rosenthal, M., 2003, "Electroelastomer Rolls and Their Application for Biomimetic Walking Robots," Synth Met, **135–136**, pp. 129–131.

[142] Pelrine, R., 2002, "Dielectric Elastomer Artificial Muscle Actuators: Toward Biomimetic Motion," Proceedings of SPIE, **4695**, pp. 126–137.

[143] Pei, Q., Pelrine, R., Rosenthal, M. a., Stanford, S., Prahlad, H., and Kornbluh, R., 2004, "Recent Progress on Electroelastomer Artifical Muscles and Their Application Biomimetic Robots," Electroactive Polymer Actuators and Devices (EAPAD), **5385**, pp. 41–50.

[144] Conn, A. T., Burgess, S., Hyde, R., and Ling, C. S., 2006, "From Natural Flyers to the Mechanical Realization of a Flapping Wing Micro Air Vehicle," 2006 IEEE International Conference on Robotics and Biomimetics, ROBIO 2006, pp. 439–444.

[145] Conn, A. T., Burgess, S. C., and Ling, C. S., 2007, "Design of a Parallel Crank-Rocker Flapping Mechanism for Insect-Inspired Micro Air Vehicles," http://dx.doi.org.proxy.lib.umich.edu/10.1243/09544062JMES517, **221**(10), pp. 1211–1222.

[146] Cao, C., Burgess, S., and Conn, A. T., 2019, "Toward a Dielectric Elastomer Resonator Driven Flapping Wing Micro Air Vehicle," Frontiers Robotics AI, **6**(JAN), p. 426316.

[147] Cao, C., Gao, X., Burgess, S., and Conn, A. T., 2020, "Power Optimization of a Conical Dielectric Elastomer Actuator for Resonant Robotic Systems," Extreme Mech Lett, **35**, p. 100619.

[148] Cacucciolo, V., Floreano, D., Maeda, S., Shea, H., and Shintake, J., 2020, "Stretchable Electrohydrodynamic Pump."

[149] Cacucciolo, V., Shintake, J., Kuwajima, Y., Maeda, S., Floreano, D., and Shea, H., 2020, "Soft Pumps for Robots and Wearables (Conference Presentation)," https://doi-org.proxy.lib.umich.edu/10.1117/12.2558595, **11375**, p. 113750U.

[150] Smith, M. J. H., Digumarti, K. M., Cacucciolo, V., and Shea, H., 2022, "A Variable Stiffness Soft Gripper with Integrated Ion-Drag Pump," Proceedings Volume PC12042, Electroactive Polymer Actuators and Devices (EAPAD) XXIV 2022, p. 19.

[151] Linnebach, P., Hau, S., Rizzello, G., and Seelecke, S., 2019, "Design of a Dielectric Elastomer Actuator Driven Pneumatic Pump," https://doi.org/10.1117/12.2514034, **10966**, pp. 242–249.

[152] Linnebach, P., Rizzello, G., Seelecke, S., and Seelecke, S., 2020, "Design and Validation of a Dielectric Elastomer Membrane Actuator Driven Pneumatic Pump," Smart Mater Struct, **29**(7), p. 075021.

[153] Gratz-Kelly, S., Rizzello, G., Fontana, M., Seelecke, S., and Moretti, G., 2022, "A Multi-Mode, Multi-Frequency Dielectric Elastomer Actuator," Adv Funct Mater, **32**(34), p. 2201889.

[154] Veale, A. J., Xie, S. Q., and Anderson, I. A., 2016, "Modeling the Peano Fluidic Muscle and the Effects of Its Material Properties on Its Static and Dynamic Behavior," Smart Mater Struct, **25**(6), p. 065014.

[155] O'Brien, B. M., Rosset, S., Shea, H., and Anderson, I. A., 2012, "Cutting the Fat: Artificial Muscle Oscillators for Lighter, Cheaper, and Slimmer Devices," https://doi.org/10.1117/12.915117, **8340**, pp. 45–52.

[156] Cao, C., Gao, X., and Conn, A. T., 2019, "A Magnetically Coupled Dielectric Elastomer Pump for Soft Robotics," Adv Mater Technol, **4**(8), p. 1900128.

[157] Cacucciolo, V., Shintake, J., Kuwajima, Y., Maeda, S., Floreano, D., and Shea, H., 2019, "Stretchable Pumps for Soft Machines," Nature 2019 572:7770, **572**(7770), pp. 516–519.

[158] Eldesoky, I. M., and Mousa, A. A., 2009, "Peristaltic Pumping of Fluid in Cylindrical Tube and Its Applications in the Field of Aerospace," Engineering, pp. 1–14.

[159] Goulbourne, N. C., Frecker, M., and Mockensturm, E. M., 2005, "Quasi-Static and Dynamic Inflation of a Dielectric Elastomer Membrane Actuator," SPIE, San Diego, CA, United states, pp. 302–313.

[160] Bowers, A. E., Rossiter, J., Walters, P. J., and Ieropoulos, I. a., 2011, "Dielectric Elastomer Pump for Artificial Organisms," **7976**, pp. 797629-797629–7.

[161] Lotz, P., Matysek, M., and Schlaak, H. F., 2009, "Peristaltic Pump Made of Dielectric Elastomer Actuators," Proceedings of SPIE, **7287**, pp. 72872D-72872D–8.

[162] Goulbourne, N., Frecker, M., Mockensturm, E., and Snyder, A., 2003, "Modeling of a Dielectric Elastomer Diaphragm for a Prosthetic Blood Pump," SPIE, San Diego, CA, United states, pp. 319–331.

[163] Goulbourne, N. C., Mockensturm, E. M., and Frecker, M. I., 2007, "Electro-Elastomers: Large Deformation Analysis of Silicone Membranes," Int J Solids Struct, **44**(9), pp. 2609–2626.

[164] Pope, K., Tews, A., Frecker, M., Mockensturm, E., Goulbourne, N. C., and Snyder, A. J., 2004, "Dielectric Elastomer Laminates for Active Membrane Pump Applications," Proc. of SPIE, **5385**, pp. 60–67.

[165] He, T., Cui, L., Chen, C., and Suo, Z., 2010, "Nonlinear Deformation Analysis of a Dielectric Elastomer Membrane–Spring System," Smart Mater Struct, **19**, p. 085017.

[166] Rosset, S., Poulin, A., Zollinger, A., Smith, M., and Shea, H., 2017, "Dielectric Elastomer Actuator for the Measurement of Cell Traction Forces with Sub-Cellular Resolution," https://doi-org.proxy.lib.umich.edu/10.1117/12.2258731, **10163**, pp. 107–115.

[167] Wingert, A., Lichter, M. D., Dubowsky, S., and Hafez, M., 2002, "Hyper-Redundant Robot Manipulators Actuated by Optimized Binary-Dielectric Polymers," https://doi.org/10.1117/12.475189, **4695**, pp. 415–423.

[168] Koh, S. J. A., Keplinger, C., Kaltseis, R., Foo, C. C., Baumgartner, R., Bauer, S., and Suo, Z., 2017, "High-Performance Electromechanical Transduction Using Laterally-Constrained Dielectric Elastomers Part I: Actuation Processes," J Mech Phys Solids, **105**, pp. 81–94.

[169] Prechtl, J., Kunze, J., Nalbach, S., Seelecke, S., and Rizzello, G., 2021, "Soft Robotic Module Actuated by Silicone-Based Rolled Dielectric Elastomer Actuators - Modeling and Simulation," International Conference and Exhibition on New Actuator Systems and Applications 2021.

[170] Randazzo, M., Buzio, R., Metta, G., Sandini, G., and Valbusa, U., 2008, "Architecture for the Semi-Automatic Fabrication and Assembly of Thin-Film Based Dielectric Elastomer Actuators," Proc. of SPIE Vol. 6927, **6927**, pp. 69272D-69272D–10.

[171] Shea, H., 2011, "Miniaturized EAPs with Compliant Electrodes Fabricated by Ion Implantation," https://doi.org/10.1117/12.882212, **7976**, pp. 235–243.

[172] Grasso, G., Rosset, S., and Shea, H., 2023, "Fully-Printed, Stretchable Arrays of Silicone-Based Zipping Actuators," https://doi-org.proxy.lib.umich.edu/10.1117/12.2657910, **PC12482**, p. PC1248205.

[173] Grasso, G., Rosset, S., and Shea, H., 2023, "Fully 3D-Printed, Stretchable, and Conformable Haptic Interfaces," Adv Funct Mater, **33**(20), p. 2213821.

[174] Kühnel, D. T., and Shea, H., 2022, "Thin, Flexible, and Scalable Mobile Robot Driven by Electrostatic Zipping Actuators," https://doi-org.proxy.lib.umich.edu/10.1117/12.2612881, **12042**, pp. 231–241.

[175] Seelecke, S., Neu, J., Croce, S., Hubertus, J., Schultes, G., and Rizzello, G., 2023, "Dielectric Elastomer Cooperative Microactuator Systems—DECMAS," Actuators 2023, Vol. 12, Page 141, **12**(4), p. 141.

[176] Pu, J., Meng, Y., Xie, Z., Peng, Z., Wu, J., Shi, Y., Plamthottam, R., Yang, W., and Pei, Q., 2022, "A Unimorph Nanocomposite Dielectric Elastomer for Large Out-of-Plane Actuation," Sci Adv, **8**(9), p. 6200.

[177] Gebbers, P., Grätzel, C., Maffli, L., Stamm, C., and Shea, H., 2012, "Zipping It up: DEAs Independent of the Elastomer's Electric Breakdown Field," Electroactive Polymer Actuators and Devices, **8340**, pp. 83402P-83402P–14.

[178] Maffli, L., Rosset, S., and Shea, H., 2013, "Zipping Dielectric Elastomer Actuators: Characterization, Design and Modeling," Smart Mater Struct, **22**(10), p. 104013.

[179] Peng, Z., Shi, Y., Chen, N., Li, Y., and Pei, Q., 2021, "Stable and High-Strain Dielectric Elastomer Actuators Based on a Carbon Nanotube-Polymer Bilayer Electrode," Adv Funct Mater, **31**(9), p. 2008321.

[180] Maffli, L., Rosset, S., and Shea, H., 2013, "Mm-Size Bistable Zipping Dielectric Elastomer Actuators for Integrated Microfluidics," https://doi.org/10.1117/12.2009367, **8687**, pp. 704–713.

[181] Price, A. K., and Culbertson, C. T., 2009, "Generation of Nonbiased Hydrodynamic Injections on Microfluidic Devices Using Integrated Dielectric Elastomer Actuators," Anal Chem, **81**(21), pp. 8942–8948.

[182] McCoul, D., Rosset, S., Schlatter, S., and Shea, H., 2017, "Inkjet 3D Printing of UV and Thermal Cure Silicone Elastomers for Dielectric Elastomer Actuators," Smart Mater Struct, **26**(12), p. 125022.

[183] Krishnan, A. S., Vargantwar, P. H., Ghosh, T. K., and Spontak, R. J., 2011, "Electroactuation of Solvated Triblock Copolymer Dielectric Elastomers: Decoupling the Roles of Mechanical Prestrain and Specimen Thickness," J Polym Sci B Polym Phys, **49**(22), pp. 1569–1582.

[184] Flittner, K., Schlosser, M., Lotz, P., Matysek, M., and Schlaak, H. F., 2010, "Integration of Dielectric Elastomer Stack Actuators into Micro Systems," **7642**, pp. 76422W-76422W–8.

[185] Piyasena, M. E., Newby, R., Miller, T. J., Shapiro, B., and Smela, E., 2009, "Electroosmotically Driven Microfluidic Actuators," Sens Actuators B Chem, **141**(1), pp. 263–269.

[186] Murray, C., McCoul, D., Sollier, E., Ruggiero, T., Niu, X., Pei, Q., and Carlo, D. Di, 2013, "Electro-Adaptive Microfluidics for Active Tuning of Channel Geometry Using Polymer Actuators," Microfluid Nanofluidics, **14**, pp. 345–358.

[187] Schlatter, S., Rosset, S., and Shea, H., 2017, "Inkjet Printing of Carbon Black Electrodes for Dielectric Elastomer Actuators," https://doi-org.proxy.lib.umich.edu/10.1117/12.2258615, **10163**, pp. 177–185.

[188] Schlatter, S., Grasso, G., Rosset, S., and Shea, H., 2020, "Inkjet Printing of Complex Soft Machines with Densely Integrated Electrostatic Actuators," Advanced Intelligent Systems, **2**(11), p. 2000136.

[189] Rosset, S., and Shea, H., 2012, "Flexible and Stretchable Electrodes for Dielectric Elastomer Actuators," Applied Physics A, **110**(2), pp. 281–307.

[190] Rosset, S., Ararom, O. A., Schlatter, S., and Shea, H., 2016, "Fabrication Process of Silicone-Based Dielectric Elastomer Actuators," JoVE (Journal of Visualized Experiments), **2016**(108), p. e53423.

[191] Rosset, S., and Shea, H., 2013, "Flexible and Stretchable Electrodes for Dielectric Elastomer Actuators," Appl Phys A Mater Sci Process, **110**(2), pp. 281–307.

[192] Li, T., Keplinger, C., Baumgartner, R., Bauer, S., Yang, W., and Suo, Z., 2013, "Giant Voltage-Induced Deformation in Dielectric Elastomers near the Verge of Snap-through Instability," J Mech Phys Solids, **61**(2), pp. 611–628.

[193] Pelrine, R., Kornbluh, R., Pei, Q., and Joseph, J., 2000, "High-Speed Electrically Actuated Elastomers with Strain Greater Than 100%," Science (1979), **287**(5454).

[194] Poulin, A., Imboden, M., Sorba, F., Grazioli, S., Martin-Olmos, C., Rosset, S., and Shea, H., 2018, "An Ultra-Fast Mechanically Active Cell Culture Substrate," Scientific Reports 2018 8:1, **8**(1), pp. 1–10.

[195] Kornbluh, R. D., Pelrine, R., Joseph, J., Heydt, R., Pei, Q., and Chiba, S., 2003, "High-Field Electrostriction of Elastomeric Polymer Dielectrics for Actuation," Smart Structures and Materials 1999: Electroactive Polymer Actuators and Devices, **3669**(May 1999), pp. 149–161.

[196] Carpi, F., De Rossi, D., Kornbluh, R., Pelrine, R., and Sommer-Larsen, P., 2011, *Dielectric Elastomers as Electromechanical Transducers: Fundamentals, Materials, Devices, Models and Applications of an Emerging Electroactive Polymer Technology*, Elsevier.

[197] Huber, J. E., Fleck, N. A., and Ashby, M. F., 1997, "The Selection of Mechanical Actuators Based on Performance Indices," Proceedings of the Royal Society of London. Series A: Mathematical, Physical and Engineering Sciences, **453**(1965), pp. 2185–2205.

[198] Shintake, J., Rosset, S., Schubert, B. E., Floreano, D., and Shea, H., 2015, "A Foldable Antagonistic Actuator," IEEE/ASME Transactions on Mechatronics, **20**(5), pp. 1997–2008.

[199] Akbari, S., Rosset, S., and Shea, H., 2013, "More than 10-Fold Increase in the Actuation Strain of Silicone Dielectric Elastomer Actuators by Applying Prestrain," https://doi.org/10.1117/12.2009912, **8687**, pp. 457–469.

[200] Pelrine, R., Kornbluh, R., and Kofod, G., 2000, "High-Strain Actuator Materials Based on Dielectric Elastomers," Advanced Materials, **12**(16), pp. 1223–1225.

[201] Plante, J.-S., and Dubowsky, S., 2006, "On the Nature of Dielectric Elastomer Actuators and Its Implications for Their Design," Proceedings of SPIE, **6168**, pp. 61681J 1–11.

[202] Chen, D., and Pei, Q., 2017, "Electronic Muscles and Skins: A Review of Soft Sensors and Actuators," Chem Rev, **117**(17), pp. 11239–11268.

[203] Zakaria, S., Yu, L., Kofod, G., and Skov, A. L., 2015, "The Influence of Static Pre-Stretching on the Mechanical Ageing of Filled Silicone Rubbers for Dielectric Elastomer Applications," Mater Today Commun, **4**, pp. 204–213.

[204] Cei, D., Costa, J., Gori, G., Frediani, G., Domenici, C., Carpi, F., and Ahluwalia, A., 2016, "A Bioreactor with an Electro-Responsive Elastomeric Membrane for Mimicking Intestinal Peristalsis," Bioinspir Biomim, **12**(1), p. 016001.

[205] Zhang, X., Wissler, M., Jaehne, B., Breonnimann, R., and Kovacs, G., 2004, "Effects of Crosslinking, Prestrain, and Dielectric Filler on the Electromechanical Response of a New Silicone and Comparison with Acrylic Elastomer," https://doi-org.proxy.lib.umich.edu/10.1117/12.540888, **5385**(27), pp. 78–86.

[206] O'Halloran, A., O'Malley, F., and McHugh, P., 2008, "A Review on Dielectric Elastomer Actuators, Technology, Applications, and Challenges," J Appl Phys, **104**(7).

[207] Cei, D., Costa, J., Gori, G., Frediani, G., Domenici, C., Carpi, F., and Ahluwalia, A., 2016, "A Bioreactor with an Electro-Responsive Elastomeric Membrane for Mimicking Intestinal Peristalsis," Bioinspir Biomim, **12**(1), p. 016001.

[208] Pei, Q., 2021, "Making Stretchy Dielectric, Conductive, and Semiconductor Polymers," https://doi.org/10.1117/12.2584462, **11587**, p. 115870H.

[209] Anderson, I. A., O'Brien, B., Brastaviceanu, T., and Spooner, G. J. R., 2010, "Artificial Muscle Membranes Fabricated Using Ultra-Short Pulse Laser Ablation," Proceedings of the ASME Conference on Smart Materials, Adaptive Structures and Intelligent Systems 2009, SMASIS2009, **2**, pp. 63–69.

[210] Wissler, M., and Mazza, E., 2005, "Modeling and Simulation of Dielectric Elastomer Actuators," Smart Mater Struct, **14**(6), pp. 1396–1402.

[211] Gisby, T., Calius, E. P., Xie, S., and Anderson, I. A., 2008, "An Adaptive Control Method for Dielectric Elastomer Devices," Proceedings of SPIE, **6927**, pp. 69271C-69271C–8.

[212] Wissler, M., Mazza, E., and Kovacs, G., 2005, "Circular Pre-Strained Dielectric Elastomer Actuator: Modeling, Simulation and Experimental Verification," Proceedings of SPIE, **5759**(0), pp. 182–193.

[213] Michel, S., Zhang, X. Q., Wissler, M., Lowe, C., and Kovacs, G., 2010, "A Comparison between Silicone and Acrylic Elastomers as Dielectric Materials in Electroactive Polymer Actuators," Polym Int, **59**(3), pp. 391–399.

[214] Kovacs, G., 2005, "Effects of Crosslinking, Prestrain, and Dielectric Filler on the Electromechanical Response of a New Silicone and Comparison with Acrylic Elastomer," Sens Actuators A Phys, **122**(2), pp. 273–283.

[215] Yuan, W., Hu, L., Yu, Z., Lam, T., Biggs, J., Ha, S. M., Xi, D., Chen, B., Senesky, M. K., Grüner, G., and Pei, Q., 2008, "Fault-Tolerant Dielectric Elastomer Actuators Using Single-Walled Carbon Nanotube Electrodes," Advanced Materials, **20**, pp. 621–625.

[216] Carpi, F., Anderson, I. A., Bauer, S., Frediani, G., Gallone, G., Gei, M., Graaf, C., Jean-Mistral, C., Kaal, W., Kofod, G., Kollosche, M., Kornbluh, R., Lassen, B., Matysek, M., Michel, S., Nowak, S., O'Brien, B., Pei, Q., Pelrine, R., Rechenbach, B., Rosset, S., and Shea, H., 2015, "Standards for Dielectric Elastomer Transducers," Smart Mater Struct, **24**(10), p. 105025.

[217] Boyce, M. C., and Arruda, E. M., 2000, "Constitutive Models of Rubber Elasticity A Review," Rubber Chemistry and Technology, **73**(3), pp. 504–523.

[218] Diani, J., Fayolle, B., and Gilormini, P., 2009, "A Review on the Mullins Effect," Eur Polym J, **45**(3), pp. 601–612.

[219] Jayatissa, S., Shim, V., Anderson, I. A., and Rosset, S., 2020, "Optimization of Prestretch and Actuation Stretch of a DEA-Based Cell Stretcher," https://doi-org.proxy.lib.umich.edu/10.1117/12.2558981, **11375**, pp. 148–159.

[220] Wang, Y., Chen, B., Bai, Y., Wang, H., and Zhou, J., 2014, "Actuating Dielectric Elastomers in Pure Shear Deformation by Elastomeric Conductors," Appl Phys Lett, **104**(6).

[221] Li, T., Qu, S., and Yang, W., 2012, "Electromechanical and Dynamic Analyses of Tunable Dielectric Elastomer Resonator," Int J Solids Struct, **49**(26), pp. 3754–3761.

[222] Zhu, J., Kollosche, M., Lu, T., Kofod, G., and Suo, Z., 2012, "Two Types of Transitions to Wrinkles in Dielectric Elastomers," Soft Matter, **8**(34), p. 8840.

[223] Kollosche, M., Kofod, G., Suo, Z., and Zhu, J., 2015, "Temporal Evolution and Instability in a Viscoelastic Dielectric Elastomer," J Mech Phys Solids, **76**, pp. 47–64.

[224] Akbari, S., Rosset, S., and Shea, H., 2013, "Improved Electromechanical Behavior in Castable Dielectric Elastomer Actuators," Appl Phys Lett, **102**(7), p. 071906.

[225] Kollosche, M., Zhu, J., Suo, Z., and Kofod, G., 2012, "Complex Interplay of Nonlinear Processes in Dielectric Elastomers," Phys Rev E, **85**(5), pp. 2–5.

[226] Li, T., Keplinger, C., Baumgartner, R., and Bauer, S., 2013, "Journal of the Mechanics and Physics of Solids Giant Voltage-Induced Deformation in Dielectric Elastomers near the Verge of Snap-through Instability," J Mech Phys Solids, **61**(2), pp. 611–628.

[227] Schlaak, H. F., 2005, "Novel Multilayer Electrostatic Solid State Actuators with Elastic Dielectric (Invited Paper)," Proceedings of SPIE, **5759**, pp. 121–133.

[228] Carpi, F., Mannini, A., and De Rossi, D., 2008, "Elastomeric Contractile Actuators for Hand Rehabilitation Splints," Proceedings of SPIE, **6927**, pp. 692705-692705–10.

[229] McKenzie, A. C., Calius, E. P., and Anderson, I. a., 2008, "Electric Field around a Dielectric Elastomer Actuator in Proximity to the Human Body," **6927**(2008), pp. 69272A-69272A–10.

[230] Karsten, R., Lotz, P., and Schlaak, H. F., 2011, "Active Suspension with Multilayer Dielectric Elastomer Actuator," **7976**, pp. 79762M-79762M–9.

[231] Karsten, R., and Schlaak, H. F., 2012, "Adaptive Absorber Based on Dielectric Elastomer Stack Actuator with Variable Stiffness," **8340**, pp. 834020-834020–8.

[232] Flittner, K., Schlosser, M., and Schlaak, H. F., 2011, "Dielectric Elastomer Stack Actuators for Integrated Gas Valves," Proceedings of SPIE, **7976**(1), pp. 79761K-79761K–7.

[233] Kovacs, G., Düring, L., Michel, S., and Terrasi, G., 2009, "Sensors and Actuators A : Physical Stacked Dielectric Elastomer Actuator for Tensile Force Transmission," **155**, pp. 299–307.

[234] Matysek, M., Lotz, P., Flittner, K., and Schlaak, H. F., 2008, "High-Precision Characterization of Dielectric Elastomer Stack Actuators and Their Material Parameters," **6927**, pp. 1–10.

[235] Carpi, F., and De Rossi, D., 2007, "Contractile Folded Dielectric Elastomer Actuators," SPIE - The International Society for Optical Engineering, USA, p. 65240D (13 pp.).

[236] Carpi, F., Migliore, A., Serra, G., and Rossi, D. De, 2005, "Helical Dielectric Elastomer Actuators," Smart Mater Struct, **14**, pp. 1210–1216.

[237] Kovacs, G., Düring, L., Michel, S., and Terrasi, G., 2009, "Stacked Dielectric Elastomer Actuator for Tensile Force Transmission," Sens Actuators A Phys, **155**, pp. 299–307.

[238] Matysek, M., Lotz, P., Flittner, K., and Schlaak, H. F., 2010, "Vibrotactile Display for Mobile Applications Based on Dielectric Elastomer Stack Actuators," Proceeding of SPIE, **7642**, p. 76420D.

[239] Pelrine, R., Kornbluh, R., and Kofod, G., 2000, "High-Strain Actuator Materials Based on Dielectric Elastomers," Advanced Materials, **12**(16), pp. 1223–1225.

[240] York, A., and Seelecke, S., 2009, "Electro-Mechanical Analysis of a Dielectric EAP Actuator," **7289**(2001), pp. 72891H-72891H–7.

[241] Ha, S. M., Park, I. S., Wissler, M., Pelrine, R., Stanford, S., Kim, K. J., Kovacs, G., and Pei, Q., 2008, "High Electromechanical Performance of Electroelastomers Based on Interpenetrating Polymer Networks," Proceedings of SPIE, **6927**, pp. 69272C-1–9.

[242] Shintake, J., Rosset, S., Floreano, D., and Shea, H. R., 2013, "Effect of Mechanical Parameters on Dielectric Elastomer Minimum Energy Structures," Proc. SPIE, **8687**, pp. 86872V-86872V–13.

[243] Kofod, G., 2006, "New Design Concept for Dielectric Elastomer Actuators," Proceedings of SPIE, **6168**, pp. 61682J-61682J–9.

[244] Plante, J.-S., and Dubowsky, S., 2007, "On the Performance Mechanisms of Dielectric Elastomer Actuators," Sens Actuators A Phys, **137**(1), pp. 96–109.

[245] Bolzmacher, C., Hafez, M., Khoudja, M. B., Bernardoni, P., and Dubowsky, S., 2004, "Polymer-Based Actuators for Virtual Reality Devices," Smart Structures and Materials: Electroactive Polymer Actuators and Devices (EAPAD), **5385**, pp. 281–289.

[246] Plante, J.-S., Devita, L. M., and Dubowsky, S., 2007, "A Road to Practical Dielectric Elastomer Actuators Based Robotics and Mechatronics: Discrete Actuation," Y. Bar-Cohen, ed., SPIE, San Diego, California, USA, pp. 652406–15.

[247] O'Brien, B., Calius, E., Xie, S., and Anderson, I., 2008, "An Experimentally Validated Model of a Dielectric Elastomer Bending Actuator," Proceedings of SPIE, **6927**, pp. 69270T-69270T–11.

[248] Lochmatter, P., Kovacs, G., and Wissler, M., 2007, "Characterization of Dielectric Elastomer Actuators Based on a Visco-Hyperelastic Film Model," Smart Mater Struct, **16**(2), pp. 477–486.

[249] Kofod, G., and Sommer-Larsen, P., 2005, "Silicone Dielectric Elastomer Actuators: Finite-Elasticity Model of Actuation," Sens Actuators A Phys, **122**(2), pp. 273–283.

[250] Bolzmacher, C., Biggs, J., and Srinivasan, M., 2006, "Flexible Dielectric Elastomer Actuators for Wearable Human-Machine Interfaces," **6168**, pp. 616804-616804–12.

[251] Balakrisnan, B., and Smela, E., 2010, "Challenges in the Microfabrication of Dielectric Elastomer Actuators," SPIE, San Diego, CA, United states, p. The Society of Photo-Optical Instrumentation Engin.

[252] Pelrine, R., Kornbluh, R., and Joseph, J. P., 1998, "Electrostriction of Polymer Dielectrics with Compliant Electrodes as a Means of Actuation," Sens Actuators A Phys, **64**(1), pp. 77–85.

[253] Yu, Z., Yuan, W., Brochu, P., Chen, B., Liu, Z., and Pei, Q., 2009, "Large-Strain, Rigid-to-Rigid Deformation of Bistable Electroactive Polymers," Appl Phys Lett, **95**, pp. 2009–2011.

[254] Shintake, J., Rosset, S., Floreano, D., and Shea, H. R., 2013, "Effect of Mechanical Parameters on Dielectric Elastomer Minimum Energy Structures," Proc. SPIE, **8687**, pp. 86872V-86872V–13.

[255] Plante, J. S., and Dubowsky, S., 2007, "On the Properties of Dielectric Elastomer Actuators and Its Implications for Their Design," J. of Smart Materials and Structures, **16**, pp. 227–236.

[256] Kornbluh, R., Pelrine, R., Pei, Q., Oh, S., and Joseph, J., 2000, "Ultrahigh Strain Response of Field-Actuated Elastomeric Polymers," SPIE 3987, Smart Structures and Materials 2000: Electroactive Polymer Actuators and Devices (EAPAD), **3987**, pp. 51–64.

[257] Zhang, X., Wissler, M., Jaehne, B., Breonnimann, R., and Kovacs, G., 2004, "Effects of Crosslinking, Prestrain and Dielectric Filler on the Electromechanical Response of a New Silicone and Comparison with Acrylic Elastomer," Proceedings of SPIE, **5385**(0), pp. 78–86.

[258] Brochu, P., and Pei, Q., 2010, "Advances in Dielectric Elastomers for Actuators and Artificial Muscles," Macromol Rapid Commun, **31**(1), pp. 10–36.

[259] Gallone, G., Galantini, F., and Carpi, F., 2010, "Perspectives for New Dielectric Elastomers with Improved Electromechanical Actuation Performance: Composites versus Blends," Polym Int, **59**(June 2009), pp. 400–406.

[260] Kornbluh, R. D., 2000, "Ultrahigh Strain Response of Field-Actuated Elastomeric Polymers," Proceedings of SPIE, **3987**, pp. 51–64.

[261] Sommer-Larsen, P., 2002, "Performance of Dielectric Elastomer Actuators and Materials," Proceedings of SPIE, **4695**(1), pp. 158–166.

[262] Pelrine, R., Kornbluh, R., and Kofod, G., 2000, "High-Strain Actuator Materials Based on Dielectric Elastomers," Advanced Materials, **12**(16), pp. 1223–1225.

[263] Kofod, G., 2008, "The Static Actuation of Dielectric Elastomer Actuators: How Does Pre-Stretch Improve Actuation?," J Phys D Appl Phys, **215405**(21), p. 215405.

[264] Kofod, G., Sommer-Larsen, P., Kornbluh, R., and Pelrine, R., 2003, "Actuation Response of Polyacrylate Dielectric Elastomers," Journal of Intelligent Materials Systems and Structures, **14**(December), pp. 787–793.

[265] Kofod, G., Sommer-Larsen, P., Kornbluh, R., and Pelrine, R., 2003, "Actuation Response of Polyacrylate Dielectric Elastomers," J Intell Mater Syst Struct, **14**(12), p. 787.

[266] Yuan, W., Li, H., Brochu, P., Niu, X., and Pei, Q., 2010, "Fault-Tolerant Silicone Dielectric Elastomers," Int J Smart Nano Mater, **1**(1), pp. 40–52.

[267] Carpi, F., and De Rossi, D., 2005, "Improvement of Electromechanical Actuating Performances of a Silicone Dielectric Elastomer by Dispersion of Titanium Dioxide Powder," IEEE Transactions on Dielectrics and Electrical Insulation, **12**(4), pp. 835–843.

[268] Mc Carthy, D. N., Risse, S., Katekomol, P., and Kofod, G., 2009, "The Effect of Dispersion on the Increased Relative Permittivity of TiO 2 /SEBS Composites," J Phys D Appl Phys, **42**(14), p. 145406.

[269] Stoyanov, H., Brochu, P., Niu, X., Lai, C., Yun, S., and Pei, Q., 2013, "Long Lifetime, Fault-Tolerant Freestanding Actuators Based on a Silicone Dielectric Elastomer and Self-Clearing Carbon Nanotube Compliant Electrodes," RSC Adv, **3**(7), p. 2272.

[270] Brochu, P., Stoyanov, H., Niu, X., and Pei, Q., 2013, "All-Silicone Prestrain-Locked Interpenetrating Polymer Network Elastomers: Free-Standing Silicone Artificial Muscles with Improved Performance and Robustness," Smart Mater Struct, **22**(5), p. 055022.

[271] Dubois, P., Rosset, S., Koster, S., Stauffer, J., Mikhaïlov, S., Dadras, M., Rooij, N. F. de, and Shea, H., 2006, "Microactuators Based on Ion Implanted Dielectric Electroactive Polymer (EAP) Membranes," Sens Actuators A Phys, **130–131**(SPEC. ISS.), pp. 147–154.

[272] Pelrine, R., Kornbluh, R., and Kofod, G., 2000, "High-Strain Actuator Materials Based on Dielectric Elastomers," Advanced Materials, **12**(16), pp. 1223–1225.

[273] Huang, J., Li, T., Chiang Foo, C., Zhu, J., Clarke, D. R., and Suo, Z., 2012, "Giant, Voltage-Actuated Deformation of a Dielectric Elastomer under Dead Load," Appl Phys Lett, **100**(4), p. 041911.

[274] Plante, J. S., and Dubowsky, S., 2006, "Large-Scale Failure Modes of Dielectric Elastomer Actuators," Int J Solids Struct, **43**, pp. 7727–7751.

[275] Huang, J. C., 2002, "Carbon Black Filled Conducting Polymers and Polymer Blends," Advances in Polymer Technology, **21**(4), pp. 299–313.

[276] Poulin, A., Rosset, S., and Shea, H., 2015, "Pad Printing 1-10 Mm Thick Elastomer Membranes for DEAs," (200020), p. 206021.

[277] Hu, L., Yuan, W., Brochu, P., Gruner, G., and Pei, Q., 2009, "Highly Stretchable, Conductive, and Transparent Nanotube Thin Films," Appl Phys Lett, **94**, pp. 2009–2011.

[278] Yuan, W., Hu, L., Ha, S., Lam, T., Grüner, G., and Pei, Q., 2008, "Self-Clearable Carbon Nanotube Electrodes for Improved Performance of Dielectric Elastomer Actuators," San Diego, California, USA, pp. 69270P-69270P–12.

[279] Pimpin, A., Suzuki, Y., and Kasagi, N., 2007, "Microelectrostrictive Actuator with Large Out-of-Plane Deformation for Flow-Control Application," Journal of Microelectromechanical Systems, **16**(3), pp. 753–764.

[280] Verplancke, R., Bossuyt, F., Cuypers, D., and Vanfleteren, J., 2012, "Thin-Film Stretchable Electronics Technology Based on Meandering Interconnections: Fabrication and Mechanical Performance," Journal of Micromechanics and Microengineering, **22**(1).

[281] Jones, R. W., Wang, P., Lassen, B., and Sarban, R., 2010, "Dielectric Elastomers and Compliant Metal Electrode Technology," Proceedings of the Mediterranean Electrotechnical Conference - MELECON, pp. 368–373.

[282] Lau, G. K., Goh, S. C. K., and Shiau, L. L., 2011, "Dielectric Elastomer Unimorph Using Flexible Electrodes of Electrolessly Deposited (ELD) Silver," Sens Actuators A Phys, **169**(1), pp. 234–241.

[283] Goh, S. C.-K., and Lau, G.-K., 2010, "Dielectric Elastomeric Bimorphs Using Electrolessly Deposited Silver Electrodes," Electroactive Polymer Actuators and Devices (EAPAD) 2010, **7642**(April 2010), p. 764215.

[284] Zakaria, S., Morshuis, P. H. F., Benslimane, M. Y., Yu, L., and Skov, A. L., 2015, "The Electrical Breakdown Strength of Pre-Stretched Elastomers, with and without Sample Volume Conservation," Smart Mater Struct, **24**(5), p. 055009.

[285] Madsen, F. B., Yu, L., Daugaard, A. E., Hvilsted, S., and Skov, A. L., 2014, "Silicone Elastomers with High Dielectric Permittivity and High Dielectric Breakdown Strength Based on Dipolar Copolymers," Polymer (Guildf), **55**(24), pp. 6212–6219.

[286] Madsen, F. B., Yu, L., and Skov, A. L., 2016, "Self-Healing, High-Permittivity Silicone Dielectric Elastomer," ACS Macro Lett, **5**(11), pp. 1196–1200.

[287] Skov, A. L., Vudayagiri, S., and Benslimane, M., 2013, "Novel Silicone Elastomer Formulations for DEAPs," Electroactive Polymer Actuators and Devices (EAPAD) 2013, **8687**, p. 86871I.

[288] Stoyanov, H., Brochu, P., Niu, X., Della Gaspera, E., and Pei, Q., 2012, "Dielectric Elastomer Transducers with Enhanced Force Output and Work Density," Appl Phys Lett, **100**(26), pp. 1–4.

[289] Yuan, B. W., Brochu, P., Ha, S. M., and Pei, Q., 2008, "Dielectric Elastomer Actuators with High Durable Electromechanical Strain," **200**, pp. 1–7.

[290] Yuan, W., Hu, L., Ha, S., Lam, T., Grűner, G., and Pei, Q., 2008, "Self-Clearable Carbon Nanotube Electrodes for Improved Performance of Dielectric Elastomer Actuators," Polymer (Guildf), **6927**, pp. 1–12.

[291] Peng, Z., Shi, Y., Xie, Z., Li, Y., Chen, N., and Pei, Q., 2021, "Self-Clearable Bilayer Electrode for Dielectric Elastomer Actuators," https://doi.org/10.1117/12.2584030, **11587**, pp. 302–306.

[292] Samuel, J., Devor, R. E., and Kapoor, S. G., 2015, "A Microstructure-Level Material Model for Simulating the Machining of Carbon Nanotube," **130**(June 2008), pp. 1–8.

[293] Yuan, W., and Pei, Q., 2010, "Novel Electrode-Elastomer Combinations for Improved Performance and Application of Dielectric Elastomers."

[294] Yuan, W., Lam, T., Biggs, J., Hu, L., Yu, Z., Ha, S., Xi, D., Senesky, M. K., Grüner, G., and Pei, Q., 2007, "New Electrode Materials for Dielectric Elastomer Actuators," Proceedings of SPIE, **6524**(2007), pp. 65240N-65240N–12.

[295] Zhu, J., Stoyanov, H., Kofod, G., and Suo, Z., 2010, "Large Deformation and Electromechanical Instability of a Dielectric Elastomer Tube Actuator," J Appl Phys, **108**(7), p. 074113.

[296] Kollosche, M., Stoyanov, H., Ragusch, H., and Kofod, G., 2010, "Dependence on Boundary Conditions for Actuation Characteristics of Dielectric Elastomer Actuators," **7642**, p. The Society of Photo-Optical Instrumentation Engin.

[297] Boyce, M., and Arruda, E., 2000, "Constitutive Models of Rubber Elasticity: A Review," Ann Rubber Chemistry and Technology, **73**(3), pp. 504–523.

[298] Carpi, F., Anderson, I., Bauer, S., Frediani, G., Gallone, G., Gei, M., Graaf, C., Jean-Mistral, C., Kaal, W., Kofod, G., Kollosche, M., Kornbluh, R. D., Lassen, B., Matysek, M., Michel, S., Nowak, S., O'Brien, B., Pei, Q., Pelrine, R., Rechenbach, B., Rosset, S., and Shea, H. R., 2015, "Standards for Dielectric Elastomer Transducers," Smart Mater Struct, **24**(10), p. 25.

[299] 2013, "Diani et al. - 2009 - A Review on the Mullins Effect.Html," **8687**, pp. 86872M-86872M–10.

[300] Han, Z., Peng, Z., Guo, Y., Wang, H., Plamthottam, R., and Pei, Q., 2023, "Hybrid Fabrication of Prestrain-Locked Acrylic Dielectric Elastomer Thin Films and Multilayer Stacks," Macromol Rapid Commun, **44**(15), p. 2300160.

[301] Moretti, G., Righi, M., Vertechy, R., and Fontana, M., 2017, "Fabrication and Test of an Inflated Circular Diaphragm Dielectric Elastomer Generator Based on PDMS Rubber Composite," Polymers 2017, Vol. 9, Page 283, **9**(7), p. 283.

[302] Chen, Y., Agostini, L., Moretti, G., Berselli, G., Fontana, M., and Vertechy, R., 2019, "Fatigue Life Performances of Silicone Elastomer Membranes for Dielectric Elastomer Transducers: Preliminary Results," https://doi-org.proxy.lib.umich.edu/10.1117/12.2515312, **10966**, pp. 158–167.

[303] Berdozzi, N., Chen, Y., Luzi, L., Fontana, M., Fassi, I., Molinari Tosatti, L., and Vertechy, R., 2020, "Rapid Fabrication of Electro-Adhesive Devices with Inkjet Printed Electrodes," IEEE Robot Autom Lett, **5**(2), pp. 2770–2776.

[304] Fasolt, B., Welsch, F., Jank, M., and Seelecke, S., 2019, "Effect of Actuation Parameters and Environment on the Breakdown Voltage of Silicone Dielectric Elastomer Films," Smart Mater Struct, **28**(9), p. 094002.

[305] Hau, S., Rizzello, G., and Seelecke, S., 2018, "A Novel Dielectric Elastomer Membrane Actuator Concept for High-Force Applications," Extreme Mech Lett, **23**, pp. 24–28.

[306] Hodgins, M., York, A., and Seelecke, S., 2017, "Systematic Experimental Characterization of Dielectric Elastomer Membranes Using a Custom-Built Tensile Test Rig," J Intell Mater Syst Struct, **28**(15), pp. 2117–2128.

[307] De Saint-Aubin, C. A., Rosset, S., Schlatter, S., and Shea, H., 2018, "High-Cycle Electromechanical Aging of Dielectric Elastomer Actuators with Carbon-Based Electrodes," Smart Mater Struct, **27**(7), p. 074002.

[308] Treloar, L. R. G., 1975, *The Physics of Rubber Elasticity*, Oxford University Press.

[309] Johnson, M. A., and Beatty, M. F., 1993, "Continuum Mechanics A Constitutive Equation for the Mullins Effect in Stress Controlled Uniaxial Extension Experiments," **5**, pp. 301–318.

[310] Babič, M., Vertechy, R., Berselli, G., Lenarčič, J., Castelli, V. P., and Vassura, G., 2010, "An Electronic Driver for Improving the Open and Closed Loop Electro-Mechanical Response of Dielectric Elastomer Actuators," Mechatronics, **20**(2), pp. 201–212.

[311] Carpi, F., Chiarelli, P., Mazzoldi, A., and De Rossi, D., 2003, "Electromechanical Characterisation of Dielectric Elastomer Planar Actuators: Comparative Evaluation of Different Electrode Materials and Different Counterloads," Sens Actuators A Phys, **107**(1), pp. 85–95.

[312] Huang, J., Li, T., Chiang Foo, C., Zhu, J., Clarke, D. R., and Suo, Z., 2012, "Giant, Voltage-Actuated Deformation of a Dielectric Elastomer under Dead Load," Appl Phys Lett, **100**.

[313] Wineman, A., and Rajagopal, K., 2000, *Mechanical Response of Polymers: An Introduction*.

[314] Suo, Z., 2010, "Theory of Dielectric Elastomers," Acta Mechanica Solida Sinica, **23**(6), pp. 549–578.

[315] Wissler, M., and Mazza, E., 2005, "Modeling of a Pre-Strained Circular Actuator Made of Dielectric Elastomers," Sens Actuators A Phys, **120**(1), pp. 184–192.

[316] Goulbourne, N., Mockensturm, E., and Frecker, M., 2005, "A Nonlinear Model for Dielectric Elastomer Membranes," J Appl Mech, **72**(6), p. 899.

[317] 2001, "Response of Dielectric Elastomer Actuators," Structures and Materials, **4329**, pp. 157–163.

[318] Gent, A. N., 1996, "A New Constitutive Relation for Rubber," Rubber Chemistry and Technology, **69**(1), pp. 59–61.

[319] Silberstein, M. N., and Boyce, M. C., 2010, "Constitutive Modeling of the Rate, Temperature, and Hydration Dependent Deformation Response of Nafion to Monotonic and Cyclic Loading," J Power Sources, **195**(17), pp. 5692–5706.

[320] Rizzello, G., Naso, D., York, A., and Seelecke, S., 2016, "Closed Loop Control of Dielectric Elastomer Actuators Based on Self-Sensing Displacement Feedback," Smart Mater Struct, **25**(3), p. 035034.

[321] Rizzello, G., Naso, D., York, A., and Seelecke, S., 2016, "Self-Sensing Control of a Bi-Stable Dielectric Elastomer Actuator Operating Against a Load," Symposium für Smarte Strukturen und Systeme (pp. 360-372).

[322] Panaro, G., Rizzello, G., Naso, D., and Seelecke, S., 2018, "Position Control of Dielectric Elastomer Actuators Based on Port-Hamiltonian Framework," Proceedings of the IEEE Conference on Decision and Control, **2018-December**, pp. 6888–6893.

[323] Massenio, P. R., Rizzello, G., Comitangelo, G., Naso, D., and Seelecke, S., 2020, "Reinforcement Learning-Based Minimum Energy Position Control of Dielectric Elastomer Actuators," IEEE Transactions on Control Systems Technology.

[324] Imai, N., Nishi, S., Yoshita, K., Ito, Y., Osawa, Y., Takahashi, K., Nakagawa, Y., Saito, K., Takahashi, K., and Narita, I., 2012, "Design and Control of a High-Speed Positioning System Based on Dielectric Elastomer Membrane Actuators," Clin Transplant, **26**(SUPPL.24), pp. 25–31.

[325] Vertechy, R., Berselli, G., Lenarc, J., and Babic, M., 2010, "Mechatronics An Electronic Driver for Improving the Open and Closed Loop Electro-Mechanical Response of Dielectric Elastomer Actuators," **20**, pp. 201–212.

[326] Rosset, S., Maffli, L., Houis, S., and Shea, H., 2014, "An Instrument to Obtain the Correct Biaxial Hyperelastic Parameters of Silicones for Accurate DEA Modelling," SPIE Smart Structures and Materials+ Nondestructive Evaluation and Health Monitoring, **9056**, pp. 90560M-90560M.

[327] Beatty, M. F., 2000, "The Mullins Effect in a Pure Shear," pp. 369–392.

[328] Chagnon, G., 2004, "On the Relevance of Continuum Damage Mechanics as Applied to the Mullins Effect in Elastomers," J Mech Phys Solids, **52**(7), pp. 1627–1650.

[329] Peng, Z., Shi, Y., Chen, N., Li, Y., and Pei, Q., 2020, "Stable and High-Strain Dielectric Elastomer Actuators Based on a Carbon Nanotube-Polymer Bilayer Electrode," Adv Funct Mater.

[330] Hu, L., Pasta, M., Mantia, F. La, Cui, L., Jeong, S., Deshazer, H., Choi, J. W., Han, S. M., and Cui, Y., 2010, "Stretchable, Porous, and Conductive Energy Textiles," Nano Lett.

[331] Czarnocki, I., Kim, W., Utter, B., Luntz, J., Brei, D., and Alexander, P., 2014, "Design of SMA Helical Actuators: An Experimental Study," ASME 2013 Conference on Smart Materials, Adaptive Structures and Intelligent Systems, SMASIS 2013, **1**.

[332] Moskalik, A., and Brei, D., 1997, "Quasi-Static Behavior of Individual C-Block Piezoelectric Actuators," J Intell Mater Syst Struct.

[333] Alexander, P. W., Brei, D., and Halloran, J. W., 2005, "The Force-Deflection Behavior of Functionally Graded Piezoceramic Actuators."

[334] Berselli, G., Vertechy, R., Vassura, G., and Castelli, V. P., 2015, "Design of a Single-Acting-Force Actuator Based on Dielectric Elastomers," **1**(August 2009), pp. 1–7.

[335] Pelrine, R., Kornbluh, R., Joseph, J., Heydt, R., Pei, Q., and Chiba, S., 2000, "High-Field Deformation of Elastomeric Dielectrics for Actuators," Materials Science and Engineering C, **11**(2), pp. 89–100.

[336] Bruch, D., Hau, S., Loew, P., Rizzello, G., and Seelecke, S., 2018, "Fast Model-Based Design of Large Stroke Dielectric Elastomer Membrane Actuators Biased with Pre-Stressed Buckled Beams," https://doi-org.proxy.lib.umich.edu/10.1117/12.2296558, **10594**, pp. 62–69.

[337] Hau, S., Bruch, D., Rizzello, G., Motzki, P., and Seelecke, S., 2018, "Silicone Based Dielectric Elastomer Strip Actuators Coupled with Nonlinear Biasing Elements for Large Actuation Strains," Smart Mater Struct, **27**(7), p. 074003.

[338] Croce, S., Neu, J., Hubertus, J., Rizzello, G., Seelecke, S., and Schultes, G., 2021, "Modeling and Simulation of Compliant Biasing Systems for Dielectric Elastomer Membranes Based on Polymeric Domes | VDE Conference Publication | IEEE Xplore," International Conference and Exhibition on New Actuator Systems and Applications 2021.

[339] Neu, J., Hubertus, J., Croce, S., Schultes, G., Seelecke, S., and Rizzello, G., 2021, "Fully Polymeric Domes as High-Stroke Biasing System for Soft Dielectric Elastomer Actuators," Front Robot AI, **8**, p. 695918.

[340] Croce, S., Neu, J., Hubertus, J., Seelecke, S., Schultes, G., and Rizzello, G., 2021, "Model-Based Design Optimization of Soft Polymeric Domes Used as Nonlinear Biasing Systems for Dielectric Elastomer Actuators," Actuators 2021, Vol. 10, Page 209, **10**(9), p. 209.

[341] Baltes, M., Kunze, J., Prechtl, J., Seelecke, S., and Rizzello, G., 2023, "Corrigendum: A Bi-Stable Soft Robotic Bendable Module Driven by Silicone Dielectric Elastomer Actuators: Design, Characterization, and Parameter Study (2022 Smart Mater. Struct. 31 114002)," Smart Mater Struct, **32**(4), p. 049501.

[342] Hodgins, M., and Seelecke, S., 2010, "Mechanical Behavior of a Bi-Stable Negative-Rate Bias Spring System," Behavior and Mechanics of Multifunctional Materials and Composites 2010, **7644**, pp. 76442H-76442H–12.

[343] Berselli, G., Vertechy, R., Vassura, G., and Castelli, V. P., 2009, "Design of a Single-Acting Constant-Force Actuator Based on Dielectric Elastomers," J Mech Robot, **1**(3), p. 031007.

[344] Gatti, D., Tropea, C., and Schlaak, H. F., 2014, "Dynamic Performance of Silicone Dielectric Elastomer Actuators with Bi-Stable Buckled Beams," Spie Eapad 2014, **9056**, p. 905638.

[345] Carpi, F., Salaris, C., and Rossi, D. De, 2007, "Folded Dielectric Elastomer Actuators," Smart Mater Struct, **16**(2), pp. S300–S305.

[346] Kovacs, G., Düring, L., Michel, S., and Terrasi, G., 2009, "Stacked Dielectric Elastomer Actuator for Tensile Force Transmission," Sens Actuators A Phys, **155**(2), pp. 299–307.

[347] Lotz, P., Matysek, M., and Schlaak, H. F., 2011, "Lifetime of Dielectric Elastomer Stack Actuators," Proceedings of SPIE, **7976**(1), pp. 79760P-79760P–9.

[348] Hodgins, M., York, A., and Seelecke, S., 2013, "Experimental Comparison of Bias Elements for Out-of-Plane DEAP Actuator System," Smart Mater Struct, **22**(9), p. 094016.

[349] Anderson, I. A., Tse, T. C. H., Inamura, T., O'Brien, B. M., McKay, T., and Gisby, T., 2011, "A Soft and Dexterous Motor," Appl Phys Lett, **98**(12), p. 123704.

[350] Ahmed, S., Ounaies, Z., and Frecker, M., 2014, "Investigating the Performance and Properties of Dielectric Elastomer Actuators as a Potential Means to Actuate Origami Structures," Smart Mater Struct, **23**(9), p. 094003.